White matter disconnection in frontal lobe disorders

D'Anna, Lucio

Awarding institution:
King's College London

White matter Disconnection in Frontal Lobe Disorders

Lucio D'Anna

Thesis submitted to King's College London

in fulfilment of the requirements for the degree of

Doctor of Philosophy

in Clinical Neuroscience

Institute of Psychiatry, Psychology & Neuroscience

King's College London

2017

Acknowledgements

I would like to express my sincere gratitude to my supervisor Professor Marco Catani for his unwavering support during my PhD research. Your guidance has been a constant help throughout my time of intellectual growth and allowed me to think as a true research scientist. Your advice on both research as well as on my career has been priceless.
I could not have imagined having a better advisor and mentor for my PhD study.

I would like to thank my supervisor Professor Declan Murphy. Your brilliant comments and suggestions have made the journey lighter and somehow amusing. This thesis would not be possible without your supervision and I am incredibly grateful for all your input during the past three years.

I thank my fellow Natbrainlab labmates for all the stimulating discussions, all the time spent working together before deadlines and for all the fun we have had in the last three years: Flavio Dell'Acqua, Michel Thiebaut De Schotten, Stephanie Forkel, Henrietta Howells, Valeria Parlantini, Luis Lacerda, Anoushka Leslie, Naianna Roberston, Claudia Cramer, Petra Gorham, Pedro Laguna, James Findon, Francisco de Santiago Requejo, Stefano Sandrone and Rachel Barrett.

My sincere gratitude also goes to Professors Marsel Mesulam, Emily Rogalski, Nigel Leigh, Laura Goldstein and Dr. Christine Ecker for the opportunity they have given me to collaborate with them and work on unique datasets.

Lastly, I would like to thank my wonderful family for all their love and encouragement. My parents, Sebastiano and Tecla raised me with a love for science and supported me in all my pursuits. Thank you for inspiring me to follow my dreams.
My sisters, Grazia and Giovanna have always believed in me and wanted the best for me. A special thank to my 6-year-old nephew Mauro for his colorfoul drawings that made me feel less far away from home.
My family are the most important people in my world and I dedicate this thesis to them.

Thank you.

London, 22 December 2016

“Have the courage to follow your heart and intuition.

They somehow know what you truly want to become.”

Steve Jobs

Abstract

In the recent years our understanding of the frontal lobe functions has greatly advanced. The advances in the field of the neuropsychology, neuroimaging and neurosciences all contributed to a rapidly changing perspective on the role of the frontal lobes in behaviour and cognition and they also changed clinical approaches to the evaluation of patients with frontal lobe disorders. The structure of the brain can be non-invasively assessed in vivo using magnetic resonance imaging (MRI). The MRI diffusion tensor imaging (DTI) can be used to reconstruct the human brain white matter and to quantify their microstructural integrity.

The aim of this thesis is to investigate the anatomy of the frontal networks underlying cognitive and behavioural functions and includes three studies: an investigation of the association between extra-motor white matter tracts and cognitive and behaviour symptoms in Motor Neuron Disease (MND); a study of the ventral fronto-temporal network and its association with behavioural symptoms in Primary Progressive Aphasia (PPA); a study to investigate the association between white matter abnormalities in several long association tracts and deficits in non-verbal and verbal communication in Autism Spectrum Disorders (ASD).

Overall, the findings of this thesis indicate that both uncinate fasciculus and cingulum are frontal lobe structures particularly vulnerable to disease regardless the nature of the underlying pathology. Damage to these tracts could manifest with abnormalities in several aspects of social behaviour and cognition. These considerations will help to broaden our understanding of the frontal lobe function beyond motor and language functions.

Table of Contents

Table of Figures

Table of Table

Chapter 1 Introduction to the Frontal lobe

This chapter provides a background of the major topics that are discussed in greater detail throughout this thesis. The emergence of the frontal lobes as an anatomical structure and the progressive expansion of its functional correlates are reviewed in the historical introduction. Structural changes from birth to old age are reviewed in the second paragraph to facilitate the interpretation of the neuroimaging findings discussed in the experimental chapters. The paragraphs on surface, sectional and connectional anatomy offer an update on the current international nomenclature used to the described the major structures of the frontal lobes. The chapter closes with an introduction to the main clinical syndromes of the frontal lobe and their anatomical correlates.

1.1 Historical overview

This historical review is not a comprehensive index although it has the aim to emphasize the key developments in frontal lobe research that have relevance to this actual thesis. Hence, greater attention has been dedicated to those milestones that have advanced our understanding of frontal lobe role in behaviour, emotion, memory and social cognition.

'*Frontal lobe*' was first proposed by the French physician and anatomist Felix Vicq d'Azyr in 1786 to indicate the most anterior part of the brain. He suggested that the old subdivision of the brain into anterior, middle and posterior lobes should be replaced by a new nomenclature that borrowed its terminology from the names of the bones forming the skull [1]. While the emergence of the '*frontal lobe*' as a distinct anatomical structure had a precise date in time, the demonstration of its functional roles in cognitive functions and behaviour has occurred slowly over the last 250 years [2].

At the beginning of the 19th century, Franz Josef Gall and Johann Gaspar Spurzheim were the first to believe that mental functions were localized in discrete parts of the brain, which they

called cortical '*organs*'. They proposed several functions of the '*frontal organs*', some of which were broadly related to memory, language and social behaviour [3]. In the mid-19th century Gall and Superzheim doctrine fell into disrepute but their idea of localized mental functions had a deep and lasting impact on many influential French academics, including Ernest Aubertin and Paul Broca. These authors provided direct demonstration of an association between damage to the frontal lobe and deficits of language production, a conclusion that was strongly opposed by those who believed in holistic ideas of brain activity [4,5]. At the same time, evidence for motor functions of the frontal cortex were brought forward by experimental physiologists and neurologists. In Germany, Gustav Theodor Fritsch and Eduard Hitzig demonstrated that the grey matter is capable of excitation and the electrical stimulation of the posterior-frontal cortex in animals produces movement in the contralateral muscles in a reproducible and orderly way[6]. These observations, coupled with the clinical report by John Hughlings Jackson of focal motor seizure spreading along the motor strip (later referred to as '*Jacksonian march*'), led to the consolidation of the idea that motor functions can be localised in the frontal lobe [7]. The third line of evidence for an association between frontal lobe and '*higher cognitive functions*' came in 1869 from the American physician, John Martyn Harlow who published the case of Phineas Gage whose remarkable 'Recovery from the Passage of an Iron Bar through the Head' provided the first evidence of the involvement of the frontal lobe in tasks related to emotion and decision making [8] [9,10] [2,11]. The description of the serendipitous case of Phineas Gage was soon followed by the work of Arnold Pick, who reported the case of a 71-year-old man with focal senile atrophy and aphasia [12]. He later refined his anatomical observations and specified that the pathology was characterised by a prominent 'bilateral frontal atrophy'[13]. In recognition of this work, the association between frontal lobe atrophy and dementia was later indicated as Pick disease. Thus, by the end of the 19th century the frontal lobe was conceptualised as a mosaic of

cortical areas specialised for language production, motor execution, emotion and decision making. While the localizationist stances of this view were rather evident, clinicians were also aware of specific disorders affecting more than one frontal function suggesting, at least from a clinical point of view, some degree of overlap. Patients with Pick's disease, for example, had often cognitive problems that extended to the language domain [12]. Those disorders affecting primarily the motor functions, such as Amyotrophic Lateral Sclerosis, were also thought to have an impact on emotion processing and language [14].

The last functional role to be ascribed to the frontal lobe has been the involvement in social cognition and personality. This aspect of the frontal lobe function was already suggested by Dr Harlow report of Phineas Gage's behavioural change after the accident [8]: '*who regarded him as the most efficient and capable foreman ... considered the change in his mind so marked that they could not give him his place again.... He is fitful, irreverent, indulging at times in the grossest profanity (which was not previously his custom), manifesting but little deference for his fellows, impatient of restraint or advice when it conflicts with his desires.... A child in his intellectual capacity and manifestations, he has the animal passions of a strong man....*'. Experimentally, the pioneering work of Leonardo Bianchi, Professor of Neurology and Psychiatry at the University of Naples, supported some of Harlow's clinical observations [15] [16] [17]. Having noted that unilateral ablations of frontal lobe in monkeys and dogs were without effect, he described the changes he observed after bilateral removals. The animals showed no sensory or motor defects but there were '*profound changes in character*'. They no longer showed affection for people whom they used to, and when approached they were likely to be fearful. They were no longer sociable with other monkeys nor did they engage in play. They were impulsive and when frustrated they became violent. Bianchi offered a broad interpretation of these changes. Bilateral prefrontal ablation '*does not so much interfere with the perception taken singly as it does disaggregate the personality'*. The animal was no

longer capable of '*serializing and synthesizing groups of representations'*. Their displays of fear and their agitation were direct consequences of this inability to integrate experiences and of their '*defective sense of personality'*. Bianchi argued that human frontal lobes were particularly dedicated to the elaboration of higher cognitive functions and they have a key role in maintaining normal behaviour and personality rather than '*general intelligence*' [18]. These results brought to the attention of many psychiatrists the frontal lobe impairment as possible cause of mental health disorders.

Common to all studies of frontal lobe pathology was the focus on cortical function and cortical pathology with little mention of the role of its connections. This changed with the emergence of histological and electrophysiological techniques for the study of the brain circuits. The work of James Papez is certainly the most celebrated example of this approach. He formulated the first network model for linking action and perception to emotion that involved part of the frontal lobe [19]. A decade later, Paul Yakovlev, independently from Papez, proposed that the orbitofrontal cortex, insula, amygdala and anterior temporal lobe form a network underlying emotion and motivation [20]. Both Papez and Yakovlev view were then incorporated into a model of the limbic system that remained unchanged since then [21,22]. The above new proposed models converged interest of neurosurgeons as they provided the anatomical rational for possible treatment of mental disorders by causing either cortical ablation (lobectomy) or disconnection (leucotomy) of the frontal lobes. A network approach to frontal lobe functions has been recently revitalized by the advent of functional and diffusion MRI and their application to neuropsychiatric disorders, such as schizophrenia and autism, whose pathology is often elusive.

1.2 Frontal lobe development and aging

Normal human brain development is a complex and protracted process that begins early

in gestation with different maturation stages that are specific to different brain regions. Brain development follows a hierarchical progression with brainstem and cerebellum maturing first, followed by primary sensory and motor cortex and finally associative areas of the frontal and parietal lobes [23].

In humans, frontal regions represent 27% of the brain size and their maturation begins in childhood continuing in the adolescence in parallel with the progress in attention control, cognitive flexibility, processing and executive functions abilities. As a consequence, a damage to frontal regions during their early development can interrupt the frontal lobe maturation and contribute to explain intellectual impairment in children. The frontal lobe development comprehends a prenatal and a postnatal phase. In the prenatal period, at approximately six months' gestation, the cortical neurogenesis is complete and neuroblasts can migrate to their permanent locations leading to differentiation and establishing connections [24].

In typical postnatal development a number of major growth periods can be identified, including (1) major dendritic growth from birth to 3 years' life [25]; (2) peak in myelination from 7 to 9 years [26]; (3) increase in grey matter volume and further myelination from 10 to 12 years [26]; (4) increase in grey matter density and decrease in gray matter volume from adolescence to early adulthood [27-30].

As for the frontal lobe, the development of the executive functions shows a stage-like progression achieving the mastery in most of them by the age of 12 years. Attentional control, cognitive flexibility, goal setting and processing speed are the main four subdomains of the executive functions with a different development trajectory. Attentional control or capacity of self-regulation emerges from the age of 7-12 months and stabilizes between the age of 6 and 7 years [31]. Cognitive flexibility defined as the capacity to learn from mistakes and plan different strategies emerges at the age of 3 years [32]. Goal setting is the ability to

enhance strategies to solve a problem and this matures from middle childhood until the late adolescence. Processing speed develops rapidly between 6 and 12 years of age. Current views demonstrated that in the developing brain the underlying basis of executive functions are more distributed than in the mature brain. As noted above, brain development follows a hierarchical progression with posterior brain region maturation preceding the development of the anterior regions. Thus, in this stage frontal lobe is less likely to be important for efficient executive functions and consequently the integrity of the entire brain appears to be more critical to carry out executive tasks when the brain is not mature.

As the brain ages, there is an increasing probability of losing neurons, synapses and transmitters. The adult human brain contains approximately 20 billion neurons. Unbiased stereological methods showed that between the age of 20 to 90 years the neocortex loses 10% of its neurons, reflecting a great vulnerability to cognitive decline [33]. Moreover, the effects of aging on the brain size are also well documented. The brain usually shows no changes in size until the 40s and 50s and then declines over many decades. Longitudinal studies showed that age-related atrophy is greater in the frontal lobe (0.9%-1.5% per year) than in the posterior brain regions and some evidence suggested that the most pronounced volumetric decline is in the prefrontal cortex with a loss of up to 5% per decade [34-36]. Significant correlations have been reported between age-related executive control deficits and prefrontal cortex atrophy in older adults [37-41]. Moreover, Cardenas et al. [42] found that smaller lateral prefrontal cortex volume predicted executive function decline.

Aging could also lead to different kind of alterations as reduced dendritic length and fewer neocortical synapses. Postmortem studies showed that age-related white matter loss occurs throughout the brain but it is more pronounced in the prefrontal cortex, where atrophy in white matter tends to be more pronounced than atrophy in gray matter [43]. Diffusion tensor imaging (DTI) is a magnetic resonance imaging (MRI) method used to quantify the

microstructural properties of biological tissue [44]. This technique is based on diffusion-weighted MRI, which sensitizes the magnetic resonance signal to the displacement of water molecules within biological tissues (see Chapter 3). The fractional anisotropy (FA) quantifies these changes and it is considered an indirect measure of white matter integrity. Reduced FA is indicative of degraded microstructural tissue integrity [45]. Although age-related FA reductions can be found throughout the brain, they tend to be most pronounced within the prefrontal cortex [46,47]. In addition, these reductions show a global anterior-to-posterior gradient as the FA reductions decreased gradually from anterior to posterior segments of longitudinal fiber tracts [48-51]. The deterioration of white matter tract could contribute to the development of cognitive deficits. For example, Diary et al. found reduced frontal lobe FA to be associated with poorer performance on several measures of frontal functioning, including verbal fluency and working memory in older adults [52]. In another study, Davis et al. found that prefrontal FA was correlated with older adults' performance in executive functions [53].

Overall, consistent with the several lines of evidence discussed above, one of the most influential ideas in cognitive neuroscience of aging is the frontal lobe hypothesis which postulates that cognitive deficits in older adults are primarily due to the anatomical and functional deterioration of the frontal lobes [54].

1.3 Surface anatomy

Dorso-lateral surface

On the dorso-lateral surface, the frontal lobes are separated posteriorly from the parietal lobes by the deep central or Rolandic sulcus and inferiorly from the temporal lobes by the lateral or Sylvian fissure. Four distinct gyri separated by three sulci are visible on the dorsolateral surface. The gyrus running anteriorly and parallel to the central sulcus and posterior to the precentral sulcus is the *precentral* or *ascending frontal gyrus*. Anteriorly to the precentral

sulcus the frontal lobe is divided into the superior, middle and inferior frontal gyri by the superior and inferior frontal sulci. The inferior frontal gyrus lies beneath the inferior frontal sulcus and its posterior part is divided into three regions by the anterior ascending and anterior horizontal limbs of the lateral sulcus. The pars opercularis is behind the anterior ascending limb of the lateral sulcus. The pars triangularis is between the anterior ascending and anterior horizontal limb of the lateral sulcus. The pars orbitalis is beneath the anterior horizontal limb. The superior, middle, and inferior frontal gyri converge anteriorly to form the frontal pole, which is separated from the orbital gyri by the frontomarginal sulcus (Figure 1).

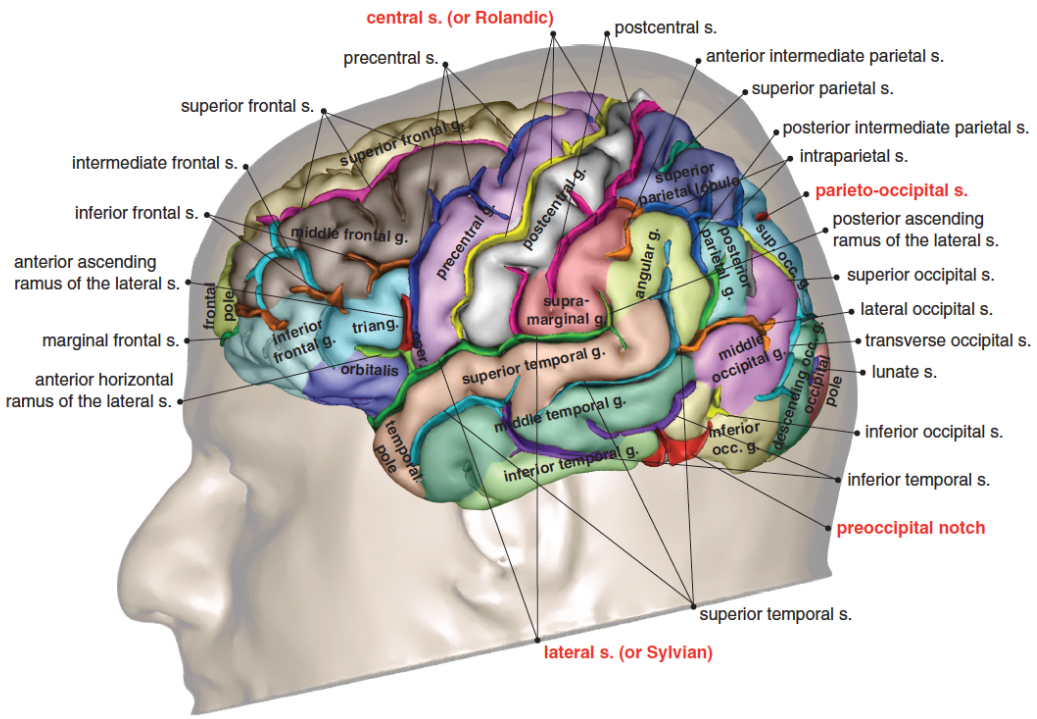

Figure 1. 3D reconstruction of the dorso-lateral surface of the left hemisphere. Interlobar sulci are in red, intralobar sulci in black [45].

Medial surface

On the medial surface the gyri and sulci are concentrically distributed around the mid-sagittal portion of the corpus callosum. The cingulate gyrus surrounds the corpus callosum, running

from the paraterminal gyrus anteriorly to the isthmus posteriorly. Around the cingulate cortex, the medial aspect of the superior frontal gyrus and frontal lobe occupy most of the medial frontal region. On the medial surface, at the level of the paracentral lobule, a vertical line extending from the central sulcus to the cingulate sulcus separates the frontal from the parietal lobe (Figure 2).

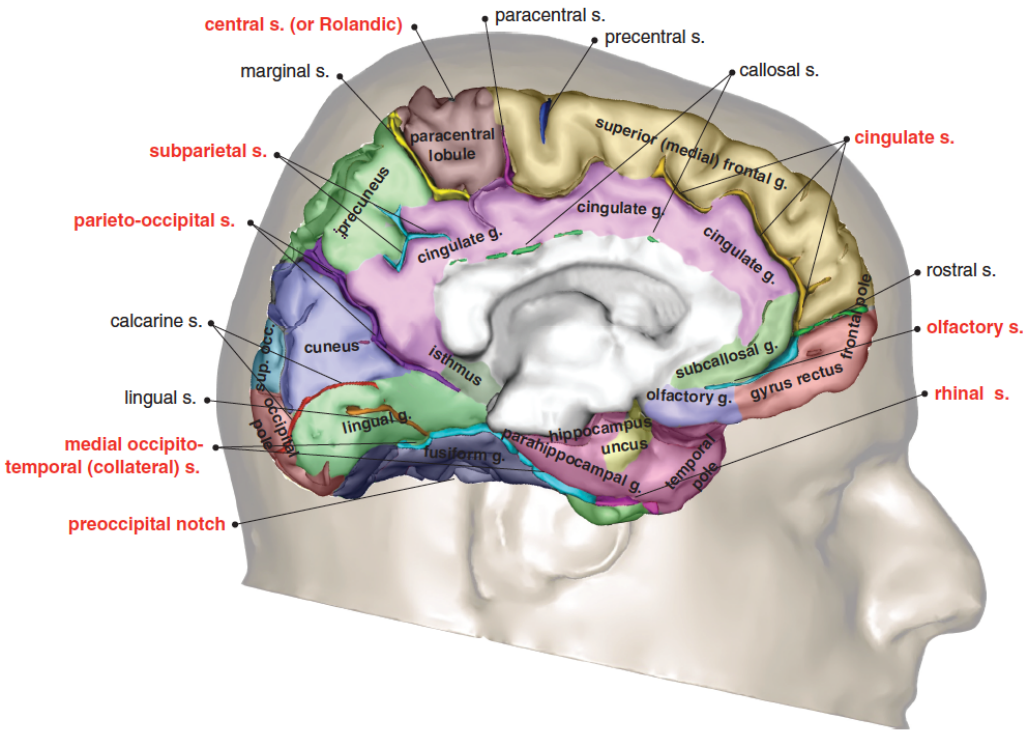

Figure 2. 3D reconstruction of the medial surface of the left hemisphere. Interlobar sulci are in red, intralobar sulci in black [45].

Ventral surface

The frontal orbital gyri, the gyrus rectus and the olfactory gyrus form the ventral aspect of the frontal lobe. In the orbitofrontal region the orbital sulcus is often in the form of a 'H' or 'X', allowing a separation between anterior, posterior, medial and lateral orbital gyri. Medially, the olfactory sulcus separates the medial orbital gyrus from the gyrus rectus and the olfactory gyrus. The gyrus rectus is a longitudinal convolution that demarcates the border between the medial and ventral surface of the frontal lobe. The frontomarginal sulcus separates the orbital

gyri from the polar frontal region (Figure 3).

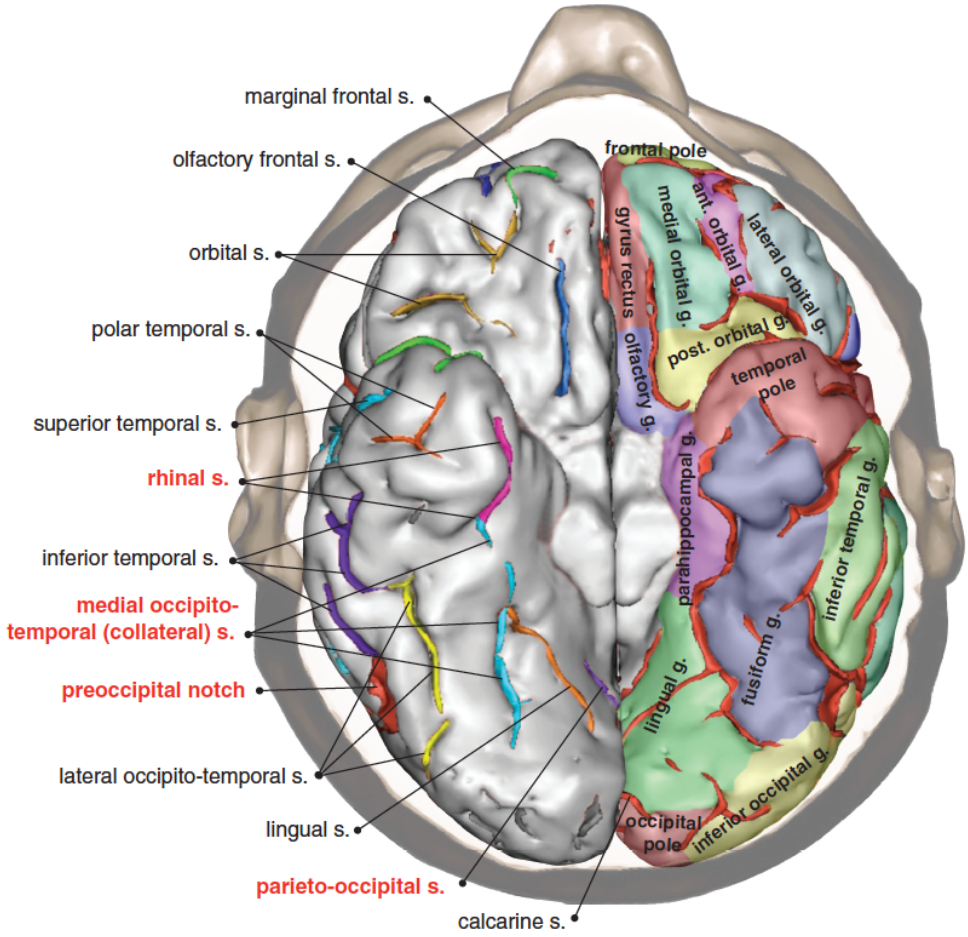

Figure 3. 3D reconstruction of the ventral surface of the left and right hemisphere. Interlobar sulci are in red, intralobar sulci in black [45].

1.4 Sectional anatomy

In the course of the phylogenetic evolution, the frontal lobes undergo a striking expansion and most recently developed its largest structure. The layering pattern of the frontal cerebral cortex changes across the brain and according to this regional variation the frontal lobe can parcellated into ten distinct fields grouped in five main regions [45]:

1. Brodmann's area 4 as primary motor cortex containing the neuronal bodies of the cortico-spinal projection fibres;
2. Brodmann's area 6 as premotor region with the lateral premotor cortex (PMC), medial

supplementary motor area (SMA) and pre-supplementary motor area (pre-SMA);

3. Brodmann's area 44 and 45 as Broca's area;
4. Brodmann's area 8, 9, 10, 46 (dorsolateral) and Brodmann's area 47 (ventrolateral) prefrontal cortex;
5. Brodmann's area 11 and 47 are the main divisions of the orbitofrontal cortex.

Mesulam has suggested a division of the frontal areas into primary, unimodal, heteromodal and supramodal cortical areas according to cytoarchitectonic features (laminar organization, myelin content, granular layer IV, pyramidal cell size, cellular density, etc.) [33]:

1. motor-premotor sector including BA4 and 6, the supplementary motor area, the frontal eye fields, the supplementary eye fields and parts of Broca's area;
2. paralimbic sector containing the cortices of the anterior cingulate complex (BA23, 32), the parolfactory gyrus (gyrus rectus, BA25) and the posterior orbitofrontal regions (BA11-13);
3. heteromodal sector containing BA9-10, anterior BA11-12, and BA45-47.

According to Mesulam, one may refer "prefrontal cortex or frontal lobe syndrome" only to the paralimbic and heteromodal sectors of the frontal lobe. The prefrontal cortex is the transmodal epicentre involved in higher order functions as working memory, executive function, attention, language and comportment.

1.5 Connectional anatomy

Frontal regions have an extensive system of connections that permits communication among frontal lobe regions or between frontal regions and other regions of the parietal, occipital and temporal lobes. Frontal lobe connections that remain with the frontal lobe constitute the *local connectivity* whereas connections between frontal regions of the two

hemispheres or between frontal and distant non-frontal regions of the same hemisphere are part of the *extended frontal network.* This *extended frontal network* includes association, projection and commissural tracts.

Local frontal lobe networks

The local connectivity is composed by three groups of connections strictly confined within the frontal lobe: *intracortical fibres, U-shaped fibres, and intralobar fibres*. The *intracortical fibres* are short connections with an average length below 1 mm running within the frontal cortex having either inhibitory or excitatory functions. They are organized in horizontal and vertical stains and most of them are unmyelinated or poorly myelinated [55]. The *U-shaped fibres* are longer, usually between 2 and 5 cm of length, discrete myelinated bundles connecting regions with different but integrated functions. As they leave the deepest cortical layers of the frontal cortex, these U-shaped bundles keep a perpendicular direction to the main sulci of the frontal lobe terminating in layers I, II and III of the target region [56].

Several major frontal U-shaped connections have been described:

- U-shaped bundles running beneath the central sulcus connecting the primary motor cortex in the precentral gyrus to the primary somatosensory cortex in the post-central gyrus having a close correspondence with the homuncular representation. This pattern is larger in the hand region compared to the mouth and tongue region, and this could suggest that they may play a key role in their precision grasping and articulatory movements [56].
- U-shaped fibres connecting the motor cortex in the precentral gyrus to premotor regions of the superior, middle and inferior frontal gyri. This pattern connects areas involved in motor planning and execution [56,57].

- U-shaped fibres of the region anterior to the precentral sulcus. One pattern connects Broca's region in the inferior frontal gyrus and the frontal eye field in the superior frontal gyrus to the middle frontal gyrus. Another set of U-shaped longitudinal fibres connect cortex in the superior and inferior frontal gyri to the cortex in the middle frontal gyrus [58,59].
- U-shaped fibres of the frontal pole connecting medial to lateral polar regions of area 10, which is involved episodic memory retrieval, monitor self-generated choices, allocating attention between simultaneous tasks and prospectively coding and deferring goals in multitasking [60-62].
- U-shaped fibres organized around the *peri-insular sulcus* connecting the inferior frontal cortex to the anterior insula of Reil. This system of insular connections to frontal regions may play a key role in integrating visceral and sensory information with limbic emotional inputs [45,63,64].

The *intralobar frontal fibres* are the longest associative tracts connecting distant specialized regions of the frontal lobes that cooperate to generate complex behaviour. The major intralobar tracts of the frontal lobe include the frontal aslant tract, the frontal orbito-polar tract and the frontal superior and frontal inferior longitudinal tracts. The *frontal aslant tract (FAT)* connects the posterior Broca's territory with medial frontal areas, including pre-supplementary motor area and cingulate cortex, which are involved in speech initiation and spontaneous verbal fluency [56,65,66]. This suggests a role of the frontal aslant tract in language as documented in patients with primary progressive aphasia [67]. The *frontal orbito-polar (FOP) tract* connects the posterior orbitofrontal cortex involved in integration of emotions and memories associated with olfactory and gustatory experiences and the anterior orbitofrontal and polar regions, which convey direct auditory and visual inputs. It is possible

that this network assembles memories and emotions associated with specific sensory inputs [63,68].

Finally, the *frontal superior longitudinal* (FSL) and *frontal inferior longitudinal* (FIL) *tracts* are two systems of fibres that connect motor, premotor and prefrontal regions and their function is to integrate the functions of all local frontal networks [56].

Extended frontal networks

The frontal lobe extended network is composed by *association, projection and commissural tracts* with the aim to connect frontal regions to distant regions of the same hemisphere and to frontal regions in the contralateral hemisphere [69].

Association tracts

The long *association tracts* connect the frontal lobe to other lobes within the same hemisphere. Five major association tracts have been described in the frontal lobe: the arcuate fasciculus, the superior longitudinal fasciculus, the cingulum, the inferior fronto-occipital fasciculus and the uncinate fasciculus.

The *arcuate fasciculus* is a dorsal association tract connecting perisylvian regions of the frontal, parietal and temporal lobe (Figure 4). The arcuate fasciculus is composed by three segments with one direct pathway or long segment connecting Wernicke's region in the temporal region with Broca's region in the frontal lobe and one indirect pathway consisting of an anterior segment that link Broca's to Geschwind's region in the parietal lobe and a posterior segment between Geschwind's and Wernicke's region[70]. The distribution of the arcuate fasciculus between Broca's and Wernicke's regions suggest its role in word learning and its absence in monkey brains may explain evolutionary differences between species. Monkey have, in fact, very poor auditory memory while humans have an exceptional ability

to learn a rich vocabulary in adult life [71]. Tractography studies have revealed an extreme degree of leftward lateralization of the long segment of the arcuate fasciculus in approximately 60% of the normal population [72].

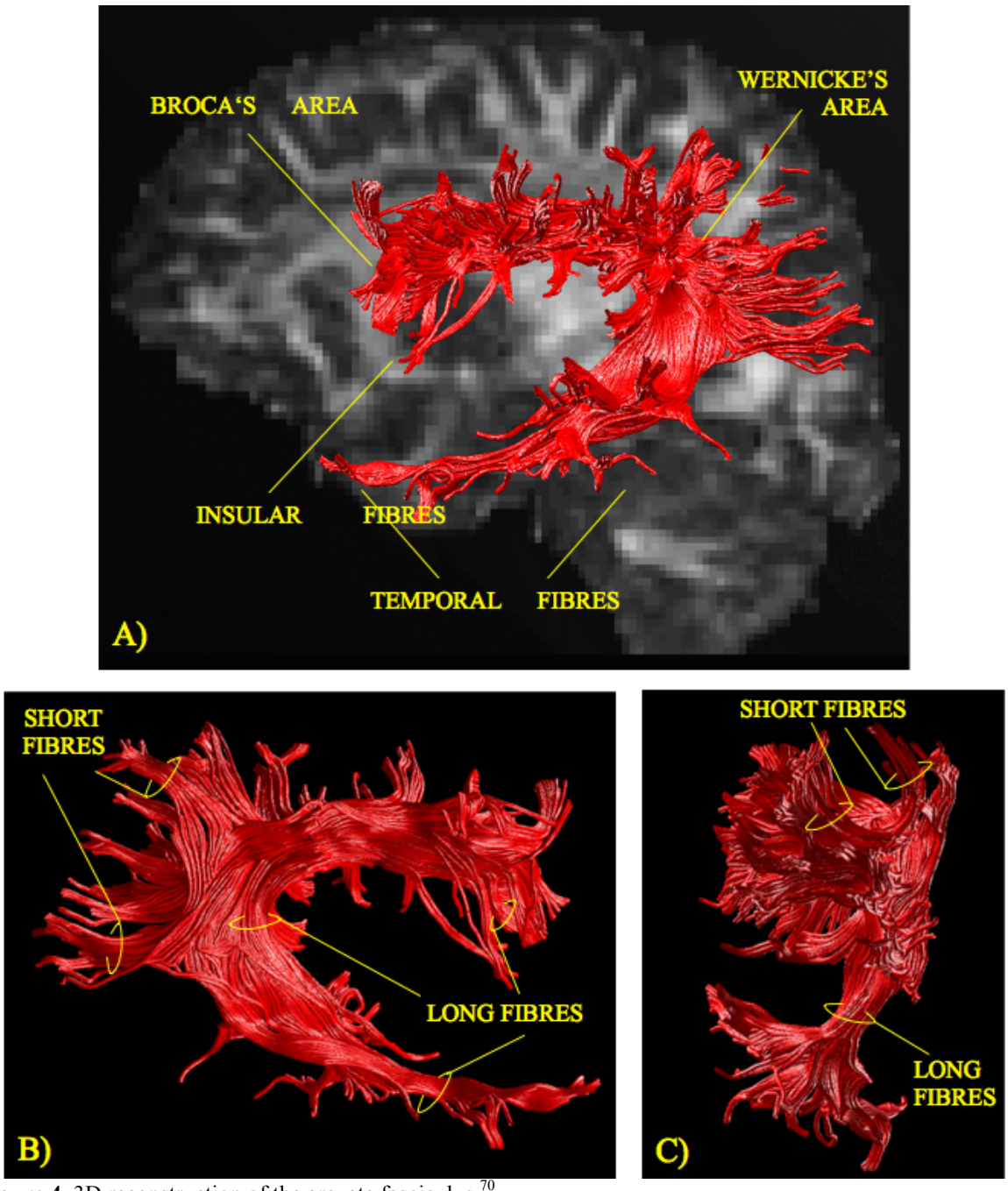

Figure 4. 3D reconstruction of the arcuate fasciculus [70].

The *superior longitudinal fasciculus (SLF)* has been defined as a group of three longitudinal separate branches connecting the dorsolateral frontal and parietal regions. The first branch of

the superior longitudinal fasciculus (SLF I) projects to the parietal precuneus and the supplementary motor area at the medial and superior surface of the superior frontal gyrus [45]. The SLF I is involved in processing of the spatial coordinates of trunk and inferior limbs, preparatory stages of movement planning, in oculomotor coordination, visual reaching, and voluntary orientation of attention [73-77]. The second component of the superior longitudinal fasciculus (SLF II) projects to the posterior region of the inferior parietal lobule (including the intraparietal sulcus) and the lateral aspect of the superior (i.e. frontal eye field) and middle frontal gyri. The main role of SLF II is processing the spatial coordinates of the upper limbs, including the hand for reaching and grasping movements and in attention, visuospatial and spatial working memory tasks [78-80]. Finally, the third branch is the SLF III which projects to the inferior parietal lobule (supramarginal and anterior angular gyrus) and the posterior region of the inferior frontal gyrus.

The *uncinate fasciculus* is a ventral tract that connects the anterior temporal lobe with the medial and lateral orbitofrontal cortex (Figure 5). This fasciculus is involved in naming and face processing and it is damaged in those patients with the semantic variant of primary progressive aphasia [67,80]. Moreover, damage to this tract has been correlated with behavioural abnormalities in psychopaths as well as frontotemporal dementia and traumatic brain injury [81-83].

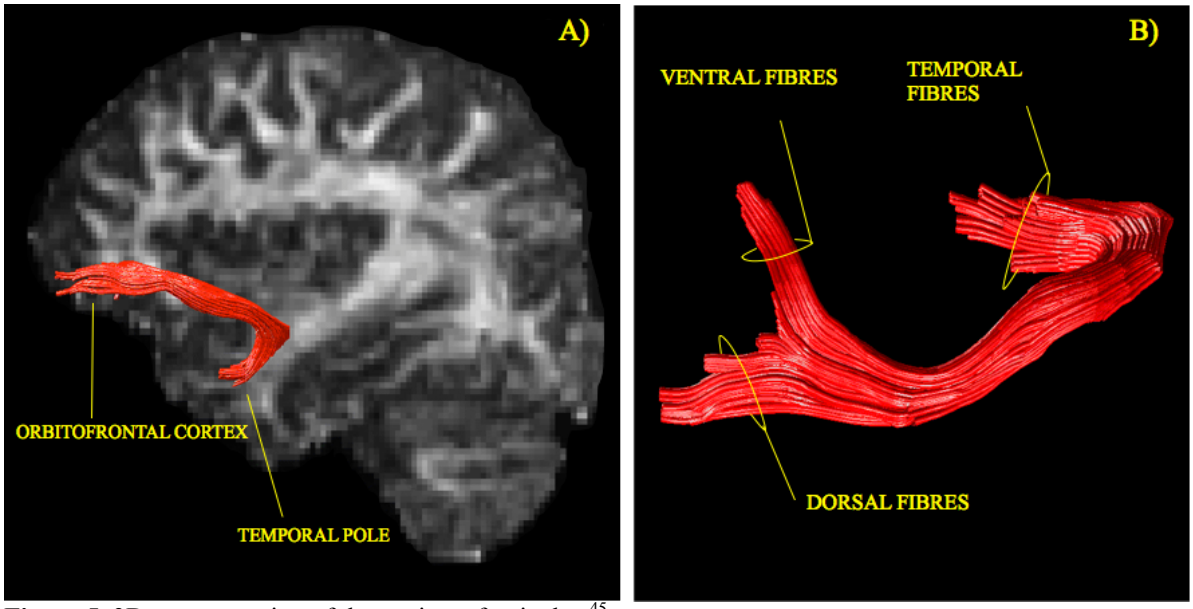

Figure 5. 3D reconstruction of the uncinate fasciculus [45].

The *cingulum* is a medial tract that runs within the cingulate gyrus around the corpus callosum (Figure 6). It contains fibres of different length, the longest of which run from the anterior temporal lobe to the orbitofrontal cortex. The short U-shaped fibres connect the medial regions of the frontal (subgenual cortex, medial frontal gyrus), parietal (precuneus), occipital (cuneus, lingual, and fusiform gyri) and temporal lobes (i.e. parahippocampal gyrus, amydgala, etc.). As part of the limbic system it is involved in attention, memory and emotion [84,85].

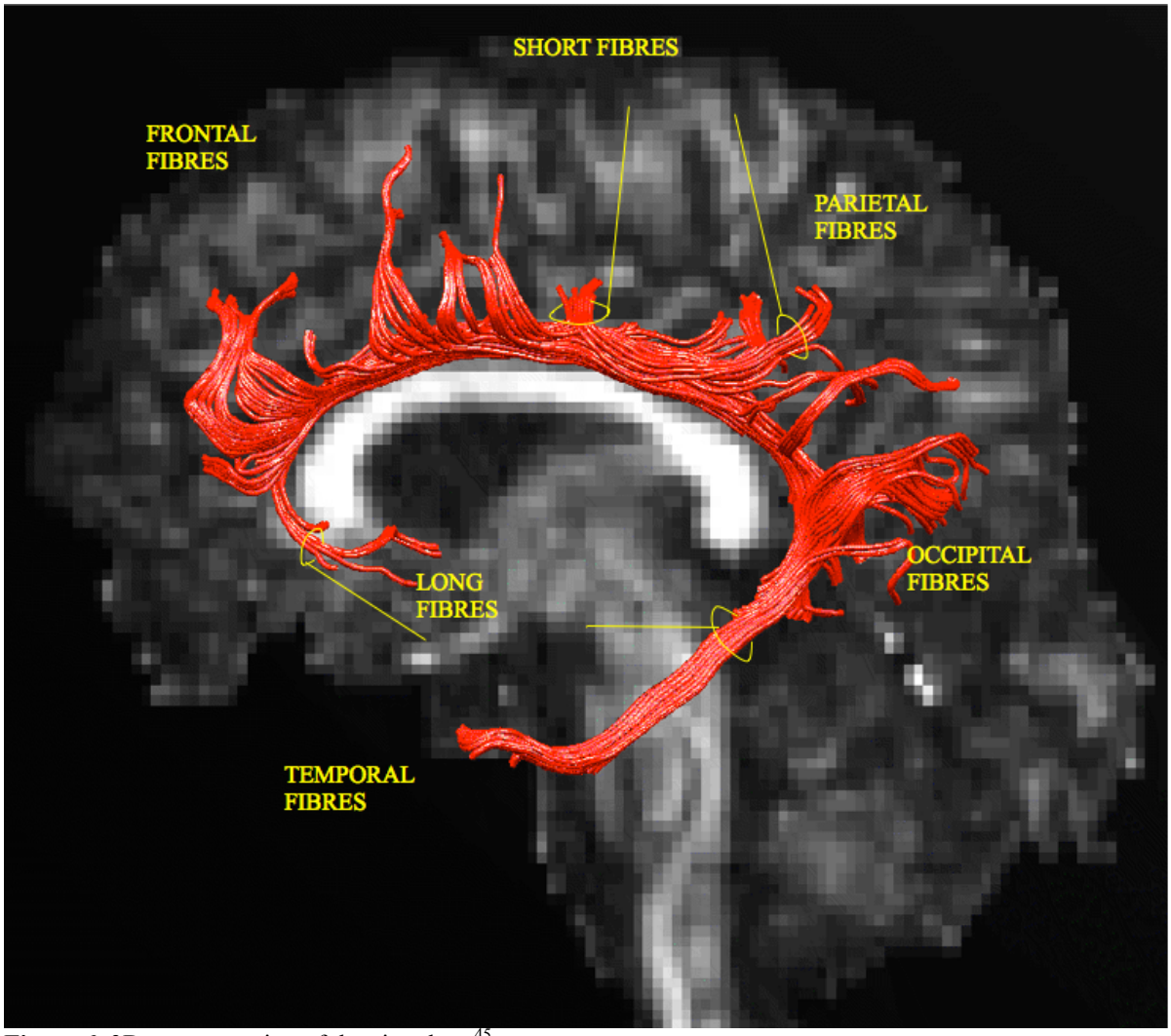

Figure 6. 3D reconstruction of the cingulum [45].

The *inferior fronto-occipital fasciculus* is a ventral tract with long and short fibres connecting the occipital and frontal cortex in the human brain. The functions of the inferior fronto-occipital fasciculus in mental rotation, space-directed attention, reading, and semantic processing remains to be clarified.

Projection tracts.

The projection pathways connecting the frontal cortex to subcortical structures and can be divided into ascending and descending pathways. The ascending projections are the *ascending thalamic pathways* carrying modulatory information from the basal ganglia and cerebellum to all areas of the frontal lobes. The three principal descending cortico-subcortical

projection systems are the *corticospinal*, *corticobulbar tracts* and the *fronto-striatal projections* to the caudate, globus pallidus and medial putamen. This complex projection system contributes to motor, cognitive, affective and behavioural functions.

Commissural pathways.

The commissural pathway connects frontal regions to their contralateral counterparts. The two major commissural tracts of the cerebral hemispheres are the *corpus callosum* and the *anterior commissure*. The corpus callosum, divided into an anterior portion (genu), a central part (body) and a posterior portion (splenium), is the largest tract of the human brain. Its function is to allow transferring input from one hemisphere to the other and it is involved in several motor, perceptual and cognitive functions. The anterior commissure connects bilaterally the anterior and ventral temporal lobes of the two hemispheres and the olfactory bulbs.

1.6 Frontal lobe functional subdivisions and frontal lobe syndromes

The frontal lobes have been subdivided into precentral, premotor and prefrontal regions according to combined anatomical and functional criteria.

The *precentral area* corresponds to the primary motor cortex (BA 4), which is located in the posterior part of the precentral gyrus. It contains somatotopically organized neuron bodies giving origin to almost 50% of the fibres of the cortico-spinal tract. The primary motor cortex is the only idiotypic cortex in the frontal lobe. Giant pyramidal neurons (Betz cells) in layer V, which project to the spinal cord, are a prominent feature. A well-developed inner granular layer (IV) characteristic of primary sensory idiotypic (koniocortical) areas is absent in BA 4, leading to its designation as agranular cortex. Lesions to the primary motor cortex and its connections manifest with moderate (hemiparesis) or severe (hemiplegia) contralateral motor

deficits of the limbs or face.

The *premotor area,* the *supplementary motor area* and the *pre-supplementary motor area* are responsible for the integrated and preparatory arousal to action and action generation. Depending on the exact location of the lesion, damage to these regions of the frontal lobe results in movement uncoordination, ideomotor apraxia and impaired organization of motor behaviour, especially if damage is in the premotor area. Conversely, symptoms like akinetic mutism, apraxia of the speech, agraphia and initiation and programming deficits are more often associated with damage to the supplementary and presupplementary motor areas.

Close to the premotor division, there is the left frontal operculum as Brodmann area 44 and 45 or Broca's area. According to Luria, here "the final common path for the generation of speech impulses" is placed. As a consequence, lesions to this area result in a breakdown in speech production and defective symbol formulation as Broca's aphasia. In keeping with Broca's area, lesions to Broca's area homologous in the right hemisphere are associated with aprosodic speech, characterized by flat intonation.

The prefrontal cortex is placed in front of the premotor cortex and it is generally considered as convergence zone between information about the external environment from the posterior cortex and information about internal states from the limbic systems. The prefrontal portion of the frontal lobes can be further subdivided in the ventromedial prefrontal cortex (vmPFC), dorsolateral prefrontal cortex (dlPFC) and superior medial prefrontal cortex.

The *ventromedial prefrontal cortex (vmPFC)* includes the medial part of the orbital region and lower part of the medial prefrontal cortex. This area plays a key role in impulse control and in regulation and maintenance of set during ongoing behaviour. The principal behavioural product of vmPFC dysfunction is impulsivity, disinhibition, aggressivity, sexual promiscuity and problems with social conduct. Cognitive impairment is manifested by defects in planning, judgment and decision making.

The *dorsolateral prefrontal cortex (dlPFC)* encompasses Brodmann areas 8, 9, 46 and 10. Most of its major functions are seen as part of the executive functions such as organizing a volitional response to environmental contingencies, recalling past events and planning current actions in a temporally informed manner, programming motor acts to follow volitional command, implementing programs to achieve the intended goal, monitoring the results of the action to determine the success of the intervention, and adjusting or stopping the action depending on the outcome of the assessment. Patients with frontal frontal lobe disorders many manifest a diverse array of clinical phenomena with only a minority showing abnormalities in all executive function domains depending on the extension of the lesion, the nature of the lesion and the premorbid level of intellectual functioning.

The *superior medial prefrontal cortex (mPFC)* comprises the medial wall of the hemispheres above the vmPFC sector including the anterior cingulate cortex. This region is linked to and shared many functions with the anterior cingulate cortex, which plays a role in motivated behaviour. Damage to these regions often manifest with amotivational apathetic syndromes. Furthermore, the following apathetic syndrome could have different components: motoric with lower motor drive, cognitive with diminished interest in learning, affective as lack of external emotional expression, and motivational as poor interest in initiating and maintaining social and vocational activities.

1.7 The present thesis

The aim of my thesis is to investigate the anatomy of the frontal networks underlying cognitive and behavioural functions. For this purpose, three different sample of patients with frontal lobe pathology were used:

1. A dataset of patients with Motor Neuron Disease (MND) and healthy controls was used to understand the effects of a degenerative process affecting extra motor regions of the frontal lobe in cognition and behaviour;
2. a dataset of patients with Primary Progressive Aphasia (PPA) and healthy controls was analyzed to investigate the role of the ventral fronto-temporal network in behaviour;
3. a dataset of patients with Autism Spectrum Disorders (ASD) and healthy controls was used to assess the anatomy of prefrontal lobe areas and pathways involved in communication and social cognition.

Chapter 2 Disorders of the Frontal lobe

The frontal cortex represents 30% of the entire cortical surface. There are many neurological and psychiatric disorders that affect the frontal lobe either directly or through a disconnection mechanism. This chapter will cover the most common neurological conditions affecting the frontal lobe with the aim to explore the link between structure abnormalities, altered function and clinical symptoms.

The first part of this chapter will be dedicated to the Fronto-Temporal lobar degeneration and its main syndromes: primary progressive aphasia and behavioural variant subtypes. Fronto-Temporal lobar degeneration is an example of a disease in which more anterior frontal cortex is affected and therefore it has been used as a model for investigating non-motor frontal function. Then a paragraph will be dedicated to the Motor Neuron Disease which manifests with motor weakness associated with specific degeneration of the primary motor cortex and surrounding areas. This chapter terminates with a paragraph on the Autism Spectrum Disorder which is a neurodevelopmental condition whose core symptoms are represented by deficits in language and social communication, impaired social interactions and repetitive behaviour. Both neuropathological and neuroimaging studies indicate frontal lobe involvement in this condition.

2.1 Frontotemporal Lobar Degeneration (FTLD)

Frontotemporal Lobar Degeneration (FTLD) is a degenerative disorder of insidious onset and slow progression, accounting for approximately 20% of all dementias. Frontotemporal Lobar Degeneration typically involves the frontal and temporal lobes with relative sparing of the posterior brain. Here the primary progressive aphasia and behavioural variant subtypes will be described.

2.1.1 Primary progressive aphasia

Introduction

Primary Progressive Aphasia (PPA) is characterized by a gradual breakdown of language functions for at least two years since the onset of symptoms with relatively sparing of other cognitive domains [86].

In the 1890s, Pick [12] [13] and Serieux [87] first described a progressive disorder of language associated with atrophy of the frontal and temporal regions of the left hemisphere and even introduced the concept of a degenerative disease beginning focally: *"Simple progressive brain atrophy can lead to symptoms of local disturbance through local accentuation of the diffuse process"*.

In the modern literature, Mesulam was the first to describe a series of cases with "*slowly progressive aphasia,*" thereafter reported under the label of "primary progressive aphasia" (PPA)[88]. In the original cases reported by Mesulam, the aphasia was predominantly nonfluent, resembling Broca's aphasia, with halting speech and reduced naming, but preserved comprehension. In the early 1990s, Hodges and colleagues provided a comprehensive characterization of semantic dementia [89]. For about two decades, cases of PPA were generally categorized as semantic dementia or progressive nonfluent aphasia, or in some studies as "fluent" vs "non fluent."

Diagnosis and classification of Primary Progressive Aphasia

Establishing a clinical diagnosis of PPA involves a 2-step process. Firstly, patients should have developed a gradual isolated language impairment of neurodegenerative nature as stated in the basic PPA inclusion and exclusion criteria which are based on Mesulam's initial observations and current guidelines. According to these inclusion criteria the most prominent clinical features are difficulties with language, which cause impairment in the activities in the daily living for at least 2 years since the onset of the disease (Table 1) [86].

Table 1. Inclusion and exclusion criteria for the diagnosis of PPA [86].

Inclusion criteria 1-3 must be answered positively for PPA diagnosis	**Exclusion criteria 1-4 must be answered negatively for PPA diagnosis**
1. Most prominent clinical features is difficulty with language	1. Pattern of deficit is better accounted for by other nondegenerative nervous system or medical disorders
2. These deficits are the principal cause of impaired daily living activities	2. Cognitive disturbances is better accounted for by a psychiatric diagnosis
3. Aphasia should the most prominent deficits at symptoms onset and for the initial phases of the disease	3. Prominent initial episodic memory, visual memory and visuoperceptual impairments
	4. Prominent, initial behavioural disturbance

Once a PPA diagnosis is established, the patient is classified according to the three main variants described in the 2011 guidelines [90]:

(i) agrammatic variant PPA (PPA-G)

(ii) logopenic variant PPA (PPA-L)

(iii) semantic variant PPA (PPA-S)

A brief clinical evaluation with 20-minute bedside language examination is considered sufficient to assess the language domains as speech production, repetition, single word and syntax comprehension, confrontation naming, semantic knowledge and reading.

Clinical criteria for each variant are reported in Tables 2,3,4.

The agrammatic variant

The PPA-G is defined as an expressive language disorder with non fluent spontaneous speech, disrupted sentence production, abnormal word order and phonemic paraphasias. Patients use effortful and broken speech with fewer number of words and phrases. However, they can have successful communicate intent. In PPA-G comprehension for simple sentences and single words is relatively preserved but not for non-canonical and grammatically complex sentences as grammar structure encoding and decoding are both affected [91,92]. As the disease advances, patients with PPA-G becomes gradually less fluent with progressive decline in naming, comprehension and repetition. Ultimately patients become mute. The anatomical correlate of these findings is the peak atrophy within the dominant left inferior frontal gyrus in the Broca's area. Atrophy in patients with PPA-G can also extend into the medial and dorsolateral premotor cortex and anterior insula, brain regions that participate in speech initiation, motor planning and syntax processing [93]. Based on the literature as for the other variants, there is no clinical pattern that is pathognomonic of a specific type of neuropathology. The agrammatic form mainly shows various forms of FTLD-tau pathology and less often FTLD-TDP type [90] (Table 2).

Table 2. Diagnostic features for the agrammatic variant of PPA [90].

1. Clinical diagnosis of agrammatic variant PPA
At least one of the following core features must be present: 1. Agrammatism in language production 2. Effortful, halting speech with inconsistent speech sound errors and distortions (apraxia of speech)
At least 2 of 3 of the following other features must be present: 1. Impaired comprehension of syntactically complex sentences 2. Spared single-word comprehension 3. Spared object knowledge
2. Imaging-supported nonfluent/agrammatic variant diagnosis
Both of the following criteria must be present: 1. Clinical diagnosis of nonfluent/agrammatic variant PPA 2. Imaging must show one or more of the following results: a. Predominant left posterior fronto-insular atrophy on MRI or b. Predominant left posterior fronto-insular hypoperfusion or hypometabolism on SPECT or PET
3. Nonfluent/agrammatic variant PPA with definite pathology
Clinical diagnosis (criterion 1 below) and either criterion 2 or 3 must be present: 1. Clinical diagnosis of nonfluent/agrammatic variant PPA 2. Histopathologic evidence of a specific neurodegenerative pathology (e.g., FTLD-tau, FTLDTDP, AD, other) 3. Presence of a known pathogenic mutation

The logopenic variant

PPA-L is the most recently described variant of PPA. Word retrieval (in spontaneous speech and confrontation naming) and sentence repetition deficits are the core features of the this variant [91]. Spontaneous speech is characterized by slow rate, with frequent pauses due to significant word-finding problems. Lack of frank agrammatic errors and preservation of articulation and prosody help distinguish the logopenic from the nonfluent variant [94]. The pattern of atrophy involves the left posterior superior temporal, inferior parietal, medial temporal, and posterior cingulate regions; more severe cases have also left frontal and right hemisphere atrophy [91 95]. The most common pathology in PPA-L is represented by the

Alzheimer disease (AD) pathology with atypical regional distribution. PPA patients with AD pathology display hemispheric asymmetry with neuronal loss and disease-specific proteinopathy in the language dominant hemisphere. In addition, neurodegeneration is most extensive in the neocortex [90] (Table 3).

Table 3. Diagnostic features for the logopenic variant of PPA [90].

1. Clinical diagnosis of logopenic variant PPA
Both of the following core features must be present: 1. Impaired single-word retrieval in spontaneous speech and naming 2. Impaired repetition of sentences and phrases
At least 3 of the following other features must be present: 1. Speech (phonologic) errors in spontaneous speech and naming 2. Spared single-word comprehension and object knowledge 3. Spared motor speech 4. Absence of frank agrammatism
2. Imaging-supported logopenic variant diagnosis
Both criteria must be present: 1. Clinical diagnosis of logopenic variant PPA 2. Imaging must show at least one of the following results: a. Predominant left posterior perisylvian or parietal atrophy on MRI b. Predominant left posterior perisylvian or parietal hypoperfusion or hypometabolism on SPECT or PET
3. Logopenic variant PPA with definite pathology
Clinical diagnosis (criterion 1 below) and either criterion 2 or 3 must be present: 1. Clinical diagnosis of logopenic variant PPA 2. Histopathologic evidence of a specific neurodegenerative pathology (e.g. AD, FTLD-tau, FTLD-TDP, other) 3. Presence of a known pathogenic mutation

The semantic variant

The main features of PPA-S are represented by an impairment in word meaning and object identity on a background of preserved grammatical structure and fluency. In PPA-S patients the language output is grammatically correct but at the same time is empty because of loss of knowledge surrounding the words and their meanings [90]. This variant is considered not

simply a language deficit but represents a fundamental loss of semantic memory and knowledge: long-memories that contain knowledge about items in the world, as well as an understanding of their relationship.

Figure 7. 63-year old man with Semantic Dementia. MRI showed striking temporal lobe volume loss with relatively well-preserved frontal gyri [108].

As the knowledge surrounding a word is lost, patients with semantic dementia use general rather than precise terms to describe objects, facts, people, or faces [96,97]. Anatomically, the semantic variant has been associated with atrophy in the ventral and lateral portions of the

anterior temporal lobes bilaterally, although damage is usually greater on the left [98] [95](Figure 7). The most common pathological feature of PPA-S is the FTLD-TDP type [90](Table 4).

Table 4. Diagnostic features for the semantic variant of PPA [90].

1. Clinical diagnosis of semantic variant PPA
Both of the following core features must be present: 1. Impaired confrontation naming 2. Impaired single-word comprehension
At least 3 of the following other diagnostic features must be present: 1. Impaired object knowledge, particularly for low frequency or low-familiarity items 2. Surface dyslexia or dysgraphia 3. Spared repetition 4. Spared speech production (grammar and motor speech)
2. Imaging-supported semantic variant diagnosis
Both of the following criteria must be present: 1. Clinical diagnosis of semantic variant PPA 2. Imaging must show one or more of the following results: a. Predominant anterior temporal lobe atrophy b. Predominant anterior temporal hypoperfusion or hypometabolism on SPECT or PET
3. Semantic variant PPA with definite pathology
Clinical diagnosis (criterion 1 below) and either criterion 2 or 3 must be present: 1. Clinical diagnosis of semantic variant PPA 2. Histopathologic evidence of a specific neurodegenerative pathology (e.g., FTLD-tau, FTLDTDP, AD, other) 3. Presence of a known pathogenic mutation

2.1.2 Frontotemporal dementia behavioural variant

Introduction

The behavioural variant of the frontotemporal dementia (bvFTD) is a clinical syndrome characterized by a profound change in social behaviour and personality that can occur several years before the diagnosis [99]. The syndrome derives from the extensive degeneration in the dorsolateral, orbital and medial frontal cortex associated with different pathologies [100]. In view of the absence of definitive biomarkers, the diagnosis of behavioural variant of the frontotemporal dementia is challenging as patients are often misdiagnosed with psychiatric

disorders or Alzheimer's disease. In 1998 the publication of consensus criteria by Neary and colleagues represented a major step forward in the field and these remain the most widely used criteria in research and clinical practice [101](Table 5).

Diagnosis and classification of behavioural variant of frontotemporal dementia

According to Neary criteria the core features of behavioural variant of frontotemporal dementia are early decline in social and personal conduct, emotional blunting and loss of insight [101]. At the beginning patients develop personality changes, such as jocularity, social disinhibition, poor judgment, irritability or affective flattening that made patients with behavioural variant of frontotemporal dementia easily confused with those with Alzheimer's disease. Nevertheless, their relatively intact cognition often helps to differentiate them from patients affected by other dementias. As the disease progresses they are likely to show perseveration, confabulations, concrete thinking and poor organization compared with behavioural variant of frontotemporal dementia. One of the first manifestation of behavioural variant of frontotemporal dementia is indeed a progressive loss of executive functions, which is often mistaken as age-related cognitive decline. This may lead to impaired planning, problem solving, abstracting and multitasking. As a consequence, these patients would perform very poorly at work and would be more prone to work at progressively simpler occupations and then get fired. Loss of decision making with consequently remarkable financial loss would be also a common presentation.

The degeneration associated with behavioural variant of frontotemporal dementia affects the insular cortex and the anterior temporal lobe [102]. The behaviour variant is usually associated with tau-negative pathology [103] [104]. As the disease progresses patients may show progressive apathy, blunted affect. In the later stage patients may develop language and motor impairment [105] [106].

Table 5. The core criteria for behavioural variant of frontotemporal dementia according to Neary criteria.

1. Core diagnostic features
A. Insidious onset and gradual progression B. Early decline in social interpersonal conduct C. Early impairment in regulation of personal conduct D. Early emotional blunting E. Early loss of insight
2. Supportive diagnostic features
A. Behavioural disorder 1. Decline in personal hygiene and grooming 2. Mental rigidity and inflexibility 3. Distractibility and impersistence 4. Hyperorality and dietary changes 5. Perseverative and stereotyped behaviour 6. Utilization behaviour
B. Speech and language 1. Altered speech output a. Aspontaneity and economy of speech b. Press of speech 2. Stereotypy of speech 3. Echolalia 4. Perseveration 5. Mutism
C. Physical signs 1. Primitive reflexes 2. Incontinence 3. Akinesia, rigidity, and tremor 4. Low and labile blood pressure
D. Investigations 1. Neuropsychology: significant impairment on frontal lobe tests in the absence of severe amnesia, aphasia, or perceptuospatial disorder 2. Electroencephalography: normal on conventional EEG despite clinically evident dementia 3. Brain imaging (structural and/or functional): predominant frontal and/or anterior temporal abnormality

2.2 Motor Neuron Disease

Introduction

At the end of the 19th century Jean-Martin Charcot (1825-1893) described for the first time a neurodegenerative disease characterized by spasticity, bulbar and motor impairment that he named Amyotrophic Lateral Sclerosis (ALS)[107]. Charcot in collaboration with Joffroy investigated the correlations between the clinical and the neuropathological aspects of the disease [108]. In 1881 at the New Sydenham Society in London, Charcot provided his most

famous comprehensive description of disease progression from the onset to the final stages. Charcot's first stage was characterized by upper limbs paresis, muscle atrophy and contractions. In the second step both upper and lower limbs are weak and the patient is no longer able to walk or to stand. Finally, the third stage has a typical bulbar involvement. This initial description made by Charcot has been recently replaced by a more modern disease staging system proposed by Roche et al. [109](Table 6). The new staging of the disease has the advantage that is based on simply clinical milestones, which tend to occur at predictable times within the natural disease progression of ALS. Moreover, this staging can be used to easily assess patient's needs of health care diagnostic services, intervention, end of life palliation and care.

Nowadays it is well recognized that ALS is the most common subtype of Motor Neuron Diseases (MNDs). This is a general umbrella term widely adopted in United Kingdom, under which different forms are classified according to whether they are inherited or sporadic, and to whether degeneration affects upper motor neurons, lower motor neurons, or both. For example, while ALS affects both upper and lower motor neurons primary lateral sclerosis is a disease of the upper motor neurons with progressive muscular atrophy affecting only lower motor neurons in the spinal cord. In progressive bulbar palsy, the lowest motor neurons of the brain stem are most affected, causing slurred speech and difficulty chewing and swallowing.

In this thesis ALS is considered synonymous with Motor Neuron Disease (MND) and the latter will be used throughout.

Table 6. ALS staging system proposed by Roche et al. [109].

Stage	Symptoms
Stage 1	Symptom onset with involvement of the first region
Stage 2A	Diagnosis
Stage 2B	Involvement of a second region
Stage 3	Involvement of a third region
Stage 4A	Need for gastrostomy
Stage 4B	Need for respiratory support (non-invasive ventilation)

Diagnosis and classification of Motor Neuron Disease

MND is a neurodegenerative disorder compromising the motor neurons and with progressive muscle weakness. Symptoms are usually noticed first in the arms and hands, legs, or swallowing muscles. Approximately 75% of people with classic MND will develop weakness and wasting of the bulbar muscles (muscles that control speech, swallowing, and chewing) [110-112]. Muscle weakness and atrophy occur on both sides of the body. Affected individuals lose strength and the ability to move their arms and legs, and to hold the body upright. Other symptoms include spasticity, spasms, muscle cramps, and fasciculations. Speech can become slurred or nasal. When muscles of the diaphragm and chest wall fail to function properly, individuals lose the ability to breathe without mechanical support. Although the disease does not usually impair a person's mind or personality, several recent studies suggest that some people with MND may develop cognitive problems involving word fluency, decision-making, and memory [113]. The MRI findings may include in a small percentage hyperintensity on the corticospinal tract on the T2-weighted and FLAIR sequences. The hyperintensity can occur anywhere from the subcortical white matter to the cerebral peduncles and pons. Changes are usually most prominent in the posterior limbs of the internal capsules and cerebral peduncles. As the corticospinal tract is normally slightly

hyperintense, this finding lacks both sensitivity and specificity as an imaging 'biomarker' for MND [114](Figure 8).

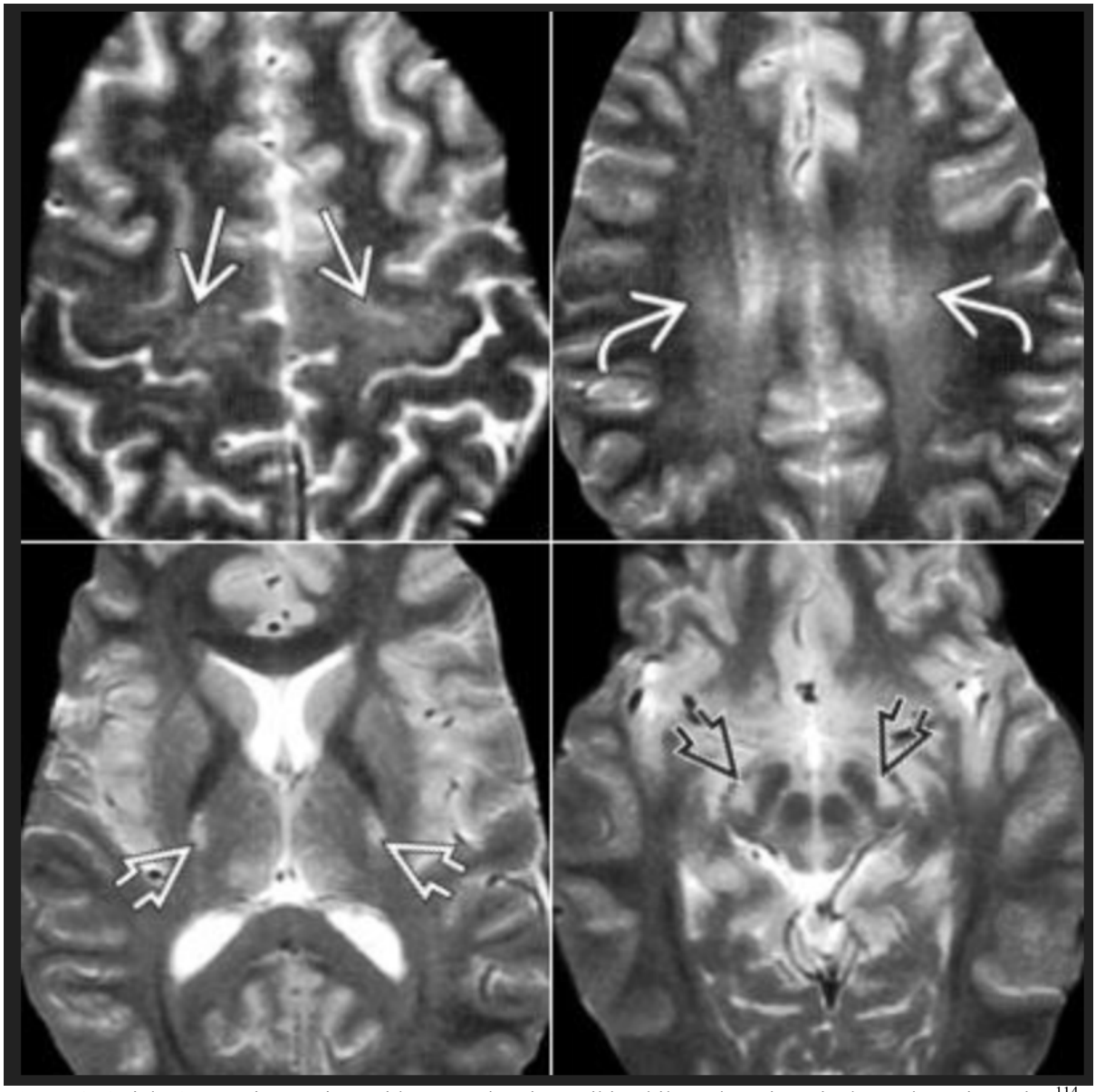

Figure 8. Axial T2 scans in a patient with MND showing striking bilateral corticospinal tract hyperintensity [114].

Most individuals with MND die from respiratory failure, usually within 3 to 5 years from the onset of symptoms. However, about 10 percent of affected individuals survive for 10 years or more [112].

The clinical diagnosis is often a complex and difficult process due to the lack of a specific diagnostic test and the high variability in the clinical presentation. The diagnostic El Escorial

revisited criteria for the diagnosis of MND are the result of a three-day workshop in Warrenton, Virginia in 1998 by the World Federation of Neurology Research Committee on Motor Neuron Diseases. These represent a consensus document accepted by MND researchers, clinicians and relevant scientific bodies [115].

On the basis of the El Escorial revisited criteria the diagnosis of MND requires:

A. the presence of:
    a. evidence of lower motor neuron (LMN) degeneration by clinical, electrophysiological or neuropathologic examination,
    b. evidence of upper motor neuron (UMN) degeneration by clinical examination, and
    c. progressive spread of symptoms or signs within a region or to other regions, as determined by history or examination,

    together with:

B. the absence of
    a. electrophysiological or pathological evidence of other disease processes that might explain the signs of LMN and/or UMN degeneration, and
    b. neuroimaging evidence of other disease processes that might explain the observed clinical and electrophysiological signs.

In the absence of pathological confirmation, these criteria allow to classify the clinical diagnosis of MND into various levels of certainty on the basis of the presence of UMN and LMN signs together in the same topographical anatomic region in either the brainstem, or the cervical, thoracic or lumbosacral spinal cord.

- Clinically definite MND: presence of UMN as well as LMN signs in the bulbar region and at least two spinal regions or the presence of UMN and LMN signs in three spinal regions;
- Clinically probable MND: presence of UMN and LMN signs in ate least two regions with some UMN signs necessarily rostral to the LMN signs;
- Clinically probable MND- laboratory supported: presence of UMN and LMN dysfunction in only one region or when UMN signs alone are present in one region, and LMN signs defined by EMG criteria are present in at least two regions with proper application of neuroimaging and clinical laboratory protocols to exclude other causes;
- Clinically possible MND: UMN and LMN dysfunction are found together in only one region or UMN signs are found alone in two or more regions; or LMN signs are found rostral to UMN signs and the diagnosis of Clinically probable MND- laboratory supported cannot be proven by evidence.

In the majority of MND brains no macroscopic abnormalities are observed. The spinal cord often reveals atrophy of the anterior nerve roots and some cases can exhibit atrophy of the precentral gyrus [116,117]. Microscopic changes include neuronal and axon loss. Cell loss is accompanied by gliosis, and some of the surviving motor neurons contain ubiquitinated cytoplasmatic inclusions of a variety of morphological types, including spherical Lewy body-like inclusions and skeins of thread-like structures [118-120]. Bunina bodies, which are bead-like eosinophilic cytoplasmic inclusions, may also be present and are very specific for classical MND. Ubiquitin-positive inclusions are negative for proteins commonly associated with neurodegenerative inclusions, such as tau and alpha-synuclein. [121,122]. TDP-43 was identified as the main component of ubiquitinated inclusions in MND and in FTD. TDP-43 is a

heterogeneous nuclear ribonucleoprotein that is expressed in the nuclei of neurons and glial cells under normal conditions. In sporadic and most familiar MND as well as FTD there is loss of nuclear TDP-43 and formation of pathological aggregates in the cytoplasm. However, TDP-43 inclusions are not pathognomonic for MND or FTD since the inclusions are also observed in Alzheimer's disease, Lewy body diseases, Guamanian Parkinsonism dementia complex and post-traumatic encephalopathy and neurodegeneration. [123-125].

2.3 Autism Spectrum Disorder

Introduction

Autism Spectrum Disorder (ASD) is a neurodevelopmental disorder that affects 1 in every 100 people in the UK [126]. ASD is characterized by a persistent, significant impairment in social interaction and communication as well as restrictive, repetitive behaviours and activities. Social communication and social interaction features include deficits in social-emotional reciprocity (e.g., deficits in joint attention, atypical social approach and response, conversational challenges, reduced sharing of interest, emotions, and affect), deficits in nonverbal communication (e.g., atypical eye contact, reduced gesture use, limited use of facial expressions in social interactions, challenges understanding nonverbal communication), and deficits in forming and maintaining relationships (e.g., diminished peer interest, challenges joining in play, difficulties adjusting behaviour to social context). ASD features of restricted, repetitive patterns of behaviour, interests, or activities may include stereotyped motor mannerisms, use of objects, or speech (e.g., simple motor stereotypies, repetitive play, echolalia, and formal or idiosyncratic speech); insistence on sameness, inflexible adherence to routines, or ritualized patterns of behaviour (e.g., distress at small changes, rigid patterns of thought and behaviour, performance of everyday activities in ritualistic manner); intense preoccupation with specific interests (e.g., strong attachment to objects, circumscribed or perseverative topics of interest); and sensory sensitivities or interests (e.g., hyper- or hypo- reactivity to pain and sensory input, sensitivity to noise, visual fascination with objects or movement). [126,127].

These symptoms cause impairment across many areas of functioning and are present early in life. However, impairments may not be fully evident until environmental demands exceed the individual capacity to compensate for the deficits. They also may be masked by learned compensatory strategies later in life. Many patients with ASD also have intellectual

impairment or language impairment [128] and the disorder has been associated with known medical, genetic, or environmental factors [129].

ASD has a strong genetic component, with heritability estimated to be between 40 and 90 percent. Autism is commonly associated with many neurogenetic disorders, such as Down's syndrome, tuberous sclerosis, neurofibromatosis and fragile X syndrome. A range of genes is implicated in susceptibility to ASD; however, environmental exposures and context also play a role in ASD development and neurogenetic expression. Current research suggests that certain metabolic and other maternal conditions (such as diabetes, hypertension, obesity, and influenza infection) during pregnancy may be associated with increased risk of ASD in offspring. Other studies have investigated the role of advanced maternal and paternal age, inter-pregnancy interval, pesticide exposure, and exposure to mercury and other heavy metals, among other potential risk factors [127,130].

Clinical diagnosis

In the *Diagnostic and Statistical Manual of Mental Disorders, Fourth Edition* (DSM-IV) disorders considered as part of the autism spectrum were divided into discrete categories including: Autistic Disorder, Asperger's Disorder, and Pervasive Developmental Disorder, Not Otherwise Specified (PDD-NOS). The DSM-5, published in May 2003, combined the previous categorical disorders into a single category of "Autism Spectrum Disorder," with varying degrees of severity depending on the amount of support required by an individual. Because no medical or biological marker exists for ASD, the diagnosis is based on clinical observations and interview with the parents. Diagnosis is established with a combination of history, observation, and/or formal testing, which may include ASD-specific screening and assessment instruments.

Diagnostic criteria for ASD according to DSM-5.

A. Persistent deficits in social communication and social interaction across multiple contexts, as manifested by the following, currently or by history:
    a. Deficits in social-emotional reciprocity, ranging, for example, from abnormal social approach and failure of normal back-and-forth conversation; to reduced sharing of interests, emotions, or affect; to failure to initiate or respond to social interactions
    b. Deficits in nonverbal communicative behaviours used for social interaction, ranging, for example, from poorly integrated verbal and nonverbal communication; to abnormalities in eye contact and body language or deficits in understanding and use of gestures; to a total lack of facial expressions and nonverbal communication.
    c. Deficits in developing, maintaining, and understanding relationships, ranging, for example, from difficulties adjusting behaviour to suit various social contexts; to difficulties in sharing imaginative play or in making friends; to absence of interest in peers.

B. Restricted, repetitive patterns of behaviour, interests, or activities, as manifested by at least two of the following, currently or by history:
    a. Stereotyped or repetitive motor movements, use of objects, or speech (e.g., simple motor stereotypies, lining up toys or flipping objects, echolalia, idiosyncratic phrases).
    b. Insistence on sameness, inflexible adherence to routines, or ritualized patterns or verbal nonverbal behaviour (e.g., extreme distress at small changes, difficulties with transitions, rigid thinking patterns, greeting rituals, need to take same route

or eat food every day).

c. Highly restricted, fixated interests that are abnormal in intensity or focus (e.g., strong attachment to or preoccupation with unusual objects, excessively circumscribed or perseverative interest).

d. Hyper- or hyporeactivity to sensory input or unusual interests in sensory aspects of the environment (e.g., apparent indifference to pain/temperature, adverse response to specific sounds or textures, excessive smelling or touching of objects, visual fascination with lights or movement).

C. Symptoms must be present in the early developmental period (but may not become fully manifest until social demands exceed limited capacities, or may be masked by learned strategies in later life).

D. Symptoms cause clinically significant impairment in social, occupational, or other important areas of current functioning.

E. These disturbances are not better explained by intellectual disability (intellectual developmental disorder) or global developmental delay. Intellectual disability and autism spectrum disorder frequently co-occur; to make comorbid diagnoses of autism spectrum disorder and intellectual disability, social communication should be below that expected for general developmental level.

Post-mortem studies of socio-emotional processing regions in ASD showed alterations in neuronal and axonal development, organization, and connectivity within frontal and temporal cortical regions [129]. However, small sample sizes and examination of a limited number of

selected regions limited the interpretation and generalizability of these results. Nonetheless, post-mortem findings included: (i) reduced neural size and increased packing density within limbic (grey matter) structures [131]; (ii) reduced mean neuron density, neuron number and perikaryal volume within output layers of the fusiform gyrus [132]; (iii) cortical dysgenesis within superior frontal and temporal grey and white matter regions [133]; (iv) increased numbers of prefrontal cortex mini-columns [134] and (v) recent evidence implicating an 67% average increase in total neuronal number within the prefrontal cortex compared to controls [135]. These findings demonstrated an early neurodevelopmental insult that affects neuronal proliferation, migration, maturation and organization in prefrontal and temporal cortical regions within ASD brain.

Preliminary examination of axonal properties within prefrontal white matter in ASD subjects found (i) increased small-diameter (representing short-range connections) and decreased large-diameter axon density (representing long-range connections) within anterior cingulate white matter, (ii) reduced myelin thickness in orbitofrontal cortex white matter, and (iii) no differences in axonal properties within lateral prefrontal cortex white matter [136].

Chapter 3 Neuroimaging methods of investigating the white and grey matter anatomy

The imaging methods used in this thesis are diffusion-based tractography and cortical morphometry. Tractography was used to identify and extract microstructural properties of tracts of interest in all three Experimental studies, whereas cortical morphometry analysis was employed only in Study 1 and 2. In this chapter a general overview of the methods is provided. A more detailed description of the methods can be found in the method section of each experimental chapter.

3.1 Introduction to Diffusion tensor imaging tractography

3.1.1 Basic principles

Diffusion imaging tractography is a magnetic resonance imaging (MRI) method used to quantify the microstructural properties of biological tissue and perform *in vivo* virtual reconstructions of white matter trajectories [45]. This technique is based on diffusion-weighted MRI, which sensitizes the magnetic resonance signal to the displacement of water molecules within biological tissues [137]. The displacement of water molecules follows Einstein's equation where the mean squared displacement ⟨r2⟩ is directly proportional to the observation time (t) according to:

$$\langle r2 \rangle = 6Dt.$$

Assuming that within a voxel of cerebrospinal fluid (CSF) the diffusion coefficient (D) is very close to the coefficient of free water (about $3x10^{-3}$ mm^2s^{-1} in a human body at the temperature of 37^o C), the water molecules are free to cover randomly an average distance of 20 μm in about

20 ms. However, the nervous tissue has a diffusion coefficient smaller than the one of the free water due to the presence of myelin, cell membranes, proteins and intracellular filaments. Here, water follows the main displacement of the brain structures in which is contained. Therefore, isotropic tissues, such as the grey matter, have equally water diffusivity along all directions. On the other hand, white matter of the brain and spinal cord is an anisotropic tissue due to the presence of parallel displaced fibres and axons and as a consequence water displacement is greater along the main direction of the fibres (Figure 9).

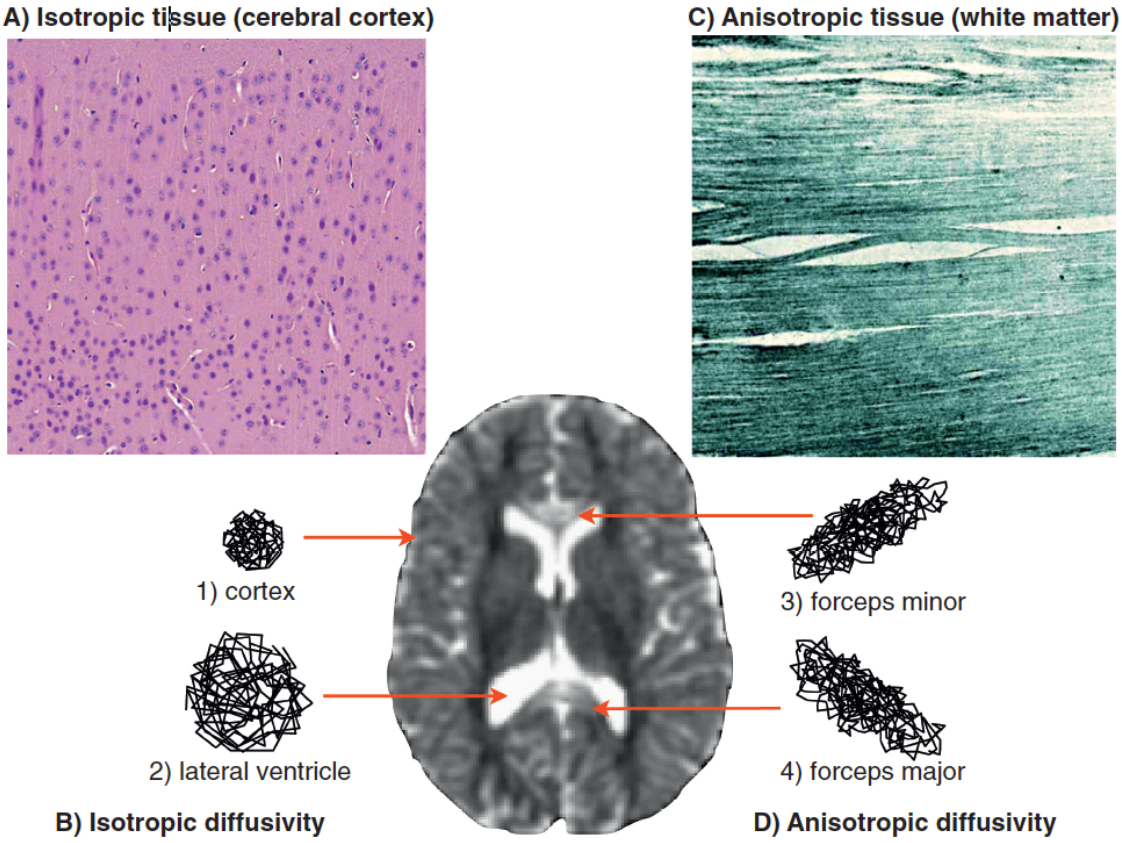

Figure 9. Histological sections of the A) cerebral cortex and B) white matter fibres in the human brain. The two tissues differ in their microstructural organization and composition of their biological constituents. In the middle, an axial ADC map of the human brain is shown together with the visualization of the 3D displacement of a water molecule in regions with different degrees of anisotropy and diffusivity: 1) low isotropic diffusivity in the frontal cortex where the overall displacement is equally hindered in all directions; 2) high isotropic diffusivity in the cerebro-spinal fluid of the lateral ventricles; 3) oblique anisotropic diffusivity along the lateral fibres of the genu in the forceps minor; 4) oblique anisotropic diffusivity along the lateral fibres of the splenium in the forceps major [45].

Diffusion-weighted imaging (DWI) is sensitive to the random motion of water molecules that is regulated by the tissue cellularity and the presence of intact cell membrane which together constitute the principal factor of impedance to water molecule diffusion. The term 'apparent diffusion coefficient' (ADC) assesses quantitatively this impedance of water molecule diffusion and it is displayed as a parametric map that reflects the degree of water diffusion through different tissues [138,139]. DWI as well as ADC maps are indispensable tools in the examination of the central nervous system and are commonly used for the early diagnosis especially in the context of acute ischaemic stroke, differentiation between brain tumors and intracranial infections (Figure 10).

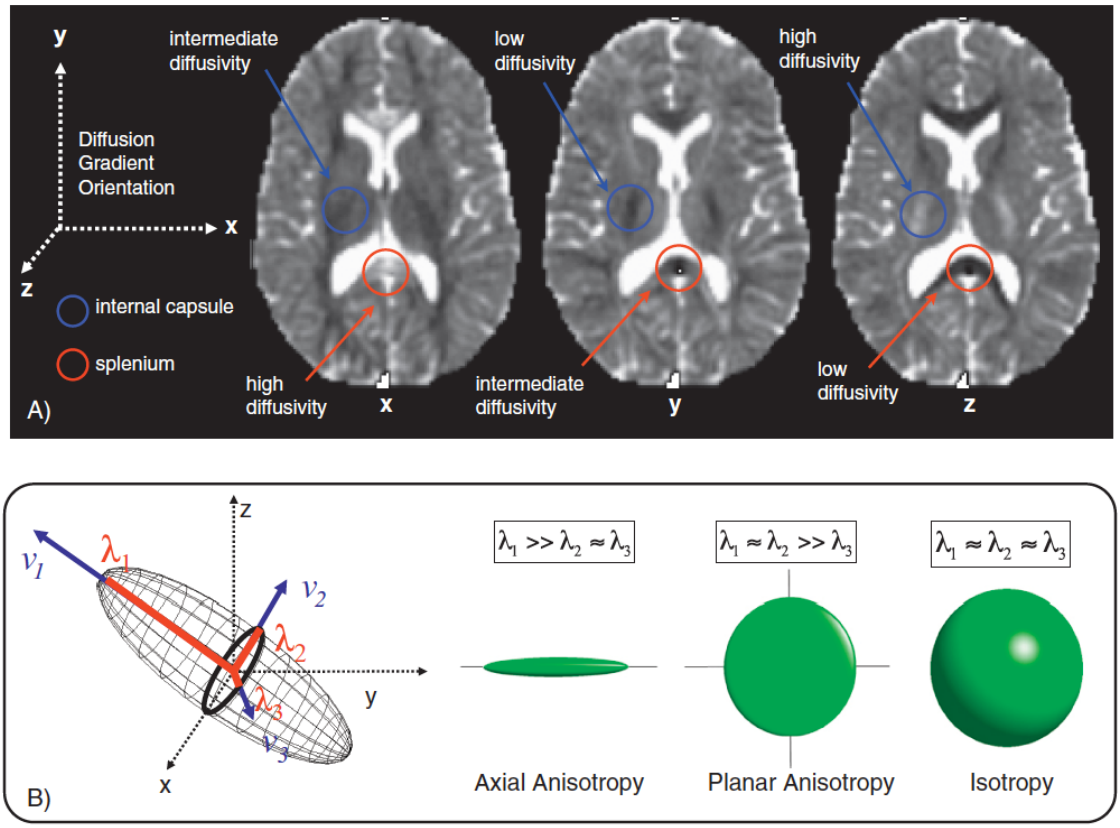

Figure 10. A) Monodirectional ADC maps where the signal is sensitized according to the displacement of water molecules along the three orthogonal planes (x, latero-lateral direction; y, antero-posterior; z, superior-inferior). The fibres of the internal capsule and splenium have a similar arrangement but different orientation. Hence, the monodirectional ADC values can differ according to the direction of the measured diffusivity. In the first figure, the fibres of the internal capsule (blue circle) are perpendicular to the diffusion direction along the axis x and show low diffusivity, while those of the central portion of the splenium (red circle) are parallel to the x directions and therefore have high diffusivity. The diffusivity of the voxels containing fibres of the internal capsule and splenium changes in the other two examples where diffusivity is measured along the axis y (i.e. anterior-posterior) and z (dorso-ventral). B) Visualization of the diffusion tensor as a diffusion ellipsoid. The size and the shape are defined by the three eigenvalues (λ1, λ2, λ3 in red) while the spatial orientation by the three eigenvectors (v1, v2, v3 in blue). In biological tissue the tensor can vary between three possible configurations: i) axial anisotropy (where λ1 is greater than λ2 and λ3), which is typical of voxels containing parallel fibres; ii) planar anisotropy (when λ1 is similar to λ1 and greater than λ3), which is common in voxels containing two groups of crossing or diverging fibres; iii) isotropy (when all three eigenvalues are similar) which is commonly observed in the grey matter [45].

3.1.2 Diffusion tensor imaging

The Diffusion tensor imaging (DTI) is a technique capable of measuring the diffusivity of water molecules and visualizing the preferential orientation of their movement. As brain white matter can be characterized to a large extent by its orientation and anisotropy, DTI can measure the anisotropy and principal orientation of an anisotropic tissue. The visualization of white matter pathways in the living brain is based on a mathematical description of the overall displacement of the water molecules which geometrically corresponds to the diffusion tensor. This is because the diffusion tensor characterizes the three-dimensional diffusion of water as a function of spatial location and describes the magnitude, the degree of anisotropy and the orientation of diffusivity anisotropy [137]. The diffusion tensor may be visualized using an 3D-ellipsoid with diffusion coefficient values (eigenvalues) and orientations (eigenvectors) of its three principal axes. The two most common measures of the 3D-ellipsoid are mean diffusivity (MD) and fractional anisotropy (FA). The MD corresponds to the average water molecular displacement within a voxel while the FA is the measure of anisotropy of a given tissue described originally by Basser and Pierpaoli [140]:

$$FA = \sqrt{\frac{(\lambda_1 - MD)^2 + (\lambda_2 - MD)^2 + (\lambda_3 - MD)^2}{2(\lambda_1{}^2 + \lambda_2{}^2 + \lambda_3{}^2)}}$$

Complementary information about the microstructural composition and architecture of the brain tissue is given by the axial diffusivity and the radial diffusivity, which represent the diffusivity along the principal direction of the diffusion tensor or perpendicular to it, respectively. The interpretation of changes in the measured diffusion tensor is complex (Figure 11). The FA ranges between 0 and 1 and have a very different distribution among gray matter (GM), white matter (WM) and CSF. The other measures in GM and WM appear

more normally distributed with the largest difference between tissue types observed for the radial diffusivity measurements. White matter neuropathology characterized by demyelination, oedema, axonal injury often causes changes in all diffusion indices [141].

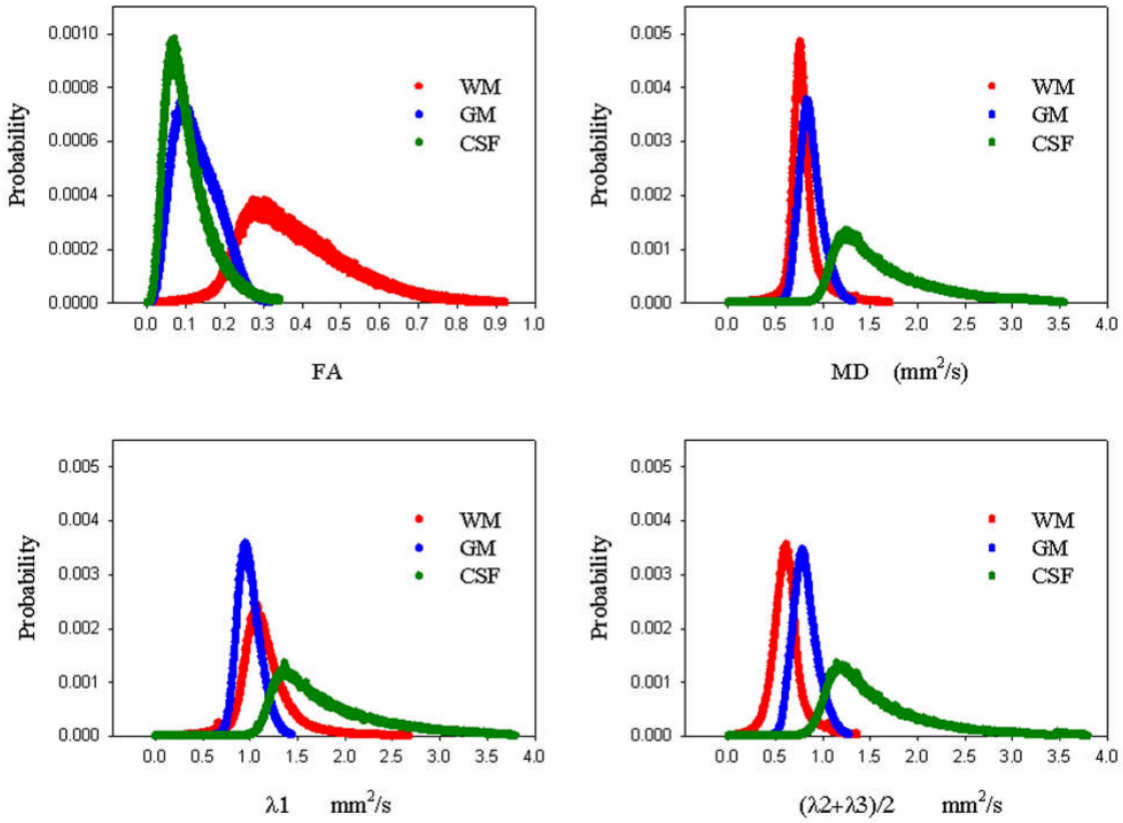

Figure 11. Histograms of FA, MD, Da and Dr in healthy gray matter (GM), white matter (WM) and CSF [141].

3.1.3 White matter tractography

White matter tractography refers to the process that pieces together contiguous voxels according to the orientation of the estimated tensors. Tractography is the only method that currently permits to delineate white matter trajectories in the living human brain. The streamlines delineated by tractography are obtained using algorithms that follow the principal eigenvector of the tensors, with specific criteria defined for starting, continuing and terminating the tracking process. Among these criteria, the most widely used are an FA

threshold (usually 0.2 for adult normal brain or lower for pathological or younger subjects) and the angle threshold between two contiguous tensors (usually between 30 and 60 degrees). The primary applications of tractography is the 3D visualization of white matter pathways and the extraction of diffusion properties along the course of each pathway [142,143].

Tractography is also used for the segmentation of cortical areas and subcortical regions, such as the thalamus, amygdala and basal ganglia. Tractography can reconstructs the main association, commissural, and projection fasciculi of the human brain (Figure 12).

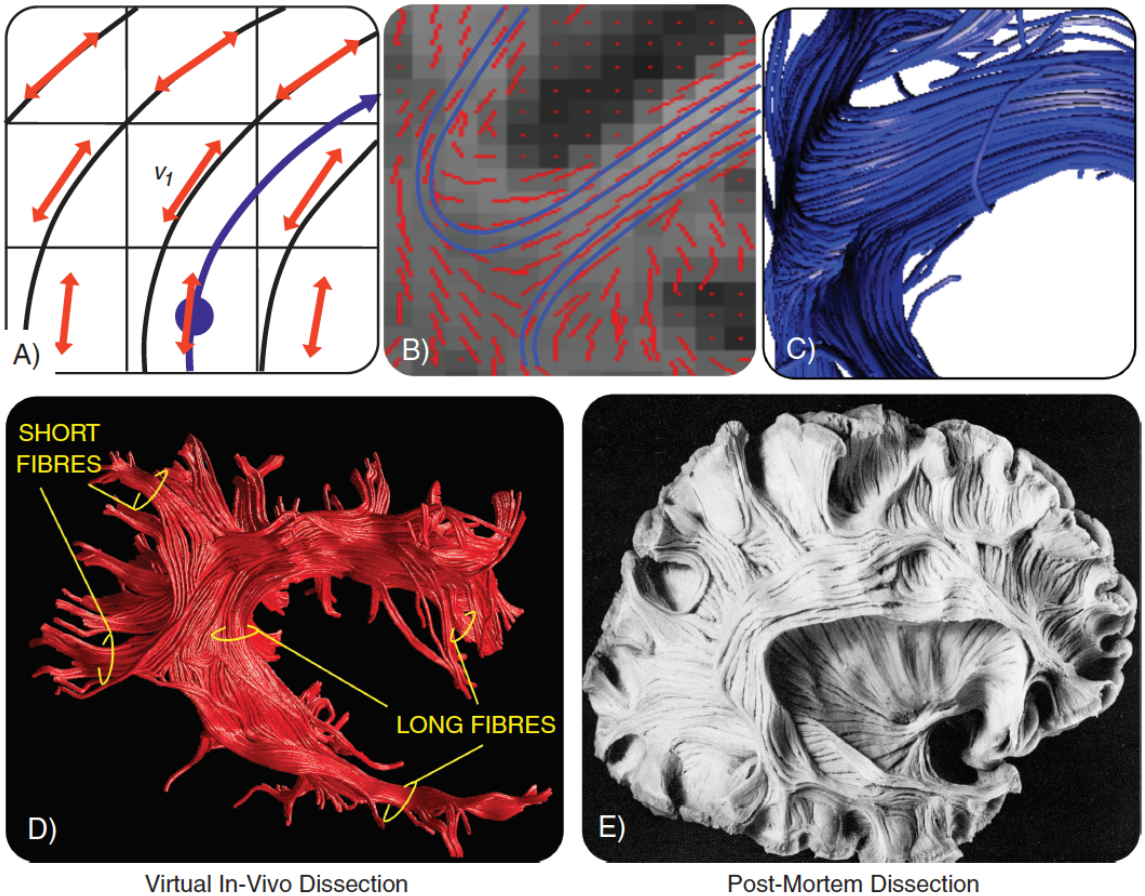

Figure 12. Tracking continuous pathways with diffusion tensor imaging. A) Streamline tractography is based on the assumption that in each white matter voxel the principal eigenvector (red arrow) is tangent to the main trajectory of the underlying fibers (black). Starting from a seed voxel (blue circle) the tractography algorithm propagates, voxel by voxel, a streamline (blue) by piecing together neighboring principal eigenvectors (v1). B) Axial section of the eigenvector map and streamlines (blue) through the lateral splenium of the corpus callosum. C) Tractography reconstruction of the splenial streamlines visualized as 3D streamtubes. D, E) Comparison between the virtual in vivo reconstruction of the arcuate fasciculus and the corresponding post-mortem dissection [45].

The association pathways (Figure 13) connect cortical regions within the same hemisphere

and there are the long association tracts connecting distant regions between lobes (the arcuate fasciculus, the cingulum, the uncinate, the inferior longitudinal fasciculus, and the inferior fronto-occipital fasciculus) and the short U-shaped fibres connecting neighboring gyri within the same lobe (intralobar fibres) or different lobes (interlobar fibres). The arcuate fasciculus is a lateral tract composed of long and short fibres connecting the perisylvian cortex of the frontal, parietal and temporal lobes. The short fibres lie more lateral than the long fibres. The cingulum is a medial tract that runs within the cingulate gyrus around the corpus callosum and contains fibres of different length, the longest of which run from the anterior temporal lobe to the orbitofrontal cortex. Short U-shaped fibres connect the medial frontal, parietal, occipital and temporal lobes and different portions of the cingulate cortex. The uncinate fasciculus is a ventral tract that connects the anterior temporal lobe with the medial and lateral orbitofrontal cortex. The inferior longitudinal fasciculus is a ventral tract with long and short fibres connecting the occipital and temporal lobes. Its long fibres, which are medial to its short fibres, connect visual areas to the temporopolar cortex, amygdala and hippocampus. The inferior fronto-occipital fasciculus is a ventral tract that connects the inferior and medial occipital lobe to the orbitofrontal cortex [44].

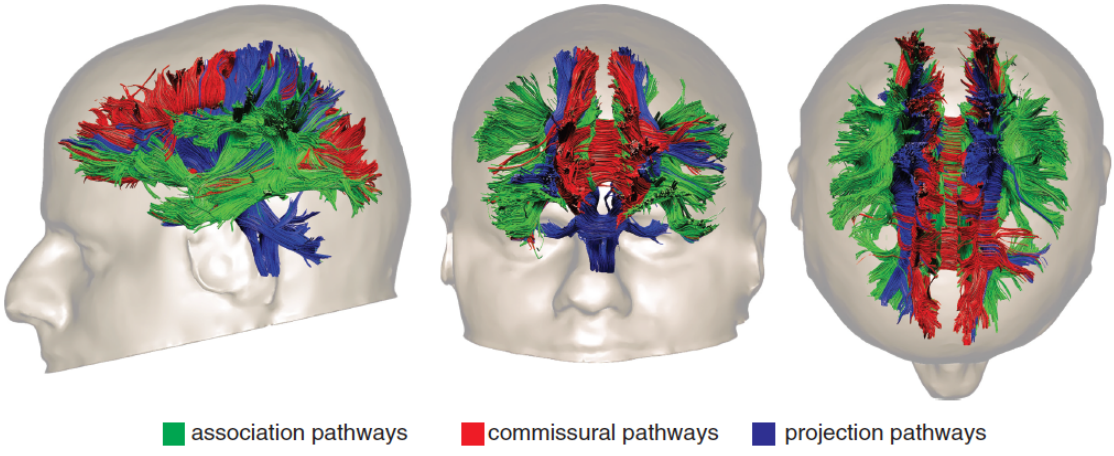

Figure 13. In vivo diffusion tensor tractography reconstruction of the association, projection, and commissural pathways of the human brain [45].

The commissural pathways (Figure 14) connect the two halves of the brain and are the corpus callosum, the anterior commissure, and the posterior (hippocampal) commissure. The corpus callosum is the largest bundle of the human brain and connects left and right cerebral hemispheres. It is conventionally divided into an anterior portion (genu) connecting the prefrontal and orbitofrontal regions, a central part (body) connecting precentral frontal regions and parietal lobes, and a posterior portion connecting the occipital lobes (splenium). The term tapetum is used for the lateral-inferior extensions of the splenial fibres connecting the posterior temporal lobes. The rostrum is a small part located just below the genu connecting the most medial regions of the orbitofrontal cortex. The fibres of the genu and rostrum arch anteriorly away from the midline and form together the anterior forceps (or forceps minor). The fibres of the splenium arch posteriorly and form the posterior forceps (or forceps major). The anterior commissure connects bilaterally the anterior and ventral temporal lobes (including the amygdalae) of the two hemispheres, and also the olfactory bulbs [44].

The projection pathways (Figure 14) connect the cortex to subcortical structures, such as deep cerebral nuclei, brainstem nuclei, and spinal cord. The fornix is a projection bundle that connects the medial temporal lobe (i.e. the hippocampus) to the septal nuclei and the mammillary bodies of the hypothalamus. The fornix belongs to the limbic system and is involved in memory functions The internal capsule and corona radiata contain ascending fibres mainly from the thalamus and descending fibres from the frontoparietal cortex to subcortical nuclei, including the basal ganglia, the brainstem nuclei, and the spinal cord [44].

3.1.4 Limitations

The development of DTI and tractography algorithms allowed, for the first time, to measure

and extract *in vivo* and non invasively the organization and integrity of white matter fibres and to reconstruct three dimensional trajectories of the major white matter pathways. Despite the fact that this technique has become the most important tool for investigating the connectional anatomy of the normal and pathological human brain, there are some limitations that will be discussed below in this paragraph [144].

The ability to reproduce three-dimensional trajectories of white matter connections in the living human brain is a unique feature of tractography. Nevertheless, for the tracts that reach cortical regions without crossing with other connections (e.g. dorsal cingulum' medial callosal fibres, and so on) the details of the 'virtual reconstructions' match those derived from human postmortem blunt dissections or histology while for other tracts the matching is rather incomplete due to the limitations of the diffusion tensor model and the intrinsic low spatial resolution of the human diffusion datasets. This is particularly evident for tracts that do not reach cortical regions with crossing with other connections [144].

Another limitation is related to the extraction of quantitative diffusion indices, such as fractional anisotropy and mean diffusivity. Along the dissected tract it is possible to characterize the microstructural properties of tissue in the normal and pathological brain and provide quantitative measurements for group comparisons or individual case studies [145-147]. However, the interpretation of these indices is not always straightforward, especially in regions containing fibre crossing. An example of the complexity of this problem is the increase of fractional anisotropy commonly seen in the normal-appearing white matter regions distant to the damaged area. Before interpreting these changes as indicative of 'plasticity or remodeling', other explanations should be taken into account. In voxels containing both degenerating and normal fibres, increases in fractional anisotropy values are, in fact, more likely due to the axonal degeneration of the perpendicular fibres. The lack of specificity of current diffusion indices (i.e., diffusion changes depend on a number of

biological, biochemical and microstructural factors) and the intrinsic voxel-specific rather than fibre-specific information derived from current indices has stimulated scientists to work on new methods and novel diffusion indices.

Recently, true tract specific indices based on spherical DE convolution that better describe the microstructural diffusion changes of individual crossing fibres within the same voxel have been proposed. Changes in the hindrance modulated orientation anisotropy, for example, have a greater sensitivity than conventional fractional anisotropy values to detect degeneration that occurs only in one population of fibres, whereas the others crossing fibres remain intact. In the future, tractography combined with other methods will allow to extract even more specific tissue microstructure indices, such as axonal diameter [148].

Finally, advanced diffusion models that resolve multiple white matter trajectories offer the possibility of describing and identify new tracts. By using spherical deconvolution tractography, for example, it is possible to visualize and quantify the volume of the three segments of the superior longitudinal fasciculus, a tract previously described only in the monkey brain. Recently, the same method has been used to reveal new details of the short frontal lobe connections. Although an exact knowledge of these short fibres represents a significant step forward in our understanding of human anatomy, it is important to be aware that tractography based on advanced diffusion methods is prone to produce a higher number of false positives compared to DTI tractography. Hence, validation of these tracts with complementary methods is necessary before applying these anatomical models to clinical populations [144,148,149].

3.2 Cortical Morphometry analysis with Freesurfer

3.2.1 Introduction

FreeSurfer is a suite of powerful tools for the analysis of neuroimaging data that provides an array of algorithms to quantify the functional, connectional and structural properties of the human brain. FreeSurfer automatically creates models of most macroscopically visible structures in the human brain given any reasonable T1-weighted input image. The structural properties of the human brain that Freesurfer can generate comprehends volumetric segmentation of most macroscopically visible brain structures, segmentation of hippocampal subfields, inter-subject alignment based on cortical folding patterns, segmentation of white matter fascicles using diffusion MRI, parcellation of cortical folding patterns, estimation of architectonic boundaries from *in vivo* data, mapping of the thickness of cortical gray matter, and the construction of surface models of the human cerebral cortex.

3.2.2 Methods

FreeSurfer analysis suite *(*http://surfer.nmr.mgh.harvard.edu/) was used to derive models of the cortical surface in each T1-weighted image in my experimental studies. These well-validated and fully automated procedures have been described extensively [150-153].

The first stage of the processing involves several intensity normalization steps, followed by skull stripping, and image segmentation using a connected components algorithm. The algorithm is a general technique for segmenting images into contiguous regions that operates by considering the image intensity values as a "watershed basin", and then gradually "flooding"

the basin with water by incrementally thresholding the image. At each increment, the separate regions are identified. If two regions or “basins”, which were previously separated, come into contact at a subsequent step of "flooding", a determination is made about whether to merge

them into one region, or to create a "dam" between them and keep them as separate regions, based on a watershed threshold of difference of "depth" between the regions and the current "flooding" level.

The next step of Freesurfer's processing pipeline is the surface tessellation for each white matter volume by fitting a deformable template. This results in a triangular cortical mesh for gray and white matter surfaces consisting of approximately 150,000 vertices (i.e. points) per hemisphere. Following standard FreeSurfer pre-processing, each reconstructed surface is then visually inspected for reconstruction errors, and images that do not reconstruct correctly (i.e. with visible anatomical abnormalities) are further excluded from the statistical analysis (dropout 5%).

Measures of cortical thickness are computed as the closest distance from the gray and white matter boundary to the gray matter and cerebrospinal fluid boundary at each vertex on the tessellated surface. Vertex-based estimates of surface area are derived as outlined by [154]. Here, the individual's native surface is initially transformed into a spherical representation, which preserves vertex identities (e.g. total numbers) and original areal quantities, and subsequently registered to a common atlas/template. This registration does not change areal quantities but shifts vertex positions to match the template. Finally, areal quantities are transferred to a common grid via areal interpolation. Here, the final amount of 'area' each face receives on the new grid depends on the overlap between the original source face and the target (i.e. common grid) face. In this way, the fixed target surface is redistributed across one of more source faces and can be used as weighting factor to account for inter-individual differences in surface reconstructions. Vertex-wise estimates of cortical volume are derived as the product of cortical thickness and surface area at each cerebral vertex. FreeSurfer can also compute mean cortical thickness, total surface area and total cortical volume (across hemispheres). To improve the ability to detect population changes, each parameter is

smoothed using a 5-mm surface-based smoothing kernel.

The statistical analysis is conducted using the SurfStat toolbox (http: //www.math.mcgill.ca/keith/surfstat/) for Matlab (R2013a; MathWorks). Parameter estimates for vertex-based measures of cortical thickness, surface area and cortical volume were estimated by regression of a general linear model (GLM) each vertex *i* and subject *j*, with (1) group and gender as categorical fixed-effects factor; and (2) age, and a total brain measure (i.e. mean CT, total SA, total CV respectively) as continuous covariates, so that

$$Y_i = \beta_0 + \beta_1 \text{Group}_j + \beta_2 \text{IQ}_j + \beta_3 \text{Age}_j + \beta_4 \text{TotalBrain}_j + \varepsilon_i.$$

Between-group differences are estimated from the fixed-effect coefficient β_1 normalized by the corresponding standard error. Corrections for multiple comparisons across the whole brain are performed using random-field theory (RFT) based cluster-corrected analysis for non-isotropic images using a $p<0.05$ (2-tailed) cluster-significance threshold [155].

Chapter 4 Neuropsychological Test Battery

For the experimental part of the thesis, several validated neuropsychological tests, structured or semi-structured interviews, and questionnaires have been used. These instruments assess several aspects of human cognition and behaviour related to frontal lobe functions. Below the individual tests and questionnaires are briefly described.

Autism Diagnostic Interview-Revised (ADI-R).

The Autism Diagnostic Interview-Revised (ADI-R) is a clinical diagnostic instrument for assessing autism in children and adults [156]. The ADI-R provides a diagnostic algorithm for autism as described in both the ICD-10 and DSM-IV. The interview contains 93 items and focuses on behaviours in three content areas or domains: quality of social interaction (e.g., emotional sharing, offering and seeking comfort, social smiling and responding to other children); communication and language (e.g., stereotyped utterances, pronoun reversal, social usage of language); and repetitive, restricted and stereotyped interests and behaviour (e.g., unusual preoccupations, hand and finger mannerisms, unusual sensory interests). The measure also includes other items relevant for treatment planning, such as self-injury and over-activity. The ADI-R interview generates scores in each of the three content areas (i.e., communication and language, social interaction, and restricted, repetitive behaviours). Elevated scores indicate problematic behaviour in a particular area. Scores are based on the clinician's judgment following the caregiver's report of the child's behaviour and development. For each item, the clinician gives a score ranging from 0 to 3. A score of 0 is given when "behaviour of the type specified in the coding is not present"; a score of 1 is given when “behaviour of the type specified is present in an abnormal form, but not sufficiently severe or frequent to meet the criteria for a 2”; a score of 2 indicates "definite abnormal behaviour” meeting the criteria specified; and a score of 3 is reserved for "extreme

severity" of the specified behaviour. (The authors of the measure recode 3 as a 2 in computing the algorithm.) There are also scores of 7 (“definite abnormality in the general area of the coding, but not of the type specified”), 8 (“not applicable”), and 9 (“not known or not asked”) given under certain circumstances, which all are converted to 0 in computing the algorithm. A classification of autism is given when scores in all three content areas of communication, social interaction, and patterns of behaviour meet or exceed the specified cutoffs, and onset of the disorder is evident by 36 months of age. The same algorithm is used for children from mental ages 18 months through adulthood, with three versions containing minor modifications: 1) a life-time version; 2) a version based on current behaviour; and 3) a version for use with children under the age of 4 years. The algorithm specifies a minimum score in each area to yield a diagnosis of autism as described in ICD-10 and DSM-IV. The total cutoff score for the communication and language domain is 8 for verbal subjects and 7 for nonverbal subjects. For all subjects, the cutoff for the social interaction domain is 10, and the cutoff for restricted and repetitive behaviours is 3.

Frontal Behaviour Inventory (FBI).

The Frontal Behaviour Inventory (FBI) is a 24-item caregiver questionnaire developed and standardized with the purpose of differentiating the behavioural variant of Frontotemporal Dementia (bvFTD) from other dementias, such as Alzheimer’s Disease (AD) and Vascular Dementia (VAD) [157]. The FBI offers an indirect method to quantify the severity of the behaviour disorder of FTD for several clinical aspects linked to negative behaviours (apathy, aspontaneity, indifference, inflexibility, concreteness, personal neglect, disorganization, inattention, loss of insight, logopenia, verbal apraxia and alien hand), and positive behaviours (perseverations/obsessions, irritability, jocularity, irresponsibility, inappropriateness, impulsivity, restlessness, aggression, hyperorality, hypersexuality, utilization behaviour and

incontinence). The inventory requires a reliable observer and the administration is about 20-30 minutes, depending on the extent and severity of symptoms and the caregiver's verbal capacity. The severity of symptoms is scored in a scale between 0 and 3 (0 = never, 1 = mild or occasional, 2 = moderate, 3 = severe or very frequent). An operational definition of FTD included a minimum FBI score of 27.

Frontal Systems Behavioral Scale (FrsBe).

The FrSBe, formerly known as the Frontal Lobe Personality Scale (FLoPS), provides a brief, reliable, and valid measure of three frontal systems behavioural syndromes: apathy, disinhibition, and executive dysfunction. It also quantifies behavioural changes over time by including both baseline (retrospective) and current assessments of behaviour. The FrSBe includes a Total Score, as well as scores on three subscales related to the three frontal systems behavioural syndromes: Apathy (14 items), Disinhibition (15 items), and Executive Dysfunction (17 items). This 46-item, paper-and-pencil behaviour rating scale is much easier and less time-consuming to administer than a neuropsychological test battery. Two hand-scorable, carbonless test booklets are available: one for self-rating and one for rating by a family member or caregiver. Each item is rated on a 5-point Likert scale. Items are written at a 6th-grade reading level. Two profile forms (Self and Family) allow comparisons of behaviours pre- and post-injury/illness. The FrSBe Professional Manual provides norms for self-ratings and family ratings. The normative sample included 436 men and women ranging in age from 18 to 95 years and in education from 10 years to doctoral level. Normative tables stratified for gender, age, and education provide T scores for the self-rating form and the family rating form [158,159].

Hospital Anxiety and Depression Scale (HADS).

Hospital Anxiety and Depression Scale (HADS) is a self-assessment scale developed to detect symptoms of depression and anxiety in hospital wards or outpatient clinics. Patients are required to complete a questionnaire composed of 14 items, each containing four statements related to four levels of symptoms severity (0 no symptoms, 1 mild symptoms, 2 moderate symptoms, 4 severe symptoms). The scores range from 0 to 21, with 0-7 indicating no symptoms of anxiety or depression, 8-10 indicating borderline case and 11-21 indicating severe symptoms. The scores are given separately for anxiety and depression [160].

Kissing and Dancing test (KDT).

Kissing and Dancing test (KDT) is a novel associative test consisting of 52 triplets of pictures depicting actions and 52 word triplets consisting of verbs, which are directly comparable with the 52 triplets of objects and nouns of the pyramids, palm trees test (PPT). The aim of this test is to assess the knowledge of actions and verbs. The authors considered the KDT to be an extension of the PPT [161].

Modified Token Test.

The Token Test [162], was initially developed to detect mild receptive language disorders in aphasic patients. The Token test is an extremely simple test to administer and to score and it is sensitive to the disrupted linguistic processes that are central to the aphasic disability. Participants whose failure on this test are mostly due to defective auditory comprehension tend to confuse colours and shape and to carry out fewer that the required instructions. They may begin to perseverate as the instructions become more complex. The commands in the Token Test are independent of redundancies in a communicative situation. All commands

consist of non-redundant words, referring to circles and (in the original Token Test) rectangles in different colours (original Token Test: red, green, blue, yellow and white) and sizes (large and small). The objects do not give a cue for a specific action. To perform the requested action, every content word has to be decoded. The original test consists of 61 commands. Because of the frequent use of the test in clinical practice, several short forms are developed. In Experimental study 1 we used a modified and shortened version of the De Renzi and Vignolo Token Test. This modified version employed Weigl's blocks presented in a random array and consisted of 15 complex but abstract commands involving these blocks. Commands were spoken and presented once only. Scoring was pass or fail on each command. Maximum score was 15 [163]. As a verbal comprehension test, poor performances on this test are usually associated with lesion in the posterior superior temporal lobe and, in same cases, in the primary auditory sensory area in the dominant hemisphere [164].

Pyramid and Palm Trees test (PPT).

Pyramid and Palm Trees test (PPT) allows comparison of semantic knowledge for words and pictures using not only cross-modal matching, but also matching within the same modality. Participants are asked to decide, by pointing, which of a pair of items, such a palm tree or a pine tree, goes better with a third (a pyramid). The stimulus can be presented as a written or spoken word, or as a picture; the target and distractor can be either pictures or written words. The basis of the match is a semantic association; in this case, the palm tree 'goes with' the pyramid, on the grounds that both are found in hot climates, or that both are found in Egypt. It was initially normalized in England with a group of 60 healthy English-speaking subjects. Participants' performance was very consistent and strong. None of the subjects made more than three errors and the authors concluded that a subject scoring 90% or better on the PPT does not have clinically significant impairment in this task; consequently, researchers and

clinicians generally consider that a score lower than 47/52 on this test indicates significant semantic memory deficit [165].

Neuropsychological and functional neuroimaging studies suggest that the semantic processing of verbal and non-verbal stimuli of the PPT may depend on partially distinct brain networks. Butler C. et al. found that the regions of gray matter that correlated with scores on the PPT word version were left and right temporal lobes, bilateral hippocampus, temporal pole and superior, middle and inferior temporal gyri. Similarly, PPT picture scores were associated with damage on the bilateral hippocampus, temporal pole and superior, middle and inferior temporal gyri. However, patients with predominant right temporal atrophy scored significantly worse than those with left-sided atrophy on the picture score while there was no difference bewteen the groups in performance on the PPT word scores [166]. These findings also parallel functional imaging findings. Vandenberghe et al. used PET to study a semantic association task derived from the PPT test and found that the verbal task preferentially activated the left superior temporal sulcus, anterior middle temporal gyrus and inferior frontal sulcus [167]. Thierry and Price, comparing conceptual processing of verbal and non-verbal stimuli in both visual and auditory modalities, found greater activation in the non-verbal trials in the right fusiform gyrus and right superior, middle and inferior temporal gyri [168].

Verbal Fluency Index (Semantic fluency, Phonemic fluency).

Verbal Fluency Index (Semantic fluency, Phonemic fluency) is a widely used tool to assess frontal executive and language abilities. This index is the difference between the specified time for the generation condition and time taken for control condition was then calculated and used to determine the fluency index *(fi)*, which represented the average time taken to think of each item. In order to generate the phonemic fluency index, participants are required to generate as many words as possible beginning with ‘S’ in 5 min and 4-letter words

beginning with 'C' in 4 min adjusted for motor disability. The semantic version of the task requires participants to generate as many words as possible belonging to a given category (e.g. animals and foods words) adjusted for motor disability in 2 minutes [169].

Different studies showed that poor performance on the phonemic verbal fluency index was associated with damage mainly to the dorsolateral prefrontal cortex. Stuss et al. demonstrated that damage to the left dorsolateral prefrontal cortex resulted in impaired on phonemic verbal fluency task [170] while Sarazin showed that reduced PET glucose metabolism in this area was correlated with poor performance on the verbal fluency task [171]. However, there are also other studies that suggest that the frontal pole, the anterior cingulate cortex, the ventrolateral prefrontal cortex and the left middle and inferior frontal gyri may be also involved in verbal fluency task performance [172-175].

Neuropsychological studies found evidence that deficit on the semantic verbal fluency task was associated with dorsolateral prefrontal damage. However, whereas phonemic verbal fluency deficits were associated with damage to the left dorsolateral prefrontal cortex, semantic verbal fluency were associated with either left or right dorsolateral prefrontal damage [176]. In addition, there is evidence to suggest that also that the ventromedial prefrontal cortex and the anterior cingulate cortex are involved in semantic verbal fluency as well as damage to more posterior brain areas as temporal and parietal regions [174,176-178]. In particular, Baldo et al. found that performance on semantic verbal fluency was mainly associated with posterior lesions in the temporal lobes [179].

In summary, according to the literature performance on verbal fluency depends on a distributed brain network of the prefrontal cortex and in particular the semantic verbal fluency relies also on more posterior regions, including the temporal lobes.

Wisconsin Card Sorting Test (WCST).

The Wisconsin Card Sorting Test (WCST) is one of the most commonly used tests for assessing executive functions in clinical settings [180,181]. Participants are presented with four target cards and two decks of 64 cards (one deck is presented at a time) all of which depict shapes of a certain number and color. Participants are required to sort the cards according to a rule set by the experimenter (e.g., color: a 'green; pile, a 'red' pile; shape: a 'triangle' pile, a 'circle' pile; number: a '2-item' pile, a '3-item' pile) by drawing cards one-at-time from the deck of cards and matching each one with one of four target cards. In the most widely used form of the WCST, participants are not told the sort rule, and are required to discover the rule for themselves through trial and error. The experimenter gives the participants feedback after each card placement by simple saying 'correct' or 'incorrect'. After a series of correct card placements, however, the sort rule changes without the participant's knowledge and the participant should work out the new sort rule. Performance is usually reported in terms of the number of contingencies achieved and the number of perseverative errors made after the sorting rule changes. However, other measures can also be reported as total correct card sorts, number of trials taken to understand the shift in the sort rule, etc. In Experimental study 1 we used a computerized version of Wisconsin Card Sorting Test [182].

Large meta-analysis of lesion studies showed that frontal lesion patients performed more poorly than posterior lesion patients [183]. However, no laterality effect was observed in the analysis, suggesting that right- and left-sided lesions have similar implications.

A number of studies investigated the neuroanatomical correlates of WCST performance. Stuss et al. observed that patients with dorsolateral prefrontal damage achieved fewer sorting categories and committed more perseverative errors than other prefrontal patients. On the other hand patients with ventromedial prefrontal lesions committed more perseverative errors and achieved fewer sorting categories than patients with posterior lesions [184]. Barcelo and

Knight fould that also patients with anterior cingulate cortex damage showed an increase rate of perseverative, non-perseverative and efficiency errors in WCST [185]. To conclude, although various studies reported that patients with frontal lesions performed significantly more poorly than non-frontal patients, the location of damage within the frontal lobes and in particular in the dorsolateral prefrontal cortex is not mutually exclusive of poor WCST performance [2].

Chapter 5 Experimental Study 1: Neuronal correlates of cognitive and behavioural performaces in Motor Neuron Disease.

5.1 Introduction

Motor Neuron Disease (MND) is a neurodegenerative disorder of unknown etiology [111,112,186,187] characterized by progressive muscular paralysis, reflecting the degeneration of both upper motor neurons (UMN) and lower motor neurons (LMN) in the spinal cord, brainstem, and motor cortex [112,188]. Although Jean-Martin Charcot did not indicate the occurrence of psychiatric and cognitive symptoms in his first report of MND [108], others included them. The first three cases reported by Wechsler in 1932, for example, presented with additional cognitive impairment, psychotic symptoms and depression that were associated with histopathological abnormalities in the cortical motor areas, underlying white matter and basal ganglia, in particular in the globus pallidus. Wechsler concluded that a common neurodegenerative mechanism underlies both motor and neuropsychiatric symptoms, except for depression, which he considered to be of a 'reactive' nature [14].

In more recent studies, non-motor symptoms in MND have been extensively studied both clinically and with neuroimaging methods. Between 5% and 15% of MND patients meet the criteria for frontotemporal dementia (FTD) whereas 35% of MND patients have a mild and isolated cognitive impairment [188-190]. The most important cognitive domains affected in MND have been reported to be executive functions and specific language deficits, particularly on tests of verbal fluency and syntactic comprehension [113,169,172,191-193]. Behavioural changes can coexist with cognitive impairment in patients with MND, or more often they present in isolation [113,193]. Depression, apathy, anxiety, difficulty with social judgment and disinhibition can affect a significant number of patients with MND [194].

Depressive disorder in MND can be associated with anxiety, pervasive anhedonia, sadness, tearfulness, hopelessness, lower quality of life, and suicidal ideation [195], with a prevalence comparable to that reported in Alzheimer's disease, Huntington's disease and other medical disorders [196,197]. Thus, MND may be associated with significant psychiatric manifestations. However, to date it remains uncertain whether mental health manifestations of MND share the same aetiology as motor symptoms or whether they are secondary to the effect of increasing neurological disability.

Several studies have used cortical thickness analysis as an *in vivo* indirect measure of cortical atrophy in MND patients. In addition to precentral regions [198-201], differences in cortical thickness have been reported in MND for the temporal lobe [202], parietal and occipital regions [199]. More recently, diffusion tensor imaging (DTI) tractography studies have evaluated the location and extent of white matter involvement in patients with MND [203]. DTI studies reported that in addition to the corticospinal tract, white matter tract degeneration often extends to extra-motor fibres of the corpus callosum, cingulum, inferior longitudinal, inferior fronto-occipital and uncinate fasciculi [204-207]. These findings suggest that during the course of the illness, the neurodegenerative process affects extra-motor cortical and subcortical regions involved in cognition and behaviour.

Despite this, few studies have investigated the association between the pattern of cortical atrophy and white matter degeneration and severity of cognitive deficits and behaviour symptoms in MND patients [208]. Schuster et al. [209] found cortical atrophy in the frontal and temporal gyri and in the posterior cingulate cortex in the MND group with cognitive impairment, although the authors did not report a relationship with severity of cognitive impairment. Sarro et al. (2011) showed an association between cognitive functions and white matter abnormalities in MND patients [207]. However, after adjusting for multiple comparisons only few of these relationships remained statistically significant.

The aim of this study was to investigate the cortical and white matter anatomical abnormalities underlying behaviour and cognitive performances in MND patients using a multimodal neuroimaging approach. In this study, a broad battery of neuropsychological tests was used to investigate executive and non-executive performance in MND patients. Previous studies (see Chapter 4) suggest that the cognitive processing of executive and non-executive tests used in this study relies on broad brain networks involving frontal but also posterior brain regions. First, an exploratory vertex-wise analysis across the entire cortex was performed to determine whether MND was associated with a cortical signature of thinning in specific motor and extra-motor regions. Second, the microstructural organization of the major association tracts underlying regions of cortical damage was explored using diffusion tractography. Finally, a possible correlation was investigated between these cortical and white matter measurements with behavioural and cognitive performances in MND patients.

The first hypothesis was that the grey and white matter damage in MND extends to extramotor regions. Based on previous studies, an involvement of a limbic medial dorso-ventral network can be hypothesized. Second, a direct correlation between atrophy of the cortical regions connected by this dorso-ventral medial network and cognitive and behavioural performances is expected.

5.2 Material and methods

Participants, inclusion and exclusion criteria

Patients with MND were recruited from The King's Motor Neurone Disease Care and Research Centre, London, UK and in part from the Barts and The London Motor Neurone Disease Centre, London, UK. Healthy control participants, recruited through a volunteer database and the local community, were matched as closely as possible to the MND group for age, gender and education.

The inclusion criteria for the patients of the present study were the following: (1) having definite, probable or possible MND using the revised El Escorial criteria after excluding other conditions [115]; (2) no family history of MND; (3) no clinical diagnosis of FTD or Primary Progressive Aphasia [90,101]; (4) no history of cerebrovascular disease or any other major systemic, psychiatric or neurological illnesses; (5) no other causes of focal or diffuse brain damage, including lacunae and other evidence of cerebrovascular disease at routine MRI scans; (6) right-handedness; (7) English as first language; (8) not taking any psychoactive medication. We excluded patients with severe dysarthria (MNDFRS-R score on bulbar items 1-3 < 9) [210], severe respiratory insufficiency (FVC < 70% predicted), and insufficiently intelligible speech.

Clinical Assessment and Neuropsychological examination

The Amyotrophic Sclerosis Functional Rating Scale Revised (ALSFRS-R) [210] was used to assess disease severity within two weeks from MRI. All patients were treated with Riluzole.

A comprehensive test battery was developed for the present study including a broad battery of tests assessing executive functions, memory and language. All the patients underwent the neuropsychological tests. Current IQ was evaluated for all subjects with the Wechsler Abbreviated Scale of Intelligence (WASI)[211]. Executive functions were tested using the computerized Wisconsin Card Sorting test (WCST) [182], and the Verbal Fluency Index (Semantic fluency, Phonemic fluency) [169]. Language functions were examined with the Pyramid and Palm Trees test (PPT) [165], the Kissing and Dancing test (KDT) (block randomization was applied) [161], Modified Token test [163]. Symptoms of anxiety and depression were assessed using the Hospital Anxiety and Depression Scale (HADS) [160]. Current behavioural involvement (measuring everyday apathy, executive dysfunction and disinhibition) was assessed using the Frontal Systems Behavioural Scale (FrsBe) [158,159].

According to current consensus criteria, to be diagnosed with MND and cognitive impairment, the patients must score at or below the 5th percentile, compared to age and education matched norms, on at least two distinct cognitive tests sensitive to executive functioning [212].

Ethics statement

The study was approved by the Joint South London and Maudsley and The Institute of Psychiatry NHS Research Ethics Committee (LREC (07/H0807/85) and all participants gave written informed consent.

MRI Data Acquisition

All participants were scanned at the Centre for Neuroimaging Sciences, Maudsley Hospital, Institute of Psychiatry, Psychology and Neuroscience, London UK, using a 3.0-GE Hdx Signa System (General-Electric, Milwaukee, WI). High-resolution structural T1-weighted volumetric images were acquired with full head cover-age, 160 contiguous slices (1.1-mm thickness, with 1.2 × 1.2-mm in-plane resolution), a 256×256×160 matrix and a repetition time/echo time/inversion time (TR/TE/TI) of 7.04/2.8/450 ms (flip angle=20 in., FOV=28 cm). A (birdcage) head coil was used for radiofrequency transmission and reception. Consistent image quality was ensured by a semi-automated quality control procedure.

Diffusion weighted imaging (DWI) data was acquired using a 3T GE Signa HDx MRI scanner (General Electric, Milwaukee, WI, USA) with actively shielded magnetic field gradients (maximum amplitude 40 mT/m). Radio Frequency (RF) signals were transmitted using a body coil and received using an 8-channel head coil. This allowed a parallel imaging (ASSET) speed up factor of two. Volume acquisition was optimized to provide precise whole-brain measurements of the diffusion tensor using a multi-slice peripherally gated twice

refocused spin-echo echo-planar imaging (SE-EPI) sequence, with an echo time (TE) = 104.5 ms and an effective repetition time (TR) that varied between 15 and 20 RR intervals. Each volume had a total of 60 contiguous near-axial slice locations with isotropic (2.4 x 2.4 x 2.4 mm) resolution, and a FoV equal to 30.7 cm and a matrix size of 128x128. In accordance with Jones et al. [213], at each slice location four SE-EPI images were acquired without diffusion gradients being applied (b = 0 s/mm2), alongside DWI with diffusion gradients applied along 32 (b =1300 s/mm2) directions uniformly distributed throughout space.

Cortical Surface Reconstruction using FreeSurfer

All individual T1-weighted scans were initially screened by a radiologist to exclude images with visible clinical abnormalities or large-scale movement artifacts. Scans of insufficient quality were excluded from the analysis.

FreeSurfer analysis suite (*vFS5.3.0) (*http://surfer.nmr.mgh.harvard.edu/) was used to derive models of the cortical surface in each T1-weighted image. These well-validated and fully automated procedures have been described extensively [150-153]. In brief, a single filled white matter volume was generated for each hemisphere after intensity normalization, skull stripping, and image segmentation using a connected components algorithm. Then, a surface tessellation was generated for each white matter volume by fitting a deformable template. This resulted in a triangular cortical mesh for gray and white matter surfaces consisting of approximately 150,000 vertices (i.e. points) per hemisphere. Following standard FreeSurfer pre-processing, each reconstructed surface was then visually inspected for reconstruction errors, and images that did not reconstruct correctly (i.e. with visible anatomical abnormalities) were further excluded from the statistical analysis (dropout 5%). Measures of cortical thickness were computed as the closest distance from the gray and white matter boundary to the gray matter and cerebrospinal fluid boundary at each vertex on the tessellated

surface. Vertex-based estimates of surface area were derived as outlined by [154]. Here, the individual's native surface is initially transformed into a spherical representation, which preserves vertex identities (e.g. total numbers) and original areal quantities, and subsequently registered to a common atlas/template. This registration does not change areal quantities but shifts vertex positions to match the template. Finally, areal quantities are transferred to a common grid via areal interpolation. Here, the final amount of 'area' each face receives on the new grid depends on the overlap between the original source face and the target (i.e. common grid) face. In this way, the fixed target surface is redistributed across one of more source faces and can be used as weighting factor to account for inter-individual's differences in surface reconstructions. Vertex-wise estimates of cortical volume were derived as the product of cortical thickness and surface area at each cerebral vertex. We also computed mean cortical thickness, total surface area and total cortical volume (across hemispheres) for each participant. To improve the ability to detect population changes, each parameter was smoothed using a 5-mm surface-based smoothing kernel.

The statistical analysis was conducted using the SurfStat toolbox (http: //www.math.mcgill.ca/keith/surfstat/) for Matlab (R2013a; MathWorks). Parameter estimates for vertex-based measures of cortical thickness, surface area and cortical volume were estimated by regression of a general linear model (GLM) each vertex *i* and subject *j*, with (1) group and gender as categorical fixed-effects factor; and (2) age, and a total brain measure (i.e. mean CT, total SA, total CV respectively) as continuous covariates, so that

$$Y_i = \beta_0 + \beta_1 \, Group_j + \beta_2 \, IQ_j + \beta_3 \, Age_j + \beta_4 \, TotalBrain_j + \varepsilon_i.$$

Between-group differences were estimated from the fixed-effect coefficient β_1 normalized by the corresponding standard error. Corrections for multiple comparisons across the whole brain were performed using random-field theory (RFT) based cluster-corrected analysis for non-isotropic images using a $p<0.05$ (2-tailed) cluster-significance threshold [155].

Diffusion tensor imaging processing and tractography dissections

ExploreDTI (http://www.exploredti.com) [214] was used to preprocess the diffusion data. Initially eddy current distortion and motion corrections were applied during preprocessing. The b-matrix was then reoriented to allow a more accurate estimation of the tensor orientations [214]. The diffusion tensors were estimated using a non-linear least squares approach. Finally, maps based on Fractional Anisotropy (FA), Mean Diffusivity (MD), Axial Diffusivity (AD) and Radial Diffusivity (RD) were created.

In addition, spherical deconvolution [215,216] was chosen to estimate multiple orientations in voxels containing different populations of crossing fibers [217]. Spherical deconvolution was calculated applying the damped version of the Richardson-Lucy algorithm with a fiber response parameter α =1.5, 200 algorithm iterations and η=0.15 and ν=15 as threshold and geometrical regularization parameters [149]. Fiber orientation estimates were then obtained by selecting the orientation corresponding to the peaks (local maxima) of the fibre orientation distribution (FOD) profiles. To exclude spurious local maxima, we applied both an absolute and a relative threshold on the FOD amplitude [148]. A first "absolute" threshold corresponding to a Hindrance Modulated Orientational Anisotropy (HMOA) threshold of 0.015 was used to exclude intrinsically small local maxima due to noise or partial volume effects with isotropic tissue. This threshold was set to select only the major fiber orientation components and exclude low amplitude spurious FOD components obtained from a gray matter and cerebro-spinal fluid isotropic voxels. A second "relative" threshold of 5% of the maximum amplitude of the FOD was applied to remove remaining unreliable local maxima with values greater than the absolute threshold but that they are still significantly smaller than the main fiber orientation [148].

Whole brain tractography was performed selecting every brain voxel with at least one fiber orientation as a seed voxel. From these voxels, and for each fiber orientation, streamlines

were propagated using a modified Euler integration with a step size of 1 mm. When entering a region with crossing white matter bundles, the algorithm followed the orientation vector of least curvature. Streamlines were halted when a voxel without fiber orientation was reached or when the curvature between two steps exceeded a threshold of 45°. All spherical deconvolution and tractography processing was performed using StarTrack, a freely available matlab software toolbox developed by Dr. Flavio Dell'Acqua at NatBrainLab, King's College London, and based on methods previously described [148].

Using TrackVis (www.trackvis.org), virtual dissections of the tracts of interest were performed in both the left and right hemisphere, were performed on each subject's FA map [218]. All dissections were performed in a systematic manner whilst the experimenter remained blind to the subject's clinical status.

The cingulum was identified as the major tract running in the proximity of those extra-motor areas whose cortical atrophy showed a significant correlation with cognitive performance and psychiatric symptoms rating [44,45]. The cingulum is a medial associative bundle that runs within the cingulated and the parahippocampal gyri all around the corpus callosum. The cingulum contains fibres of different lengths, the longest running from the amygdala, uncus, and parahippocampal gyrus to sub-genual areas of the frontal lobe [84,219]. From the medial temporal lobe, these fibres reach the occipital lobe and arch almost 180 degrees around the splenium to continue anteriorly within the white matter of the cingulate gyrus. The dorsal and anterior fibres of the cingulum follow the shape of the superior aspect of the corpus callosum. After curving around the genu of the corpus callosum, the fibre terminate in the subcallosal gyrus and the paraolfactory area. Shorter fibre connects adjacent areas of the medial frontal gyrus, paracentral lobule, precuneus, cuneus, cingulate, lingual and fusiform gyrus [220]. The cingulum can be divided into an anterior-dorsal component of the cingulum, which constitutes most of the white matter of the cingulate gyrus, and a posterior-ventral component

of the left and right cingulum, running within the parahippocampal gyrus and posterior precuneus [221-223]. To dissect the cingulum a single region of interest is delineated on the fractional anisotropy map. Then, in order to split the cingulum into the anterior-dorsal and posterior-ventral components, a region of interest is defined on a coronal slice identifying the midline of the splenium of the corpus callosum [45].

Statistical analysis

Statistical analysis was performed using SPSS software package (version 21). Independent samples t-tests were used to test differences between MND patients and control in relation to the demographic data, neuropsychological scores and diffusion measurements. Multiple one-way analysis of covariances (ANCOVAs) was done to test differences in neuropsychological tests between MND patients and controls using PPT, KDT, Modified token test as covariates. Shapiro-Wilk normality test was used to assess the normality of distribution of our variables. In the patient group, Pearson or Spearman rank bivariate correlation analysis were used to detect the strength of the correlation between parameter estimates of cortical volume, diffusion measurements and neuropsychological scores. The Pearson correlation coefficient was used when variables were normally distributed and Spearman rank correlation method when variables were not normally distributed. A Bonferroni correction was applied to correct for multiple comparisons (threshold at $p \leq 0.001$).

Role of the PhD student in this experimental study

In this experimental study, my role involved participating in the overall research design, analysing the cortical morphometry using FreeSurfer and performing diffusion tensor imaging processing and tractography dissections. I was also responsible for the statistical analysis and preparation of the manuscript for publication.

5.3 Results

Twenty-four patients with MND and 21 age, education, and gender matched healthy controls were included in the study (Table 7). Shapiro-Wilk test indicated a normal distribution for all the measurements extracted from the neuropsychological tests collected in our MND cohort. One patient (0.04%) scored below the cutoff in at least 2 executive cognitive tests and was classified as MND with cognitive impairment. Table 8 illustrated the ANCOVA analysis to test differences in neuropsychological tests between MND patients and controls using PPT, KDT, Modified token test as covariates.

Table 7. Distribution of characteristics of MND and healthy controls

	Healthy controls (n=21) (N and % or mean ± sd)	**MND (n=24) (N and % or mean ± sd)**	***p***
Age	49.47 (± 8.27)	53.11 (± 12.57)	0.258
Male	17 (80.95%)	21 (87.50%)	0.556
Education (years)	14.71 (± 4.82)	13.58 (± 3.93)	0.392
IQ-WASI	118.04 (± 11.52)	114.33 (± 15.53)	0.364
Limb/bulbar/limb+bulbar onset	NA	22/2/0	-
Disease duration (months)	NA	24.66 (± 14.67)	-
ALSFRS-R	NA	40.60 (± 4.28)	-

sd: standard deviation
WASI= Wechsler Abbreviated Scale of Intelligence. ALSFRS-R: Amyotrophic Lateral Sclerosis Functional Rating Scale Revised. NA= nor applicable

Table 8. ANCOVA analysis between MND patients and healthy controls.

Test	**Healthy controls (mean ± sd)**	**MND (mean ± sd)**	***p***
WCST total errors	48.20 ± 2.06	53.47 ± 2.43	0.206
WCST perseverative responses	50.62 ± 2.62	55.40 ± 3.21	0.312
WCST non perseverative errors	47.78 ± 1.92	52.46 ± 2.26	0.172
WCST perseverative errors	49.79 ± 2.68	53.27 ± 3.15	0.462
Semantic fluency Index	4.11 ± 0.62	3.96 ± 0.67	0.883
Phonemic fluency Index	12.80 ± 1.30	10.68 ± 1.40	0.323
HADS Anxiety	1.78 ± 0.50	1.98 ± 0.54	0.810
HADS Depression	3.70 ± 0.70	2.89 ± 0.75	0.477

Between-group differences in cortical volume and surface area

Patients with MND had significantly reduced total gray matter volume ($t(47) = -8.54$, $p < 0.0001$) and total surface area ($t(47) = -7.45$, $p < 0.001$) relative to controls but no differences in the mean cortical thickness. After covarying for total brain measures, compared with healthy controls, the MND group showed three regions of reduced cortical volume in the left hemisphere: the lateral precentral gyrus ($t_{min} = -4.4164$ $N_{vertices} = 6,552$, $p_{cluster} = 0.000028$), the mid-cingulate cortex ($t_{min} = -4.345$, $N_{vertices} = 2,827$, $p_{cluster} = 0.00049$), and the parahippocampal gyrus ($t_{min} = -4.243$, $N_{vertices} = 1,248$, $p_{cluster} = 0.00783$). In right hemisphere two regions of reduced cortical volume were identified: the medial ($t_{min} = -4.2423$ $N_{vertices} = 2,774$ $p_{cluster} = 0.0005800$) and lateral precentral gyrus ($t_{min} = -4.2436$ $N_{vertices} = 1,248$ $p_{cluster} = 0.0078347$) (Figure 14).

MND patients also showed regions of reduced surface area in the left lateral precentral gyrus ($t_{min} = -3.810$, $N_{vertices} = 7,305$, $p_{cluster} = 0.000019$) and the right lateral ($t_{min} = -3.507$, $N_{vertices} = 3,929$, $p_{cluster} = 0.000049$) and medial precentral gyrus ($t_{min} = -4.689$, $N_{vertices} = 3,890$, $p_{cluster} = 0.000331$). There were no significant clusters of reduced cortical thickness.

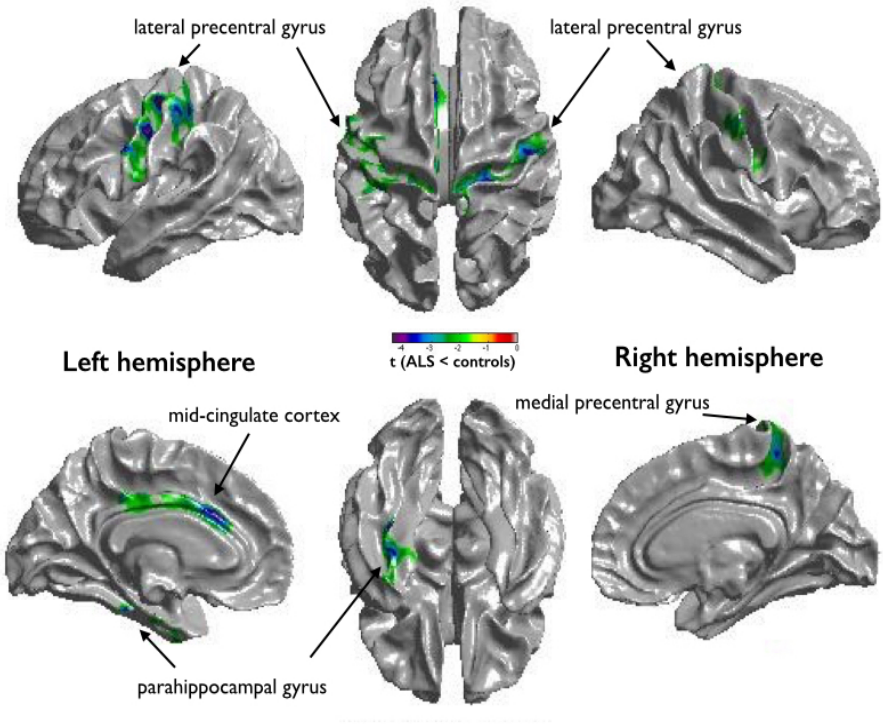

Figure 14. Between-group differences in cortical volume in MND compared to controls.

Correlations between measures of cortical volume and the Amyotrophic Sclerosis Functional Rating Scale Revised (ALSFRS-R)

In the MND group, cortical volume of the left precentral gyrus positively correlated with the ALSFRS-R total score (Rho Spearman = 0.834, $p < 0.001$), ALSFRS-R climbing (Rho Spearman = 0.712, $p < 0.001$) and walking (Rho Spearman = 0.687, $p < 0.001$) items. In the right hemisphere, measures of cortical volume of the medial precentral gyrus were significantly correlated with the ALSFRS-R total score (Rho Spearman = 0.688, $p < 0.001$), ALSFRS-R climbing (Rho Spearman = 0.647, $p = 0.001$) and ALSFRS-R walking (Rho Spearman = 0.647, $p = 0.001$) items. Moreover, we found that cortical volume of right lateral precentral gyrus was positively correlated with the ALSFRS-R total score (Rho Spearman =

0.578, p = 0.003), ALSFRS-R climbing (Rho Spearman = 0.537, p = 0.007) and walking (Rho Spearman = 0.486, p = 0.006) items even though these correlations with cortical volume in the right hemisphere did not survive Bonferroni corrections.

Correlations between measures of cortical volume and neuropsychological assessment

In the MND group, measures of cortical volume of the left mid-cingulate cortex were negatively correlated with HADS depression (Pearson = -0.801, p < 0.001) and anxiety scores (Pearson = -0.809, p < 0.001), WCST total errors (Pearson = -0.620, p = 0.001), WCST perseverative responses (Pearson = -0.620, p = 0.001), WCST perseverative errors (Pearson = -0.613, p = 0.001), and WCST non-perseverative errors (Pearson = -0.619, p = 0.001). Cortical volume of the left parahippocampal gyrus was positively correlated with the PPT words (Pearson = 0.709, p < 0.001), the KDT words (Pearson = 0.713, p < 0.001), and the Modified Token Test Score (Pearson = 0.734, p < 0.001), and was negatively correlated with the Semantic fluency index (Pearson = -0.500, p < 0.001) (Figure 15).

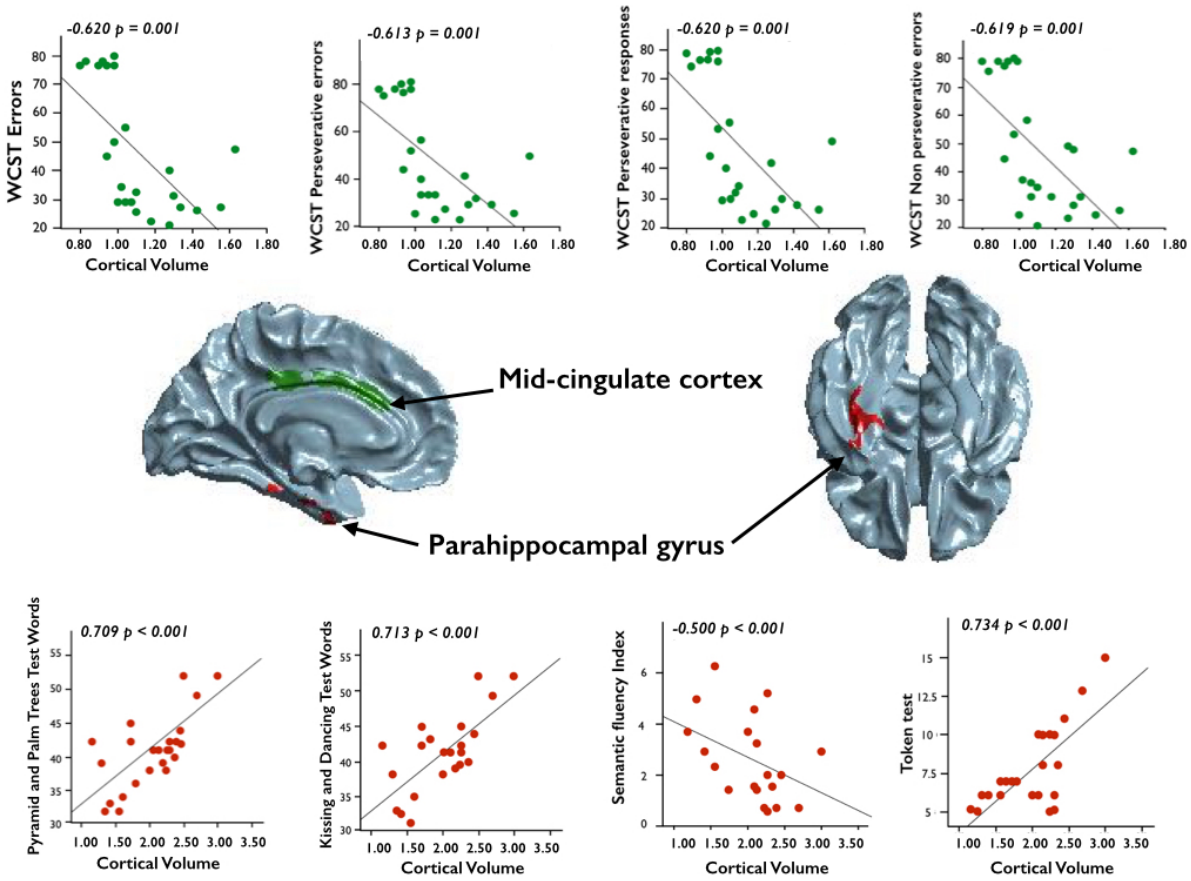

Figure 15. Correlations between measures of cortical volume of the left Mid-cingulate cortex and left parahippocampal gyrus with Neuropsychological test scores.

Between-group differences in white matter tracts and correlations with neuropsychological and clinical scores

In the left dorsal cingulum, MND patients showed significantly reduced number of streamlines ($p = 0.003$, $t_{(47)} = 3.180$) and lower fractional anisotropy ($p < 0.001$, $t_{(47)} = 4.306$) compared with controls. The axial ($t_{(47)} = -4.085$; $p < 0.001$,) and perpendicular diffusivity ($t_{(47)} = -2.915$; $p = 0.005$,) of the left dorsal cingulum were significantly increased when compared with healthy controls (Figure 16).

In the right hemisphere, the dorsal component of the cingulum showed significantly reduced number of streamlines ($p < 0.001$, $t_{(47)} = 4.180$) and lower fractional anisotropy ($p = 0.002$, $t_{(47)} = 3.306$). The axial and perpendicular diffusivity were significantly increased when compared with healthy controls (respectively $p < 0.001$, $t_{(47)} = -4.085$, and $p = 0.005$, $t_{(47)} = -2.915$) (Figure 17).

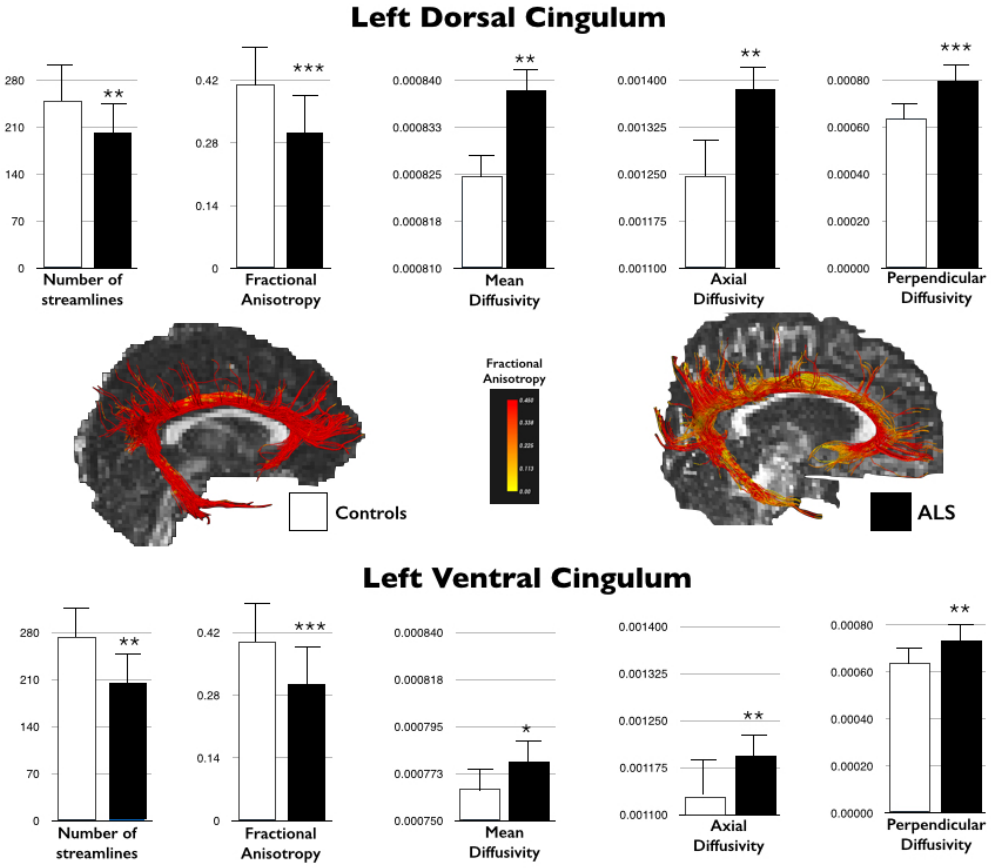

Figure 16. Differences in tract-specific measurements of the Left Dorsal and Ventral Cingulum between control subjects and patients with MND.

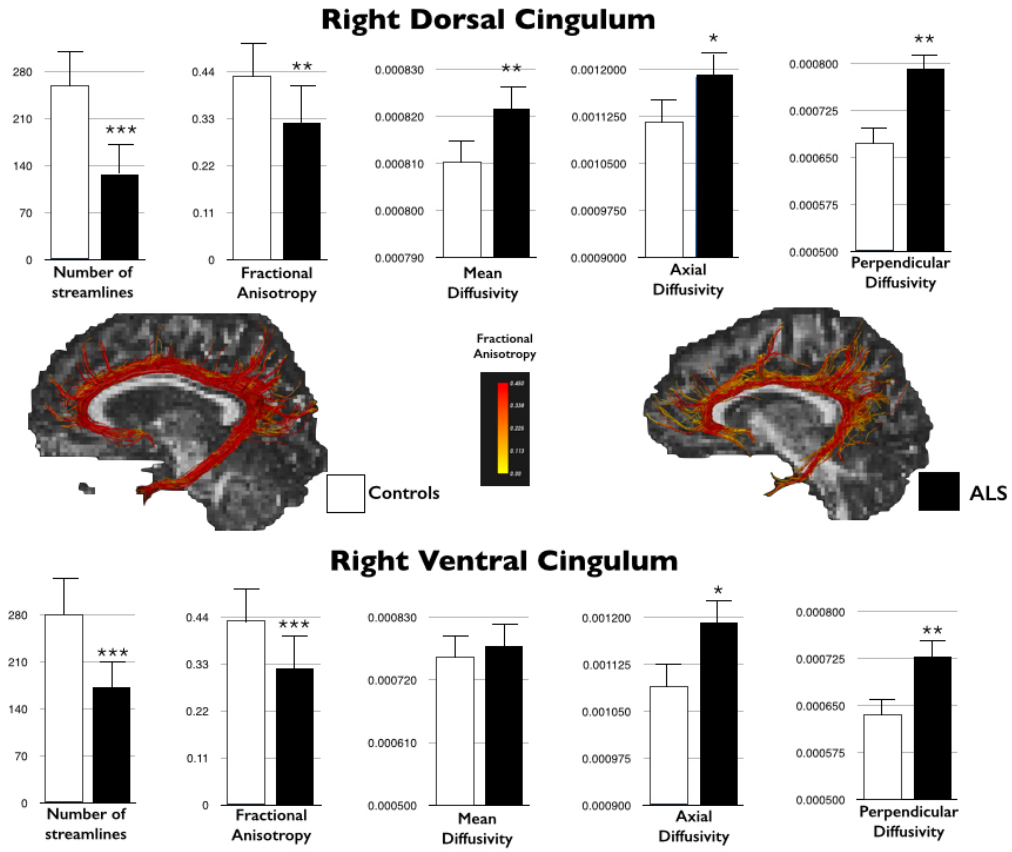

Figure 17. Differences in tract-specific measurements of the Right Dorsal and Ventral Cingulum between control subjects and patients with MND.

In the MND group, diffusion measurements of the left and right dorsal cingulum were significantly correlated with Depression and Anxiety HADS scores. Significant correlations were also found between DTI measurements of the left and right dorsal cingulum and performance in terms of WCST total errors, WCST perseverative responses, WCST perseverative errors, and WCST non-perseverative errors tests (Figure 18).

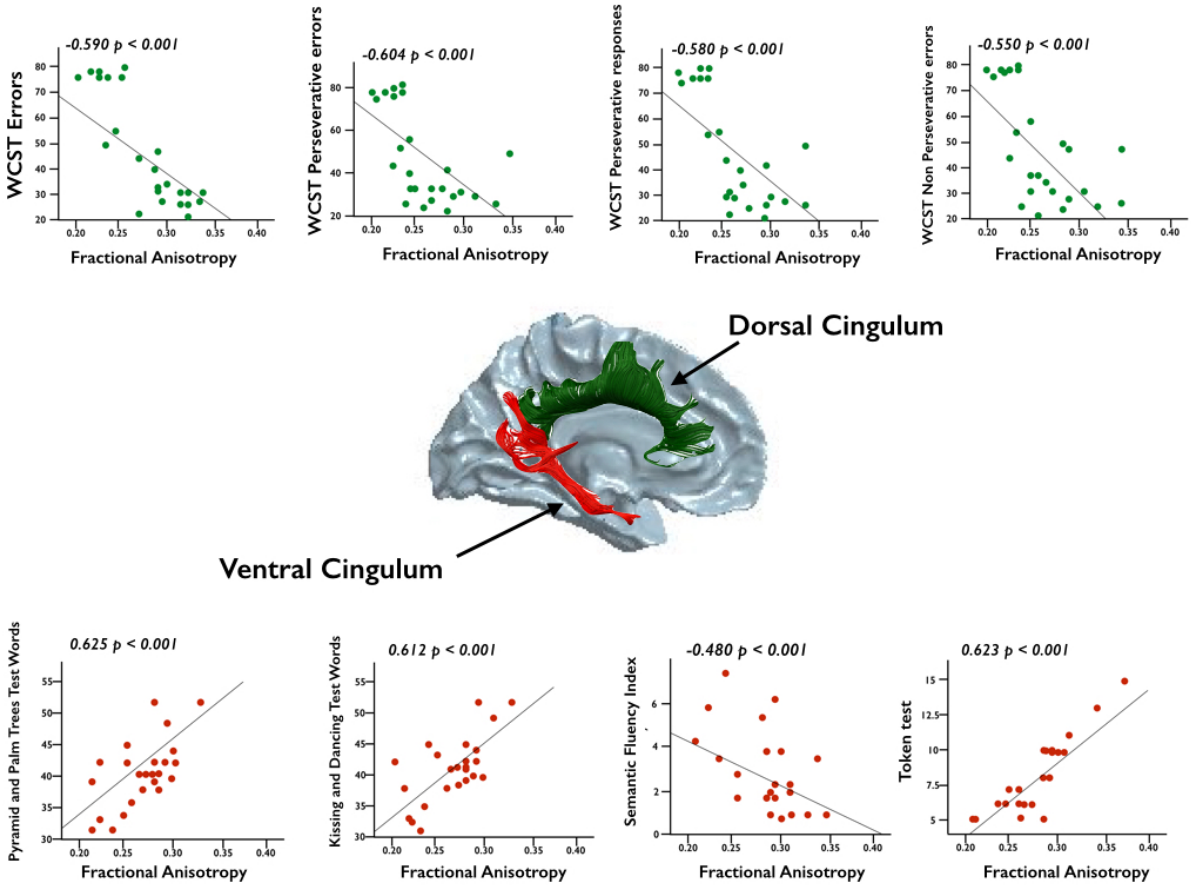

Figure 18. Correlations between fractional anisotropy of the left dorsal and ventral cingulum with Neuropsychological test scores.

In the left ventral cingulum, patients with MND showed significantly reduced number of streamlines ($p = 0.003$, $t_{(47)} = 3.078$), fractional anisotropy ($p < 0.001$, $t_{(47)} = 4.244$), and higher axial ($p = 0.005$, $t_{(47)} = -2.234$) and perpendicular diffusivity ($p = 0.002$, $t_{(47)} = -2.122$) when compared with healthy controls (Figure 16).

Abnormalities in the DTI measurements were also evident in the right ventral cingulum. Number of streamlines and fractional of the right ventral cingulum were significantly lower in the MND group when compared with healthy controls (respectively $p < 0.001$, $t_{(47)} = 4.134$; $p = 0.003$, $t_{(47)} = 3.236$;). Moreover, axial and perpendicular diffusivity were significantly increased when compared with healthy controls (respectively $p < 0.03$, $t_{(47)} = -1.865$, and $p = 0.004$, $t_{(47)} = -2.932$) (Figure 17).

Diffusion measurements of the left ventral cingulum were significantly correlated with Semantic fluency index, PPT-words and KDT-words scores and with the Modified Token Test Score (Figure 18).

Correlations between the Amyotrophic Sclerosis Functional Rating Scale Revised (ALSFRS-R), linguist tests and neuropsychological tests.

Table 9 showed correlations between the ALSFRS-R and neuropsychological tests in MND sample. As reported in the table there is no statistical significant correlation between the ALSFRS-R and the neuropsychological tests under investigation.

Table 10 showed the Pearson correlations between linguist tests and neuropsychological tests in MND sample. As reported in the table there is no statistical significant correlation between the linguistic tests and the neuropsychological tests under investigation.

Table 9. Correlations between Amyotrophic Lateral Sclerosis Functional Rating Scale Revised (ALSFRS-R) and neuropsychological tests.

HADS	**ALSFRS-R**	**Language functions**	**ALSFRS-R**
HADS Anxiety	Pearson = -0.371 p = 0.740	Pyramid and Palm Trees Test words	Pearson = 0.182 p = 0.395
HADS Depression	Pearson = -0.125 0.561	Pyramid and Palm Trees Test pictures	Pearson = -0.041 p = 0.848
FrSBe score		Kissing and Dancing Test words	Pearson = 0.101 p = 0.638
FrsBe post-illness disinhibition score	Pearson = 0.149 p = 0.530	Kissing and Dancing Test pictures	Pearson = -0.239 p = 0.262
FrsBe post-illness apathy score	Pearson = -0.277 p = 0.237	Modified Token Test score	Pearson = 0.042 p = 0.850
FrsBe post-illness executive dysfunction score	Pearson = 0.061 p = 0.804		
FrsBe post-illness total score	Pearson = 0.026 p = 0.916		
Executive functions			
WCST total errors	Pearson = 0.399 p = 0.900		
WCST perseverative responses	Pearson = 0.186 p = 0.461		
WCST non perseverative errors	Pearson = 0.199 p = 0.415		
WCST perseverative errors	Pearson = 0.174 p = 0.476		
Semantic fluency Index	Pearson = -0.117 p = 0.587		
Phonemic fluency Index	Pearson = 0.056 p = 0.797		

Table 10. Pearson correlations between linguist tests and neuropsychological tests.

Test	Pyramid and Palm Trees Test words	Pyramid and Palm Trees Test pictures	Kissing and Dancing Test words	Kissing and Dancing Test pictures	Modified Token Test score
HADS Anxiety	-0.039 p = 0.792	0.265 p = 0.066	0.101 p = 0.492	0.257 p = 0.075	-0.012 p = 0.933
HADS Depression	0.073 p = 0.619	0.177 p = 0.223	0.017 p = 0.907	0.040 p = 0.784	0.097 p = 0.511
FrSBe score	-0.098 p = 0.543	-0.239 p = 0.132	-0.036 p = 0.824	-0.022 p = 0.890	-0.254 p = 0.114
FrsBe post-illness disinhibition score	-0.086 p = 0.587	-0.208 p = 0.187	-0.037 p = 0.818	-0.004 p = 0.981	-0.132 p = 0.411
FrsBe post-illness apathy score	-0.125 p = 0.658	-0.193 p = 0.430	0.013 p = 0.959	0.179 p = 0.464	0.147 p = 0.213
FrsBe post-illness executive dysfunction score	0.044 p = 0.857	-0.296 p = 0.218	0.020 p = 0.935	-0.005 p = 0.984	0.119 p = 0.626
FrsBe post-illness total score	-0.025 p = 0.920	-0.312 p = 0.193	0.014 p = 0.954	0.039 p = 0.872	0.060 p = 0.808
WCST total errors	-0.461 p = 0.054	-0.163 p = 0.518	0.318 p = 0.198	0.522 p = 0.046	0.353 0.151
WCST perseverative responses	0.211 p = 0.417	0.308 p = 0.229	0.301 p = 0.241	0.212 p = 0.414	-0.019 p = 0.944
WCST non perseverative errors	0.230 p = 0.358	0.474 p = 0.047	0.309 p = 0.212	0.155 p = 0.539	0.138 p = 0.585
WCST perseverative errors	0.340 p = 0.168	0.573 p = 0.150	0.316 p = 0.202	0.361 p = 0.141	0.238 p = 0.341
Semantic fluency Index	-0.163 p = 0.457	-0.105 p = 0.635	-0.043 p = 0.846	0.239 p = 0.271	-0.223 p = 0.307
Phonemic fluency Index	-0.057 p = 0.795	-0.260 p = 0.231	-0.050 p = 0.820	-0.104 p = 0.635	-0.170 p = 0.439

5.4 Discussion

This study reported evidence of cortical thinning of the left mid-cingulate cortex and left parahippocampal gyrus and abnormalities of the underlying white matter in MND patients regardless of the presence of pathological cognitive and behavioral dysfunctions.

Abnormalities of the anatomy, metabolism and function of mid-cingulate cortex and parahippocampal gyrus in MND were previously documented using measures of cortical thickness [199], voxel-based morphometry [224], MR spectroscopy [225] and resting-state functional MRI connectivity [226]. Previous studies attributed multiple functions to the mid-cingulate cortex [227-230]. The mid-cingulate cortex receives afferents from orbitofrontal cortex and amygdala [45,84,227,231], which in turn are involved in processing negative emotion states [232]. In addition nociceptive input from the thalamus activates the mid-cingulate cortex and this induces fear and anxiety related to aversive stimuli that trigger avoidance responses [233]. Hence, the mid-cingulate cortex is considered as the region where converging information related to negative emotion states and nociception is elaborated to produce the most appropriate response between reward/approach and fear/avoidance [230]. Degeneration of mid-cingulate cortex could therefore explain abnormal reaction to emotional distress, altered fear activation and distorted punishment/reward processing that may predispose to clinically significant depression and anxiety. Moreover, the mid-cingulate cortex plays a central role in cognitive tasks related to attention for action [234] through its widespread connections to the dorsolateral prefrontal cortex and other cortical and subcortical regions. It is part of the fronto-parietal network for the selection of where and to what to allocate attention and maintenance of goals. The degree of hypoperfusion in the mid-cingulate cortex has been shown to correlate with the Stroop test, WCST categories and with behavioural deficits in frontotemporal dementia and progressive supranuclear palsy [235,236]. These imaging abnormalities in the mid-cingulate cortex have also been reported in familiar frontotemporal

dementia even before symptom onset [237].

The parahippocampal gyrus has been ascribed many functions such as episodic memory, source memory, recollection and visuospatial processing [238]. Beyond these functions, the parahippocampal gyrus is involved in language comprehension [239] underpinning processes of semantic integration [240]. This region plays a central role in object memory and recognition by collecting various inputs of an object from multiple sensory areas in order to constitute a real representation. The cortical areas that form the parahippocampal gyrus are susceptible to pathological and imaging abnormalities in several progressive neurodegenerative disease [241,242]. In Semantic Dementia, which is characterized by impairment of knowledge surrounding word and object identity [90], the severity of semantic deficits has been correlated with loss of integrity of the left anterior temporal lobe and parahippocampal cortex [243].

Our study also showed the involvement of a non-motor white matter tract, the cingulum, in MND [244,245]. In particular, the cingulum was analysed separately in its two components: the dorsal cingulum running within the cingulate gyrus and the ventral cingulum running within the parahippocampal gyrus. Previous studied reported that the dorsal cingulum is involved in emotion processing and attention while the ventral cingulum participates in semantic knowledge and memory [221-223]. These findings support a recent proposal for an anatomical and functional division of the limbic system into three distinct but interconnected networks [84].

In this study, it was found that reduced cortical volume to the left mid-cingulate cortex and damage to the underlying anterior-dorsal component of the cingulum were associated with anxiety, depression and performance on executive function tests. Furthermore, this study showed that damage to the left parahippocampal gyrus and underlying posterior-ventral component of the cingulum was significantly correlated with semantic performance. Overall, in the individual measures of psychiatric symptoms, executive and non-executive tests most

of the MND patients do not show pathological performances. Importantly, only one patient with MND had a mild cognitive impairment according to current consensus criteria while some other patients only showed executive or non-executive deficits. This is not the first study in literature that investigated the anatomical abnormalities and their relationship with cognitive performance in non-demented MND patients. Mioshi E. et al reported a similar pattern of grey matter atrophy in extra-motor regions of the temporal and parietal lobe between patients with MND and cognitive decline and patients with MND without cognitive decline [224]. However, atrophy was much more marked in the MND group with cognitive decline. Sarro L. et al investigated the relationship between DTI tractography imaging metrics of the corpus callosum, cingulum and uncinate fasciculus and cognitive and behavioral functions in 16 non-demented patients with MND [207]. Among these, only two of them had a mild executive impairment and 11 out of 16 scored below the fifth percentile in at least one cognitive test. Interestingly, they found that in the MND group the severity of white matter tract degeneration of the long association tracts was associated with neuropsychological performance. This could give further support to this hypothesis that even though our MND sample does not show evidence of marked pathological cognitive deficits and psychiatric symptoms, the anatomical differences identified in MND patients could indicate a vulnerability to subsequent development of executive and non-executive deficits and psychiatric symptoms. Future longitudinal studies are necessary to understand the predictive value of the *in vivo* cortical measures and the link between anatomical abnormalities and neuropsychiatric symptoms.

This study is not without limitations. First, the effect of motor impairment on cognitive performance in MND is not well established in the literature [246-249]. In this study, patients with severe dysarthria, respiratory insufficiency and insufficiently intelligible speech were

not included. The final cohort included patients with mild motor disability (mean ALSFRS-R was 40.60). The ANCOVA analysis showed (Table 8) that there were no statistical significant differences in terms of neuropsychological test performances between MND patients and controls even when PPT, KDT, Modified token test are used as covariates. Indeed, Table 9 shows no statistically significant correlations between ALSFRS-R score and neuropsychological performance and Table 10 shows no statistically significant correlations between KDT scores and other cognitive performance and between language performance in general and other cognitive tests. Second, correlations between neuroimaging measurements and neuropsychological scores may have been driven by a binomial distribution of the MND group. Indeed, Figures 16 and 19 show a group of 7 patients with significant impaired performance on the WSCT while the rest of participants had performance within the normal range. However, a Shapiro-Wilk test indicated a normal distribution for all the measurements extracted from the neuropsychological tests collected in our MND cohort. We are therefore confident that our results demonstrate a direct link between executive performance and anatomical measurements of cortical and white matter anatomy that is not mediated by the motor and language deficits. The lack of correlation between impairment in motor and language performance and scores in depression/anxiety tests suggests a similar conclusion can be drawn for these clinical scores. Finally, we were unable to verify the underlying pathology and severity of the anatomical changes in all our patients. Neuroimaging methods employed in this study offer only an indirect measurement of cortical and white matter integrity and often several factors may affect the sensitivity and specificity of these approaches [250].

In conclusion, our findings suggest that neuronal damage to specific limbic regions is associated with emotional processing and cognitive performances in MND. These findings

are in line with previous studies that attributed multiple roles in cognition and behaviour to the mid-cingulate cortex and parahippocampal gyrus. MRI assessment of cortical damage and underlying white matter anatomy could have clinical applications for early detection of patients at high risk of developing psychiatric and cognitive symptoms in MND.

Chapter 6 Experimental Study 2: Fronto-temporal networks and behavioural symptoms in primary progressive aphasia.

6.1 Introduction

Patients with Primary Progressive Aphasia (PPA) show a gradual decline in the language functioning with a relative sparing of other cognitive domains [88]. However, as the disease progresses, patients with PPA are at high risk of developing other problems. For instance, in the first report of PPA, four out of six patients were described as displaying additional symptoms of 'distress', 'sadness and reactive depression' after the onset of the language deficits [88]. A more recent prevalence study conducted in 55 patients with PPA indicates that apathy and depression are very common in almost half of the patients, followed by changes in eating, aberrant motor behaviour, night-time behaviour, agitation, disinhibition and irritability, which are observed in about one fifth of the patients [251]. These behavioural symptoms further aggravate their autonomy in the activities of daily living [252].

The prevalence and severity of behavioural symptoms in PPA change over time. Banks and Weintraub (2008) showed that patients with PPA of short illness duration (<5 years) had higher prevalence of mood-related symptoms compared to PPA patients with longer duration [253]. The latter group showed a higher prevalence of symptoms typical of the behavioural variant of fronto-temporal dementia (bvFTD) [253]. In advanced stages of the disease the overlap between the PPA and bvFTD is significant: approximately 75% of patients with PPA develop severe behavioural problems whereas 65% of patients with bvFTD manifest clear language impairment [254]. This overlap of the two forms supports the contention that these

diseases belong to a common family of focal degenerations and that the individual clinical syndromes reflect the differential anatomy of the disease onset and progression trajectory [255]. This is particularly true for patients with the semantic variant of PPA who are at higher risk of developing behavioural symptoms compared with the other variants and in which the anatomical hallmark is represented by a marked atrophy of the anterior temporal lobes [256]. Rohrer and Warren [257] found that in addition to anterior temporal lobe atrophy, the most significant anatomical cortical changes in PPA patients with behavioural symptoms occur in the orbitofrontal cortex. Moreover, these authors reported that atrophy of the orbitofrontal cortex correlated mainly with anxiety, apathy, irritability and abnormal eating behaviour, whereas damage to the anterior temporal lobe correlated predominantly with disinhibition.

The anterior temporal and orbitofrontal regions are directly linked by the uncinate fasciculus, a major associative tract already reported as significantly damaged in PPA [67,258]. While the association between degeneration of the uncinate fasciculus and semantic deficits is well documented, the role of the uncinate fasciculus in behavioural symptoms associated with PPA is not known.

The aim of this study was to determine the anatomical abnormalities underlying behavioural symptoms in relatively early PPA patients. Diffusion tensor imaging tractography was used to assess the microstructural organization of the major association tracts connecting to the orbitofrontal cortex and/or anterior temporal lobe. It was also measured the cortical thickness of the orbitofrontal cortex and anterior temporal lobe to determine whether white matter degeneration correlates with the degree of cortical atrophy. The first hypothesis was that severity of behavioural symptoms in PPA is associated with damage to the network that directly connects orbitofrontal cortex and anterior temporal lobe, namely the uncinate fasciculus. Furthermore, based on previous studies a direct correlation between atrophy of these brain cortices and severity of behavioural symptoms can be hypothesized. Finally, a

direct correlation between cortical atrophy of the orbitofrontal cortex and anterior temporal lobe and white matter integrity of the uncinate fasciculus is expected.

6.2 Material and methods

Participants and Clinical Assessment

Thirty-three patients with PPA and twenty-six healthy controls matched for age, gender and handedness, were recruited through the Primary Progressive Aphasia Program at the Cognitive Neurology and Alzheimer's Disease Centre, Northwestern University Feinberg School of Medicine.

An experienced clinician (Prof. Marsel Mesulam) made the diagnosis of PPA. According to the current criteria, establishing a clinical diagnosis of PPA involves a 2-step process as described in Gorno-Tempini et al. (2011)[90]. Patients should first meet basic PPA criteria based on Mesulam's initial and current guidelines (Mesulam 2001)[86]. A PPA clinical diagnosis requires a progressive, isolated deterioration of speech and/or language functions during the initial phase of the disease. Exclusion criteria include specific cause of aphasia such as stroke or tumor. Behavioral disturbances should not be the main cause of functional impairment. Once a PPA diagnosis is established, the clinical classification of PPA patients into one of the variants described in Gorno-Tempini's et al. (2011) occurs on the basis of the speech and language features that are characteristic of a specific variant [90]. Behavioural symptoms were assessed using the Frontal Behavioural Inventory (FBI). The Frontal Behavioural Inventory (FBI) was originally developed and standardized with the purpose of differentiate the behavioural variant of Frontotemporal Dementia (bvFTD) from other dementias and to quantify the severity of behavioural symptoms [259]. The FBI is based on the evaluation of the patient's caregiver that for each item scores the severity of symptoms in a scale between 0 and 3 (0 = never, 1 = mild or occasional, 2 = moderate, 3 = severe or very

frequent). The FBI is composed of 24 items divided into twelve items for negative behaviour symptoms (FBI negative symptoms score) and twelve for positive symptoms (FBI positive symptoms score). The FBI negative symptoms score contains three items that evaluate behavioural symptoms in relation to language impairment (item 9 logopenia; item 10, aphasia and verbal apraxia; item 11, comprehension and semantic deficits). An operational definition of FTD included a minimum FBI score of 27.

To effectively evaluate the behavioural symptoms in the PPA patients, we subtracted these three language-related items from the FBI negative symptoms score and the FBI total scores. All statistical analyses were therefore performed using corrected scores for the total FBI and negative FBI.

Magnetic resonance image acquisition, diffusion tensor imaging and data processing

Magnetic resonance imaging (MRI) acquisitions were carried out on a 3T Siemens Trio MRI system at the Centre for Translational Imaging, Northwestern University of Chicago. T1-weighted MPRAGE sequences were acquired with the following parameters: repetition time 2300 ms; echo time 2.86 ms; flip angle, 9; field of view, 256 mm; 60 slices; slice thickness 1.0mm. FreeSurfer image analysis suite (version 4.5.0) (http://surfer. nmr.mgh.harvard.edu/) was used to measure cortical thickness on T1-weighted MPRAGE images. Cortical thickness estimates were calculated by measuring the distance between representations of the white–grey and pial–CSF boundaries across each point of the cortical surface [260]. Statistical surface maps were generated using a general linear model that displayed differences in cortical thickness between PPA patients and healthy controls for each vertex along surface representations of the entire neocortex using an FDR of 0.001 [67,261].

For the tractography analysis a total of 72 contiguous near-axial slices were acquired, using an acquisition sequence fully optimized for diffusion imaging, providing isotropic (2 x 2 x 2

mm) resolution and whole head coverage. Sixty diffusion-weighted images (b-value of 1000s/mm2) were acquired together with eight images with no diffusion gradient applied. DTI processing was performed using Explore DTI (http://www.exploredti.com). Subject motion and geometrical distortions were corrected simultaneously with reorientation of the b-matrix. Remaining outliers due to subject motion and cardiac pulsation were excluded using the RESTORE function [262]. The tensor model was fitted to the data using a non-linear least square fitting procedure. DTI scalar maps, including fractional anisotropy and radial diffusivity were calculated and exported. Whole brain tractography was performed using a b-spline interpolated streamline algorithm (step size 0.5mm; fractional an- isotropy threshold 0.15; angle threshold 35). The whole brain tractography was imported in TrackVis (http://www.trackvis.org) using software written in Matlab 2009b (http://www.matworks.com) [263].

Virtual dissections and tract-specific measurements

TrackVis was used to perform the virtual in vivo dissection of the three tracts of interest according to previously published methods [44,45,67,68,82,264]. Tractography dissections were obtained using manually defined regions of interest on the axial, coronal, and sagittal fractional anisotropy images. The following tracts were dissected.

The uncinate fasciculus originates from the temporal pole, uncus, parahippocampal gyrus, and amygdala, then after a U-turn, enter the floor of the external/extreme capsule. Between the insula and the putamen, the uncinate fasciculus runs inferior to the inferior fronto-occipital fasciculus before entering the orbital region of the frontal lobe. Here, the uncinate splits into a ventro-lateral branch, which terminates in the anterior insula and lateral orbitofrontal cortex, and an antero-medial branch that continues towards the olfactory cortex, the medial orbitofrontal cortex and the frontal pole. To dissect the uncinate fasciculus, a

temporal region of interest was defined around the white matter of the anterior temporal lobe and a second region of interest was defined around the white matter of the anterior floor of the external/extreme capsule [44,219].

The inferior fronto-occipital fasciculus originates from the inferior and medial surface of the occipital lobe. As it leaves the temporal lobe, the inferior fronto-occipital fasciculus narrows in section and its fibres gather together at the level of the extreme/external capsule just above the uncinate fasciculus. In the frontal lobe its fibres spread to form a thin sheet curving dorsolaterally to terminate mainly in the inferior frontal gyrus. The most ventral fibres continue anteriorly and terminate in the medial fronto-orbital region and frontal pole [219]. To dissect the inferior fronto-occipital fasciculus a first region of interest was delineated around the white matter of the occipital lobe and a second region of interest was delineated around the white matter the external/extreme capsule [44].

Finally, the inferior longitudinal fasciculus is a ventral associative bundle connecting the occipital and temporal lobes. To dissect the inferior longitudinal fasciculus the first region of interest was defined around the white matter of the anterior temporal lobe and the second region of interest around the white matter of the occipital lobe [44].

For each tract of interest, number of streamlines, fractional anisotropy, mean diffusivity, axial and perpendicular diffusivity were extracted as indices of microstructural composition and architecture of the brain tissue. The number of streamlines was considered a surrogate of tract volume and atrophy. In dementia syndromes the number of streamlines is reduced in association with the severity of the pathology and clinical symptoms [265].

Fractional anisotropy is a quantitative index of the degree of anisotropy of the biological tissue and of microstructural integrity. Fractional anisotropy gives information about the organization of the tissue and the microarchitecture of the fibres. In normal brain it varies from 0.1 (e.g. in the grey matter) to 0.8 or higher in the white matter. In pathological tissue

(e.g. demyelination, oedema, degeneration etc.) fractional anisotropy reduces [144]. Perpendicular and radial diffusivity correspond to the the diffusivity along the principal directions of the diffusion tensor. Perpendicular diffusivity is generally considered a sensitive measure for axonal/myelin damage, although interpretation of their changes in regions with crossing fibres is not always straightforward [144]. The dissector (L.D.), blind to the results of the cortical atrophy analysis and to the identity of the individual data sets, was trained by an expert tractographer (M.C.) on 10 practice data sets and dissections for this study began only when high reliability was achieved.

Statistical analysis

All statistical analyses were performed using SPSS software package (version 21). Independent samples t-test were run to examine group differences in number of streamlines, fractional anisotropy, axial and radial diffusivity of the different tracts of interest. One-way ANOVA for independent samples was used to investigate differences among controls and all PPA subtypes except the mixed variant that included only 2 patients. Bonferroni correction was applied to correct for multiple comparisons. All p values are provided uncorrected. Spearman bivariate correlation analysis was used to detect the strength of the correlations between tract specific measurements and severity of behavioural symptoms.

Role of the PhD student in this experimental study

In this experimental study, my role involved study design, cortical surface morphometry using FreeSurfer, diffusion tensor imaging processing and tractography dissections. I was

also responsible for the statistical analysis and writing up of the manuscript which has been published in Neurology in 2016 as a full article.

6.3 Results

Demographic, clinical and behavioural features of our sample are reported in Table 11 and Table 12. Among the PPA patients, eight received a descriptive diagnosis of logopenic variant (PPA-L), eight of non-fluent/agrammatic variant (PPA-G), seven of semantic (PPA-S), two of mixed variant and eight of unclassified/severe variant.

The PPA-S group were younger compared to the other variants and had higher prevalence of behavioural symptoms as reported in the FBI total scores and FBI positive symptoms scores. Neither PPA variants scored above the minimum operational score to define FTD.

Table 11. Demographic, clinical data and behavioural features of PPA and healthy controls.

	Patients with PPA (n= 33) *(N or mean ± sd)*	**Healthy controls (n= 26)** *(N or mean ± sd)*	**Group comparisons**
Age, years	64.88 (±6.60)	62.61 (±8.19)	p=0.282
Duration of illness, years	3.63 (±1.80)	-	-
Sex, n			
Male	13	14	
Female	20	12	p=0.269
Handedness (EHI score)	97.12 (±7.70)	93.65 (±9.85)	p=0.135
FBI negative score	6.39 (±5.53)	-	-
FBI positive score	3.93 (±5.15)	-	-
FBI total score	10.51 (±9.63)	-	-

FBI = Frontal Behavioural Inventory; EHI = Edinburgh Handedness Inventory. Group comparisons were by t-test or Chi-squared.

Variable	PPA-L (n=8) *(mean ± sd)*	PPA-G (n=8) *(mean ± sd)*	PPA-S (n=7) *(mean ± sd)*	PPA mixed (n=2) *(mean ± sd)*	PPA unclassified (n=8) *(mean ± sd)*
Age, years	66.13 (±6.98)	65.13 (±5.64)	57.14 (±3.71)*	68.50 (±10.60)	69.25 (±10.53)
Duration of illness, years	3.36 (±2.17)	3.61 (±1.19)	3.47 (±1.25)	5.75 (±6.01)	3.56 (±0.86)
FBI negative score	4.00 (±3.74)	4.93 (±5.17)	10.79 (±6.05)	6.00 (±8.48)	6.50 (±5.42)
FBI positive score	1.25 (±1.38)	2.50 (±4.10)	9.71 (±6.67)*	6.50 (±7.77)	2.37 (±2.61)
FBI total score	6.00 (±3.66)	7.43 (±8.68)	20.50 (±11.75)*	12.50 (±16.26)	8.87 (±6.40)

Table 12. Demographic, clinical and behavioural features of the PPA variants.
FBI = Frontal Behavioural Inventory; Statistically different versus other variants ($p < 0.05$). PPA-L = logopenic variant; PPA-G = nonfluent/agrammatic variant; PPA-S = semantic dementia; PPA mixed = mixed or unclassified/severe; PPA unclassified = unclassified variant.

White matter connections analysis

The left uncinate fasciculus of PPA patients showed a significantly reduced number of streamlines ($p < 0.001$, $t_{(54)}$ value = 7.942), lower fractional anisotropy ($p < 0.001$, $t_{(54)}$ = 3.253) and a significant increase in axial ($p < 0.001$, $t_{(54)}$ = -2.849) and perpendicular diffusivity ($p = 0.020$, $t_{(54)}$ = -2.264) compared with healthy controls.

The number of streamlines was significantly reduced also in the right uncinate fasciculus of PPA patients when compared with healthy controls ($p < 0.001$, $t_{(54)}$ = 5.193) (Figure 19). ANOVA between PPA subtypes and controls showed statistically significant differences between groups in the number of streamlines ($F = 4.933$; $p = 0.001$), axial diffusivity ($F = 5.038$; $p < 0.001$) perpendicular diffusivity ($F = 7.902$; $p < 0.001$) and medial diffusivity ($F = 7.243$; $p < 0.001$). Abnormalities in the left uncinate fasciculus were particularly evident for the semantic subtype (Figure 20).

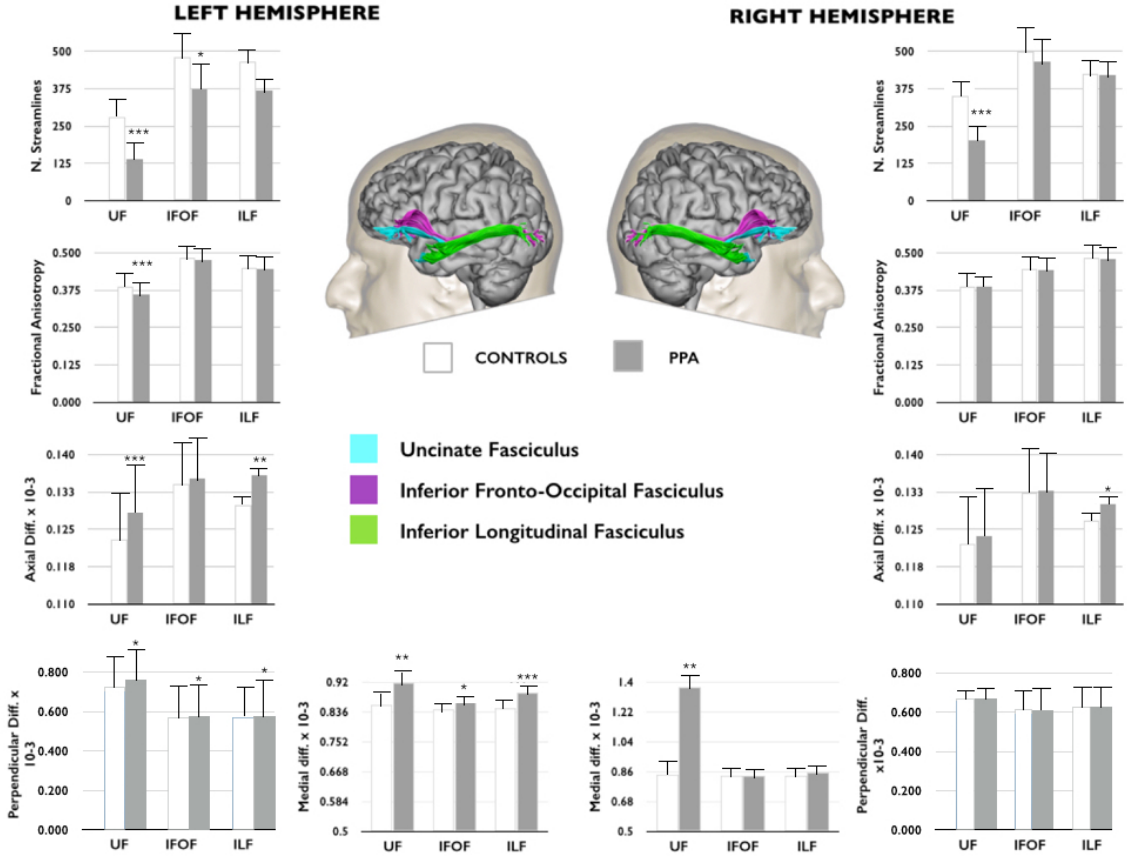

Figure 19. Differences in tract-specific measurements.
Differences in tract-specific measurements of the uncinate fasciculus (UF), inferior fronto-occipital fasciculus (IFOF) and inferior longitudinal fasciculus (ILF) between controls and patients with primary progressive aphasia (PPA). Measurements of the number of streamlines, fractional anisotropy, axial diffusivity and perpendicular diffusivity are reported for the tracts of interest. Statistically significant differences between controls and patients within each tract are indicated with asterisks (*p < 0.05; **p < 0.01; ***p < 0.001; Bonferroni threshold for significance = 0.0016).

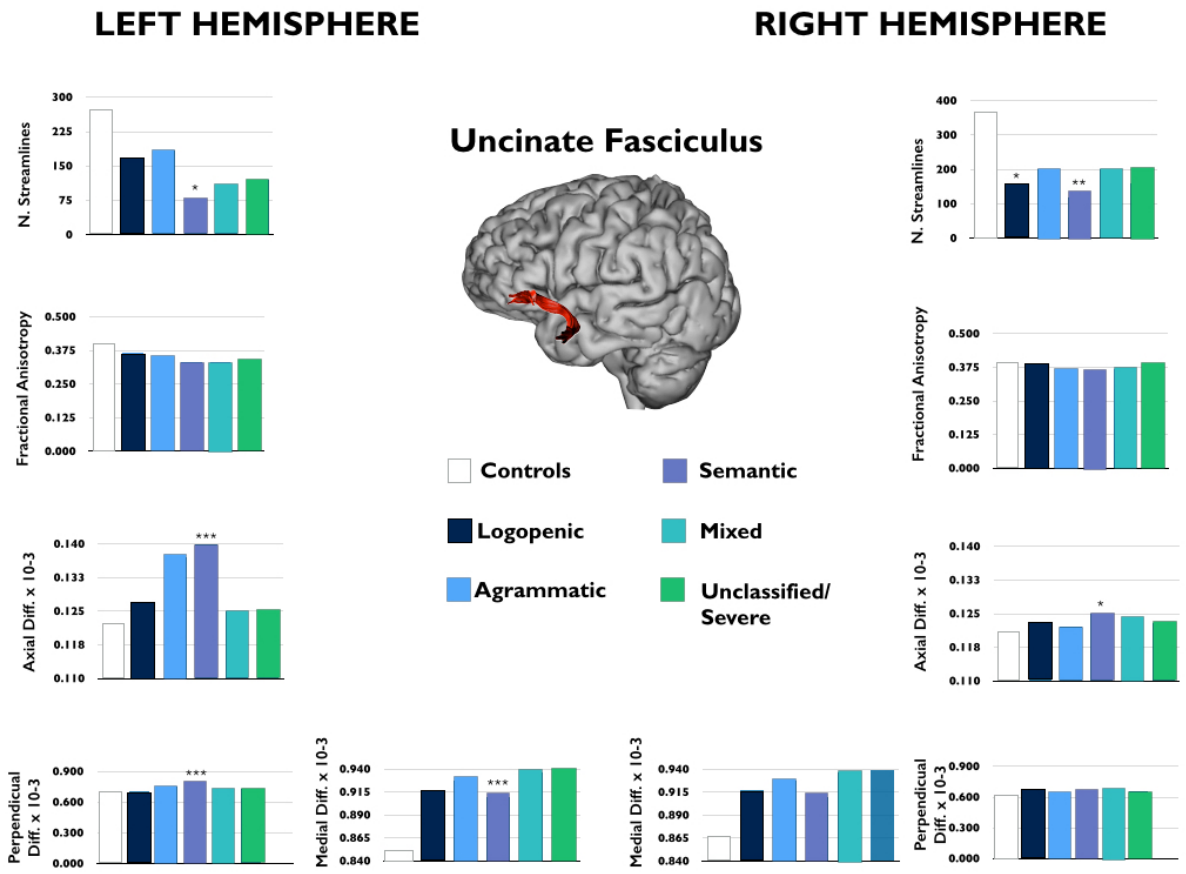

Figure 20. Differences in tract-specific measurements of the uncinate fasciculus among the different PPA variants. Statistically significant differences between controls and patients are indicated with asterisks (*p < 0.05; **p < 0.01; ***p < 0.001.

In the left uncinate fasciculus, the number of streamlines and fractional anisotropy were inversely correlated with total FBI scores (Spearman = -0.549, p = 0.001 and Spearman = -0.490, p < 0.001, respectively) and with both positive (Spearman = -0.530, p = 0.001 and Spearman = -0.500, p < 0.001, respectively) and negative FBI scores (Spearman = -0.460, p < 0.001 and Spearman = -0.450, p < 0.001, respectively), whereas axial and perpendicular diffusivity correlated directly with total FBI scores (Spearman = 0.450, p < 0.001 and Spearman = 0.540, p < 0.001, respectively) and with both positive (Spearman = 0.400, p < 0.001 and Spearman = 0.600, p < 0.001, respectively) and negative FBI scores (Spearman = 0.575, p < 0.001 and Spearman = 0.540, p < 0.001, respectively). These correlations indicate that behavioural symptoms are associated with poorer white matter integrity (Table 13)

(Figure 21). In the right uncinate fasciculus axial diffusivity was correlated with negative (Spearman = 0.443, p = 0.005), positive (Spearman = 0.432, p = 0.005) and total FBI scores (Spearman = 0.421, p = 0.001); perpendicular diffusivity was correlated with FBI negative, positive and total scores (Spearman = 0.497, p < 0.001; Spearman = 0.576, p < 0.001; Spearman = 0.580, p < 0.001) (Table 5.3). ANOVA between PPA subtypes and controls showed statistically significant differences in the number of streamlines (F = 4.840; p = 0.003) and axial diffusivity (F = 3.943; p < 0.04), which were particularly evident for the semantic subtype (Figure 21).

Table 13. Correlations between tract-specific measurements of the tracts of interest and neuropsychiatric assessments in PPA patients**.**

Tract	DTI	FBI negative scores	FBI positive scores	FBI total scores
Left UF	N streamlines	Rho Spearman = -0.460 p < 0.001	Rho Spearman = -0.530 p = 0.001	Rho Spearman = -0.549 p = 0.001
	Fractional anisotropy	Rho Spearman = -0.450 p < 0.001	Rho Spearman = -0.500 p < 0.001	Rho Spearman = -0.490 p < 0.001
	Axial diffusivity	Rho Spearman = 0.575 p < 0.001	Rho Spearman = 0.400 p < 0.001	Rho Spearman = 0.450 p < 0.001
	Perpendicular diffusivity	Rho Spearman = 0.540 p < 0.001	Rho Spearman = 0.600 p < 0.001	Rho Spearman = 0.540 p < 0.001
Right UF	N streamlines	Rho Spearman = 0.120 p = 0.045	Rho Spearman = -0.038 p = 0.915	Rho Spearman = 0.071 p = 0.852
	Fractional anisotropy	Rho Spearman = -0.120 p = 0.321	Rho Spearman = -0.231 p = 0.609	Rho Spearman = -0.321 p = 0.432

	Axial diffusivity	Rho Spearman = 0.443 p = 0.005	Rho Spearman = 0.432 p = 0.005	Rho Spearman = 0.421 p = 0.001
	Perpendicular diffusivity	Rho Spearman = 0.497 p < 0.001	Rho Spearman = 0.576 p < 0.001	Rho Spearman = 0.580 p < 0.001
Left IFOF	N streamlines	Rho Spearman = 0.111 p = 0.787	Rho Spearman = 0.243 p = 0.154	Rho Spearman = 0.221 p = 0.432
	Fractional anisotropy	Rho Spearman = -0.332 p = 0.143	Rho Spearman = -0.076 p = 0.667	Rho Spearman = -0.259 p = 0.780
	Axial diffusivity	Rho Spearman = 0.456 p = 0.235	Rho Spearman = -0.045 p = 0.987	Rho Spearman = 0.234 p = 0.567
	Perpendicular diffusivity	Rho Spearman = 0.768 p = 0.078	Rho Spearman = 0.346 p = 0.890	Rho Spearman = 0.789 p = 0.567
Right IFOF	N streamlines	Rho Spearman = 0.678 p = 0.908	Rho Spearman = 0.531 p = 0.543	Rho Spearman = 0.721 p = 0.772
	Fractional anisotropy	Rho Spearman = -0.523 p = 0.852	Rho Spearman = -0.863 p = 0.642	Rho Spearman = -0.074 p = 0.732
	Axial diffusivity	Rho Spearman = 0.532 p = 0.345	Rho Spearman = 0.563 p = 0.563	Rho Spearman = 0.341 p = 0.145
	Perpendicular diffusivity	Rho Spearman = 0.342 p = 0.126	Rho Spearman = 0.231 p = 0.453	Rho Spearman = 0.171 p = 0.876
Left ILF	N streamlines	Rho Spearman = 0.753 p = 0.654	Rho Spearman = 0.165 p = 0.456	Rho Spearman = 0.176 p = 0.765
	Fractional anisotropy	Rho Spearman = -0.564 p = 0.900	Rho Spearman = 0.453 p = 0.653	Rho Spearman = -0.078 p = 0.564
	Axial diffusivity	Rho Spearman = 0.546 p = 0.098	Rho Spearman = 0.075 p = 0.908	Rho Spearman = 0.234 p = 0.567
	Perpendicular diffusivity	Rho Spearman = 0.456 p = 0.455	Rho Spearman = -0.567 p = 0.564	Rho Spearman = 0.456 p = 0.456

Right ILF	N streamlines	Rho Spearman = 0.056 p = 0.456	Rho Spearman = 0.123 p = 0.389	Rho Spearman = 0.245 p = 0.489
	Fractional anisotropy	Rho Spearman = -0.345 p = 0.134	Rho Spearman = -0.089 p = 0.789	Rho Spearman = -0.453 p = 0.378
	Axial diffusivity	Rho Spearman = 0.345 p = 0.231	Rho Spearman = 0.245 p = 0.456	Rho Spearman = 0.345 p = 0.567
	Perpendicular diffusivity	Rho Spearman = 0.456 p = 0.078	Rho Spearman = 0.678 p = 0.890	Rho Spearman = 0.356 p = 0.145

UF = Uncinate Fasciculus; IFOF = Inferior Fronto-Occipital Fasciculus; ILF = Inferior Longitudinal Fasciculus; FBI = Frontal Behavioural Inventory. N streamlines = Number of streamline

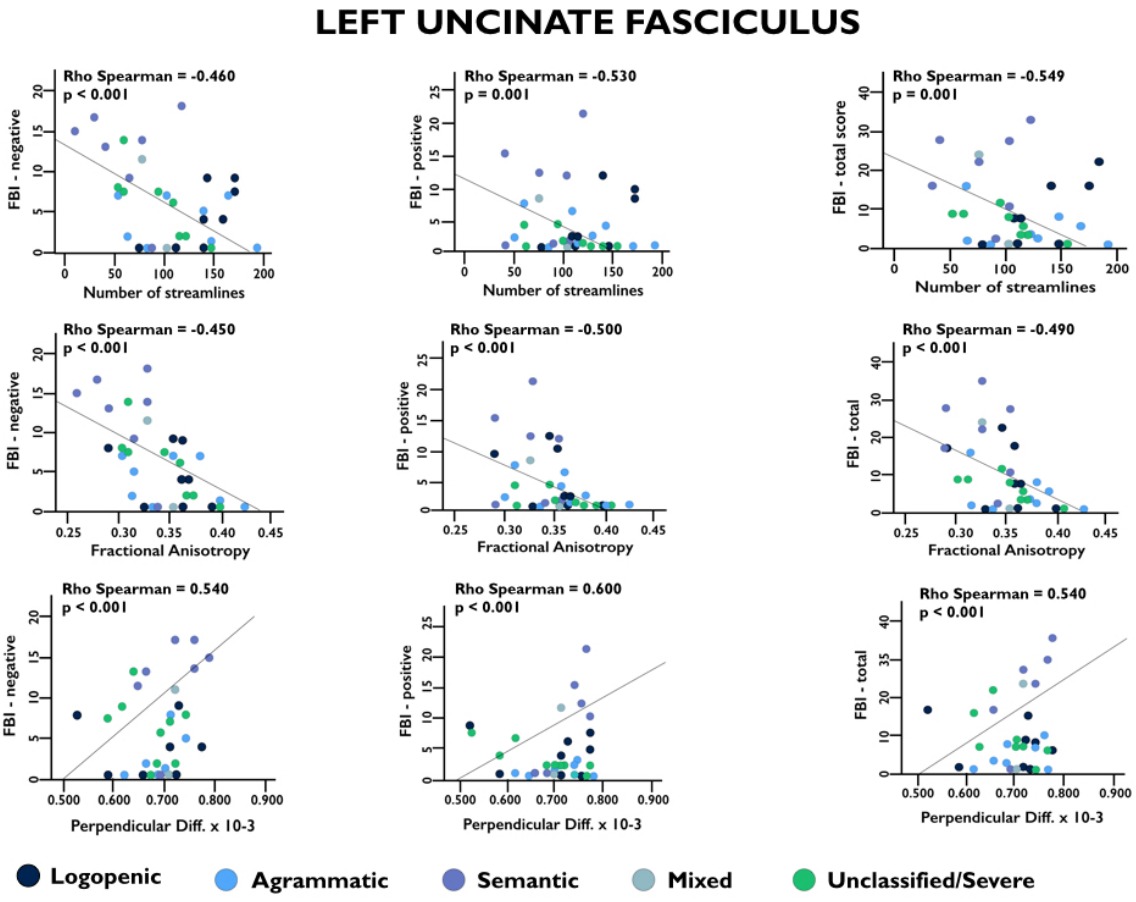

Figure 21. Correlations between left uncinate diffusion measurements and FBI scores.

In the left inferior fronto-occipital fasciculus, the patients with PPA showed significantly fewer streamlines ($p = 0.036$, $t_{(54)} = 2.256$) and higher perpendicular diffusivity ($p = 0.028$, $t_{(54)} = -2.145$) when compared with healthy controls. No statistically significant differences were found for this tract in the right hemisphere (Figure 19). ANOVA between PPA subtypes and controls did not show statistically significant differences between groups in terms of DTI measurements (Figure 22). No statistically significant correlations between any of the tractography measurements of the inferior fronto-occipital fasciculus and the scores of the FBI were found (Table 13).

In the inferior longitudinal fasciculus, PPA patients showed a statistically significant increase of axial diffusivity in both sides (left: $p = 0.002$, $t_{(54)} = -3.342$; right: $p = 0.030$, $t_{(54)} = -2.223$) and perpendicular diffusivity in the left side ($p = 0.020$, $t_{(54)} = -2.396$) (Figure 19). ANOVA between PPA subtypes and controls did not show statistically significant differences between groups in terms of DTI measurements (Figure 23). No significant correlations were found between diffusivity measurements of the inferior longitudinal fasciculus and scores on the FBI (Table 13).

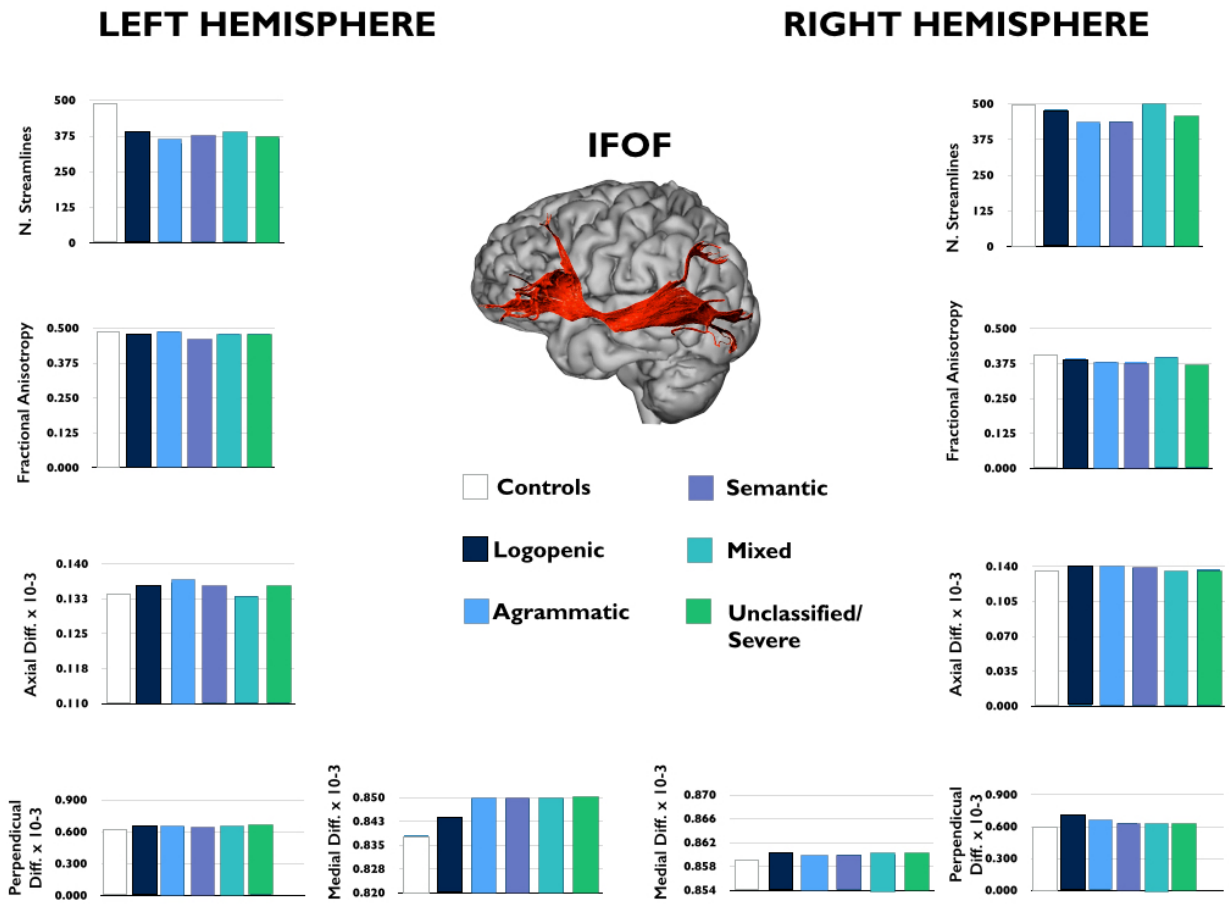

Figure 22. Differences in tract-specific measurements of the inferior fronto-occipital fasciculus among the different PPA variants.
Statistically significant differences between controls and patients are indicated with asterisks (*p < 0.05; **p < 0.01; ***p < 0.001.

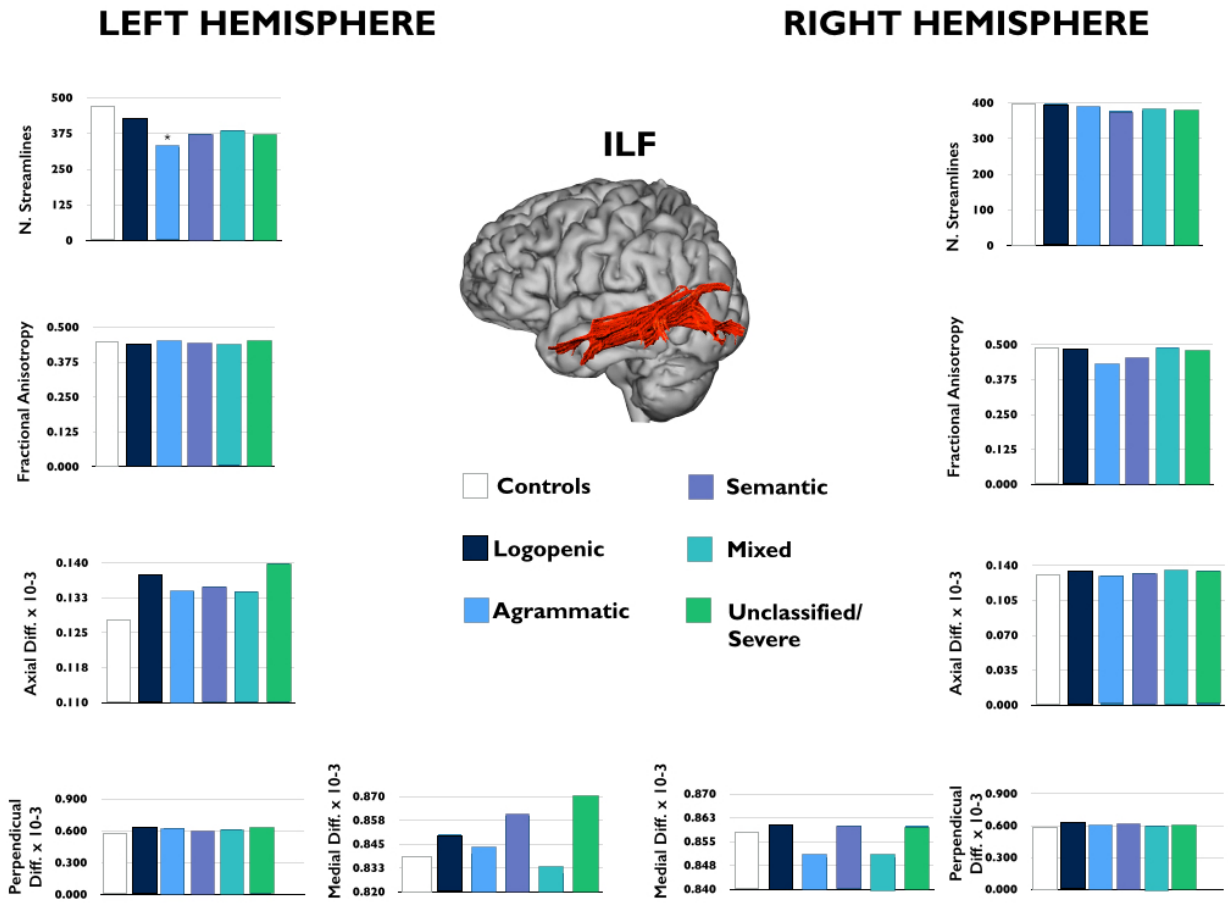

Figure 23. Differences in tract-specific measurements of the inferior longitudinal fasciculus among the different PPA variants.
Statistically significant differences between controls and patients are indicated with asterisks (*p < 0.05; **p < 0.01; ***p < 0.001.

Cortical Thickness analysis

A whole brain analysis showed significant cortical atrophy of the left temporal-parietal and frontal regions in the PPA compared with controls (Figure 24). A region of interest approach confirmed that compared with healthy controls, PPA patients showed significant atrophy in the left ($p < 0.001$, $t_{(57)} = 4.367$) and right ($p = 0.014$, $t_{(57)} = 2.537$) orbitofrontal cortex and in the left ($p = 0.001$, $t_{(57)} = 3.391$) and right ($p = 0.004$, $t_{(57)} = 2.996$) anterior temporal lobe. Cortical thickness of the regions of interest in the left orbitofrontal and anterior temporal cortex were inversely correlated with negative scores (Spearman = -0.460, $p = 0.001$ and

Spearman = -0.521, p = 0.001, respectively), positive scores (Spearman = -0.523, p = 0.001 and Spearman = -0.590, p < 0.001, respectively), and total scores in the FBI (Spearman = -0.534, p = 0.001 and Spearman = -0.580, p < 0.001, respectively) (Figure 24). Correlations between the right anterior temporal lobe and the scores on the FBI were less significant (Table 14).

In addition, cortical thickness measurements of both AT and OFC cortex were directly correlated with fractional anisotropy (Spearman = 0.488, p = 0.003 and Spearman = 0.524, p = 0.001, respectively), and inversely correlated with axial diffusivity (Spearman = -0.570, p = 0.001 and Spearman = -0.378, p = 0.007, respectively) and perpendicular (Spearman = -0.580, p = 0.001 and Spearman = -0.513, p = 0.002, respectively) (Table 15). Similar correlations were found for the right uncinate fasciculus (Table 16). No correlations were found between cortical thickness measurements and DTI measurements of the inferior fronto-occipital fasciculus and inferior longitudinal fasciculus (Table 15 and 16).

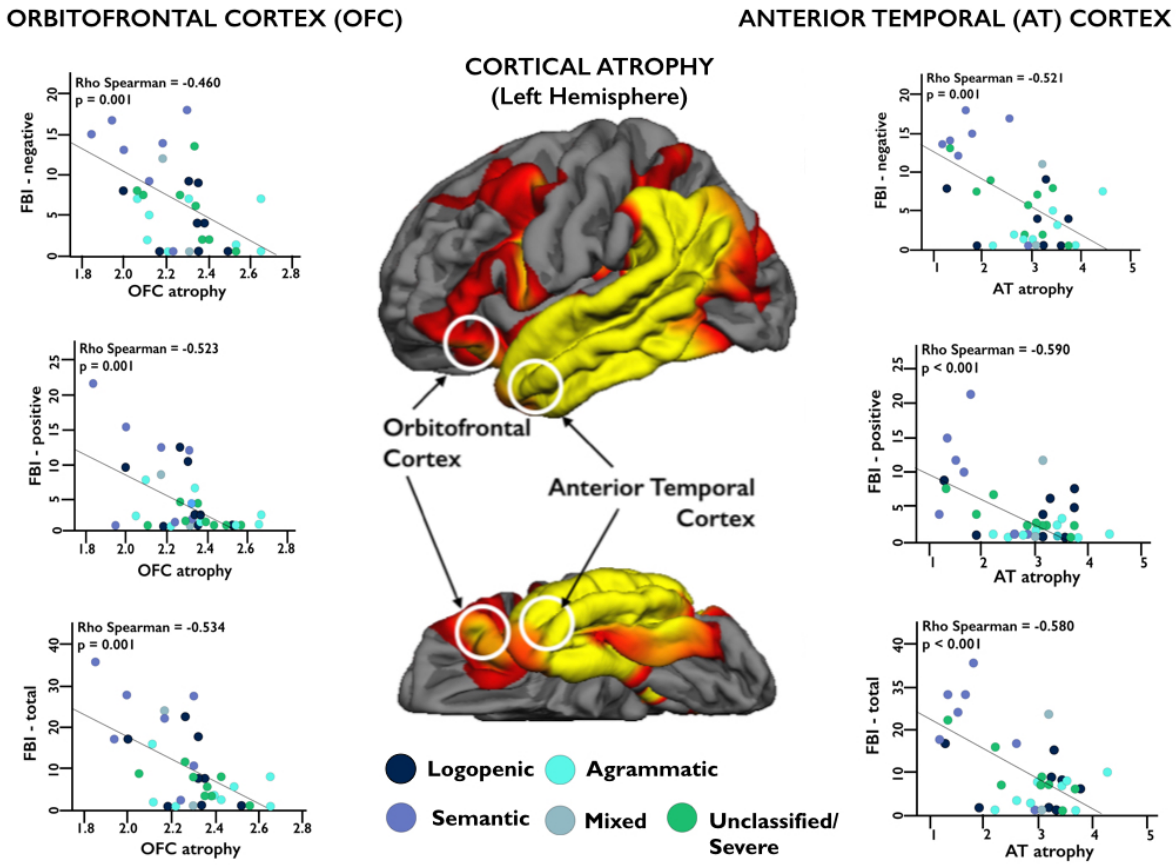

Figure 24. Correlations between cortical thickness and FBI scores.
Correlations between left orbito-frontal cortex (OFC) and anterior temporal lobe (AT) and Frontal Battery Inventory (FBI) negative, positive and total scores.

Table 14. Correlations between cortical thickness analysis of the orbitofrontal and anterior temporal lobe cortices and neuropsychiatric assessments in PPA patients.

Region	FBI negative scores	FBI positive scores	FBI total scores
Left OFC	Rho Spearman = -0.460 p = 0.001	Rho Spearman = -0.523 p = 0.001	Rho Spearman = -0.534 p = 0.001
Right OFC	Rho Spearman = -0.323 p = 0.099	Rho Spearman = -0.467 p = 0.004	Rho Spearman = -0.379 p = 0.015
Left ATL	Rho Spearman = -0.521 p = 0.001	Rho Spearman = -0.590 p < 0.001	Rho Spearman = -0.580 p < 0.001
Right ATL	Rho Spearman = -0.332 p = 0.049	Rho Spearman = -0.499 p = 0.004	Rho Spearman = -0.467 p = 0.010

FBI = Frontal Behavioural Inventory; OFC = orbitofrontal cortex; ATL= anterior temporal lobe cortex.

Table 15. Correlations between cortical thickness analysis of the left orbitofrontal and left anterior temporal lobe cortices and tract-specific measurements of the tracts of interest in the left hemisphere.

		Left OFC	Left ATL
Left Uncinate fasciculus	N streamlines	Rho Spearman = 0.324 p = 0.125	Rho Spearman = 0.567 p = 0.004
	Fractional anisotropy	Rho Spearman = 0.524 p = 0.001	Rho Spearman = 0.488 p = 0.003
	Axial diffusivity	Rho Spearman = -0.378 p = 0.007	Rho Spearman = -0.570 p = 0.001
	Perpendicular diffusivity	Rho Spearman = -0.513 p = 0.002	Rho Spearman = -0.580 p = 0.001
Left Inferior frontooccipital fasciculus	N streamlines	Rho Spearman = 0.008 p = 0.689	Rho Spearman = 0.089 p = 0.956
	Fractional anisotropy	Rho Spearman = 0.342 p = 0.132	Rho Spearman = 0.035 p = 0.918
	Axial diffusivity	Rho Spearman = -0.090 p = 0.943	Rho Spearman = -0.090 p = 0.678
	Perpendicular diffusivity	Rho Spearman = -0.453 p = 0.178	Rho Spearman = 0.089 p = 0.900
Left Inferior longitudinal fasciculus	N streamlines	Rho Spearman = -0.345 p = 0.234	Rho Spearman = -0.278 p = 0.342
	Fractional anisotropy	Rho Spearman = -0.198 p = 0.456	Rho Spearman = -0.147 p = 0.564
	Axial diffusivity	Rho Spearman = -0.089 p = 0.456	Rho Spearman = -0.189 p = 0.390
	Perpendicular diffusivity	Rho Spearman = 0.089 p = 0.889	Rho Spearman = -0.078 p = 0.990

OFC = orbitofrontal cortex; ATL= anterior temporal lobe cortex. N streamlines = Number of streamlines

Table 16. Correlations between cortical thickness analysis of the right orbitofrontal and right anterior temporal lobe cortices and tract-specific measurements of the tracts of interest in the right hemisphere.

		Right OFC	**Right ATL**
Right Uncinate fasciculus	N streamlines	Rho Spearman = 0.023 p = 0.901	Rho Spearman = 0.236 p = 0.187
	Fractional anisotropy	Rho Spearman = 0.043 p = 0.812	Rho Spearman = 0.067 p = 0.712
	Axial diffusivity	Rho Spearman = -0.007 p = 0.968	Rho Spearman = -0.464 p = 0.007
	Perpendicular diffusivity	Rho Spearman = -0.207 p = 0.248	Rho Spearman = -0.615 p < 0.001
Right Inferior frontooccipital fasciculus	N streamlines	Rho Spearman = -0.036 p = 0.841	Rho Spearman = -0.181 p = 0.312
	Fractional anisotropy	Rho Spearman = -0.140 p = 0.438	Rho Spearman = 0.085 p = 0.639
	Axial diffusivity	Rho Spearman = 0.023 p = 0.899	Rho Spearman = -0.011 p = 0.953
	Perpendicular diffusivity	Rho Spearman = 0.077 p = 0.668	Rho Spearman = -0.106 p = 0.557
Right Inferior longitudinal fasciculus	N streamlines	Rho Spearman = -0.347 p = 0.048	Rho Spearman = -0.157 p = 0.384
	Fractional anisotropy	Rho Spearman = -0.076 p = 0.672	Rho Spearman = 0.118 p = 0.514
	Axial diffusivity	Rho Spearman = 0.309 p = 0.081	Rho Spearman = -0.148 p = 0.412
	Perpendicular diffusivity	Rho Spearman = 0.211 p = 0.238	Rho Spearman = -0.189 p = 0.292

OFC = orbitofrontal cortex; ATL= anterior temporal lobe cortex. N streamlines = Number of streamlines

6.4 Discussion

In the present study diffusion tensor imaging tractography was used to demonstrate that damage to the uncinate fasciculus, which directly connects the orbitofrontal and anterior temporal cortex is associated with behavioural symptoms in PPA. This study also reported that atrophy to the anterior temporal and orbitofrontal regions correlates with behavioural symptoms in PPA patients. Furthermore, severity of white matter damage of the uncinate

fasciculus correlated with cortical atrophy of both anterior temporal and orbitofrontal regions. These findings suggest a link between damage to a fronto-temporal network and behavioural symptoms in PPA.

Despite clear evidence of damage to other ventral tracts, the lack of a statistical correlation between integrity of the inferior fronto-occipital fasciculus or the inferior longitudinal fasciculus and behavioural symptoms confirms the functional specialization of the uncinate network. In previous studies, degeneration of the uncinate fasciculus has been found to correlate with semantic processing deficits in PPA patients [67,258]. There are, however, no previous studies that reported an association between degeneration of the uncinate fasciculus and behavioural symptoms in PPA. This association has been frequently described in other conditions affecting anterior temporal and orbitofrontal regions. In bvFTD, for example, the white matter damage in the uncinate fasciculus correlates with severity of apathy, impulsivity, inappropriate sexual behaviour and hoarding [83]. In patients with anterior temporal lobe epilepsy the emergence of psychotic symptoms is associated with damage to the white matter of the uncinate fasciculus [266]. Finally, in subjects with psychopathy [82] altered integrity of the uncinate fasciculus correlates with severity of antisocial behaviour, which include poor behavioural control, impulsivity, need for stimulation, proneness to boredom, lack of realistic goals, and irresponsibility. Overall these studies confirm that the uncinate fasciculus has a major role in a wide range of comportments and that its damage is associated with behavioural deficits irrespective of the underlying pathology.

The uncinate fasciculus is the major association pathway between the anterior part of the temporal lobe and the ventral frontal region [44]. In the anterior temporal lobe, the uncinate fasciculus originates primarily from the temporopolar cortex and the amydgala. In the ventral frontal region, the uncinate fasciculus projects directly to the olfactory cortex, orbitofrontal cortex and subgenual cortex. The temporopolar cortex is a multimodal ‘convergence zone’

that integrates sensory information for object-identity representation [33,267]. Here the stimuli are processed independently of their reward or punishment value [232]. Sensory stimuli are also conveyed directly to the amydgala, where they are processed for their emotional/affective valence. Information that reaches the temporopolar cortex and amygdala is then projected onto the ventral frontal regions through the uncinate fasciculus. The orbitofrontal cortex in turn computes the reward values of primary reinforces [268] (e.g. taste, touch and smell) and associate them with the stimuli carried through the uncinate fasciculus. The associative learning realized by the neurons in the orbitofrontal cortex provides the goals for subsequent decision-making and appropriate motor response [83]. In light of this, our findings suggest that behavioural symptoms in PPA could be attributed to impaired associative learning for sensory information associated with object-identity representation and processing of emotional/affective valence of stimuli [269,270].

Among all PPA patients, we confirmed that those with the semantic variant have higher prevalence of behavioural symptoms. Neuropathological causes of PPA are heterogeneous and the neuroimaging measurements are indirect and do not allow to infer the underlying anatomical abnormalities. Autoptic studies show that 45% of cases with PPA have been found to have Alzheimer disease (AD) pathology; the remaining 55% of cases present evidence of frontotemporal lobar degeneration (FLTD) pathology, distributed approximately equally between TAR DNA-binding protein 43 (TDP-43), proteinopathy (FTLD-TDP) and tauopathy (FTLD-tau) [271]. Although there is no a direct correspondence between each clinical subtype of PPA and specific neuropathological causes [90], previous studies revealed that FTLD-TDP of type C is the most common pathology in the semantic variant. FTLD-TDP of type C is characterized by numerous dystrophic neuritis (DNs) [271,272] with associated neuronal and synaptic loss [33,273]. One could therefore speculate that cortical atrophy reflects

neuronal loss at cortical level while diffusivity measurements are secondary axonal degeneration of the white matter fibres connecting cortical regions affected by the pathology.

Some limitations of the study deserve further discussion. The PPA cohort we investigated was of a relatively small size and its composition rather heterogeneous. Large cohorts of PPA patients are difficult to recruit especially in the early stage of the disease and when assessment involves extensive neuropsychological and neuroimaging measurements. While the sample size of our study is similar to previous reports, a larger sample could help to generalise our findings and reach a better characterisation of the anatomy underpinning each variant. In fact, due to the small number of subjects in the mixed group, we had to exclude from the ANOVA analysis this variant.

Another important limitation to acknowledge is the use of FBI to assess behavioural symptoms. Objective assessment and quantification of behavioural symptoms is difficult to obtain, especially in patients that do not reach clinical criteria for FTD. Indeed, FBI scores are provided by the caregiver and therefore are highly subjective and variable over time. The FBI were not obtained from the healthy controls as they were all independent and had no need for a caregiver. While we can assume that all controls had no behavioural symptoms, the lack of scores limited our ability to test for between-group differences in FBI scores and understand the degree of deviation from normality. While it is evident that the semantic variant presented with the most severe behavioural scores, other variants significantly contributed to the correlations between FBI scores and anatomical measurements. Of the 7 patients with semantic variant, only three showed scores that were above the cut-off (27 out of a maximum of 72) for clinically significant symptoms. The second variant with high scores was the logopenic group with 3 out of 8 patients presenting scores above 15 but below the cut-off. This indicates that while at the group level only the semantic variant presented

with statistically significant high scores compared to the other variants, a large degree of overlap between all variants was evident. Finally, another limitation of the study is the cross-sectional design, which does not allow to understand the predictive values of our findings for the detection of those subjects at higher risk of developing fronto-temporal dementia.

In conclusion, these findings support the conclusion that the emergence of neuropsychiatric symptoms in PPA patients is associated with degeneration of the uncinate fasciculus and atrophy of its cortical projections. These results identify the ventral temporo-frontal connections as a major network underlying normal behaviour in humans. These findings could have important implications for early detection of behavioural changes in PPA and in other neurodegenerative disorders in general. Future studies using higher resolution datasets and advanced methods for fibre crossing [148,149] could help distinguish within the uncinate fasciculus different networks responsible for different behavioural manifestations. Moreover, longitudinal studies are necessary to determine the predictive value of brain imaging methods looking at the anatomical integrity of the fronto-temporal networks in PPA.

Chapter 7 Experimental Study 3: Frontal networks in adults with autism spectrum disorder.

7.1 Introduction

In Autistic Spectrum Disorder (ASD), structural and functional neuroimaging studies showed that damage to the frontal and temporal cortex, caudate nucleus, cerebellum, amygdala and hippocampus was associated with the impairment in social, emotion and language processing [274-286]. These cortical and subcortical structures are connected by a system of white matter tracts composed of short and long white matter bundles [287]. In the recent years the development of diffusion imaging has permitted to study these bundles in the living human brain and understand disconnection mechanism in ASD.

Different electrophysiological and imaging studies have suggested that in ASD several higher-order areas have reduced or increased connectivity since early development. These findings led to the proposal of 'atypical connectivity' theories to explain higher-order task deficits in ASD [288-292]. Within this framework ASD is considered as a neurodevelopmental disorder characterized by aberrant network development. However, it remains unclear whether disconnectivity is specific to individual tracts or rather part of a more generalized brain abnormality.

In this experimental study two complementary approaches were used to analyse white matter connections in adults with ASD. In the first part of the study, Tract-Based-Spatial Statistics (TBSS) was applied for a whole-brain analysis of white matter integrity [293-296].

TBSS is a fully automated, operator-independent approach with the potential to identify white matter differences at the whole-brain level. TBSS has the advantage of being operator-

independent but can be limited in identifying between-group differences within specific tracts as differences can be often found in regions containing more than one tract. For this reason, in the second part of the study DT-MRI tractography was used to focus on specific tracts in greater detail. DT-MRI tractography is a MRI method for the virtual reconstruction of 3D white matter trajectories and the quantification of tissue microstructural integrity in the living human brain [44]. DT-MRI tractography permits tract-specific analysis of white matter bundles and indirect volumetric measurements (e.g. number of streamlines and tract volume) that cannot be extracted with TBSS. Tractography has been applied to a large number of neurodevelopmental conditions, including psychopathy, dyslexia, callosal agenesis and schizophrenia [45,82,264,297-301]. In these conditions DT-MRI tractography has demonstrated that white matter abnormalities are present along the entire course of the fibre rather than be localized within circumscribed areas.

In this study, the first aim was to determine if the white matter damage in ASD is diffuse of localized to specific tracts and whether these white matter abnormalities were associated with the severity of symptoms in social interactions, repetitive behaviour and communication.

The first hypothesis was that ASD is underpinned by an 'atypical connectivity' involving associative tracts. Based on previous studies, an involvement of the arcuate fasciculus, uncinate fasciculus and cingulum is expected. Finally, a direct correlation between the degree of microstructural alteration of the associative tracts and autistic symptom severity can be hypothesized.

7.2 Material and methods

Participants, inclusion and exclusion criteria

61 male right-handed adults with ASD and 61 matched neurotypical male controls aged 18 to 45 years were recruited by advertisement and assessed in the Institute of Psychiatry at Kings

College London and the Autism Research Centre at the University of Cambridge. The Wechsler Abbreviated Scale of Intelligence [211] was used to assess the overall intellectual ability of the participants. Patients with ASD were diagnosed according to International Statistical Classification of Diseases, 10th Revision research criteria (ICD10-R), confirmed using the Autism Diagnostic Interview-Revised (ADI-R)[156]. All cases of ASD reached ADI-R algorithm cut-off values in the three domains of autism characteristics (social reciprocity A1-A4 subscores, language and communication B1-B4 subscores, repetitive and restricted behaviours and interests C1-C4 subscores), although failure to reach cut-off in one of the domains by one point was permitted. Current symptoms were assessed using the Autism Diagnostic Observation Schedule (ADOS)[302] but were not used as inclusion criteria. The ADOS is a semi-structured assessment of communication, social interaction and imaginative use of materials. Module 4 is designed for use with verbally fluent adolescents or adults, and describes a standardized interview/observational assessment consisting of 9-14 activities with 31 accompanying ratings. Autism-Spectrum Quotient (AQ), Empathy Quotient (EQ) and Systemizing Quotient (SQ) were also used.

The exclusion criteria for the patients of the present study were as follows: (1) a history of psychotic disorders; (2) head injury; (3) genetic disorder associated with ASD; (4) any medical condition affecting brain function (e.g. epilepsy); (5) current use of antipsychotic medication, mood stabilizers, or benzodiazepines; (6) or a history of substance misuse (including alcohol).

All participants gave informed written consent in accordance with ethics approval by the National Research Ethics Committee, Suffolk, England.

MRI Data Acquisition

All participants were scanned with MRI scanners operating at 3T (GE Medical Systems

HDx).

High-resolution structural T1-weighted volumetric images were acquired with full-head coverage, 196 contiguous slices (1.1mm thickness, with 1.09 x 1.09mm in-plane resolution), a 256 x 256 x 196 matrix and a repetition time/echo time of 7/2.8ms (flip angle 20°, field of view 28cm). An 8-channel head-coil was used for radiofrequency transmission and reception allowing a parallel imaging (ASSET) speed up factor of 2. Consistent image quality was ensured by a semi-automated quality control procedure. DT-MRI data were acquired using a spin-echo echo-planar imaging double refocused sequence providing whole head coverage with isotropic image resolution (2.4 x 2.4 x 2.4mm; 32 diffusion-weighted volumes with different non-collinear diffusion directions with b-factor 1300 s/mm^2, and six non-diffusion-weighted volumes; 60 slices without slice gap; echo time = 104.5ms; repetition time = 20R-R intervals; 128 x 128 acquisition matrix; field of view 307 x 307mm). The acquisition was gated to the cardiac cycle using a digital pulse oximeter placed on participants' forefinger.

Diffusion tensor imaging processing and tractography dissections

ExploreDTI (http://www.exploredti.com) was used to preprocess the diffusion data [214]. Initially eddy current distortion and motion corrections were applied during preprocessing. The b-matrix was then reoriented to allow a more accurate estimation of the tensor orientations [214]. The diffusion tensors were estimated using a non-linear least squares approach [303]. Finally, maps based on Fractional Anisotropy (FA), Mean Diffusivity (MD), Axial Diffusivity (AD) and Radial Diffusivity (RD) were created. Whole brain tractography was performed selecting every brain voxel with at least one fiber orientation as a seed voxel. From these voxels, and for each fiber orientation, streamlines were propagated using a modified Euler integration with a step size of 1 mm. When entering a region with crossing white matter bundles, the algorithm followed the orientation vector of least curvature.

Streamlines were halted when a voxel without fiber orientation was reached or when the curvature between two steps exceeded a threshold of 45°. Each participant's fractional anisotropy map was transformed into standard stereotactic space (using FMRIB58 template) and a mean fractional anisotropy map for the whole sample used to create the average core 'skeleton'. By using only the core of the sample's white matter the peripheral tract regions are not involved in further analysis, thus removing partial volume effects [304]. Skeleton images of each participant's fractional anisotropy map were then produced and projected onto the mean skeleton to identify voxels where fractional anisotropy value differs significantly between these skeletons using voxel-wise statistics. The design matrix used centre, performance IQ, and age as covariates. Five thousand permutations were applied (confidence limits for P = 0.05 is = 0.0062). The TFCE value images are reported fully corrected for multiple comparisons across space using threshold free cluster enhancement with a specified significance level of P = 0.05 [126].

Following the TBSS analysis, white matter regions that were found to be atypical in ASD were localized using a probabilistic digital atlas of the major white matter tracts [45]. Tracts that were identified to be atypical in ASD by the TBSS analysis were dissected using one or two region of interest approach [44]. The tractographer was blind to group membership of each subject and brain side.

Virtual dissections of the left and right arcuate fasciculus and its segments connecting frontal, parietal and temporal regions were performed according to previous publications [70]. Virtual dissections of the three major limbic pathways including the cingulum, uncinate fasciculus and fornix were also performed [44]. In addition, the inferior longitudinal fasciculus and the inferior fronto-occipital fasciculus dissections were done to extend the analysis to pathways that contain parts of the fibres connecting limbic structures to visual and auditory associative areas. The corpus callosum was dissected using a single region of interest defined on the two

most medial slices of the fractional anisotropy maps. Individual portions of the corpus callosum were analyzed separately according to Witelson's criteria [305] (Figure 25).

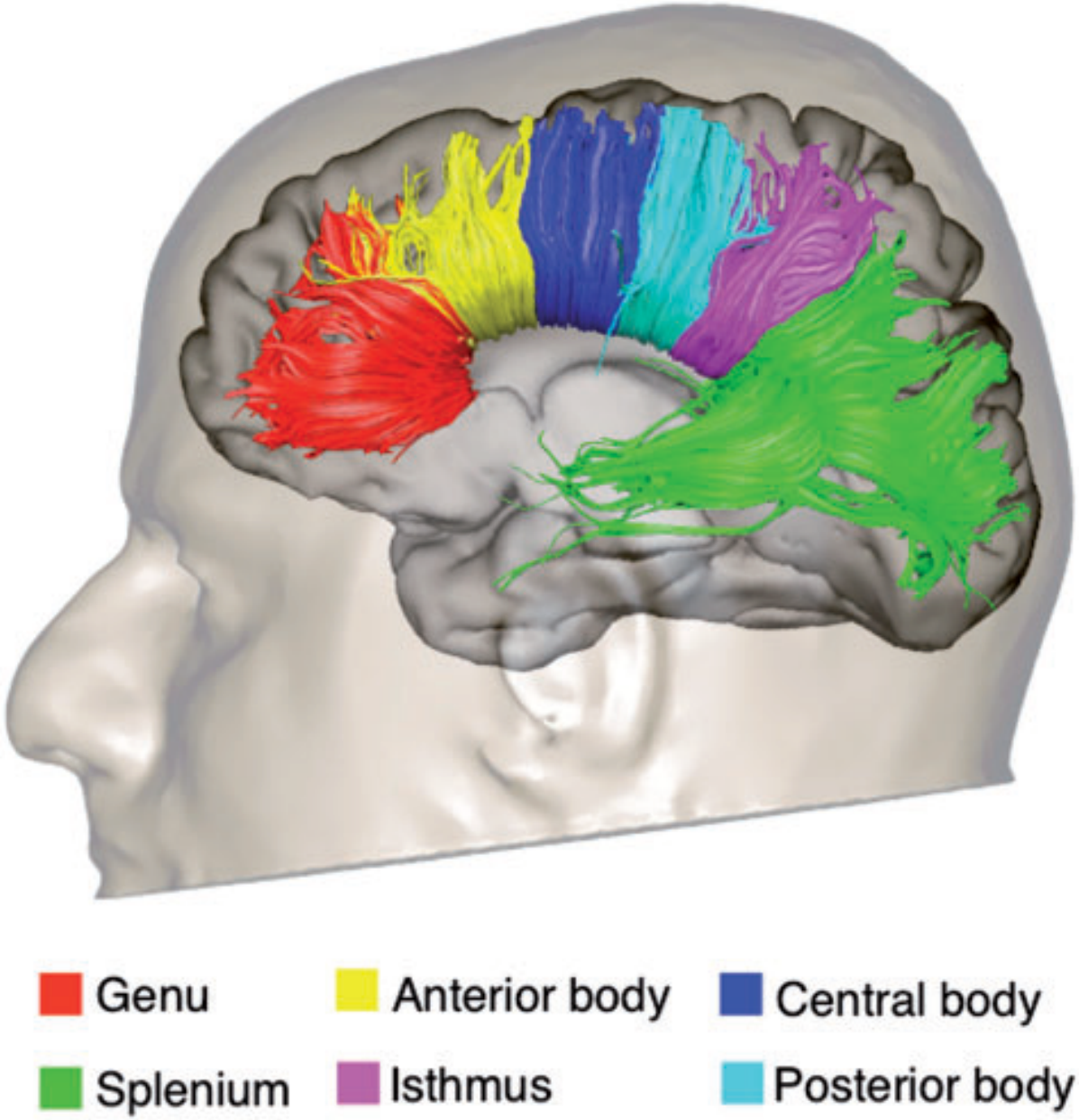

Figure 25. Tractography reconstruction of the segments of the corpus callosum according to Witelson's division [305].

Statistical analysis

Statistical analysis was performed using SPSS software package (version 21). Demographic and behavioural differences between ASD and control groups were analyzed using independent-samples t-tests. Repeated measures ANOVA analyses were performed separately for each measurement (i.e. number of streamlines, volume, fractional anisotropy, mean diffusivity, and perpendicular diffusivity) to examine group differences (i.e. the fixed factor) for the perisylvian network (long, posterior and anterior segments of the arcuate fasciculus) and the limbic association pathways (cingulum and uncinate fasciculus). Corpus callosum's group differences were estimated separately for each measurement (i.e. number of streamlines, volume, fractional anisotropy, mean diffusivity, and perpendicular diffusivity) using univariate

ANOVA analyses. Age, centre and performance IQ were entered as covariates in all analyses. Post hoc comparisons for specific tracts were considered as statistically significant if they survived Bonferroni correction for multiple comparisons (P = 0.0045, five tracts for each hemisphere; P = 0.008 for the corpus callosum). Both streamline count and tract volume were calculated for each tract. Considering that both measures yielded to similar results only streamline count is reported. To study possible associations between tract abnormalities and symptom severity within the ASD group differences in tracts were related to symptom severity as measured by the relevant ADIR and ADOS scores using Pearson correlation.

Role of the PhD student in this experimental study.

In this experimental study, I was primarily involved in processing the diffusion tensor data and performing tractography dissections for the statistical analysis.

7.3 Results

The ASD sample included 24 males with a diagnosis of childhood autism and 37 with a

diagnosis of Asperger syndrome (Table 17).

Table 17. Demographics of the ASD group and healthy controls.

Characteristics	**Healthy Controls (n=61)**	**ASD group (n=61)**
Age, y	28 (±6.7) [18-45]	26 (±6.9) [18-41]
Full-scale IQ, WASI	114 (±11.1) [86-137]	111 (±13) [77-135]
Performance IQ, WASI[b]	116 (±10.5) [94-135]	109 (±14.9) [75-138]
Verbal IQ, WASI	110 (±12.5) [71-137]	110 (±13.2) [84-139]
EHI	96 (±7.6) [65-100]	93 (±14.2) [25-100]
ADI-R Score		
- Social[c]	-	18.1 (±5.3)
- Communication[c]	-	13.6 (±4.2)
- Repetitive Behaviour[c]	-	4.8 (±2.2)
ADOS Score		
- Social[d]	-	6.1 (±2.9)
- Communication[d]	-	3.3 (±1.7)
- Repetitive Behaviour[d]	-	1.2 (±1.2)
AQ	-	23.6 (±10.7)
EQ	-	32.7 (±15.5)
SQ	-	64.3 (±22.3)

Numbers are means ± standard deviations. Ranges are between square brackets. Abbreviations: ADI-R, Autism Diagnostic Interview–Revised; ADOS, Autism Diagnostic Observation Schedule; ASD, autism spectrum disorder; WASI, Wechsler Abbreviated Scale of Intelligence.

[a]There were no significant differences between the ASD and control groups in age, full-scale IQ, or verbal IQ at $p < .05$ (2-tailed).

[b] There was a significant difference in performance IQ (P = .005).

[c] Information was available for all 61 individuals with ASD. The following cutoff scores were used: ADI-R Social, greater than 10; Communication, greater than 8; and Repetitive Behaviour, greater than 3.

[d] Information was available for 59 individuals with ASD. A cut-off of 7 was used for Communication plus Social interaction.

TBSS analysis

There was a significant lower fractional anisotropy in the ASD group (corrected for multiple comparisons) compared to controls in the left arcuate fasciculus (P = 0.026), external capsule (P = 0.046), anterior (P = 0.044) and posterior (P = 0.032) cingulum, and anterior corpus callosum (P = 0.015).

Diffusion tractography analysis

Arcuate fasciculus

In the arcuate fasciculus, ASD showed a significant difference in terms of mean diffusivity [F(1 120) = 5.618; P = 0.020] and radial diffusivity [F(1 120), 4.629; P = 0.034]. A statistically significant Group x Hemisphere interaction for the number of streamlines [F(2 116) = 6.817; P = 0.010] and Group x Tract interaction for the number of streamlines [F(2, 113) = 4.045; P = 0.02] was also found. After Bonferroni correction for multiple comparisons, the ASD group showed higher mean and radial diffusivity in the left long and left anterior segments while differences in the number of streamlines of the left long and anterior segments and mean diffusivity of the posterior right segment did not survive correction for multiple comparisons.

In the ASD group, the number of streamlines of the left anterior segment of the arcuate fasciculus was significantly negative correlated with the ADI-R B3 score for stereotyped, repetitive and idiosyncratic speech (Pearson's correlation = -0.340; P = 0.005).

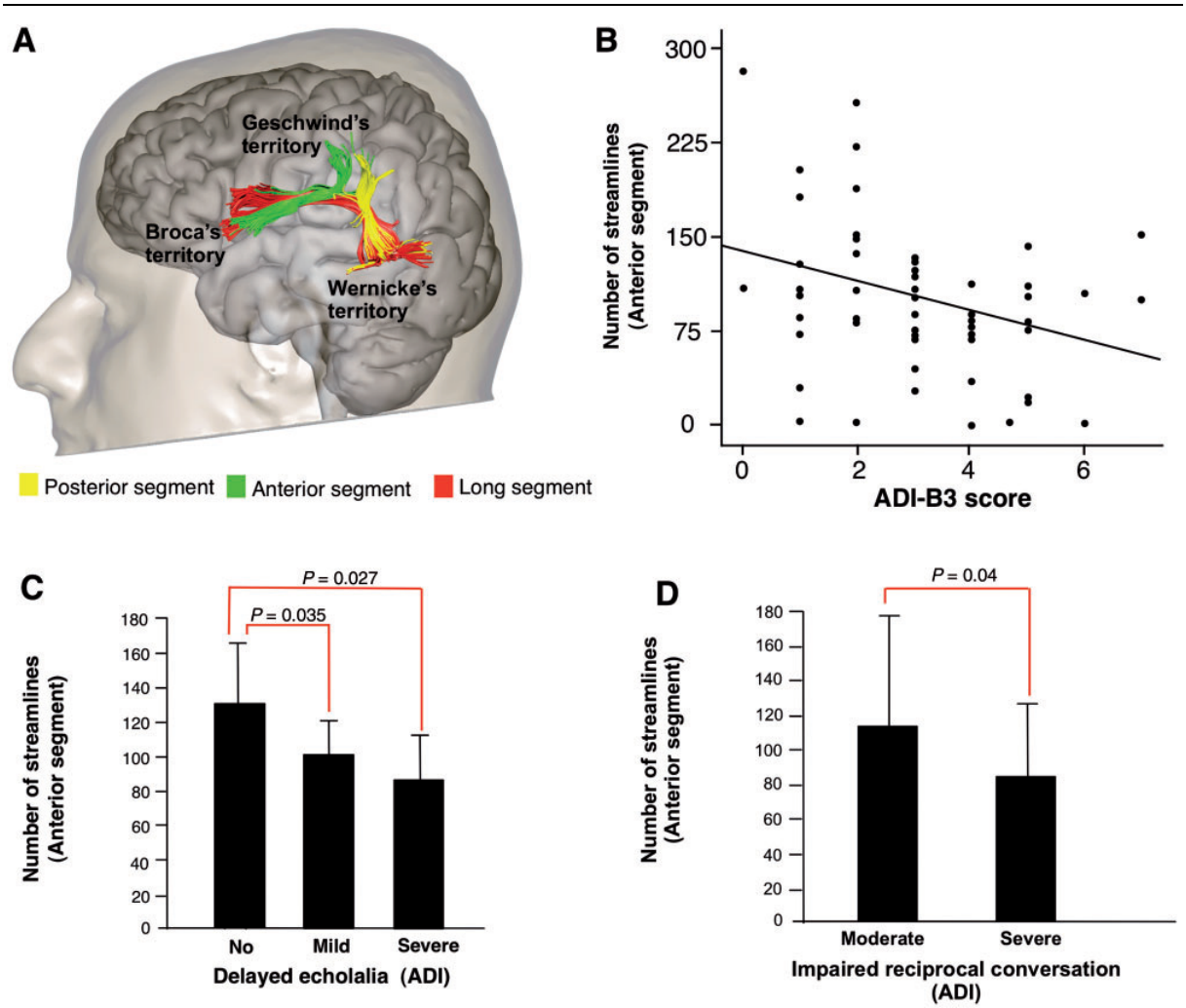

Figure 26. The anatomy of the arcuate fasciculus in relation to childhood ASD symptoms. (A) Tractography dissections of the three segments of the arcuate fasciculus. (B) Negative correlation between the number of streamlines of the left anterior segment and the B3 score (stereotyped, repetitive and idiosyncratic speech) of the ADI-R (r = -0.340; P = 0.005) in the ASD group. (C) In the ASD group, participants with a significant history of stereotyped utterance and delayed echolalia in childhood had a significantly lower number of streamlines in the anterior segment of the arcuate fasciculus. (D) Similarly, ASD subjects with severely impaired reciprocal conversation in childhood had a significantly lower number of streamlines in the anterior segment of the arcuate fasciculus compared to ASD subjects with moderate symptoms.

Limbic tracts

A statistically significant Group x Hemisphere interaction for fractional anisotropy [F(2 118) = 6.197; P = 0.014] was found. The ASD group showed a higher mean diffusivity and radial diffusivity in the left uncinate and lower fractional anisotropy in the left cingulum after Bonferroni correction for multiple comparisons.

Table 18. Tract-specific measurements of the three segments of the arcuate fasciculus.

Segments	Measurements	Controls	ASD	p-value
Long_left	Streamlines	292±108	246±108	0.023
	FA	0.504±.020	0.496±.023	0.042
	MD	0.74±.02 x 10^{-3}	0.75±.02 x 10^{-3}	0.002*
	RD	0.51±.02 x 10^{-3}	0.52±.02 x 10^{-3}	0.003*
Long_right	Streamlines	153±116	120±88	0.084
	FA	0.480±.024	0.470±.025	0.21
	MD	0.49±.02 x 10^{-3}	0.48±.06 x 10^{-3}	0.163
	RD	0.52±.02 x 10^{-3}	0.52±.02 x 10^{-3}	0.09
Anterior_left	Streamlines	132±78	101±63	0.018
	FA	0.459±.026	0.448±.030	0.039
	MD	0.75±.02 x 10^{-3}	0.77±.03 x 10^{-3}	0.003*
	RD	0.55±.02 x 10^{-3}	0.57±.03 x 10^{-3}	0.003*
Anterior_right	Streamlines	210±125	192±119	0.431
	FA	0.470±.027	0.464±.024	0.188
	MD	0.76±.02 x 10^{-3}	0.77±.02 x 10^{-3}	0.083
	RD	0.55±.02 x 10^{-3}	0.55±.02 x 10^{-3}	0.078
Posterior_left	Streamlines	156±67	170±94	0.353
	FA	0.454±.026	0.453±.023	0.885
	MD	0.75±.02 x 10^{-3}	0.76±.02 x 10^{-3}	0.007*
	RD	0.54±.02 x 10^{-3}	0.55±.03 x 10^{-3}	0.057
Posterior_right	Streamlines	132±75	131±83	0.947
	FA	0.452±.028	0.451±.026	0.878
	MD	0.76±.02 x 10^{-3}	0.77±.03 x 10^{-3}	0.011
	RD	0.55±.02 x 10^{-3}	0.56±.03 x 10^{-3}	0.055

Numbers are means ± standard deviations. * Indicates values that survive Bonferroni correction for multiple comparisons.

In ASD group, statistically significant correlation between the number of streamlines of the left uncinate and the ADI-R total score for qualitative abnormalities in reciprocal social

interactions (r = -0.269; P = 0.01), and A4 score for impaired socio-emotional reciprocity (r = -0.295; P = 0.01) was found. A similar correlation was found between fractional anisotropy of the left uncinate and the A4 score for impaired socio-emotional reciprocity (r = -0.301; P50.01). The correlation with A4 score was mainly driven by the severity of 'inappropriate use of facial expression'.

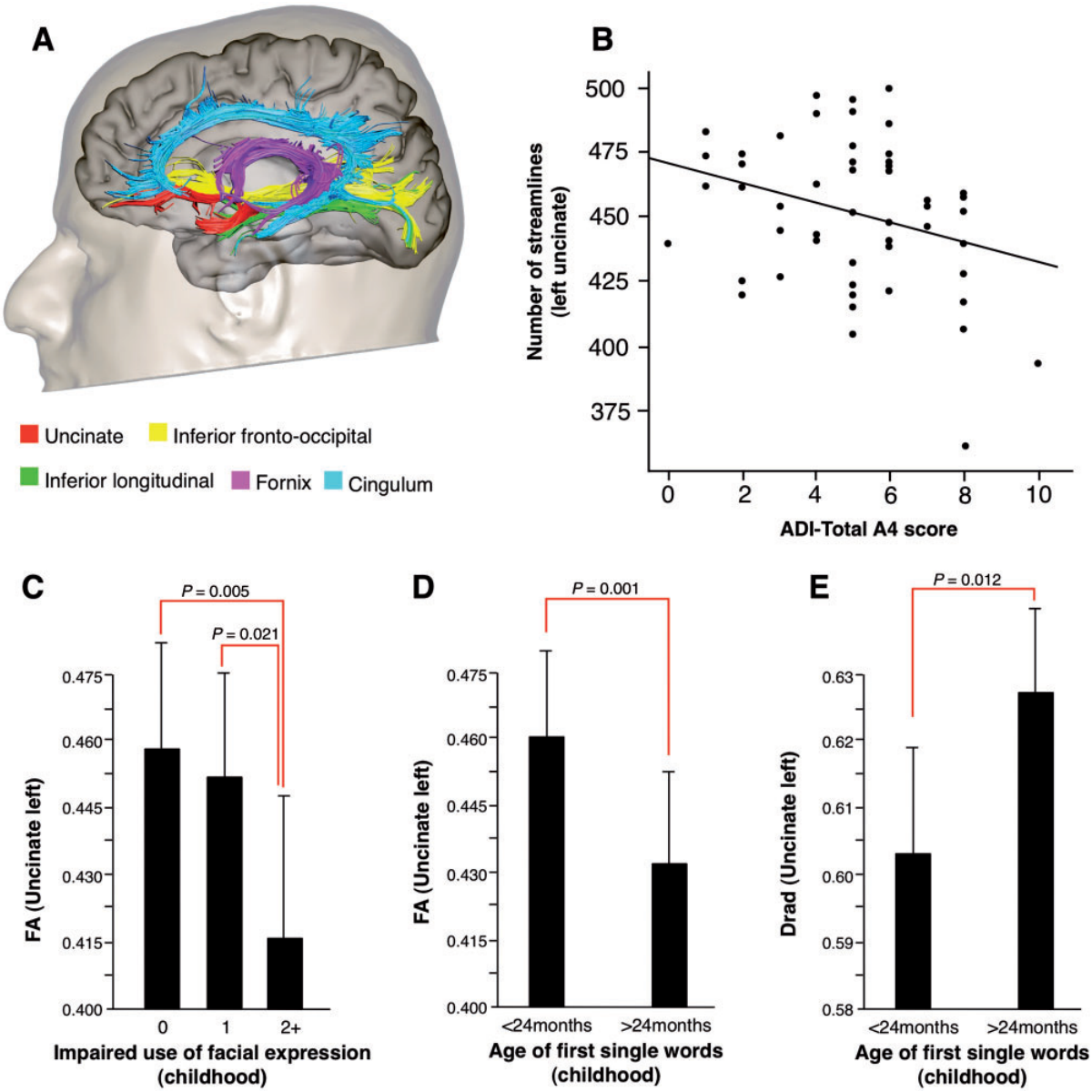

Figure 27. The anatomy of the limbic tracts in relation to childhood ASD symptoms. (A) Tractography reconstructions of the limbic pathways. (B) Negative correlation between the number of streamlines of the left uncinate fasciculus and the total A4 score for impaired socioemotional reciprocity in the ADI-R (Pearson's correlation = -0.295; P = 0.01) in the ASD group. ASD participants with a (C) significant history of impaired use of facial expression in childhood and (D and E) late use of first single words had a significantly lower fractional anisotropy (FA) and higher radial diffusivity in the left uncinate fasciculus.

Corpus callosum

In the number of streamlines, fractional anisotropy, mean diffusivity and radial diffusivity of the total corpus callosum there were not statistically significant differences between participants with ASD and controls. No significant correlations between diffusion indices of the corpus callosum and symptom severity as measured by the ADI-R and ADOS were found in the ASD group. The analysis of the segments of the corpus callosum revealed a statistically significant increase in mean diffusivity and radial diffusivity in the genu and anterior body in the ASD group as compared to controls. Differences in fractional anisotropy and radial diffusivity of the central body did not survive correction for multiple comparisons. No statistically significant differences were found in the posterior body, isthmus and splenium. There no significant correlations between diffusion indices of the corpus callosum and symptom severity as measured by the ADI-R and ADOS.

Table 19. Tract-specific measurements of the callosal tracts.

Callosal Segments	Measurements	Controls	ASD	p-value
Genu	Streamlines	914±304	853±192	0.197
	FA	0.572±.022	0.566±.020	0.178
	MD	0.82±.04 x 10^{-3}	0.84±.03 x 10^{-3}	0.006*
	RD	0.51±.03 x 10^{-3}	0.53±.03 x 10^{-3}	0.011
Anterior Body	Streamlines	412±156	427±143	0.534
	FA	0.539±.022	0.532±.018	0.062
	MD	0.82±.03 x 10^{-3}	0.83±.03 x 10^{-3}	0.003*
	RD	0.53±.03 x 10^{-3}	0.55±.05 x 10^{-3}	0.004*
Centre Body	Streamlines	460±149	427±111	0.191
	FA	0.558±.022	0.550±.020	0.04
	MD	0.81±.03 x 10^{-3}	0.82±.03 x 10^{-3}	0.04
	RD	0.51±.03 x 10^{-3}	0.52±.03 x 10^{-3}	0.022
Posterior Body	Streamlines	464±120	463±118	0.98
	FA	0.572±.022	0.574±.018	0.537
	MD	0.79±.03 x 10^{-3}	0.79±.02 x 10^{-3}	0.741
	RD	0.49±.03 x 10^{-3}	0.49±.02 x 10^{-3}	0.994
Isthmus	Streamlines	474±143	453±131	0.363
	FA	0.559±.024	0.557±.020	0.723
	MD	0.80±.03 x 10^{-3}	0.79±.02 x 10^{-3}	0.532
	RD	0.50±.03 x 10^{-3}	0.50±.02 x 10^{-3}	0.722
Splenium	Streamlines	1514±295	1498±315	0.774
	FA	0.611±.017	0.608±.018	0.424
	MD	0.79±.02 x 10^{-3}	0.79±.02 x 10^{-3}	0.584
	RD	0.46±.02 x 10^{-3}	0.47±.02 x 10^{-3}	0.44

Numbers are means ± standard deviations. * Indicates values that survive Bonferroni correction for multiple comparisons.

Table 20. Tract-specific measurements of the limbic tracts.

Limbic Tracts	Measurements	Controls	ASD	p-value
Uncinate_left	Streamlines	180±80	147±68	0.019
	FA	0.462±.022	0.452±.027	0.023
	MD	0.82±.02 x 10^{-3}	0.84±.02 x 10^{-3}	0.003*
	RD	0.59±.03 x 10^{-3}	0.61±.03 x 10^{-3}	0.001*
Uncinate_right	Streamlines	206±81	183±78	0.149
	FA	0.468±.022	0.459±.029	0.044
	MD	0.82±.02 x 10^{-3}	0.83±.40 x 10^{-3}	0.014
	RD	0.58±.02 x 10^{-3}	0.60±.04 x 10^{-3}	0.025
Cingulum_left	Streamlines	666±139	607±149	0.036
	FA	0.479±.025	0.466±.023	0.003*
	MD	0.78±.02 x 10^{-3}	0.79±.02 x 10^{-3}	0.199
	RD	0.55±.02 x 10^{-3}	0.56±.02 x 10^{-3}	0.007*
Cingulum_right	Streamlines	596±126	562±137	0.158
	FA	0.464±.024	0.457±.025	0.083
	MD	0.78±.02 x 10^{-3}	0.79±.02 x 10^{-3}	0.147
	RD	0.56±.02 x 10^{-3}	0.58±.03 x 10^{-3}	0.064
IFOF_left	Streamlines	182±80	167±88	0.481
	FA	0.499±.025	0.493±.025	0.272
	MD	0.78±.02 x 10^{-3}	0.80±.03 x 10^{-3}	0.008
	RD	0.54±.03 x 10^{-3}	0.55±.03 x 10^{-3}	0.025
IFOF_right	Streamlines	166±81	177±93	0.35
	FA	0.488±.020	0.491±.025	0.5
	MD	0.79±.02 x 10^{-3}	0.80±.03 x 10^{-3}	0.023
	RD	0.55±.02 x 10^{-3}	0.56±.03 x 10^{-3}	0.277
ILF_left	Streamlines	235±74	222±118	0.469
	FA	0.529±.027	0.524±.023	0.138
	MD	0.79±.03 x 10^{-3}	0.81±.03 x 10^{-3}	0.035
	RD	0.53±.02 x 10^{-3}	0.54±.03 x 10^{-3}	0.024
ILF_right	Streamlines	265±103	228±93	0.021
	FA	0.516±.070	0.524±.021	0.894
	MD	0.80±.02 x 10^{-3}	0.81±.02 x 10^{-3}	0.02
	RD	0.53±.02 x 10^{-3}	0.54±.03 x 10^{-3}	0.086

Numbers are means ± standard deviations. * Indicates values that survive Bonferroni correction for multiple comparisons.

7.4 Discussion

In this experimental study, white matter abnormalities in ASD were showed to persist into adult life. It was found that white matter damage is mainly to the major association and commissural tracts of the frontal lobe connecting frontal lobe to more posterior areas of the parietal, limbic and temporal lobe. Moreover, these white matter differences were associated with specific childhood ASD behavioural characteristics.

These results are in line with previous studies that reported differences in white matter tracts in ASD. A recent meta-analysis of diffusion tensor imaging (voxel-based) studies with 330 people with ASD and 313 controls showed decreased fractional anisotropy of the left arcuate fasciculus, uncinate fasciculus and corpus callosum, and increased mean diffusivity in the same regions [306]. Most of the tractography studies reported differences in the uncinate and arcuate fasciculi in ASD while a smaller number of studies demonstrated abnormalities in additional tracts, including the cingulum bundle, the inferior longitudinal and inferior fronto-occipital fasciculus.

However, only a few studies showed a direct correlation between white matter abnormalities and clinical symptoms [129]. A recent study used DTI to find a positive correlation between the fractional anisotropy of the uncinate fasciculus and both therapy duration and symptom improvement measured by the Child Autism Rating Scale [307]. Despite the fact that all of these findings suggest that ASD is characterized by differences in white matter tracts, the exact biological mechanism modulating these differences cannot be elucidated by diffusion techniques but may be understood by other methodologies, including post-mortem studies.

Post-mortem studies have reported that ASD is associated with white matter inflammation and reduced neural size and increased packing density within frontal and temporal limbic (grey matter) structures and increased number of neuronal processing units, known as cortical mini-columns within frontal and temporal cortices [131,133,308]. These are highly interconnected,

and a greater number of mini-columns could result in increased formation of short-range (intracortical) connections and disrupted maturation of long-range connections linking distant regions [309-311]. These findings may give support to the results of this study as they suggest that ASD pathology may lead to white matter changes in the long white matter connections, which can explain the reduced fractional anisotropy and increased radial diffusivity in the long-range connections of the frontal lobe identified in the present study. This hypothesis is also supported by a recent post-mortem study in ASD, which reported reduced myelin thickness in the frontal white matter [312].

In our study, we analysed only adult and it is therefore difficult to establish the onset of white matter abnormalities in ASD. A recent in vivo longitudinal study found that in infants at high-risk of developing ASD later in life, reduced fractional anisotropy in limbic and association tracts, including those reported in our current study, was already evident by the age they showed obvious signs of autism. In addition, these white matter differences are evident as early as 6 months of age in infants at risk of ASD, although abnormalities are often in the opposite direction (i.e. increased fractional anisotropy in the risk group). These findings suggest that ASD progresses through different stages during early neurodevelopment [313].

Differences in tract-specific measurements between neurotypical adults and ASD were found to be particularly significant for the mean diffusivity and radial diffusivity. These findings may suggest that mean diffusivity and radial diffusivity have greater intrinsic sensitivity to in vivo abnormalities associated with ASD pathology but also that the biophysical meaning of these indices is different. Fractional anisotropy as measure of diffusion anisotropy is sensitive to changes in the overall structural organization of the tissue or the fibre architecture but does not provide information regarding how the diffusion proceeds in different directions. On the other hand, mean diffusivity and radial diffusivity are able to provide quantitative measures

of water mobility within the tissue, either as average (mean diffusivity) or radially to the direction of maximum diffusivity (radial diffusivity). Mean diffusivity and radial diffusivity could be considered as more specific biomarkers related to abnormalities, such as changes in axonal membrane, extra-axonal volume density or in the myelin sheet because they may capture something not visible in a ratio or a difference in diffusivities. This is in line with previous study that have reported differences between typically developing adolescents and individuals with ASD only for diffusivity measures [314].

This study is not without limitations. First, the cross-sectional design and exclusion of children, females and participants with intellectual disability limited the capability for generalization or confirming causal and temporal developmental effects. For example, there is a sex difference in arcuate tract development in the typically developing population [72].Therefore, these results may not generalize to females with ASD, suggesting the need for future studies to include comparable samples of females. Similarly, the exclusion of individuals with below average IQ may mean that these results are not generalizable to the proportion of those with both ASD and intellectual disability. It could be argued that the significant difference in the IQ performance between the two groups may have confounded these findings. However, this difference was dealt with by co-varying for this across all of this analysis and these criteria were implemented in order to optimize sample homogeneity. Second, a multicentre design was used for MRI data acquisition, which may carry additional limitations. However, the same scanner model and acquisition parameters across scanning sites were used. In addition, inter-site effects were accounted for in the statistical model [315,316]. Therefore, the detected between-group differences cannot be fully explained by these limitations. Finally, some of the negative findings (e.g. lack of correlation between anatomy of the corpus callosum and ASD symptoms) could be explained by the use of the tensor

method, which is limited in resolving fibre crossing. Future studies are necessary to improve the complete visualization of callosal tracts using advanced diffusion models [148].

To conclude, this experimental study demonstrated that the specific structural abnormalities of white matter fibres found in this sample of ASD are compatible with the concept of autism being associated with atypical developmental connectivity of the frontal lobes. Future studies are needed to confirm these findings and to extend them across a wider range of autistic spectrum conditions.

Chapter 8 Conclusions

This chapter brings together the main conclusions of the experimental work reported in this thesis and discuss them in the context of our current understanding of the link between network anatomy and some non-motor functions of the frontal lobe.

General considerations on the approach proposed in this thesis

The overall aim of this thesis was to investigate the anatomy of the frontal networks underlying behavioural functions in frontal lobe disorders. Tractography analysis was performed in three distinct disorders that have been previously demonstrated to affect different but partially overlapping regions of the frontal lobe. MND is a neurodegenerative disorder that affects primarily precentral and premotor cortex [198-201]. PPA is a heterogeneous neurodegenerative disorder that involves perisylvian language areas of the temporal, parietal and frontal lobe of the left hemisphere. In the frontal lobe, the premotor and posterior prefrontal cortex are severely affected, especially in those forms presenting with a non-fluent/agrammatic form [90,93,317]. ASD is a neurodevelopmental condition that has been linked to anatomical abnormalities of the prefrontal and in part premotor cortex [129]. One advantage of using three cohorts of disorders affecting distinct regions of the frontal lobe is the possibility of probing the functional anatomy of the networks originating or projecting to the three broad divisions of the frontal lobe in motor, premotor and prefrontal. At the same time the partial overlap between the anatomy of the three disorders permits to understand the consequences of damage to a specific tract irrespective of the underlying condition. For example, in this thesis damage to the uncinate fasciculus was found to be correlated with behavioural symptoms in both PPA and ASD (see below), which indicates that the proposed clinico-anatomical correlative approach across disorders is valid and informative. In addition,

by collecting complementary evidence from different pathologies, a more comprehensive map of the behavioural correlates of frontal lobe dysfunction can be depicted.

At the same time, the differences between the three disorders in terms of genetic vulnerability, age of onset, clinical progression and neuropathology should be taken into account when interpreting the results derived from the three studies. ASD, for example, is a clinical condition not always accompanied by evident and specific neuroradiological or neuropathological abnormalities [129] and therefore anatomical changes in cortical and white matter anatomy may be difficult to detect with neuroimaging. Furthermore, compensatory changes are likely to occur with time, which may affect the possibility to identify a one-to-one correspondence between lesion location and symptoms, as demonstrated in Experimental study 3. Conversely, PPA and MND are progressive neurodegenerative disorders in which meaningful correlations between anatomical abnormalities and severity of clinical symptoms are frequently reported [67,207]. However, in these disorders the extension of the anatomical abnormalities beyond the language and motor areas is often highly variable and biased by the composition of the studied cohort. This may explain the lack of significant correlations between, for example, the uncinate fasciculus and behavioural manifestations in our MND study.

Discussion of the conclusions from the three studies

The first study investigated the cortical and white matter abnormalities underlying cognitive and behavior performances in MND patients using a cortical morphometry analysis and diffusion tensor tractography. The whole brain vertex-wise cortical analysis showed reduced cortical volume in the left lateral precentral gyrus, mid-cingulate cortex, parahippocampal gyrus and right medial and lateral precentral gyrus in the MND group compared with healthy controls. The diffusion tractography demonstrated white matter damage of the cortico-spinal

tract and of the cingulum in the MND group when compared with healthy controls. Furthermore, in this study the dorsal and ventral components of the cingulum were analysed separately. A correlation analysis showed that the reduced cortical volume of the mid-cingulate cortex and the underlying dorsal component of the cingulum were associated with anxiety, depression and performance in executive functions while the reduced volume of the parahippocampal gyrus and the underlying ventral component of the cingulum with semantic performances. Two main conclusions can be derived from these findings. First, we were able to confirm the sensitivity of current imaging methods to detect motor abnormalities whose severity correlates with the degree of motor impairment. Second, both cortical morphometry and tractography demonstrated the involvement of extra-motor regions that have been traditionally associated with the limbic system, such as dorsal cingulum and parahippocampal gyrus. The pattern of involvement of the limbic areas is of interest as it suggests two possible spreading mechanisms: i) by contiguity to those limbic areas adjacent to the motor cortex (e.g. dorsal cingulate cortex); ii) by diffusion along the long fibres of the cingulum connecting the medial-dorsal frontal cortex and cingulate cortex to the parahippocampal cortex. The possibility that white matter fibres represent a vehicle for the diffusion of the neuropathological process to distant cerebral regions has been suggested by post-mortem studies that demonstrated, for example, that patients with PPA and localized cortical degeneration in Broca's region develop concomitant symptoms of bulbar onset MND if the neurogenerative process affects the hypoglossal nucleus [192]. Our tractography findings of a white matter damage along the cingulum fibres suggest that the neurodegenerative process extends along white matter connections. Future histological studies are necessary to confirm this hypothesis by demonstrating white matter pathology of tracts connecting distant cortical regions affected by the neuropathological process. These findings also support a recent

proposal for an anatomical and functional division of the limbic system into three distinct but interconnected networks. This aspect will be discussed more in detail in the final paragraph.

The second study investigated if behavioral symptoms in patients with PPA were associated with degeneration of a ventral frontotemporal network through a multimodal neuroimaging approach. Diffusion tensor imaging tractography was used to quantify abnormalities of the uncinate fasciculus that connects the anterior temporal lobe and the ventrolateral frontal cortex and of the inferior fronto-occipital fasciculus and the inferior longitudinal fasciculus. Cortical thickness of anterior temporal and orbitofrontal regions interconnected by these tracts was also measured. The findings showed that although all three tracts had structural abnormalities as determined by tractography, significant correlations with behavioural scores were found only for the uncinate fasciculus. Cortical atrophy of the orbitofrontal and anterior temporal lobe cortex was also correlated with these scores. These findings indicate that damage to a frontotemporal network mediated by the uncinate fasciculus may underlie the emergence of behavioral symptoms in patients with PPA. Similar to the MND study, we were able to demonstrate the sensitivity of neuroimaging methods to anatomical changes in both cortical and white matter fibres of the tracts affected in PPA. The sensitivity extends to non-language functions as demonstrated by the correlations with subclinical behavioural symptoms in a group at high risk of developing a full-fledged fronto-temporal dementia. In addition, these findings confirm the role of the uncinated fasciculus in human behavior and suggest hypothesis for future studies that will be taken into account more in detail below.

The third study analysed the relationship between the ‘atypical connectivity’ of the higher-order association brain regions and autistic symptom severity in a large cohort of adults with ASD using a multimodal neuroimaging approach. TBSS showed that the white matter

microstructure was altered in regions that included frontal lobe pathways in ASD. Tractography analysis of these specific pathways detected diffusion abnormalities in the anterior and long segments of the arcuate fasciculus, cingulum and uncinate and in the anterior portions of the corpus callosum. Damage to the uncinate tract correlated with severity of symptoms in social reciprocity. The findings provide evidence that ASD is a development condition associated with abnormal connectivity of the frontal lobes and these aberrant development trajectories of the frontal networks persist in adult life. The neurodevelopmental hypothesis of ASD is a relatively recent advancement in our understanding of this disorder and followed many decades of psychoanalytical and social explanations [318]. The possibility of detecting white matter abnormalities in these patients reinforce the idea of neurobiological origin of the disorder and helps to develop network models of ASD symptoms. At the same time this is a disorder that occurs in developing brains in which structural, functional and behavioural changes have been observed before and after the onset of symptoms. The dynamic nature of this condition, especially in the milder forms such as Asperger's syndrome, may represent a limitation when a traditional clinic-anatomical correlative approach is adopted. In adults, characteristic ASD symptoms are difficult to quantify and often high functioning individuals have developed compensatory strategies to overcome their social, communication and behavioural difficulties. This may explain the lack of correlation between current symptoms and frontal lobe anatomy in our study. Nevertheless, the anatomical abnormalities we detected were localized in the dorsal cingulum and the uncinate fasciculus. These findings together with those of the first two experiments allow to put forward a general model of frontal lobe networks for human social behaviour.

Frontal lobe networks underlying human social behavior and emotions

The results of this thesis suggest the existence of two main frontal tracts involved in behaviour and emotion processing in humans. A ventral fronto-temporal network composed of long fibres of the uncinate fasciculus is responsible for behaviour symptoms in our PPA sample and severity of social reciprocity in our ASD group. A more dorso-medial frontal-parietal network that corresponds to the dorsal cingulum associated with anxiety, depression and performance in executive functions. In the classical literature, these two tracts have been considered as part of the limbic system and therefore should not be strictly considered as purely frontal lobe tracts.

The *uncinate fasciculus* is a tract that Paul Yakovlev proposed to form a network linked to emotion processing and motivation [319]. Indeed, the experimental study 3 of this thesis identified a correlation between diffusion abnormalities of the uncinate fasciculus and impaired socio-emotional reciprocity in ASD. On the other hand, we also found in experimental study 2 that in our PPA sample damage to the uncinate fasciculus was associated with severity of total negative behaviour symptoms which included apathy, aspontaneity, indifference and emotional flatness. The role of the uncinate fasciculus in emotion processing and motivation is extensively reported in the tractography literature. For example, decreased fractional anisotropy values in both left and right uncinate fasciculus have been described in patients with bvFTD [320,321]. Similar findings have been reported in neurodevelopmental disorders characterized by impaired emotional processing and motivation. Craig et al. (2009) found that altered microstructural integrity of the uncinate fasciculus in young men diagnosed with psychopathy correlated with measures of antisocial behaviour [82]. Several studies reported reduced fractional anisotropy values in the uncinate

fasciculus of patients with schizophrenia [322-324]and significant correlations with specific symptoms of schizophrenia such as flattened affect and lack of social engagement [323]. There is also evidence that the uncinate fasciculus is involved in cognitive functions such as recognition of famous faces [325], naming and single words comprehension. This suggests that the uncinate fasciculus may represent a complex network involved in functions that can be broadly separated into a cognitive domain and a behavioural domain. Post-morterm and tractography studies showed that before entering the orbital region of the frontal lobe, the uncinate fasciculus splits into a ventro-lateral branch terminating in the lateral orbitofrontal cortex and inferior frontal gyrus, and an antero-medial branch that connects to the medial orbitofrontal cortex, olfactory cortex and frontal pole [44,326,327]. Considering that the lateral branch originates from anterior and lateral temporo-polar cortex involved in semantic cognition, we hypothesise that this branch of the uncinate fasciculus has a prominent role in cognitive functions. Conversely, the anterior-medial branch originates from the medial temporal lobe (amygdala and hippocampus), we hypothesise that this component of the uncinate fasciculus is involved in behavioural aspects. This hypothesis can be validated in the future studies using tractography applied to conditions characterized by temporo-frontal network dysfunction with either predominant cognitive or behavioral symptoms.

The *cingulum* was originally described as a single tract forming the main cortical associative network of Papez circuit [328]. More recently the cingulum has been proposed to represent a network composed of at least two separate segments: i) an anterior-dorsal branch connecting anterior medial prefrontal cortex and cingulate cortex to precuneus and posterior cingulate cortex; ii) a posterior-ventral branch connecting the posterior precuneus and cingulate cortex to the parahippocampal gyrus [45]. The results of our experimental study 1 support this division of the cingulum and confirm a different functional role of the two branches. Previous studies

have demonstrated that the dorsal segment forms the medial portion of the default-mode network. The default-mode network is active during the 'resting state' while a synchronous deactivation of the default network is observed in the transition between the 'resting state' and the execution of goal directed tasks, irrespective of the nature of the task. The deactivation of the default-mode network may be crucial for tasks requiring attention, mentalising, response selection and action monitoring, autobiographical memory, self-knowledge, pain perception, empathy and person perception [22,85]. In clinical populations, abnormal activation of the default network has been reported in major depression, autism spectrum disorder, attention deficit and hyperactivity disorder, and in obsessive-compulsive disorder [22,329-331]. This literature gives support to our interpretation of anatomical differences identified in MND as indicative of a vulnerability to develop executive and non-executive deficits and psychiatric symptoms. Conversely, the fibres constituting the ventral branch of the cingulum are important for episodic memory, a conclusion that is supported by tractography studies that demonstrated early atrophy of the ventral cingulum fibres in early Alzheimer disease [332].

Asymmetry of the frontal lobe networks underlying human social behavior and emotions

Structural network asymmetry is an emerging topic in the current neuroimaging literature. The demonstration of inter-individual differences in network asymmetry for the language pathways [72] has important implications for language recovery in patients with aphasia after stroke [333]. In neurodegenerative and neurodevelopmental disorders the concept of network asymmetry has not been thoroughly explored. The presence of bilateral networks may represent a mechanism of resilience in disorders predominantly affecting one hemisphere. In healthy subjects, both uncinate and cingulum tracts are structurally symmetrical [263]. If we take into account the results of the three experiments in the context of network asymmetry,

the lack of specific correlations between current symptoms and left hemisphere tract abnormalities can be explained by possible compensatory mechanisms occurring in the relatively spared right hemisphere. Conversely, the experimental study 1 demonstrated bilaterally diffusion abnormalities of the cingulum in MND and these correlated significantly with anxiety, depression and performance in executive functions. This is in line with previous studies that suggested that there is no clear effect of laterality on these performances [2,334]. In addition, our PPA sample also showed bilateral damage to the uncinate fasciculus that correlated significantly with severity of behavioural symptoms. Although it is well known that language deficits in PPA are largely driven by a degeneration in the left hemisphere, most of the PPA patients with behavioural and emotional changes strongly show also right-sided damage. It is believed that the disease spreads from hemisphere to the other over the course of the disease [261,317,335]. Future longitudinal studies may clarify the role of white matter asymmetry in disease resilience and progression.

In conclusion, this thesis demonstrated that current neuroimaging methods such as cortical thickness and diffusion imaging are sensitive to brain abnormalities associated not only to neurodegeneration but also to neurodevelopmental pathology. Second, damage to specific networks will manifest with similar symptoms irrespective of the underlying pathology. In particular damage to the uncinate fasciculus and dorsal cingulum seems to be shared across the three pathologies. These considerations will help to broaden our understanding of the frontal lobe function beyond motor and language functions.

References

1. d'Azyr FV. Traite“ d”anatomie et de physiologie. Epub 1786 Jan 1.

2. MacPherson SE, Sala Della S, Cox S, Iveson MH, Girardi A. Handbook of Frontal Lobe Assessment. Oxford University Press, USA; 2015.

3. Gall FJ, Spurzheim JC. Anatomie et physiologie du système nerveux en général, et du cerveau en particulier. 1810.

4. Gratiolet L. Anatomie comparée du système nerveux. Epub 1857.

5. Flourens MJP. Recherches experimentales sur les proprietes et les fonctions du systeme nerveux dans les animaux vertebres. Epub 1824.

6. Fritsch GT, Hitzig E. Uber die elektrische Erregbarkeit des Grosshirns. Arch f Anat, Physiol und wissenschaftl Mediz. Epub 1870.

7. Jackson JH. Remarks on dissolution of the nervous system as exemplified by certain post-epileptic conditions. Med Press Circ. Epub 1881.

8. Harlow JM. Recovery from the Passage of an Iron Bar Through the Head. Epub 1869.

9. Thiebaut de Schotten M, Dell'Acqua F, Ratiu P, et al. From Phineas Gage and Monsieur Leborgne to H.M.: Revisiting Disconnection Syndromes. Cereb Cortex. 2015;25:4812–4827.

10. Macmillan M. John Martyn Harlow: "Obscure country physician"? J Hist Neurosci Taylor & Francis Group; 2001. p. 149–162.

11. Sala Della S. A daguerreotype of Phineas Gage? Cortex 2011.

12. Pick A. Uber die Beziehungen der senilen Hirnatrophie zur Aphasie. Prager Medizinische Wochenschrift. 17:165–167.

13. Pick A. Uber einen weiteren Symptomenkomplex im Rahmen der Dementia senilis, bedingt durch umschriebene starkere Hirnatrophie: Vortrag, gehalten im Wiener Vereine fur Psychiatrie und Neurologie. Monatsschr Psychiatr. 1906;19:97–108.

14. Wechsler I, Davison C. Amyotrophic lateral sclerosis with mental symptoms: A clinicopathologic study. Archives of Neurology and Psychiatry. 1932;27:859–880.

15. Bianchi L. The functions of the frontal lobe. Brain. 1895;18:497–522.

16. Bianchi L. La meccanica del cervello. Epub 1920.

17. Bianchi L. The Mechanism of the Brain and the Function of the Frontal Lobes. Epub 1922.

18. Levin HS, Eisenberg HM, Benton AL. Frontal Lobe Function and Dysfunction. Oxford University Press, USA; 1991.

19. Papez JW. A proposed mechanism of emotion. Arch Neurol Psychiatry. American Psychiatric Publishing; 1937;7:103–112.

20. Yakovlev PI, Locke S. Limbic nuclei of thalamus and connections of limbic cortex. III. Corticocortical connections of the anterior cingulate gyrus, the cingulum, and the subcallosal bundle in monkey. Arch Neurol. 1961;5:364–400.

21. MacLean PD. Psychosomatic disease and the visceral brain; recent developments bearing on the Papez theory of emotion. Psychosom Med. 1949;11:338–353.

22. Catani M, Dell'Acqua F, Thiebaut de Schotten M. A revised limbic system model for memory, emotion and behaviour. Neurosci Biobehav Rev. 2013;37:1724–1737.

23. Flechsig Of Leipsic P. Developmental (myelogenetic) localisation of the cerebral cortex in the human subject. The Lancet. Elsevier; 1901;158:1027–1030.

24. Altman J, Bayer SA. "Are new neurons formed in the brains of adult mammals?." Neuronal Cell Death and Repair. Elsevier; 1993. p. 203–225.

25. Eyre JA, Miller S, Clowry GJ, Conway EA, Watts C. Functional corticospinal projections are established prenatally in the human foetus permitting involvement in the development of spinal motor centres. Brain. 2000;123 (Pt 1):51–64.

26. Thatcher RW. Cyclic cortical reorganization during early childhood. Brain Cogn. 1992;20:24–50.

27. Sowell ER, Thompson PM, Welcome SE, Henkenius AL, Toga AW, Peterson BS. Cortical abnormalities in children and adolescents with attention-deficit hyperactivity disorder. Lancet. Elsevier; 2003;362:1699–1707.

28. Sowell ER, Delis D, Stiles J, Jernigan TL. Improved memory functioning and frontal lobe maturation between childhood and adolescence: a structural MRI study. J Int Neuropsychol Soc. 2001;7:312–322.

29. Sowell ER, Thompson PM, Leonard CM, Welcome SE, Kan E, Toga AW. Longitudinal mapping of cortical thickness and brain growth in normal children. J Neurosci. Society for Neuroscience; 2004;24:8223–8231.

30. Sowell ER, Thompson PM, Toga AW. Mapping changes in the human cortex throughout the span of life. Neuroscientist. 2nd ed. Sage PublicationsSage CA: Thousand Oaks, CA; 2004;10:372–392.

31. Anderson V, Jacobs R, Harvey AS. Prefrontal lesions and attentional skills in childhood. J Int Neuropsychol Soc. 2005;11:817–831.

32. Espy KA. The shape school: Assessing executive function in preschool children. Developmental Neuropsychology. 1997;13:495–499.

33. Mesulam MM. Principles of Behavioral and Cognitive Neurology. Oxford University Press; 2000.

34. Driscoll I, Davatzikos C, An Y, et al. Longitudinal pattern of regional brain volume

change differentiates normal aging from MCI. Neurology. Lippincott Williams & Wilkins; 2009;72:1906–1913.

35. Pfefferbaum A, Sullivan EV, Rosenbloom MJ, Mathalon DH, Lim KO. A controlled study of cortical gray matter and ventricular changes in alcoholic men over a 5-year interval. Arch Gen Psychiatry. 1998;55:905–912.

36. Resnick SM, Pham DL, Kraut MA, Zonderman AB, Davatzikos C. Longitudinal magnetic resonance imaging studies of older adults: a shrinking brain. J Neurosci. 2003;23:3295–3301.

37. Head D, Kennedy KM, Rodrigue KM, Raz N. Age differences in perseveration: cognitive and neuroanatomical mediators of performance on the Wisconsin Card Sorting Test. Neuropsychologia. 2009;47:1200–1203.

38. Head D, Raz N, Gunning-Dixon F, Williamson A, Acker JD. Age-related differences in the course of cognitive skill acquisition: the role of regional cortical shrinkage and cognitive resources. Psychol Aging. 2002;17:72–84.

39. Head D, Rodrigue KM, Kennedy KM, Raz N. Neuroanatomical and cognitive mediators of age-related differences in episodic memory. Neuropsychology. 2008;22:491–507.

40. Gunning-Dixon FM, Gur RC, Perkins AC, et al. Age-related differences in brain activation during emotional face processing. Neurobiol Aging. 2003;24:285–295.

41. Gunning-Dixon FM, Raz N. Neuroanatomical correlates of selected executive functions in middle-aged and older adults: a prospective MRI study. Neuropsychologia. 2003;41:1929–1941.

42. Cardenas VA, Chao LL, Studholme C, et al. Brain atrophy associated with baseline and longitudinal measures of cognition. Neurobiol Aging. 2011;32:572–580.

43. Double KL, Halliday GM, Kril JJ, et al. Topography of brain atrophy during normal aging and Alzheimer's disease. Neurobiol Aging. 1996;17:513–521.

44. Catani M, Thiebaut de Schotten M. A diffusion tensor imaging tractography atlas for virtual in vivo dissections. Cortex. 2008;44:1105–1132.

45. Catani M, Thiebaut de Schotten M. Atlas of Human Brain Connections. Oxford University Press; 2012.

46. Madden DJ, Whiting WL, Huettel SA, White LE, MacFall JR, Provenzale JM. Diffusion tensor imaging of adult age differences in cerebral white matter: relation to response time. Neuroimage. 2004;21:1174–1181.

47. O'Sullivan M, Jones DK, Summers PE, Morris RG, Williams SC, Markus HS. Evidence for cortical “disconnection” as a mechanism of age-related cognitive decline. Neurology. 2001;57:632–638.

48. Bennett IJ, Madden DJ, Vaidya CJ, Howard DV, Howard JH. Age-related differences in multiple measures of white matter integrity: A diffusion tensor

imaging study of healthy aging. Hum Brain Mapp. Wiley Subscription Services, Inc., A Wiley Company; 2010;31:378–390.

49. Bennett IJ, Madden DJ, Vaidya CJ, Howard JH, Howard DV. White matter integrity correlates of implicit sequence learning in healthy aging. Neurobiol Aging. Elsevier; 2011;32:2317.e1–.e12.

50. Salat DH, Tuch DS, Greve DN, et al. Age-related alterations in white matter microstructure measured by diffusion tensor imaging. Neurobiol Aging. Elsevier; 2005;26:1215–1227.

51. Salat DH, Tuch DS, Hevelone ND, et al. Age-related changes in prefrontal white matter measured by diffusion tensor imaging. Ann N Y Acad Sci. Blackwell Publishing Ltd; 2005;1064:37–49.

52. Deary IJ, Bastin ME, Pattie A, et al. White matter integrity and cognition in childhood and old age. Neurology. Lippincott Williams & Wilkins; 2006;66:505–512.

53. Davis SW, Dennis NA, Buchler NG, White LE, Madden DJ, Cabeza R. Assessing the effects of age on long white matter tracts using diffusion tensor tractography. Neuroimage. NIH Public Access; 2009;46:530–541.

54. West RL. An application of prefrontal cortex function theory to cognitive aging. Psychol Bull. 1996;120:272–292.

55. Gordon Shepherd SG. Handbook of Brain Microcircuits. Oxford University Press; 2010.

56. Catani M, Dell'Acqua F, Vergani F, et al. Short frontal lobe connections of the human brain. Cortex. 2012;48:273–291.

57. Davare M, Kraskov A, Rothwell JC, Lemon RN. Interactions between areas of the cortical grasping network. Curr Opin Neurobiol. 2011;21:565–570.

58. Fuster J. The Prefrontal Cortex. Academic Press; 2015.

59. Barbey AK, Koenigs M, Grafman J. Dorsolateral prefrontal contributions to human working memory. Cortex. 2013;49:1195–1205.

60. Christoff K, Ream JM, Geddes LPT, Gabrieli JDE. Evaluating self-generated information: anterior prefrontal contributions to human cognition. Behav Neurosci. 2003;117:1161–1168.

61. Koechlin E, Basso G, Pietrini P, Panzer S, Grafman J. The role of the anterior prefrontal cortex in human cognition. Nature. 1999;399:148–151.

62. Burgess PW, Dumontheil I, Gilbert SJ. The gateway hypothesis of rostral prefrontal cortex (area 10) function. Trends Cogn Sci (Regul Ed). 2007;11:290–298.

63. Yeterian EH, Pandya DN, Tomaiuolo F, Petrides M. The cortical connectivity of the prefrontal cortex in the monkey brain. Cortex. 2012;48:58–81.

64. Cerliani L, Thomas RM, Jbabdi S, et al. Probabilistic tractography recovers a rostrocaudal trajectory of connectivity variability in the human insular cortex. Hum Brain Mapp. Wiley Subscription Services, Inc., A Wiley Company; 2012;33:2005–2034.

65. Guevara P, Poupon C, Rivière D, et al. Robust clustering of massive tractography datasets. Neuroimage. 2011;54:1975–1993.

66. Ford A, McGregor KM, Case K, Crosson B, White KD. Structural connectivity of Broca's area and medial frontal cortex. Neuroimage. 2010;52:1230–1237.

67. Catani M, Mesulam MM, Jakobsen E, et al. A novel frontal pathway underlies verbal fluency in primary progressive aphasia. Brain. 2013;136:2619–2628.

68. Thiebaut de Schotten M, Dell'Acqua F, Valabregue R, Catani M. Monkey to human comparative anatomy of the frontal lobe association tracts. Cortex. 2012;48:82–96.

69. Catani M, Dell'Acqua F, Bizzi A, et al. Beyond cortical localization in clinico-anatomical correlation. Cortex. 2012;48:1262–1287.

70. Catani M, Jones DK, ffytche DH. Perisylvian language networks of the human brain. Annals of Neurology. Wiley Subscription Services, Inc., A Wiley Company; 2005;57:8–16.

71. Schulze K, Vargha-Khadem F, Mishkin M. Test of a motor theory of long-term auditory memory. Proc Natl Acad Sci USA. 2012;109:7121–7125.

72. Catani M, Allin MPG, Husain M, et al. Symmetries in human brain language pathways correlate with verbal recall. PNAS. National Acad Sciences; 2007;104:17163–17168.

73. Duffy FH, Burchfiel JL. Somatosensory system: organizational hierarchy from single units in monkey area 5. Science. 1971;172:273–275.

74. Leiguarda RC, Marsden CD. Limb apraxias: higher-order disorders of sensorimotor integration. Brain. 2000;123 (Pt 5):860–879.

75. Anderson EJ, Jones DK, O'Gorman RL, Leemans A, Catani M, Husain M. Cortical network for gaze control in humans revealed using multimodal MRI. Cereb Cortex. 2012;22:765–775.

76. Corbetta M, Shulman GL. Control of goal-directed and stimulus-driven attention in the brain. Nat Rev Neurosci. 2002;3:201–215.

77. Johnson PB, Ferraina S, Bianchi L, Caminiti R. Cortical Networks for Visual Reaching: Physiological and Anatomical Organization of Frontal and Parietal Lobe Arm Regions. Cereb Cortex. Oxford University Press; 1996;6:102–119.

78. Goldenberg G, Spatt J. The neural basis of tool use. Brain. 2009;132:1645–1655.

79. Levy R, Goldman-Rakic PS. Segregation of working memory functions within the dorsolateral prefrontal cortex. Exp Brain Res. 2000;133:23–32.

80. Thiebaut de Schotten M, Urbanski M, Duffau H, et al. Direct evidence for a parietal-frontal pathway subserving spatial awareness in humans. Science. 2005;309:2226–2228.

81. Zappalà G, Thiebaut de Schotten M, Eslinger PJ. Traumatic brain injury and the frontal lobes: what can we gain with diffusion tensor imaging? Cortex. 2012;48:156–165.

82. Craig MC, Catani M, Deeley Q, et al. Altered connections on the road to psychopathy. Mol Psychiatry. Nature Publishing Group; 2009;14:946–53–907.

83. Heide Von Der RJ, Skipper LM, Klobusicky E, Olson IR. Dissecting the uncinate fasciculus: disorders, controversies and a hypothesis. Brain. 2013;136:1692–1707.

84. Catani M, Dell'Acqua F, Thiebaut de Schotten M. A revised limbic system model for memory, emotion and behaviour. Neurosci Biobehav Rev. 2013;37:1724–1737.

85. Amodio DM, Frith CD. Meeting of minds: the medial frontal cortex and social cognition. Nat Rev Neurosci. 2006;7:268–277.

86. Mesulam MM. Primary progressive aphasia. Annals of Neurology. 2001;49:425–432.

87. Serieux P. Sur un cas de surdite verbale pure. Rev Med. 11:592–598.

88. Mesulam MM. Slowly progressive aphasia without generalized dementia. Annals of Neurology. Wiley Subscription Services, Inc., A Wiley Company; 1982;11:592–598.

89. Hodges JR, Patterson K, Oxbury S, Funnell E. Semantic dementia. Progressive fluent aphasia with temporal lobe atrophy. Brain. 1992;115 (Pt 6):1783–1806.

90. Gorno-Tempini ML, Hillis AE, Weintraub S, et al. Classification of primary progressive aphasia and its variants. Neurology. Lippincott Williams & Wilkins; 2011.76:1006–1014.

91. Gorno-Tempini ML, Dronkers NF, Rankin KP, et al. Cognition and anatomy in three variants of primary progressive aphasia. Annals of Neurology. Wiley Subscription Services, Inc., A Wiley Company; 2004;55:335–346.

92. Josephs KA, Duffy JR, Strand EA, et al. Clinicopathological and imaging correlates of progressive aphasia and apraxia of speech. Brain. 2006;129:1385–1398.

93. Nestor PJ, Graham NL, Fryer TD, Williams GB, Patterson K, Hodges JR. Progressive non-fluent aphasia is associated with hypometabolism centred on the left anterior insula. Brain. 2003;126:2406–2418.

94. Ash S, Moore P, Vesely L, et al. Non-Fluent Speech in Frontotemporal Lobar Degeneration. J Neurolinguistics. 2009;22:370–383.

95. Tu S, Leyton CE, Hodges JR, Piguet O, Hornberger M. Divergent Longitudinal Propagation of White Matter Degradation in Logopenic and Semantic Variants of Primary Progressive Aphasia. Naismith S, editor. J Alzheimers Dis. IOS Press;

2016;49:853–861.

96. Seeley WW, Bauer AM, Miller BL, et al. The natural history of temporal variant frontotemporal dementia. Neurology. Lippincott Williams & Wilkins; 2005;64:1384–1390.

97. Gainotti G. Different patterns of famous people recognition disorders in patients with right and left anterior temporal lesions: a systematic review. Neuropsychologia. 2007;45:1591–1607.

98. Rosen HJ, Kramer JH, Gorno-Tempini ML, Schuff N, Weiner M, Miller BL. Patterns of cerebral atrophy in primary progressive aphasia. Am J Geriatr Psychiatry. 2002;10:89–97.

99. Ramanan S, Bertoux M, Flanagan E, et al. Longitudinal Executive Function and Episodic Memory Profiles in Behavioral-Variant Frontotemporal Dementia and Alzheimer's Disease. Journal of the International Neuropsychological Society. 2017;23:34–43.

100. Lindau M, Almkvist O, Kushi J, et al. First symptoms--frontotemporal dementia versus Alzheimer's disease. DEM. 2000;11:286–293.

101. Neary D, Snowden JS, Gustafson L, et al. Frontotemporal lobar degeneration: a consensus on clinical diagnostic criteria. Neurology. Lippincott Williams & Wilkins; 1998. p. 1546–1554.

102. Hornberger M, Yew B, Gilardoni S, et al. Ventromedial-frontopolar prefrontal cortex atrophy correlates with insight loss in frontotemporal dementia and Alzheimer's disease. Hum Brain Mapp. 2014;35:616–626.

103. Hornberger M. Clinicopathologic differences among patients with behavioral variant frontotemporal dementia. Neurology. Lippincott Williams & Wilkins; 2013;81:775–775.

104. Hornberger M, Geng J, Hodges JR. Convergent grey and white matter evidence of orbitofrontal cortex changes related to disinhibition in behavioural variant frontotemporal dementia. Brain. 2011;134:2502–2512.

105. Gräsbeck A, Englund E, Horstmann V, Passant U, Gustafson L. Predictors of mortality in frontotemporal dementia: a retrospective study of the prognostic influence of pre-diagnostic features. Int J Geriatr Psychiatry. John Wiley & Sons, Ltd; 2003;18:594–601.

106. Hodges JR, Davies R, Xuereb J, Kril J, Halliday G. Survival in frontotemporal dementia. Neurology. 2003;61:349–354.

107. Charcot JM. Deux cas d'atrophie musculaire progressive avec lesions de la substance grise et des faisceaux anterolaterax de la moelle epiniere. Pathol. Pathol; 1869;2:354–367.

108. Charcot JM, Joffroy A. Deux cas d'atrophie musculaire progressive: avec lésions de la substance grise et des faisceaux antérolatéraux de la moelle épinière. 1869.

109. Roche JC, Rojas-Garcia R, Scott KM, et al. A proposed staging system for amyotrophic lateral sclerosis. Brain. 2012;135:847–852.

110. Turner MR, Bowser R, Bruijn L, et al. Mechanisms, models and biomarkers in amyotrophic lateral sclerosis. Amyotroph Lateral Scler Frontotemporal Degener. Taylor & Francis; 2013;14 Suppl 1:19–32.

111. Turner MR, Swash M. The expanding syndrome of amyotrophic lateral sclerosis: a clinical and molecular odyssey. J Neurol Neurosurg Psychiatr. 2015;86:667–673.

112. Kiernan MC, Vucic S, Cheah BC, et al. Amyotrophic lateral sclerosis. The Lancet. 2011;377:942–955.

113. Tsermentseli S, Leigh PN, Goldstein LH. The anatomy of cognitive impairment in amyotrophic lateral sclerosis: more than frontal lobe dysfunction. Cortex. 2012;48:166–182.

114. Osborn AG, Salzman KL, Jhaveri MD, Barkovich AJ. Diagnostic Imaging: Brain. Elsevier Health Sciences; 2015.

115. El Escorial revisited: revised criteria for the diagnosis of amyotrophic lateral sclerosis. Epub 2000.

116. Saberi S, Stauffer JE, Schulte DJ, Ravits J. Neuropathology of Amyotrophic Lateral Sclerosis and Its Variants. Neurol Clin. 2015;33:855–876.

117. Abrahams S, Goldstein LH, Suckling J, et al. Frontotemporal white matter changes in amyotrophic lateral sclerosis. J Neurol. Steinkopff-Verlag; 2005;252:321–331.

118. Hammer RP, Tomiyasu U, Scheibel AB. Degeneration of the human Betz cell due to amyotrophic lateral sclerosis. Exp Neurol. 1979;63:336–346.

119. Nihei K, McKee AC, Kowall NW. Patterns of neuronal degeneration in the motor cortex of amyotrophic lateral sclerosis patients. Acta Neuropathol. Springer-Verlag; 1993;86:55–64.

120. Stephens B, Guiloff RJ, Navarrete R, Newman P, Nikhar N, Lewis P. Widespread loss of neuronal populations in the spinal ventral horn in sporadic motor neuron disease. A morphometric study. J Neurol Sci. Elsevier; 2006;244:41–58.

121. Tomonaga M, Saito M, Yoshimura M, Shimada H, Tohgi H. Ultrastructure of the Bunina bodies in anterior horn cells of amyotrophic lateral sclerosis. Acta Neuropathol. 1978;42:81–86.

122. Kuroda S, Ishizu H, Kawai K, Otsuki S. Bunina bodies in dendrites of patients with amyotrophic lateral sclerosis. Acta Med Okayama. 1990;44:41–45.

123. Giordana MT, Piccinini M, Grifoni S, et al. TDP-43 redistribution is an early event in sporadic amyotrophic lateral sclerosis. Brain Pathol. Blackwell Publishing Ltd; 2010;20:351–360.

124. Thorpe JR, Tang H, Atherton J, Cairns NJ. Fine structural analysis of the neuronal

inclusions of frontotemporal lobar degeneration with TDP-43 proteinopathy. J Neural Transm (Vienna). Springer Vienna; 2008;115:1661–1671.

125. Geser F, Prvulovic D, O'Dwyer L, et al. On the development of markers for pathological TDP-43 in amyotrophic lateral sclerosis with and without dementia. Prog Neurobiol. 2011;95:649–662.

126. Catani M, Dell'Acqua F, Budisavljevic S, et al. Frontal networks in adults with autism spectrum disorder. Brain. 2016;139:616–630.

127. Filipek PA, Accardo PJ, Baranek GT, et al. The screening and diagnosis of autistic spectrum disorders. J Autism Dev Disord. 1999;29:439–484.

128. García-Villamisar D, Sala Della S. Dual-task performance in adults with autism. Cogn Neuropsychiatry. 2002;7:63–74.

129. Ameis SH, Catani M. Altered white matter connectivity as a neural substrate for social impairment in Autism Spectrum Disorder. Cortex. 2015;62:158–181.

130. Folstein SE, Rosen-Sheidley B. Genetics of autism: complex aetiology for a heterogeneous disorder. Nat Rev Genet. 2001;2:943–955.

131. Bauman ML, Kemper TL. Neuroanatomic observations of the brain in autism: a review and future directions. Int J Dev Neurosci. 2005;23:183–187.

132. van Kooten IAJ, Palmen SJMC, Cappeln von P, et al. Neurons in the fusiform gyrus are fewer and smaller in autism. Brain. 2008;131:987–999.

133. Bailey A, Luthert P, Dean A, et al. A clinicopathological study of autism. Brain. 1998;121 (Pt 5):889–905.

134. Casanova MF. White matter volume increase and minicolumns in autism. Annals of Neurology. Wiley Subscription Services, Inc., A Wiley Company; 2004;56:453–453.

135. Courchesne E, Mouton PR, Calhoun ME, et al. Neuron number and size in prefrontal cortex of children with autism. JAMA. 2011;306:2001–2010.

136. Zikopoulos B, Barbas H. Altered neural connectivity in excitatory and inhibitory cortical circuits in autism. Front Hum Neurosci. Frontiers; 2013;7:609.

137. Basser PJ, Mattiello J, LeBihan D. MR diffusion tensor spectroscopy and imaging. Biophys J. 1994;66:259–267.

138. Le Bihan D, Breton E, Lallemand D, Grenier P, Cabanis E, Laval-Jeantet M. MR imaging of intravoxel incoherent motions: application to diffusion and perfusion in neurologic disorders. Radiology. 1986;161:401–407.

139. Tanner JE. Transient diffusion in a system partitioned by permeable barriers. Application to NMR measurements with a pulsed field gradient. The Journal of Chemical Physics. American Institute of Physics; 2008;69:1748–1754.

140. Pierpaoli C, Basser PJ. Toward a quantitative assessment of diffusion anisotropy.

Magn Reson Med. 1996;36:893–906.

141. Alexander AL, Lee JE, Lazar M, Field AS. Diffusion tensor imaging of the brain. Neurotherapeutics. 2007;4:316–329.

142. Basser PJ, Pajevic S, Pierpaoli C, Duda J, Aldroubi A. In vivo fiber tractography using DT-MRI data. Magn Reson Med. 2000;44:625–632.

143. Conturo TE, Lori NF, Cull TS, et al. Tracking neuronal fiber pathways in the living human brain. PNAS. National Academy of Sciences; 1999;96:10422–10427.

144. Dell'Acqua F, Catani M. Structural human brain networks: hot topics in diffusion tractography. Current Opinion in Neurology. 2012;25:375–383.

145. Berman JI, Mukherjee P, Partridge SC, et al. Quantitative diffusion tensor MRI fiber tractography of sensorimotor white matter development in premature infants. Neuroimage. 2005;27:862–871.

146. Jones DK, Catani M, Pierpaoli C, et al. Age effects on diffusion tensor magnetic resonance imaging tractography measures of frontal cortex connections in schizophrenia. Hum Brain Mapp. Wiley Subscription Services, Inc., A Wiley Company; 2006;27:230–238.

147. Wheeler-Kingshott CAM, Cercignani M. About "axial" and "radial" diffusivities. Magn Reson Med. Wiley Subscription Services, Inc., A Wiley Company; 2009;61:1255–1260.

148. Dell'Acqua F, Simmons A, Williams SCR, Catani M. Can spherical deconvolution provide more information than fiber orientations? Hindrance modulated orientational anisotropy, a true-tract specific index to characterize white matter diffusion. Hum Brain Mapp. 2013;34:2464–2483.

149. Dell'Acqua F, Scifo P, Rizzo G, et al. A modified damped Richardson-Lucy algorithm to reduce isotropic background effects in spherical deconvolution. Neuroimage. 2010;49:1446–1458.

150. Dale AM, Fischl B, Sereno MI. Cortical surface-based analysis. I. Segmentation and surface reconstruction. Neuroimage. 1999;9:179–194.

151. Fischl B, Sereno MI, Dale AM. Cortical surface-based analysis. II: Inflation, flattening, and a surface-based coordinate system. Neuroimage. 1999;9:195–207.

152. Fischl B, Sereno MI, Tootell RB, Dale AM. High-resolution intersubject averaging and a coordinate system for the cortical surface. Hum Brain Mapp. 1999;8:272–284.

153. Ségonne F, Dale AM, Busa E, et al. A hybrid approach to the skull stripping problem in MRI. Neuroimage. 2004;22:1060–1075.

154. Winkler AM, Sabuncu MR, Yeo BTT, et al. Measuring and comparing brain cortical surface area and other areal quantities. Neuroimage. 2012;61:1428–1443.

155. Worsley KJ, Andermann M, Koulis T, MacDonald D, Evans AC. Detecting changes

in nonisotropic images. Hum Brain Mapp. 1999;8:98–101.

156. Lord C, Rutter M, Le Couteur A. Autism Diagnostic Interview-Revised: a revised version of a diagnostic interview for caregivers of individuals with possible pervasive developmental disorders. J Autism Dev Disord. 1994;24:659–685.

157. Kertesz A, Nadkarni N, Davidson W, Thomas AW. The Frontal Behavioral Inventory in the differential diagnosis of frontotemporal dementia. Journal of the International Neuropsychological Society. Cambridge University Press; 2000;6:460–468.

158. Stout JC, Ready RE, Grace J, Malloy PF, Paulsen JS. Factor analysis of the frontal systems behavior scale (FrSBe). Assessment. 3rd ed. SAGE PublicationsSage UK: London, England; 2003;10:79–85.

159. Grace J, Stout JC, Malloy PF. Assessing frontal lobe behavioral syndromes with the frontal lobe personality scale. Assessment. Sage PublicationsSage CA: Thousand Oaks, CA; 1999;6:269–284.

160. Zigmond AS, Snaith RP. The hospital anxiety and depression scale. Acta Psychiatr Scand. 1983;67:361–370.

161. Bak TH, Hodges JR. Kissing and dancing—a test to distinguish the lexical and conceptual contributions to noun/verb and action/object dissociation. Preliminary results in patients with frontotemporal dementia. J Neurolinguistics. 2003;16:169–181.

162. De Renzi E, Vignolo LA. The token test: A sensitive test to detect receptive disturbances in aphasics. Brain. 1962;85:665–678.

163. Coughlan AK, Warrington EK. Word-comprehension and word-retrieval in patients with localized cerebral lesions. Brain. 1978;101:163–185.

164. Yudofsky SC, Hales RE. The American Psychiatric Press Textbook of Neuropsychiatry and Behavioral Sciences. 2008.

165. Howard D, Education H, Patterson K. Pyramids and Palm Trees Manual. Epub 2004.

166. Butler CR, Brambati SM, Miller BL, Gorno-Tempini ML. The neural correlates of verbal and non-verbal semantic processing deficits in neurodegenerative disease. Cognitive and behavioral neurology : official journal of the Society for Behavioral and Cognitive Neurology. NIH Public Access; 2009;22:73–80.

167. Vandenberghe R, Price C, Wise R, Josephs O, Frackowiak RS. Functional anatomy of a common semantic system for words and pictures. Nature. 1996;383:254–256.

168. Thierry G, Price CJ. Dissociating verbal and nonverbal conceptual processing in the human brain. J Cogn Neurosci. MIT Press 238 Main St., Suite 500, Cambridge, MA 02142-1046USA journals-info@mit.edu; 2006;18:1018–1028.

169. Abrahams S, Leigh PN, Harvey A, Vythelingum GN, Grisé D, Goldstein LH. Verbal fluency and executive dysfunction in amyotrophic lateral sclerosis (ALS).

Neuropsychologia. 2000;38:734–747.

170. Stuss DT, Alexander MP, Hamer L, et al. The effects of focal anterior and posterior brain lesions on verbal fluency. J Int Neuropsychol Soc. 1998;4:265–278.

171. Sarazin M, Pillon B, Giannakopoulos P, Rancurel G, Samson Y, Dubois B. Clinicometabolic dissociation of cognitive functions and social behavior in frontal lobe lesions. Neurology. 1998;51:142–148.

172. Abrahams S, Goldstein LH, Kew JJ, et al. Frontal lobe dysfunction in amyotrophic lateral sclerosis. A PET study. Brain. 1996;119 (Pt 6):2105–2120.

173. Cicerone KD, Tanenbaum LN. Disturbance of social cognition after traumatic orbitofrontal brain injury. Arch Clin Neuropsychol. 1997;12:173–188.

174. Baird A, Dewar B-K, Critchley H, Gilbert SJ, Dolan RJ, Cipolotti L. Cognitive functioning after medial frontal lobe damage including the anterior cingulate cortex: a preliminary investigation. Brain Cogn. 2006;60:166–175.

175. McDonald CR, Swartz BE, Halgren E, Patell A, Daimes R, Mandelkern M. The relationship of regional frontal hypometabolism to executive function: a resting fluorodeoxyglucose PET study of patients with epilepsy and healthy controls. Epilepsy Behav. Elsevier; 2006;9:58–67.

176. Szatkowska I, Grabowska A, Szymańska O. Phonological and semantic fluencies are mediated by different regions of the prefrontal cortex. Acta Neurobiol Exp (Wars). 2000;60:503–508.

177. Troyer AK, Moscovitch M, Winocur G, Alexander MP, Stuss D. Clustering and switching on verbal fluency: the effects of focal frontal- and temporal-lobe lesions. Neuropsychologia. 1998;36:499–504.

178. Cilia R, Siri C, Marotta G, et al. Brain networks underlining verbal fluency decline during STN-DBS in Parkinson's disease: an ECD-SPECT study. Parkinsonism Relat Disord. Elsevier; 2007;13:290–294.

179. Baldo JV, Schwartz S, Wilkins D, Dronkers NF. Role of frontal versus temporal cortex in verbal fluency as revealed by voxel-based lesion symptom mapping. Journal of the International Neuropsychological Society. Cambridge University Press; 2006;12:896–900.

180. Grant DA, Berg EA. A behavioral analysis of degree of reinforcement and ease of shifting to new responses in a Weigl-type card-sorting problem. J Exp Psychol. 1948;38:404–411.

181. Nelson HE. A Modified Card Sorting Test Sensitive to Frontal Lobe Defects. Cortex. 1976;12:313–324.

182. Heaton RK. Wisconsin Card Sort Task Version 4 Research Edition. Psychological Assessment Resources; 2003.

183. Demakis GJ. Frontal lobe damage and tests of executive processing: a meta-analysis

of the category test, stroop test, and trail-making test. J Clin Exp Neuropsychol. 2004;26:441–450.

184. Stuss DT, Alexander MP. Executive functions and the frontal lobes: a conceptual view. Psychol Res. 2000;63:289–298.

185. Barceló F, Knight RT. Both random and perseverative errors underlie WCST deficits in prefrontal patients. Neuropsychologia. 2002;40:349–356.

186. Goodall EF, Greenway MJ, van Marion I, Carroll CB, Hardiman O, Morrison KE. Association of the H63D polymorphism in the hemochromatosis gene with sporadic ALS. Neurology. Lippincott Williams & Wilkins; 2005;65:934–937.

187. Sage CA, Peeters RR, Görner A, Robberecht W, Sunaert S. Quantitative diffusion tensor imaging in amyotrophic lateral sclerosis. Neuroimage. 2007;34:486–499.

188. Turner MR, Hardiman O, Benatar M, et al. Controversies and priorities in amyotrophic lateral sclerosis. The Lancet Neurology. Elsevier; 2013;12:310–322.

189. Bak TH, Hodges JR. Motor neurone disease, dementia and aphasia: coincidence, co-occurrence or continuum? J Neurol. 2001;248:260–270.

190. Phukan J, Elamin M, Bede P, et al. The syndrome of cognitive impairment in amyotrophic lateral sclerosis: a population-based study. J Neurol Neurosurg Psychiatr. BMJ Publishing Group Ltd; 2012;83:102–108.

191. Abrahams S, Leigh PN, Goldstein LH. Cognitive change in ALS: a prospective study. Neurology. Lippincott Williams & Wilkins; 2005;64:1222–1226.

192. Catani M, Piccirilli M, Cherubini A, et al. Axonal injury within language network in primary progressive aphasia. Annals of Neurology. Wiley Subscription Services, Inc., A Wiley Company; 2003;53:242–247.

193. Goldstein LH, Abrahams S. Changes in cognition and behaviour in amyotrophic lateral sclerosis: nature of impairment and implications for assessment. The Lancet Neurology. Elsevier; 2013;12:368–380.

194. Grossman AB, Woolley-Levine S, Bradley WG, Miller RG. Detecting neurobehavioral changes in amyotrophic lateral sclerosis. Amyotroph Lateral Scler. 2007;8:56–61.

195. Rabkin JG, Goetz R, Factor-Litvak P, et al. Depression and wish to die in a multicenter cohort of ALS patients. Amyotroph Lateral Scler Frontotemporal Degener. 4 ed. 2015;16:265–273.

196. Lyketsos CG, Lopez O, Jones B, Fitzpatrick AL, Breitner J, DeKosky S. Prevalence of neuropsychiatric symptoms in dementia and mild cognitive impairment: results from the cardiovascular health study. JAMA: The Journal of the American Medical Association. 2002;288:1475–1483.

197. Huey ED, Koppel J, Armstrong N, Grafman J, Floeter MK. A pilot study of the prevalence of psychiatric disorders in PLS and ALS. Amyotroph Lateral Scler.

2010;11:293–297.

198. Roccatagliata L, Bonzano L, Mancardi G, Canepa C, Caponnetto C. Detection of motor cortex thinning and corticospinal tract involvement by quantitative MRI in amyotrophic lateral sclerosis. Amyotroph Lateral Scler. 2009;10:47–52.

199. Agosta F, Valsasina P, Riva N, et al. The cortical signature of amyotrophic lateral sclerosis. Le W, editor. PLoS ONE. Public Library of Science; 2012;7:e42816.

200. Kwan JY, Meoded A, Danielian LE, Wu T, Floeter MK. Structural imaging differences and longitudinal changes in primary lateral sclerosis and amyotrophic lateral sclerosis. Neuroimage Clin. 2012;2:151–160.

201. Verstraete E, Veldink JH, Hendrikse J, Schelhaas HJ, van den Heuvel MP, van den Berg LH. Structural MRI reveals cortical thinning in amyotrophic lateral sclerosis. J Neurol Neurosurg Psychiatr. BMJ Publishing Group Ltd; 2012;83:383–388.

202. Walhout R, Westeneng H-J, Verstraete E, et al. Cortical thickness in ALS: towards a marker for upper motor neuron involvement. J Neurol Neurosurg Psychiatr. 2015;86:288–294.

203. Hornberger M, Kiernan MC. Emergence of an imaging biomarker for amyotrophic lateral sclerosis: is the end point near? J Neurol Neurosurg Psychiatr. BMJ Publishing Group Ltd; 2016;87:569–569.

204. Ellis CM, Simmons A, Jones DK, et al. Diffusion tensor MRI assesses corticospinal tract damage in ALS. Neurology. 1999;53:1051–1058.

205. Sato K, Aoki S, Iwata NK, et al. Diffusion tensor tract-specific analysis of the uncinate fasciculus in patients with amyotrophic lateral sclerosis. Neuroradiology. 2010;52:729–733.

206. Blain CRV, Brunton S, Williams VC, et al. Differential corticospinal tract degeneration in homozygous “D90A” SOD-1 ALS and sporadic ALS. J Neurol Neurosurg Psychiatr. 2011;82:843–849.

207. Sarro L, Agosta F, Canu E, et al. Cognitive functions and white matter tract damage in amyotrophic lateral sclerosis: a diffusion tensor tractography study. AJNR Am J Neuroradiol. 2011;32:1866–1872.

208. Mioshi E, Roberts R, Hornberger M. Neuropsychiatric symptoms and survival in amyotrophic lateral sclerosis: a missing link? Neurodegener Dis Manag. Future Medicine Ltd London, UK; 2015;5:89–91.

209. Schuster C, Kasper E, Dyrba M, et al. Cortical thinning and its relation to cognition in amyotrophic lateral sclerosis. Neurobiol Aging. Elsevier; 2014;35:240–246.

210. Cedarbaum JM, Stambler N, Malta E, et al. The ALSFRS-R: a revised ALS functional rating scale that incorporates assessments of respiratory function. BDNF ALS Study Group (Phase III). J Neurol Sci. 1999;169:13–21.

211. Wechsler D. Wechsler Abbreviated Scale of Intelligence. San Antonio, Texas; Epub

1999.

212. Strong MJ, Grace GM, Freedman M, et al. Consensus criteria for the diagnosis of frontotemporal cognitive and behavioural syndromes in amyotrophic lateral sclerosis. Amyotroph Lateral Scler. 2009;10:131–146.

213. Jones DK, Williams SCR, Gasston D, Horsfield MA, Simmons A, Howard R. Isotropic resolution diffusion tensor imaging with whole brain acquisition in a clinically acceptable time. Hum Brain Mapp. 2002;15:216–230.

214. Leemans A, Jones DK. The B-matrix must be rotated when correcting for subject motion in DTI data. Magn Reson Med. Wiley Subscription Services, Inc., A Wiley Company; 2009;61:1336–1349.

215. Tournier J-D, Calamante F, Gadian DG, Connelly A. Direct estimation of the fiber orientation density function from diffusion-weighted MRI data using spherical deconvolution. Neuroimage. 2004;23:1176–1185.

216. Tournier J-D, Calamante F, Connelly A. Robust determination of the fibre orientation distribution in diffusion MRI: non-negativity constrained super-resolved spherical deconvolution. Neuroimage. 2007;35:1459–1472.

217. Alexander DC. Maximum entropy spherical deconvolution for diffusion MRI. Inf Process Med Imaging. 2005;19:76–87.

218. Jones DK. Studying connections in the living human brain with diffusion MRI. Cortex. 2008;44:936–952.

219. Catani M, Howard RJ, Pajevic S, Jones DK. Virtual in vivo interactive dissection of white matter fasciculi in the human brain. Neuroimage. 2002;17:77–94.

220. Dejerine J. Anatomie des centres nerveux. 1901.

221. Metzler-Baddeley C, Jones DK, Steventon J, Westacott L, Aggleton JP, O'Sullivan MJ. Cingulum microstructure predicts cognitive control in older age and mild cognitive impairment. J Neurosci. Society for Neuroscience; 2012;32:17612–17619.

222. Metzler-Baddeley C, Jones DK, Belaroussi B, Aggleton JP, O'Sullivan MJ. Frontotemporal connections in episodic memory and aging: a diffusion MRI tractography study. J Neurosci. Society for Neuroscience; 2011;31:13236–13245.

223. Jones DK, Christiansen KF, Chapman RJ, Aggleton JP. Distinct subdivisions of the cingulum bundle revealed by diffusion MRI fibre tracking: implications for neuropsychological investigations. Neuropsychologia. 2013;51:67–78.

224. Mioshi E, Lillo P, Yew B, et al. Cortical atrophy in ALS is critically associated with neuropsychiatric and cognitive changes. Neurology. Lippincott Williams & Wilkins; 2013;80:1117–1123.

225. Sudharshan N, Hanstock C, Hui B, Pyra T, Johnston W, Kalra S. Degeneration of the mid-cingulate cortex in amyotrophic lateral sclerosis detected in vivo with MR spectroscopy. AJNR Am J Neuroradiol. 2011;32:403–407.

226. Agosta F, Valsasina P, Absinta M, et al. Sensorimotor functional connectivity changes in amyotrophic lateral sclerosis. Cereb Cortex. 2011;21:2291–2298.

227. Shackman AJ, Salomons TV, Slagter HA, Fox AS, Winter JJ, Davidson RJ. The integration of negative affect, pain and cognitive control in the cingulate cortex. Nat Rev Neurosci. 2011;12:154–167.

228. Koch K, Schultz CC, Wagner G, et al. Disrupted white matter connectivity is associated with reduced cortical thickness in the cingulate cortex in schizophrenia. Cortex. 2013;49:722–729.

229. Kühn S, Kaufmann C, Simon D, Endrass T, Gallinat J, Kathmann N. Reduced thickness of anterior cingulate cortex in obsessive-compulsive disorder. Cortex. 2013;49:2178–2185.

230. Vogt BA. Submodalities of emotion in the context of cingulate subregions. Cortex. 2014;59:197–202.

231. Hoffstaedter F, Grefkes C, Caspers S, et al. The role of anterior midcingulate cortex in cognitive motor control: evidence from functional connectivity analyses. Hum Brain Mapp. 2014;35:2741–2753.

232. Rolls ET. Limbic systems for emotion and for memory, but no single limbic system. Cortex. 2015;62:119–157.

233. Vogt BA, Berger GR, Derbyshire SWG. Structural and functional dichotomy of human midcingulate cortex. Eur J Neurosci. NIH Public Access; 2003;18:3134–3144.

234. Posner MI, Petersen SE, Fox PT, Raichle ME. Localization of cognitive operations in the human brain. Science. 1988;240:1627–1631.

235. Raczka KA, Becker G, Seese A, et al. Executive and behavioral deficits share common neural substrates in frontotemporal lobar degeneration - a pilot FDG-PET study. Psychiatry Res. Elsevier; 2010;182:274–280.

236. Chiu WZ, Papma JM, de Koning I, et al. Midcingulate involvement in progressive supranuclear palsy and tau positive frontotemporal dementia. J Neurol Neurosurg Psychiatr. 2012;83:910–915.

237. Dopper EGP, Rombouts SARB, Jiskoot LC, et al. Structural and functional brain connectivity in presymptomatic familial frontotemporal dementia. Neurology. Lippincott Williams & Wilkins; 2013;80:814–823.

238. Aminoff EM, Kveraga K, Bar M. The role of the parahippocampal cortex in cognition. Trends Cogn Sci (Regul Ed). Elsevier; 2013;17:379–390.

239. Binder JR, Desai RH, Graves WW, Conant LL. Where is the semantic system? A critical review and meta-analysis of 120 functional neuroimaging studies. Cereb Cortex. 2009;19:2767–2796.

240. Meyer P, Mecklinger A, Grunwald T, Fell J, Elger CE, Friederici AD. Language

processing within the human medial temporal lobe. Hippocampus. Wiley Subscription Services, Inc., A Wiley Company; 2005;15:451–459.

241. Braak H, Del Tredici K, Bohl J, Bratzke H, Braak E. Pathological changes in the parahippocampal region in select non-Alzheimer's dementias. Ann N Y Acad Sci. 2000;911:221–239.

242. Van Hoesen GW, Augustinack JC, Dierking J, Redman SJ, Thangavel R. The parahippocampal gyrus in Alzheimer's disease. Clinical and preclinical neuroanatomical correlates. Ann N Y Acad Sci. 2000;911:254–274.

243. Rohrer JD, Warren JD, Modat M, et al. Patterns of cortical thinning in the language variants of frontotemporal lobar degeneration. Neurology. Lippincott Williams & Wilkins; 2009;72:1562–1569.

244. Agosta F, Pagani E, Petrolini M, et al. Assessment of white matter tract damage in patients with amyotrophic lateral sclerosis: a diffusion tensor MR imaging tractography study. AJNR Am J Neuroradiol. American Journal of Neuroradiology; 2010;31:1457–1461.

245. Sarica A, Cerasa A, Vasta R, et al. Tractography in amyotrophic lateral sclerosis using a novel probabilistic tool: a study with tract-based reconstruction compared to voxel-based approach. J Neurosci Methods. 2014;224:79–87.

246. Jelsone-Swain L, Persad C, Votruba KL, et al. The Relationship between Depressive Symptoms, Disease State, and Cognition in Amyotrophic Lateral Sclerosis. Front Psychol. Frontiers; 2012;3:542.

247. Gordon PH, Delgadillo D, Piquard A, et al. The range and clinical impact of cognitive impairment in French patients with ALS: a cross-sectional study of neuropsychological test performance. Amyotroph Lateral Scler. 3rd ed. 2011;12:372–378.

248. Rusina R, Ridzon P, Kulist'ák P, et al. Relationship between ALS and the degree of cognitive impairment, markers of neurodegeneration and predictors for poor outcome. A prospective study. Eur J Neurol. Blackwell Publishing Ltd; 2010;17:23–30.

249. Diamond BJ, Johnson SK, Kaufman M, Graves L. Relationships between information processing, depression, fatigue and cognition in multiple sclerosis. Arch Clin Neuropsychol. 2008;23:189–199.

250. Zilles K, Amunts K, Smaers JB. Three brain collections for comparative neuroanatomy and neuroimaging. Ann N Y Acad Sci. Blackwell Publishing Inc; 2011;1225 Suppl 1:E94–E104.

251. Fatemi Y, Boeve BF, Duffy J, et al. Neuropsychiatric aspects of primary progressive aphasia. J Neuropsychiatry Clin Neurosci. American Psychiatric Publishing, Inc. Arlington, VA; 2011;23:168–172.

252. Kertesz A, Davidson W, Munoz DG. Clinical and Pathological Overlap between Frontotemporal Dementia, Primary Progressive Aphasia and Corticobasal

Degeneration: The Pick Complex. DEM. Karger Publishers; 1999;10:46–49.

253. Banks SJ, Weintraub S. Cognitive deficits and reduced insight in primary progressive aphasia. Am J Alzheimers Dis Other Demen. SAGE PublicationsSage CA: Los Angeles, CA; 2008;23:363–371.

254. Marczinski CA, Davidson W, Kertesz A. A longitudinal study of behavior in frontotemporal dementia and primary progressive aphasia. Cognitive and behavioral neurology : official journal of the Society for Behavioral and Cognitive Neurology. 2004;17:185–190.

255. Mesulam MM, Grossman M, Hillis A, Kertesz A, Weintraub S. The core and halo of primary progressive aphasia and semantic dementia. Annals of Neurology. Wiley Subscription Services, Inc., A Wiley Company; 2003;54 Suppl 5:S11–S14.

256. Rosen HJ, Allison SC, Ogar JM, et al. Behavioral features in semantic dementia vs other forms of progressive aphasias. Neurology. Lippincott Williams & Wilkins; 2006;67:1752–1756.

257. Rohrer JD, Warren JD. Phenomenology and anatomy of abnormal behaviours in primary progressive aphasia. J Neurol Sci. Elsevier; 2010;293:35–38.

258. Galantucci S, Tartaglia MC, Wilson SM, et al. White matter damage in primary progressive aphasias: a diffusion tensor tractography study. Brain. 2011;134:3011–3029.

259. Kertesz A, Nadkarni N, Davidson W, Thomas AW. The Frontal Behavioral Inventory in the differential diagnosis of frontotemporal dementia. J Int Neuropsychol Soc. 2000;6:460–468.

260. Fischl B, Dale AM. Measuring the thickness of the human cerebral cortex from magnetic resonance images. PNAS. 2000;97:11050–11055.

261. Rogalski E, Cobia D, Harrison TM, Wieneke C, Weintraub S, Mesulam MM. Progression of language decline and cortical atrophy in subtypes of primary progressive aphasia. Neurology. Lippincott Williams & Wilkins; 2011;76:1804–1810.

262. Chang LC, Jones DK, Pierpaoli C. RESTORE: Robust estimation of tensors by outlier rejection. Magn Reson Med. Wiley Subscription Services, Inc., A Wiley Company; 2005;53:1088–1095.

263. Thiebaut de Schotten M, ffytche DH, Bizzi A, et al. Atlasing location, asymmetry and inter-subject variability of white matter tracts in the human brain with MR diffusion tractography. Neuroimage. 2011;54:49–59.

264. Forkel SJ, Thiebaut de Schotten M, Kawadler JM, Dell'Acqua F, Danek A, Catani M. The anatomy of fronto-occipital connections from early blunt dissections to contemporary tractography. Cortex. 2014;56:73–84.

265. Catani M. Diffusion tensor magnetic resonance imaging tractography in cognitive disorders. Current Opinion in Neurology. 2006;19:599–606.

266. Flügel D, Cercignani M, Symms MR, et al. Diffusion tensor imaging findings and their correlation with neuropsychological deficits in patients with temporal lobe epilepsy and interictal psychosis. Epilepsia. Blackwell Publishing Inc; 2006;47:941–944.

267. Gaffan D, Wilson CRE. Medial temporal and prefrontal function: recent behavioural disconnection studies in the macaque monkey. Cortex. 2008;44:928–935.

268. Kumfor F, Irish M, Hodges JR, Piguet O. The orbitofrontal cortex is involved in emotional enhancement of memory: evidence from the dementias. Brain. 2013;136:2992–3003.

269. Tan RH, Wong S, Kril JJ, et al. Beyond the temporal pole: limbic memory circuit in the semantic variant of primary progressive aphasia. Brain. 2014;137:2065–2076.

270. Hughes LE, Rowe JB. The impact of neurodegeneration on network connectivity: a study of change detection in frontotemporal dementia. J Cogn Neurosci. MIT Press55 Hayward Street, Cambridge, MA 02142-1315USAjournals-info@mit.edu; 2013;25:802–813.

271. Mesulam MM, Rogalski EJ, Wieneke C, et al. Primary progressive aphasia and the evolving neurology of the language network. Nature Reviews Neurology. 2014;10:554–569.

272. Arai T, Hasegawa M, Nonoka T, et al. Phosphorylated and cleaved TDP-43 in ALS, FTLD and other neurodegenerative disorders and in cellular models of TDP-43 proteinopathy. Neuropathology. Blackwell Publishing Asia; 2010;30:170–181.

273. Budini M, Romano V, Quadri Z, Buratti E, Baralle FE. TDP-43 loss of cellular function through aggregation requires additional structural determinants beyond its C-terminal Q/N prion-like domain. Hum Mol Genet. Oxford University Press; 2015;24:9–20.

274. Abell F, Krams M, Ashburner J, et al. The neuroanatomy of autism: a voxel-based whole brain analysis of structural scans. Neuroreport. 1999;10:1647–1651.

275. Waiter GD, Williams JHG, Murray AD, Gilchrist A, Perrett DI, Whiten A. A voxel-based investigation of brain structure in male adolescents with autistic spectrum disorder. Neuroimage. 2004;22:619–625.

276. McAlonan GM, Cheung V, Cheung C, et al. Mapping the brain in autism. A voxel-based MRI study of volumetric differences and intercorrelations in autism. Brain. 2005;128:268–276.

277. McAlonan GM, Suckling J, Wong N, et al. Distinct patterns of grey matter abnormality in high-functioning autism and Asperger's syndrome. J Child Psychol Psychiatry. Blackwell Publishing Ltd; 2008;49:1287–1295.

278. Brieber S, Neufang S, Bruning N, et al. Structural brain abnormalities in adolescents with autism spectrum disorder and patients with attention deficit/hyperactivity disorder. J Child Psychol Psychiatry. Blackwell Publishing Ltd; 2007;48:1251–1258.

279. Bonilha L, Cendes F, Rorden C, et al. Gray and white matter imbalance--typical structural abnormality underlying classic autism? Brain Dev. Elsevier; 2008;30:396–401.

280. Ke X, Hong S, Tang T, et al. Voxel-based morphometry study on brain structure in children with high-functioning autism. Neuroreport. 2008;19:921–925.

281. Lange N, DuBray MB, Lee JE, et al. Atypical diffusion tensor hemispheric asymmetry in autism. Autism Res. John Wiley & Sons, Inc; 2010;3:350–358.

282. Toal F, Daly EM, Page L, et al. Clinical and anatomical heterogeneity in autistic spectrum disorder: a structural MRI study. Psychol Med. Cambridge University Press; 2010;40:1171–1181.

283. Cauda F, Costa T, Palermo S, et al. Concordance of white matter and gray matter abnormalities in autism spectrum disorders: a voxel-based meta-analysis study. Hum Brain Mapp. 2014;35:2073–2098.

284. Via E, Radua J, Cardoner N, Happé F, Mataix-Cols D. Meta-analysis of gray matter abnormalities in autism spectrum disorder: should Asperger disorder be subsumed under a broader umbrella of autistic spectrum disorder? Arch Gen Psychiatry. 2011;68:409–418.

285. Nickl-Jockschat T, Habel U, Michel TM, et al. Brain structure anomalies in autism spectrum disorder--a meta-analysis of VBM studies using anatomic likelihood estimation. Hum Brain Mapp. Wiley Subscription Services, Inc., A Wiley Company; 2012;33:1470–1489.

286. Nordahl CW, Scholz R, Yang X, et al. Increased rate of amygdala growth in children aged 2 to 4 years with autism spectrum disorders: a longitudinal study. Arch Gen Psychiatry. American Medical Association; 2012;69:53–61.

287. Catani M, Bambini V. A model for Social Communication And Language Evolution and Development (SCALED). Curr Opin Neurobiol. 2014;28:165–171.

288. Belmonte MK, Allen G, Beckel-Mitchener A, Boulanger LM, Carper RA, Webb SJ. Autism and abnormal development of brain connectivity. J Neurosci. Society for Neuroscience; 2004;24:9228–9231.

289. Frith C. Is autism a disconnection disorder? The Lancet Neurology. Elsevier; 2004;3:577.

290. Courchesne E, Pierce K. Brain overgrowth in autism during a critical time in development: implications for frontal pyramidal neuron and interneuron development and connectivity. Int J Dev Neurosci. 2005;23:153–170.

291. Geschwind DH, Levitt P. Autism spectrum disorders: developmental disconnection syndromes. Curr Opin Neurobiol. 2007;17:103–111.

292. Just MA, Keller TA, Malave VL, Kana RK, Varma S. Autism as a neural systems disorder: a theory of frontal-posterior underconnectivity. Neurosci Biobehav Rev. 2012;36:1292–1313.

293. Barnea-Goraly N, Lotspeich LJ, Reiss AL. Similar white matter aberrations in children with autism and their unaffected siblings: a diffusion tensor imaging study using tract-based spatial statistics. Arch Gen Psychiatry. 2010;67:1052–1060.

294. Sahyoun CP, Belliveau JW, Mody M. White matter integrity and pictorial reasoning in high-functioning children with autism. Brain Cogn. 2010;73:180–188.

295. Jou RJ, Mateljevic N, Kaiser MD, Sugrue DR, Volkmar FR, Pelphrey KA. Structural neural phenotype of autism: preliminary evidence from a diffusion tensor imaging study using tract-based spatial statistics. AJNR Am J Neuroradiol. American Journal of Neuroradiology; 2011;32:1607–1613.

296. Walker L, Gozzi M, Lenroot R, et al. Diffusion tensor imaging in young children with autism: biological effects and potential confounds. Biol Psychiatry. Elsevier; 2012;72:1043–1051.

297. Catani M, Craig MC, Forkel SJ, et al. Altered integrity of perisylvian language pathways in schizophrenia: relationship to auditory hallucinations. Biol Psychiatry. Elsevier; 2011;70:1143–1150.

298. Sethi A, Gregory S, Dell'Acqua F, et al. Emotional detachment in psychopathy: Involvement of dorsal default-mode connections. Cortex. 2015;62:11–19.

299. Vanderauwera J, Vandermosten M, Dell'Acqua F, Wouters J, Ghesquière P. Disentangling the relation between left temporoparietal white matter and reading: A spherical deconvolution tractography study. Hum Brain Mapp. 4 ed. 2015;36:3273–3287.

300. Bénézit A, Hertz-Pannier L, Dehaene-Lambertz G, et al. Organising white matter in a brain without corpus callosum fibres. Cortex. 2015;63:155–171.

301. Kanaan RAA, Borgwardt S, McGuire PK, et al. Microstructural organization of cerebellar tracts in schizophrenia. Biol Psychiatry. Elsevier; 2009;66:1067–1069.

302. Lord C, Risi S, Lambrecht L, et al. The autism diagnostic observation schedule-generic: a standard measure of social and communication deficits associated with the spectrum of autism. J Autism Dev Disord. 2000;30:205–223.

303. Jones DK, Basser PJ. "Squashing peanuts and smashing pumpkins": how noise distorts diffusion-weighted MR data. Magn Reson Med. Wiley Subscription Services, Inc., A Wiley Company; 2004;52:979–993.

304. Smith SM, Jenkinson M, Johansen-Berg H, et al. Tract-based spatial statistics: voxelwise analysis of multi-subject diffusion data. Neuroimage. 2006;31:1487–1505.

305. Witelson SF. Hand and sex differences in the isthmus and genu of the human corpus callosum. A postmortem morphological study. Brain. 1989;112 (Pt 3):799–835.

306. Aoki Y, Abe O, Nippashi Y, Yamasue H. Comparison of white matter integrity between autism spectrum disorder subjects and typically developing individuals: a meta-analysis of diffusion tensor imaging tractography studies. Mol Autism. BioMed Central; 2013;4:25.

307. Pardini M, Elia M, Garaci FG, et al. Long-term cognitive and behavioral therapies, combined with augmentative communication, are related to uncinate fasciculus integrity in autism. J Autism Dev Disord. 4 ed. 2012;42:585–592.

308. Vargas DL, Nascimbene C, Krishnan C, Zimmerman AW, Pardo CA. Neuroglial activation and neuroinflammation in the brain of patients with autism. Annals of Neurology. Wiley Subscription Services, Inc., A Wiley Company; 2005;57:67–81.

309. Mountcastle VB. The columnar organization of the neocortex. Brain. 1997;120 (Pt 4):701–722.

310. Casanova MF, Buxhoeveden DP, Switala AE, Roy E. Asperger's Syndrome and Cortical Neuropathology. Journal of Child Neurology. Sage PublicationsSage CA: Thousand Oaks, CA; 2016;17:142–145.

311. Casanova MF, Buxhoeveden DP, Switala AE, Roy E. Minicolumnar pathology in autism. Neurology. Lippincott Williams & Wilkins; 2002;58:428–432.

312. Zikopoulos B, Barbas H. Changes in prefrontal axons may disrupt the network in autism. J Neurosci. Society for Neuroscience; 2010;30:14595–14609.

313. Wolff JJ, Gu H, Gerig G, et al. Differences in white matter fiber tract development present from 6 to 24 months in infants with autism. Am J Psychiatry. American Psychiatric Publishing Arlington, VA; 2012;169:589–600.

314. Lisiecka DM, Holt R, Tait R, et al. Developmental white matter microstructure in autism phenotype and corresponding endophenotype during adolescence. Transl Psychiatry. Nature Publishing Group; 2015;5:e529.

315. Suckling J, Barnes A, Job D, et al. Power calculations for multicenter imaging studies controlled by the false discovery rate. Hum Brain Mapp. Wiley Subscription Services, Inc., A Wiley Company; 2010;31:1183–1195.

316. Suckling J, Barnes A, Job D, et al. The Neuro/PsyGRID calibration experiment: identifying sources of variance and bias in multicenter MRI studies. Hum Brain Mapp. Wiley Subscription Services, Inc., A Wiley Company; 2012;33:373–386.

317. Rogalski E, Cobia D, Harrison TM, et al. Anatomy of language impairments in primary progressive aphasia. J Neurosci. Society for Neuroscience; 2011;31:3344–3350.

318. Tantam D. Autism Spectrum Disorders Through the Life Span. Jessica Kingsley Publishers; 2012.

319. Yakovlev PI. Motility, behavior and the brain; stereodynamic organization and neural coordinates of behavior. The Journal of Nervous and Mental Disease. 1948;107:313–335.

320. Piguet O, Hornberger M, Mioshi E, Hodges JR. Behavioural-variant frontotemporal dementia: diagnosis, clinical staging, and management. The Lancet Neurology. 2011;10:162–172.

321. Zhang Y, Schuff N, Du A-T, et al. White matter damage in frontotemporal dementia and Alzheimer's disease measured by diffusion MRI. Brain. 2009;132:2579–2592.

322. Kawashima T, Nakamura M, Bouix S, et al. Uncinate fasciculus abnormalities in recent onset schizophrenia and affective psychosis: a diffusion tensor imaging study. Schizophr Res. 2009;110:119–126.

323. Kitis O, Ozalay O, Zengin EB, et al. Reduced left uncinate fasciculus fractional anisotropy in deficit schizophrenia but not in non-deficit schizophrenia. Psychiatry Clin Neurosci. Blackwell Publishing Asia; 2012;66:34–43.

324. Kubicki M, McCarley R, Westin C-F, et al. A review of diffusion tensor imaging studies in schizophrenia. J Psychiatr Res. 2007;41:15–30.

325. Papagno C, Miracapillo C, Casarotti A, et al. What is the role of the uncinate fasciculus? Surgical removal and proper name retrieval. Brain. 2011;134:405–414.

326. Crosby EC. Correlative Anatomy of the Nervous System. 1962.

327. Klinger J, Gloor P. The connections of the amygdala and of the anterior temporal cortex in the human brain. J Comp Neurol. 1960;115:333–369.

328. Papez JW. A proposed mechanism of emotion. Arch Neurol Psychiatry. Epub 1937.

329. Mayberg HS, Brannan SK, Tekell JL, et al. Regional metabolic effects of fluoxetine in major depression: serial changes and relationship to clinical response. Biol Psychiatry. 2000;48:830–843.

330. Pugliese L, Catani M, Ameis S, et al. The anatomy of extended limbic pathways in Asperger syndrome: a preliminary diffusion tensor imaging tractography study. Neuroimage. 2009;47:427–434.

331. Radua J, Mataix-Cols D. Voxel-wise meta-analysis of grey matter changes in obsessive-compulsive disorder. Br J Psychiatry. The Royal College of Psychiatrists; 2009;195:393–402.

332. Acosta-Cabronero J, Williams GB, Pengas G, Nestor PJ. Absolute diffusivities define the landscape of white matter degeneration in Alzheimer's disease. Brain. 2010;133:529–539.

333. Forkel SJ, Thiebaut de Schotten M, Dell'Acqua F, et al. Anatomical predictors of aphasia recovery: a tractography study of bilateral perisylvian language networks. Brain. 2014;137:2027–2039.

334. Miller BL, Cummings JL. The human frontal lobes. 2007.

335. Seeley WW, Bauer AM, Miller BL, et al. The natural history of temporal variant frontotemporal dementia. Neurology. Lippincott Williams & Wilkins; 2005;64:1384–1390.

Appendix A: Publications attributed to this thesis

D'Anna L, Mesulam Marsel M, Thiebaut de Schotten M, Dell'Acqua F, Murphy D, Wieneke C, Martersteck A, Cobia D, Rogalsky E, Catani M. *Fronto-temporal networks and behavioral symptoms in primary progressive aphasia.* Neurology. 2016 Apr 12;86(15):1393-9

Catani M, Dell'Acqua F, Howells H, Budisavljevic S, Thiebaut de Schotten M, Walsh S, **D'Anna L**, Abigal T, Edward T, Simon J, Michael V, Bhismadev S J, Meng-Chuan J, Amber NV, Ecker C, MRCAIMS, Murphy D. *Frontal networks in adults with autism spectrum disorder*. Brain. 2016 Feb;139(Pt 2):616-30.

D'Anna L, Tsermenteli S, Ecker C, Dell'Acqua F, Leigh PN, Murphy D, Goldstein LH, Catani M. *Neuronal correlates of cognitive and behavioural symptoms in Amyotrophic Lateral Sclerosis.* Under review on Psychological Medicine.

Neurology®
Volume 86, Number 15, April 12, 2016
Neurology.org
AMERICAN ACADEMY OF NEUROLOGY

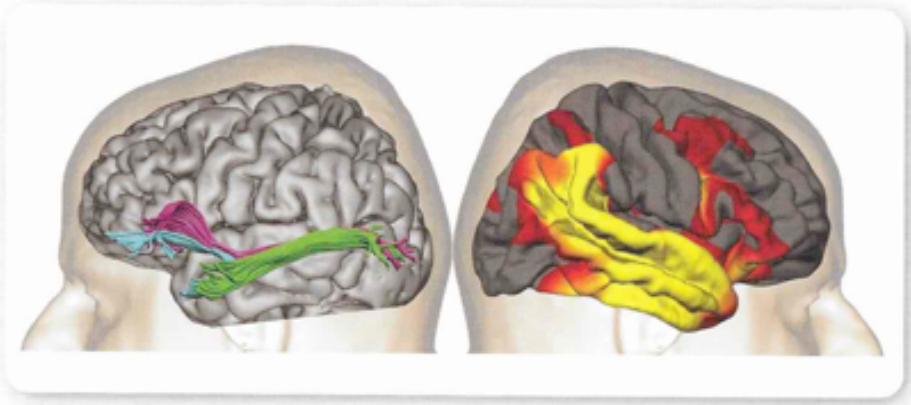

Better verbal memory in women than men in MCI despite similar levels of hippocampal atrophy, **p 1368**

Randomized, placebo-controlled trials of dichlorphenamide in periodic paralysis, **p 1408**

Health-related quality of life in multiple sclerosis: Direct and indirect effects of comorbidity, **p 1417**

AAN • 68th Annual Meeting
Vancouver, Canada • April 15–21, 2016

The most widely read and highly cited peer-reviewed neurology journal
THE OFFICIAL JOURNAL OF THE AMERICAN ACADEMY OF NEUROLOGY

Frontotemporal networks and behavioral symptoms in primary progressive aphasia

OPEN

Lucio D'Anna, MD
Marsel M. Mesulam, MD
Michel Thiebaut de Schotten, PhD
Flavio Dell'Acqua, PhD
Declan Murphy, MD
Christina Wieneke, BA
Adam Martersteck, BS
Derin Cobia, PhD
Emily Rogalski, PhD
Marco Catani, MD

Correspondence to Dr. Catani: m.catani@iop.kcl.ac.uk or Dr. D'Anna: lucio.d'anna@kcl.ac.uk

ABSTRACT

Objective: To determine if behavioral symptoms in patients with primary progressive aphasia (PPA) were associated with degeneration of a ventral frontotemporal network.

Methods: We used diffusion tensor imaging tractography to quantify abnormalities of the uncinate fasciculus that connects the anterior temporal lobe and the ventrolateral frontal cortex. Two additional ventral tracts were studied: the inferior fronto-occipital fasciculus and the inferior longitudinal fasciculus. We also measured cortical thickness of anterior temporal and orbitofrontal regions interconnected by these tracts. Thirty-three patients with PPA and 26 healthy controls were recruited.

Results: In keeping with the PPA diagnosis, behavioral symptoms were distinctly less prominent than the language deficits. Although all 3 tracts had structural pathology as determined by tractography, significant correlations with scores on the Frontal Behavioral Inventory were found only for the uncinate fasciculus. Cortical atrophy of the orbitofrontal and anterior temporal lobe cortex was also correlated with these scores.

Conclusions: Our findings indicate that damage to a frontotemporal network mediated by the uncinate fasciculus may underlie the emergence of behavioral symptoms in patients with PPA.

Neurology® 2016;86:1393–1399

GLOSSARY

ANOVA = analysis of variance; **bvFTD** = behavioral variant frontotemporal dementia; **DTI** = diffusion tensor imaging; **FBI** = Frontal Behavioral Inventory; **MPRAGE** = magnetization-prepared rapid gradient echo; **PPA** = primary progressive aphasia; **PPA-S** = primary progressive aphasia–semantic variant; **ROI** = region of interest.

Patients with primary progressive aphasia (PPA) show a gradual decline in language functioning with a relative sparing of other cognitive domains.[1] Although the aphasia is the major cause of impaired function, additional symptoms such as distress, sadness, apathy, and depression can be seen in almost half of patients with PPA, followed by changes in eating, aberrant motor behavior, agitation, disinhibition, and irritability.[1,2] In keeping with the progressive neurodegenerative etiologies of both PPA and behavioral variant frontotemporal dementia (bvFTD), it is not surprising that the symptom overlap between these 2 syndromes becomes increasingly more prominent as the disease progresses. In fact, approximately 75% of patients with PPA eventually develop severe behavioral problems, whereas 65% of patients with bvFTD manifest clear language impairment.[3]

Among the 3 variants of PPA, patients with the semantic form, in which the anatomical hallmark is represented by a marked atrophy of the anterior temporal lobes,[3] are at higher risk of developing behavioral symptoms compared with the other variants. Rohrer and Warren[4] found

Supplemental data at Neurology.org

From Natbrainlab, Department of Forensic and Neurodevelopmental Sciences (L.D., M.T.d.S., F.D., M.C.), Department of Neuroimaging (F.D.), and Sackler Institute of Translational Neurodevelopment (D.M.), Institute of Psychiatry, Psychology and Neuroscience (IoPPN), King's College London, UK; Neurology Clinic, Department of Experimental and Clinical Medical Sciences (L.D.), University of Udine Medical School; Department of Neurosciences (L.D.), "S. Maria della Misericordia" University Hospital, Udine, Italy; Cognitive Neurology and Alzheimer's Disease Center (M.M.M., C.W., A.M., D.C., E.R.) and Department of Neurology (M.M.M., A.M., D.C.), Northwestern University Feinberg School of Medicine, Chicago, IL; and Brain Connectivity and Behaviour, Brain and Spine Institute (M.T.d.S.), CNRS UMR 7225 INSERM-UPMC UMRS 1127 La Salpêtrière, Paris, France.

Go to Neurology.org for full disclosures. Funding information and disclosures deemed relevant by the authors, if any, are provided at the end of the article. The Article Processing Charge was paid by Wellcome Trust.

that in addition to anterior temporal lobe atrophy, the most significant anatomical cortical changes in patients with PPA and behavioral symptoms occur in the orbitofrontal cortex.

The anterior temporal and orbitofrontal regions are directly linked by the uncinate fasciculus. Although the association between degeneration of the uncinate fasciculus and semantic deficits is well-documented,[5,6] the role of the uncinate fasciculus in patients with PPA and behavioral symptoms is unknown.

The aim of our study was to determine, through a multimodal neuroimaging approach, the anatomical abnormalities underlying behavioral symptoms in patients with PPA. We used diffusion tensor imaging (DTI) tractography to assess the microstructural organization of the major association tracts connecting to the orbitofrontal cortex or the anterior temporal lobe.[7,8] We also measured cortical thickness of the orbitofrontal cortex and the anterior temporal lobe to determine whether white matter degeneration correlates with the degree of cortical atrophy.

METHODS **Participants and clinical assessment.** Thirty-three patients with PPA and 26 healthy controls matched for age, sex, and handedness were enrolled through the Primary Progressive Aphasia Program at the Cognitive Neurology and Alzheimer's Disease Centre, Northwestern University Feinberg School of Medicine.

The diagnosis of PPA was based on at least a 2-year history of progressive, isolated deterioration of speech or language functions. All patients were then classified into 1 of the 5 PPA variants based on several recent diagnostic classification guidelines.[1,3,10] Patients with PPA who presented a severe (e.g., Boston Naming Test <50%) single isolated language symptom (anomia or dyslexia) without fulfilling the criteria for the other variants were classified as unclassified variant.[10] Patients with PPA with a combination of agrammatism and semantic impairments were classified as mixed PPA.[11–13]

The Frontal Behavioral Inventory (FBI), originally developed and standardized with the purpose of differentiating bvFTD from other dementias and quantifying the severity of behavioral symptoms,[14,15] was used to assess behavioral symptoms.

The FBI is based on the evaluation of the patient's caregiver that for each item scores the severity of symptoms in a scale between 0 and 3 (0 = never, 1 = mild or occasional, 2 = moderate, 3 = severe or very frequent). The FBI is composed of 24 items divided into 12 items for negative behavior symptoms (FBI negative symptoms score) and 12 for positive symptoms (FBI positive symptoms score). The FBI negative symptoms score contains 3 items that evaluate behavioral symptoms in relation to language impairment (item 9, logopenia; item 10, aphasia and verbal apraxia; item 11, comprehension and semantic deficits). To effectively evaluate the behavioral symptoms in the patients with PPA, we subtracted these 3 language-related items from the FBI negative symptoms score and the FBI total scores. All statistical analyses were therefore performed using corrected scores for the total FBI and negative FBI.

MRI acquisition, DTI, and data processing. MRI acquisitions were carried out on a 3T Siemens Trio MRI system at the Centre for Translational Imaging, Northwestern University of Chicago. T1-weighted magnetization-prepared rapid gradient echo (MPRAGE) sequences were acquired with the following parameters: repetition time 2,300 ms; echo time 2.86 ms; flip angle, 9; field of view, 256 mm; 60 slices; slice thickness 1.0 mm, as previously described.[6] FreeSurfer image analysis suite (version 4.5.0) (http://surfer.nmr.mgh.harvard.edu/) was used to measure cortical thickness on T1-weighted MPRAGE images. Measures of cortical thickness were obtained by estimating the closest distance between the gray/white matter boundary and the gray matter/CSF boundary at each vertex of the tessellated surface.[6,16] Differences in cortical thickness between patients with PPA and healthy controls were shown on the entire surface area of the neocortex using an FDR of 0.001.[6,17] Cortical thickness was measured from a 20-mm region of interest (ROI) placed in the most atrophic anterior temporal and lateral orbitofrontal cortex, within the cortical projections areas of the uncinate fasciculus.

For the tractography analysis, we acquired a total of 72 contiguous near-axial slices using an acquisition sequence fully optimized for diffusion imaging, providing isotropic (2 × 2 × 2 mm) resolution and whole head coverage. At each slice location, 8 images were acquired with no diffusion gradient applied, together with 60 diffusion-weighted images (b value of 1,000 s/mm^2). Explore DTI (http://www.exploredti.com) was used to perform DTI processing and to correct simultaneously subject motion and geometrical distortions with reorientation of the b matrix. RESTORE function excluded the remaining outliers and robustly fitted the tensor model in all voxels of the brain.[18,19] Fractional anisotropy and radial diffusivity maps were calculated and saved in nifti format. A spline interpolated streamline algorithm was used to perform whole brain tractography (stepsize 0.5 mm; fractional anisotropy threshold 0.15; angle threshold 35). Finally, the whole brain tractography was imported in TrackVis (http://www.trackvis.org) for visualization.[6]

Tract-specific reconstructions and measurements. TrackVis was used to perform the virtual in vivo dissection of the 3 tracts of interest according to previously published methods.[6,20–25] Tractography dissections were obtained using manually defined ROIs on the orthogonal fractional anisotropy images. The following tracts were dissected as previously described.[7,21]

The uncinate fasciculus is a U-shaped bundle that arises in the temporal pole, lateral to the parahippocampal gyrus and amygdala. In the temporal lobe, the uncinate fasciculus is ventral to the inferior fronto-occipital fasciculus. Arching forward, the uncinate then enters the external capsule and splits into a ventrolateral and an anteromedial branch.[7] The ventrolateral component ends in the anterior insula and lateral orbitofrontal cortex, while the anteromedial branch reaches the olfactory cortex, the medial orbitofrontal cortex, and the frontal pole.[7] Dissections of the uncinate fasciculus were performed by placing a ROI in the anterior temporal lobe and a second ROI in the external/extreme capsule.[6,20,26]

The inferior fronto-occipital fasciculus originates from the inferior and medial surface of the occipital lobe. When the inferior fronto-occipital fasciculus leaves the temporal lobe, it reduces its section and its fibers come together when they reach the extreme/external capsule at higher level respect to the uncinate fasciculus. In the frontal lobe, the dorsolateral fibers of the inferior fronto-occipital fasciculus end mainly in the inferior frontal gyrus, while the most ventral fibers gather together, ending in the medial fronto-orbital region and frontal pole.[21,26]

Two ROIs were used to dissect the inferior fronto-occipital fasciculus, one placed in the occipital white matter and a second region in the external/extreme capsule.[20]

Finally, the inferior longitudinal fasciculus is a ventral associative bundle connecting the occipital and temporal lobes. To dissect the inferior longitudinal fasciculus, the first region was placed in the anterior temporal lobe and the second in the occipital white matter.[20,25]

For each tract of interest, number of streamlines, fractional anisotropy, mean diffusivity, and axial and perpendicular diffusivity were extracted as indices of microstructural composition and architecture of the brain tissue.[25] The number of streamlines was considered a surrogate of tract volume and atrophy.[6] In dementia syndromes, the number of streamlines is reduced according to the severity of the pathology and clinical symptoms.[6,27]

Fractional anisotropy is a quantitative index of the degree of anisotropy of the biological tissue and indirectly of microstructural integrity. Fractional anisotropy provides information about the biological properties and the microarchitecture of the white matter fibers. Reduced fractional anisotropy values have been reported in disorders characterized by demyelination, edema, or degeneration.[28]

Perpendicular and axial diffusivities correspond to the diffusivity along the principal directions of the diffusion tensor and are generally used to quantify changes due to axonal/myelin damage.[25,28]

Ten practice datasets were used to train the dissector (L.D.), who was blind to any information about the cortical thickness results and the identity of the participants. L.D. began the dissections for this study only when he achieved high reliability.

Statistical analysis. All statistical analyses were performed using SPSS (Chicago, IL) software (version 21). Independent-samples *t* tests were run to examine group differences in number of streamlines, fractional anisotropy, and axial and perpendicular diffusivity of the different tracts of interest. Bonferroni correction was applied to correct for multiple comparisons (threshold at $p \leq 0.001$). All *p* values are provided uncorrected. We used one-way analysis of variance (ANOVA) between groups to compare the differences between PPA subtypes and controls. Rho Spearman analysis was used to describe the strength and direction of the linear relationship between severity of behavioral symptoms and tract-specific measurements.

Standard protocol approvals, registrations, and patient consents. For this study, we received approval from an ethical standards committee on human experimentation for any experiments using human participants. We obtained written informed consents from all patients (or guardians of patients) participating in this study.

Table 1 Demographic and clinical data and behavioral features of the participants

	Patients with PPA (n = 33), n or mean ± SD	Healthy controls (n = 26), n or mean ± SD	Group comparisons
Age, y	64.88 ± 6.60	62.61 ± 8.19	p = 0.282
Duration of illness, y	3.63 ± 1.80	—	—
Sex, n			
Male	13	14	
Female	20	12	p = 0.269
Handedness (EHI score)	97.12 ± 7.70	93.65 ± 9.85	p = 0.135
FBI negative score	6.39 ± 5.53	—	—
FBI positive score	3.93 ± 5.15	—	—
FBI total score	10.51 ± 9.63	—	—

Abbreviations: EHI = Edinburgh Handedness Inventory; FBI = Frontal Behavioral Inventory. Group comparisons were performed using *t* test or χ^2.

RESULTS Demographic, clinical, and behavioral features of our sample are reported in tables 1 and 2. Among the patients with PPA, 8 received a descriptive diagnosis of logopenic variant, 8 of nonfluent/agrammatic variant, 7 of semantic variant (PPA-S), 2 of mixed variant, and 8 of unclassified/severe variant.[1,9,10] The PPA-S group were younger compared to the other variants and had higher prevalence of behavioral symptoms as reported in the FBI total scores and FBI positive symptoms scores.

White matter connections analysis. After Bonferroni correction the left uncinate fasciculus of patients with PPA showed a significantly reduced number of streamlines ($p < 0.001$, $t_{[54]}$ value = 7.942), lower fractional anisotropy ($p < 0.001$, $t_{[54]} = 3.253$), and a significant increase in axial ($p < 0.001$, $t_{[54]} = -2.849$) and perpendicular diffusivity ($p = 0.020$, $t_{[54]} = -2.264$) compared with healthy controls (figure 1, left). In the right hemisphere only the number of streamlines was significantly reduced also in the uncinate fasciculus of patients with PPA when compared with healthy controls ($p < 0.001$, $t_{[54]} = 5.193$) (figure 1).

ANOVA between PPA subtypes and controls showed statistically significant differences between groups in the number of streamlines ($F = 4.933$; $p = 0.001$), axial diffusivity ($F = 5.038$; $p < 0.001$), perpendicular diffusivity ($F = 7.902$; $p < 0.001$), and mean diffusivity ($F = 7.243$; $p < 0.001$). Abnormalities in the left uncinate fasciculus were particularly evident for the semantic subtype when compared with the other variants (figure e-1 on the *Neurology*® Web site at Neurology.org).

In the left uncinate fasciculus, the number of streamlines and fractional anisotropy were inversely correlated with total FBI scores (Spearman = −0.549, $p = 0.001$ and Spearman = −0.490, $p < 0.001$, respectively) and with both positive (Spearman = −0.530, $p = 0.001$ and Spearman = −0.500, $p < 0.001$, respectively) and negative FBI scores (Spearman = −0.460, $p < 0.001$ and Spearman = −0.450, $p < 0.001$, respectively), whereas axial and perpendicular diffusivity correlated directly with total FBI scores (Spearman = 0.450, $p < 0.001$ and Spearman = 0.540, $p < 0.001$, respectively) and with both positive (Spearman = 0.400, $p < 0.001$ and Spearman = 0.600, $p < 0.001$, respectively) and negative FBI scores (Spearman = 0.575, $p < 0.001$ and Spearman = 0.540, $p < 0.001$, respectively). These correlations indicate that behavioral symptoms are associated with poorer white matter integrity (table e-1, figure e-2). In the right uncinate fasciculus, axial

Table 2 Demographic and clinical and behavioral features of the PPA variants

Variable	PPA-L (n = 8), mean ± SD	PPA-G (n = 8), mean ± SD	PPA-S (n = 7), mean ± SD	PPA mixed (n = 2), mean ± SD	PPA unclassified (n = 8), mean ± SD
Age, y	66.13 ± 6.98	65.13 ± 5.64	57.14 ± 3.71[a]	68.50 ± 10.60	69.25 ± 10.53
Duration of illness, y	3.36 ± 2.17	3.61 ± 1.19	3.47 ± 1.25	5.75 ± 6.01	3.56 ± 0.86
FBI-negative score	4.00 ± 3.74	4.93 ± 5.17	10.79 ± 6.05	6.00 ± 8.48	6.50 ± 5.42
FBI-positive score	1.25 ± 1.38	2.50 ± 4.10	9.71 ± 6.67[a]	6.50 ± 7.77	2.37 ± 2.61
FBI total score	6.00 ± 3.66	7.43 ± 8.68	20.50 ± 11.75[a]	12.50 ± 16.26	8.87 ± 6.40

Abbreviations: FBI = Frontal Behavioral Inventory; PPA = primary progressive aphasia; PPA mixed = mixed primary progressive aphasia; PPA unclassified = unclassified/severe primary progressive aphasia variant; PPA-L = primary progressive aphasia-logopenic variant; PPA-G = primary progressive aphasia-nonfluent/agrammatic variant; PPA-S = primary progressive aphasia-semantic variant.
[a] Statistically different vs other variants ($p < 0.05$).

diffusivity was correlated with negative (Spearman = 0.443, $p = 0.005$), positive (Spearman = 0.432, $p = 0.005$), and total FBI scores (Spearman = 0.421, $p = 0.001$); perpendicular diffusivity was correlated with FBI negative, positive, and total scores (Spearman = 0.497, $p < 0.001$; Spearman = 0.576, $p < 0.001$; Spearman = 0.580, $p < 0.001$) (table e-1). ANOVA between PPA subtypes and controls showed statistically

Figure 1 Tract-specific measurements

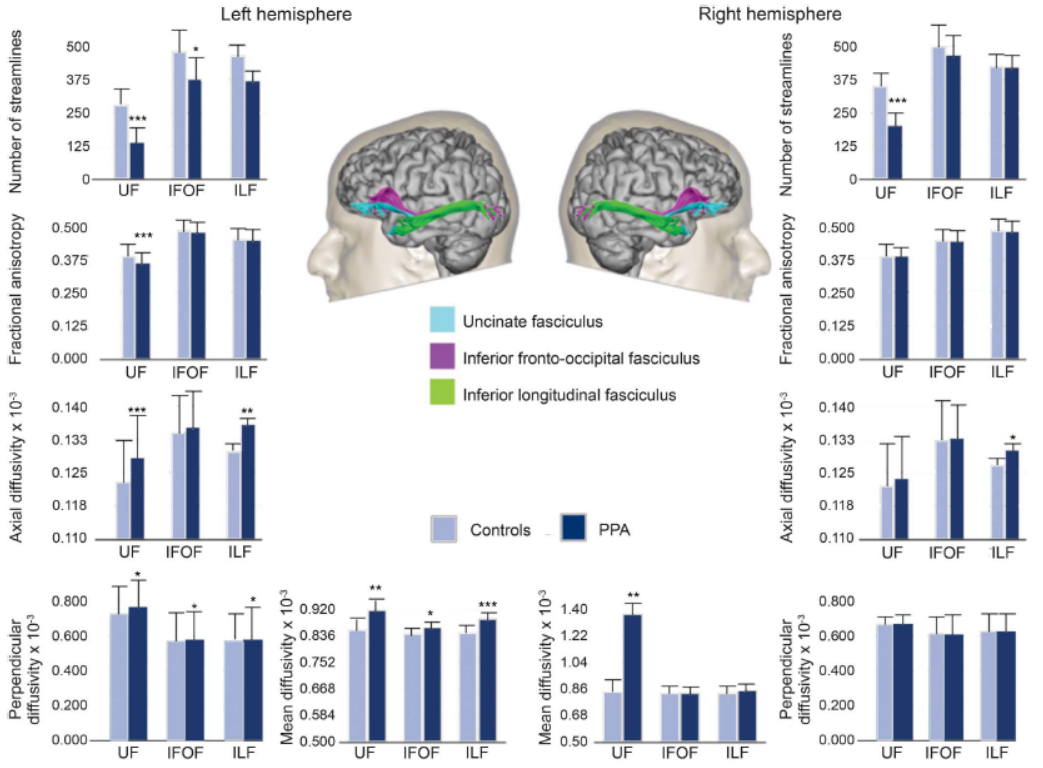

Differences in tract-specific measurements of the uncinate fasciculus (UF), inferior fronto-occipital fasciculus (IFOF), and inferior longitudinal fasciculus (ILF) between controls and patients with primary progressive aphasia (PPA). Measurements of the number of streamlines, fractional anisotropy, mean diffusivity, axial diffusivity, and perpendicular diffusivity are reported for the tracts of interest. Statistically significant differences between controls and patients within each tract are indicated with asterisks (*$p < 0.05$; **$p < 0.01$; ***$p < 0.001$; Bonferroni threshold for significance = 0.0016).

significant differences in the number of streamlines ($F = 4.840$; $p = 0.003$) and axial diffusivity ($F = 3.943$; $p < 0.04$), which were particularly evident for the semantic subtype when compared to the other variants (figure e-1).

In the left inferior fronto-occipital fasciculus, the patients with PPA showed significantly fewer streamlines ($p = 0.036$, $t_{[54]} = 2.256$) and higher perpendicular diffusivity ($p = 0.028$, $t_{[54]} = -2.145$) when compared with healthy controls. No statistically significant differences were found for this tract in the right hemisphere (figure 1). ANOVA between PPA subtypes and controls did not show statistically significant differences between groups in terms of DTI measurements (figure e-3). We found no statistically significant correlations between any of the tractography measurements of the inferior fronto-occipital fasciculus and the scores of the FBI (table e-1).

In the inferior longitudinal fasciculus, patients with PPA showed a statistically significant increase of axial diffusivity in both sides (left: $p = 0.002$, $t_{[54]} = -3.342$; right: $p = 0.030$, $t_{[54]} = -2.223$) and perpendicular diffusivity in the left side ($p = 0.020$, $t_{[54]} = -2.396$) (figure 1). ANOVA between PPA subtypes and controls did not show statistically significant differences between groups in terms of DTI measurements (figure e-4). No significant correlations were found between diffusivity measurements of the inferior longitudinal fasciculus and scores on the FBI (table e-1).

Cortical thickness analysis. A whole brain analysis showed significant cortical atrophy of the left temporal-parietal and frontal regions in the PPA compared with controls (figure 2). A ROI approach confirmed that compared with healthy controls, patients with PPA showed significant atrophy in the left ($p < 0.001$, $t_{[57]} = 4.367$) and right ($p = 0.014$, $t_{[57]} = 2.537$) orbitofrontal cortex and in the left ($p = 0.001$, $t_{[57]} = 3.391$) and right ($p = 0.004$, $t_{[57]} = 2.996$) anterior temporal lobe. Cortical thickness of the ROIs in the left orbitofrontal and anterior temporal cortex were inversely correlated with negative scores (Spearman = −0.460, $p = 0.001$ and Spearman = −0.521, $p = 0.001$, respectively), positive scores (Spearman = −0.523, $p = 0.001$ and Spearman = −0.590, $p < 0.001$, respectively), and total scores in the FBI (Spearman = −0.534, $p = 0.001$ and Spearman = −0.580, $p < 0.001$, respectively) (figure 2). Correlations between the

Figure 2 **Correlations between left cortical thickness and Frontal Battery Inventory (FBI) scores**

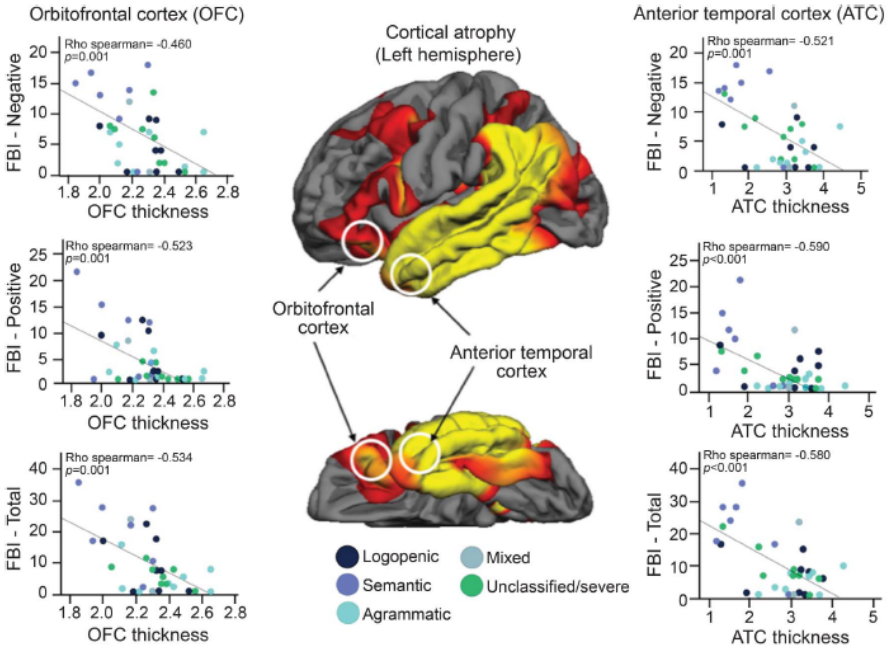

The cortical thickness measurements of the left orbitofrontal cortex and anterior temporal lobe showed a statistically significant correlation with FBI negative, positive, and total scores.

right anterior temporal lobe and the scores on the FBI were less significant (table e-2).

In addition, cortical thickness measurements of both anterior temporal lobe and orbitofrontal cortex were directly correlated with fractional anisotropy (Spearman = 0.488, $p = 0.003$ and Spearman = 0.524, $p = 0.001$, respectively), and inversely correlated with axial diffusivity (Spearman = −0.570, $p = 0.001$ and Spearman = −0.378, $p = 0.007$, respectively) and perpendicular diffusivity (Spearman = −0.580, $p = 0.001$ and Spearman = −0.513, $p = 0.002$, respectively) (table e-3). Similar correlations were found for the right uncinate fasciculus (table e-4). No correlations were found between cortical thickness measurements and DTI measurements of the inferior fronto-occipital fasciculus and inferior longitudinal fasciculus (tables e-3 and e-4).

DISCUSSION Our findings showed that damage to a ventral frontotemporal network is correlated with behavioral symptoms in PPA (tables e-5 to e-8).

In previous studies,[29] degeneration of the uncinate fasciculus has been found to correlate with behavioral symptoms in several other conditions affecting anterior temporal and orbitofrontal regions. In bvFTD, for example, the white matter damage in the uncinate fasciculus correlates with severity of apathy, impulsivity, inappropriate sexual behavior, and hoarding.[30] In patients with idiopathic psychopathy,[22] altered integrity of the uncinate fasciculus correlates with severity of antisocial behavior, which includes poor behavioral control, impulsivity, need for stimulation, proneness to boredom, lack of realistic goals, and irresponsibility. We had previously shown that damage to the uncinate fasciculus was correlated with semantic processing deficits in PPA.[5,6] The current results reveal the additional association of this fasciculus with behavioral symptoms in this group of patients. Overall, these studies confirm that the uncinate fasciculus has a major role in a wide range of comportments and that its damage is associated with behavioral deficits irrespective of the presenting syndrome and underlying etiology.[7,31]

The uncinate fasciculus is the major association pathway between the anterior part of the temporal lobe, including the amygdala, and the ventral frontal (orbitofrontal) region.[20] The temporopolar and ventral frontal cortices constitute multimodal convergence zones for sensory information.[32] Here the stimuli are processed independently of their reward or punishment value.[33] These cortical areas, and the amygdala with which they are interconnected, collectively play pivotal roles in multimodal integration as well as the motivational guidance and cognitive filtering of behavior.[30] Our findings suggest that disruption of this network may underlie some of the behavioral abnormalities that emerge in PPA.[34,35] The lack of a correlation between FBI scores and damage to the inferior fronto-occipital and inferior longitudinal fasciculi supports the relative specificity of this relationship. It appears therefore that the uncinate fasciculus has a dual functionality, one related to lexico-semantic processing[8] and the other to a broad range of behaviors.[7]

In our study, we confirmed that among the patients with PPA, those with the semantic variant have the most severe damage to the uncinate fasciculus. Postmortem studies revealed that the most common pathology affecting the semantic variant is ubiquitin/TDP43-positive frontotemporal lobar degeneration, which is characterized by numerous dystrophic neurites associated with neuronal and synaptic loss.[10] It is therefore most likely that diffusivity abnormalities in the uncinate fasciculus reflect axonal degeneration of the white matter fibers secondary to the cortical pathology.

Our findings confirm the existence of significant white matter damage in PPA[36] and support the importance of anterior frontotemporal connections in sustaining normal behavior in humans. Future studies using higher resolution datasets and advanced methods for fiber crossing[37] could help to isolate individual components of the uncinate fasciculus and their different functional correlates.

AUTHOR CONTRIBUTIONS

Dr. D'Anna: analysis and interpretation, acquisition of data, revision of the manuscript for important intellectual content. Dr. Mesulam: revision of the manuscript for important intellectual content, study supervision, study concept and design. Dr. Thiebaut de Schotten: acquisition of data, revision of the manuscript for important intellectual content. Dr. Dell'Acqua: acquisition of data. Prof. Murphy: revision of the manuscript for important intellectual content. Dr. Wieneke: acquisition of data. Dr. Martersteck: acquisition of data. Dr. Cobia: acquisition of data. Dr. Rogalski: revision of the manuscript for important intellectual content, study supervision, study concept and design. Dr. Catani: revision of the manuscript for important intellectual content, study supervision, study concept and design.

ACKNOWLEDGMENT

The authors thank the NatBrainLab (www.natbrainlab.com) for discussion.

STUDY FUNDING

Marco Catani is the recipient of the Welcome Trust New Investigator Award number 103759/Z/14/Z. This work was supported by the following grants: DC008552 from the National Institute on Deafness and Communication Disorders (NIDCD), AG13854 (the Alzheimer Disease Centre) from the National Institute on Aging (NIA), NS075075 from the National Institute of Neurological Disorders and Stroke (NINDS), and 5KL2RR025740 from the National Centre for Research Resources. The content of this manuscript is solely the responsibility of the authors and does not necessarily represent the official views of the National Centre for Research Resources or the NIH. Michel Thiebaut de Schotten is funded by the "Agence Nationale de la Recherche" (grant ANR-13-JSV4-0001-01).

DISCLOSURE

The authors report no disclosures relevant to the manuscript. Go to Neurology.org for full disclosures.

Received March 3, 2015. Accepted in final form January 7, 2016.

REFERENCES

1. Mesulam MM. Slowly progressive aphasia without generalized dementia. Ann Neurol 1982;11:592–598.
2. Fatemi Y, Boeve BF, Duffy J, et al. Neuropsychiatric aspects of primary progressive aphasia. J Neuropsychiatry Clin Neurosci 2011;23:168–172.
3. Rosen HJ, Allison SC, Ogar JM, et al. Behavioral features in semantic dementia vs other forms of progressive aphasias. Neurology 2006;67:1752–1756.
4. Rohrer JD, Warren JD. Phenomenology and anatomy of abnormal behaviours in primary progressive aphasia. J Neurol Sci 2010;293:35–38.
5. Galantucci S, Tartaglia MC, Wilson SM, et al. White matter damage in primary progressive aphasias: a diffusion tensor tractography study. Brain 2011;134:3011–3029.
6. Catani M, Mesulam MM, Jakobsen E, et al. A novel frontal pathway underlies verbal fluency in primary progressive aphasia. Brain 2013;136:2619–2628.
7. Catani M, Dell'Acqua F, Thiebaut de Schotten M. A revised limbic system model for memory, emotion and behaviour. Neurosci Biobehav Rev 2013;37:1724–1737.
8. Catani M, Bambini V. A model for Social Communication And Language Evolution and Development (SCALED). Curr Opin Neurobiol 2014;28:165–171.
9. Mesulam MM. Primary progressive aphasia. Ann Neurol 2001;49:425–432.
10. Gorno-Tempini ML, Hillis AE, Weintraub S, et al. Classification of primary progressive aphasia and its variants. Neurology 2011;76:1006–1014.
11. Mesulam MM, Weintraub S. Is it time to revisit the classification guidelines for primary progressive aphasia? Neurology 2014;82:1108–1109.
12. Mesulam MM, Wieneke C, Thompson C, Rogalski E, Weintraub S. Quantitative classification of primary progressive aphasia at early and mild impairment stages. Brain 2012;135:1537–1553.
13. Mesulam M, Wieneke C, Rogalski E, Cobia D, Thompson C, Weintraub S. Quantitative template for subtyping primary progressive aphasia. Arch Neurol 2009;66:1545–1551.
14. Kertesz A, Nadkarni N, Davidson W, Thomas AW. The frontal behavioral inventory in the differential diagnosis of frontotemporal dementia. J Int Neuropsychol Soc 2000;6:460–468.
15. Kertesz A, Davidson W, Fox H. Frontal behavioral inventory: diagnostic criteria for frontal lobe dementia. Can J Neurol Sci 1997;24:29–36.
16. Fischl B, Dale AM. Measuring the thickness of the human cerebral cortex from magnetic resonance images. Proc Natl Acad Sci USA 2000;97:11050–11055.
17. Rogalski E, Cobia D, Harrison TM, Wieneke C, Weintraub S, Mesulam MM. Progression of language decline and cortical atrophy in subtypes of primary progressive aphasia. Neurology 2011;76:1804–1810.
18. Chang L-C, Jones DK, Pierpaoli C. RESTORE: robust estimation of tensors by outlier rejection. Magn Reson Med 2005;53:1088–1095.
19. Jones DK, Basser PJ. "Squashing peanuts and smashing pumpkins": how noise distorts diffusion-weighted MR data. Magn Reson Med 2004;52:979–993.
20. Catani M, Thiebaut de Schotten M. A diffusion tensor imaging tractography atlas for virtual in vivo dissections. Cortex 2008;44:1105–1132.
21. Forkel SJ, Thiebaut de Schotten M, Kawadler JM, Dell'Acqua F, Danek A, Catani M. The anatomy of fronto-occipital connections from early blunt dissections to contemporary tractography. Cortex 2014;56:73–84.
22. Craig MC, Catani M, Deeley Q, et al. Altered connections on the road to psychopathy. Mol Psychiatry 2009;14:1–8.
23. Catani M, Thiebaut de Schotten M. Atlas of Human Brain Connections. New York: Oxford University Press; 2012.
24. Thiebaut de Schotten M, Dell'Acqua F, Valabregue R, Catani M. Monkey to human comparative anatomy of the frontal lobe association tracts. Cortex 2012;48:82–96.
25. Catani M. Occipito-temporal connections in the human brain. Brain 2003;126:2093–2107.
26. Catani M, Howard RJ, Pajevic S, Jones DK. Virtual in vivo interactive dissection of white matter fasciculi in the human brain. Neuroimage 2002;17:77–94.
27. Catani M. Diffusion tensor magnetic resonance imaging tractography in cognitive disorders. Curr Opin Neurol 2006;19:599–606.
28. Dell'Acqua F, Catani M. Structural human brain networks: hot topics in diffusion tractography. Curr Opin Neurol 2012;25:375–383.
29. Oishi K, Faria AV, Hsu J, Tippett D, Mori S, Hillis AE. Critical role of the right uncinate fasciculus in emotional empathy. Ann Neurol 2015;77:68–74.
30. Heide Von Der RJ, Skipper LM, Klobusicky E, Olson IR. Dissecting the uncinate fasciculus: disorders, controversies and a hypothesis. Brain 2013;136:1692–1707.
31. Ameis SH, Catani M. Altered white matter connectivity as a neural substrate for social impairment in Autism Spectrum Disorder. Cortex 2015;62:158–181.
32. Mesulam M-M. Principles of Behavioural and Cognitive Neurology. New York: Oxford University Press; 2000.
33. Rolls ET. Limbic systems for emotion and for memory, but no single limbic system. Cortex 2015;62:119–157.
34. Hughes LE, Rowe JB. The impact of neurodegeneration on network connectivity: a study of change detection in frontotemporal dementia. J Cogn Neurosci 2013;25:802–813.
35. Tan RH, Wong S, Kril JJ, et al. Beyond the temporal pole: limbic memory circuit in the semantic variant of primary progressive aphasia. Brain 2014;137:2065–2076.
36. Catani M, Piccirilli M, Cherubini A, et al. Axonal injury within language network in primary progressive aphasia. Ann Neurol 2003;53:242–247.
37. Dell'Acqua F, Scifo P, Rizzo G, et al. A modified damped Richardson–Lucy algorithm to reduce isotropic background effects in spherical deconvolution. Neuroimage 2010;49:1446–1458.

doi:10.1093/brain/awv351 BRAIN 2016: 139; 616–630 | 616

BRAIN
A JOURNAL OF NEUROLOGY

Frontal networks in adults with autism spectrum disorder

Marco Catani,[1,2] Flavio Dell'Acqua,[2] Sanja Budisavljevic,[1] Henrietta Howells,[1] Michel Thiebaut de Schotten,[1] Seán Froudist-Walsh,[1] Lucio D'Anna,[1] Abigail Thompson,[1] Stefano Sandrone,[1] Edward T. Bullmore,[3,4] John Suckling,[3,4,5] Simon Baron-Cohen,[3,5] Michael V. Lombardo,[5,6] Sally J. Wheelwright,[5] Bhismadev Chakrabarti,[5,7] Meng-Chuan Lai,[5,8,9] Amber N. V. Ruigrok,[5] Alexander Leemans,[10] Christine Ecker,[1] MRC AIMS Consortium,[†] Michael C. Craig[1,11,*] and Declan G. M. Murphy[1,*]

*These authors contributed equally to this work.

[†]See Appendix 1.

It has been postulated that autism spectrum disorder is underpinned by an 'atypical connectivity' involving higher-order association brain regions. To test this hypothesis in a large cohort of adults with autism spectrum disorder we compared the white matter networks of 61 adult males with autism spectrum disorder and 61 neurotypical controls, using two complementary approaches to diffusion tensor magnetic resonance imaging. First, we applied tract-based spatial statistics, a 'whole brain' non-hypothesis driven method, to identify differences in white matter networks in adults with autism spectrum disorder. Following this we used a tract-specific analysis, based on tractography, to carry out a more detailed analysis of individual tracts identified by tract-based spatial statistics. Finally, within the autism spectrum disorder group, we studied the relationship between diffusion measures and autistic symptom severity. Tract-based spatial statistics revealed that autism spectrum disorder was associated with significantly reduced fractional anisotropy in regions that included frontal lobe pathways. Tractography analysis of these specific pathways showed increased mean and perpendicular diffusivity, and reduced number of streamlines in the anterior and long segments of the arcuate fasciculus, cingulum and uncinate—predominantly in the left hemisphere. Abnormalities were also evident in the anterior portions of the corpus callosum connecting left and right frontal lobes. The degree of microstructural alteration of the arcuate and uncinate fasciculi was associated with severity of symptoms in language and social reciprocity in childhood. Our results indicated that autism spectrum disorder is a developmental condition associated with abnormal connectivity of the frontal lobes. Furthermore our findings showed that male adults with autism spectrum disorder have regional differences in brain anatomy, which correlate with specific aspects of autistic symptoms. Overall these results suggest that autism spectrum disorder is a condition linked to aberrant developmental trajectories of the frontal networks that persist in adult life.

1 Sackler Institute for Translational Neurodevelopment, and Department of Forensic and Neurodevelopmental Sciences, Institute of Psychiatry, King's College, London, UK
2 NatBrainLab, Centre for Neuroimaging Sciences, Institute of Psychiatry, King's College, London, UK
3 Cambridgeshire and Peterborough NHS Foundation Trust
4 Brain Mapping Unit, Department of Psychiatry, University of Cambridge, UK
5 Autism Research Centre, Department of Psychiatry, University of Cambridge, UK
6 Department of Psychology and Center for Applied Neuroscience, University of Cyprus, Cyprus
7 Centre for Integrative Neuroscience and Neurodynamics, School of Psychology and Clinical Language Sciences, University of Reading, Reading, UK
8 Centre for Addiction and Mental Health and Department of Psychiatry, University of Toronto, Canada

Received July 21, 2015. Revised September 30, 2015. Accepted October 2, 2015

9 Department of Psychiatry, National Taiwan University Hospital and College of Medicine, Taiwan
10 Image Sciences Institute, University Medical Center Utrecht, Utrecht, The Netherlands
11 National Autism Unit, South London and Maudsley NHS Foundation Trust, Bethlem Royal Hospital, Beckenham, UK

Correspondence to: Marco Catani,
NatBrainLab, PO50,
Institute of Psychiatry, Psychology and Neuroscience,
De Crespigny Park, London SE5 8AF, UK
E-mail: m.catani@iop.kcl.ac.uk

Keywords: autism spectrum disorder; diffusion tractography; frontal networks; language; arcuate fasciculus;

Abbreviations: ADI-R = Autism Diagnostic Interview–Revised; ADOS = Autism Diagnostic Observation Schedule; ASD = autism spectrum disorder; TBSS = tract-based spatial statistics

Introduction

Approximately 1% of the population have an autistic spectrum disorder (ASD), with a male:female ratio of 2.5:1 (Lai *et al.*, 2014). Recent advances in brain imaging have enabled *in vivo* mapping of the structural and functional characteristics associated with ASD. Several structural neuroimaging studies have implicated abnormalities in a number of brain regions, including the frontal and temporal cortex, the caudate nucleus, cerebellum, amygdala and hippocampus (Abell *et al.*, 1999; Waiter *et al.*, 2004; McAlonan *et al.*, 2005, 2008; Brieber *et al.*, 2007; Craig *et al.*, 2007; Bonilha *et al.*, 2008; Ke *et al.*, 2008; Lange *et al.*, 2010; Toal *et al.*, 2010; Cauda *et al.*, 2011; Via *et al.*, 2011; Nickl-Jockschat *et al.*, 2012; Nordahl *et al.*, 2012). Functional neuroimaging studies have also reported altered activation of these regions during tasks involving social, emotion and language processing (Baron-Cohen *et al.*, 1999; Pierce *et al.*, 2001; Just *et al.*, 2004; Ashwin *et al.*, 2007; Philip *et al.*, 2012). However, some of these findings have not been consistently replicated (Stigler *et al.*, 2011).

Inconsistency amongst previous findings is probably due to a variety of factors including small sample sizes, failure to apply strict diagnostic criteria and variability in confounding factors such as age and IQ (Freitag *et al.*, 2009). In addition, the majority of previous studies analysed only grey matter at the cortical and subcortical level. However, these regions do not function independently; rather they are interconnected through a complex system of short- and long-range tracts running within the white matter of each hemisphere (Catani and Bambini, 2014). White matter tract 'connectivity' regulates the speed and timing of activation across neural networks. These factors are necessary for optimum performance of higher-order tasks that rely on integrated information processing (Fields, 2008).

'Atypical connectivity' theories of ASD have postulated that higher-order association areas of the brain are partially disconnected during development (Belmonte *et al.*, 2004; Frith, 2004; Courchesne and Pierce, 2005; Geschwind and Levitt, 2007; Just *et al.*, 2012). Regional white matter structural abnormalities in ASD have been reported using different methods, from early region of interest approaches on structural MRI scans to, more recently, tract-specific virtual dissections of diffusion tensor MRI (DT-MRI) datasets (for a recent review see Ameis and Catani, 2015). Both approaches are mainly hypothesis driven and have therefore usually been limited to single regions or specific tracts (Aoki *et al.*, 2013), such as the midsagittal portion of the corpus callosum (Frazier and Hardan, 2009), or the core of the arcuate and uncinate fasciculus (Hardan *et al.*, 2000; Fletcher *et al.*, 2010), but sample sizes have tended to be small (Billeci *et al.*, 2012; Travers *et al.*, 2012; Mueller *et al.*, 2013). Other studies based on meta-analytical approaches (Radua *et al.*, 2011; Aoki *et al.*, 2013; Cauda *et al.*, 2014), voxel-based morphometry (Barnea-Goraly *et al.*, 2004; Keller *et al.*, 2007; Cheung *et al.*, 2009; Ke *et al.*, 2009; Lee *et al.*, 2009; Bloemen *et al.*, 2010; Noriuchi *et al.*, 2010; Groen *et al.*, 2011; Jou *et al.*, 2011), and tract-based spatial statistics (TBSS) (Barnea-Goraly *et al.*, 2010; Cheng *et al.*, 2010; Sahyoun *et al.*, 2010; Jou *et al.*, 2011; Shukla *et al.*, 2010; Walker *et al.*, 2012) have attempted to overcome some of the limitations attributable to small sample size and/or operator-dependent biases. However, it remains unclear whether the findings, if replicated in larger studies, are indicative of tract-specific anomalies in ASD or part of a more generalized brain abnormality (Wolff *et al.*, 2012). Therefore in this study we used two complementary approaches to analyse white matter connections in adults with ASD.

First, we applied TBSS (Smith *et al.*, 2006). This is a fully automated, operator-independent approach that permits a whole-brain analysis of white matter integrity in a voxel-wise manner. It has the potential to identify white matter differences in regions not previously considered to be of importance in a particular cohort and is resistant to operator bias. However, TBSS is affected by partial volume effects in regions accurate localization of between-group differences within specific tracts can be difficult with TBSS, as differences are often found in regions containing more than one tract (Catani, 2006). Therefore, after identifying regions of interest using TBSS, our second approach focused on specific tracts in greater detail using an approach based on DT-MRI tractography.

DT-MRI tractography facilitates the reconstruction of 3D trajectories of specific white matter tracts and probe their microstructural integrity. It permits a more detailed analysis of specific subpopulations of fibres, and indirect volumetric indices (e.g. number of streamlines and tract volume), which cannot be measured with TBSS. It has been applied to a wide range of neurodevelopmental conditions in addition to ASD (Catani *et al.*, 2011), including psychopathy (Craig *et al.*, 2009; Sethi *et al.*, 2015), dyslexia (Vanderauwera *et al.*, 2015), acallosal brain (Forkel *et al.*, 2014; Bénézit *et al.*, 2015) and schizophrenia (Kanaan *et al.*, 2009; Catani *et al.*, 2011). These studies suggest that this method of white matter sampling may be particularly well suited for neurodevelopmental conditions, including ASD, as changes are likely to occur along the entire course of the fibres, rather than be localized within circumscribed areas.

In summary, our aim was to understand whether white matter abnormalities in ASD are diffuse or localized to specific tracts. We also hypothesized that in adults with ASD the intensity of the white matter differences would be linked to the severity of symptoms in social interactions, repetitive behaviour and communication.

Materials and methods

Participants

Sixty-one male right-handed adults with ASD and 61 matched neurotypical male controls aged 18 to 45 years were recruited by advertisement and subsequently assessed at one of two collaborating autism research centres in the UK that make up the Medical Research Council UK Autism Imaging Multicentre Study (MRC AIMS) Consortium: the Institute of Psychiatry at Kings College London and the Autism Research Centre at the University of Cambridge. Equal ratios of cases to controls were recruited at each site: London, 34:34; Cambridge, 27:27. Overall intellectual ability was assessed using the Wechsler Abbreviated Scale of Intelligence (Wechsler, 1999). All participants fell within the high-functioning range on the spectrum defined by a full-scale IQ > 70. All participants with ASD were diagnosed according to International Statistical Classification of Diseases, 10th Revision research criteria (ICD10-R) (WHO, 1983), confirmed using the Autism Diagnostic Interview-Revised (ADI-R) (Lord *et al.*, 1994). The ADI-R is a semi-structured interview of parents that focuses primarily on the key diagnostic characteristics specified in the ICD10-R and DSM IV-R (Diagnostic and Statistical Manual of Mental Disorders); namely those features concerned with developmental delays, differences in reciprocal social interactions, language, communication and play, and restricted and stereotyped behaviours and interests. Many items concentrate on the age 4 to 5 year period.

All cases of ASD reached ADI-R algorithm cut-off values in the three domains of autism characteristics (social reciprocity, communication, repetitive and restricted behaviours and interests), although failure to reach cut-off in one of the domains by one point was permitted. Current symptoms were assessed using the Autism Diagnostic Observation Schedule (ADOS) (Lord *et al.*, 2000) but were not used as inclusion criteria. The ADOS is a semi-structured assessment of communication, social interaction and imaginative use of materials. Module 4 is designed for use with verbally fluent adolescents or adults, and describes a standardized interview/observational assessment consisting of 9–14 activities with 31 accompanying

Table 1 Subject demographics

Characteristics[a]	Healthy controls ($n = 61$)	ASD group ($n = 61$)
Age, years	28 (±6.7) [18–45]	26 (±6.9) [18–41]
Full-scale IQ, WASI	114 (±11.1) [86–137]	111 (±13) [77–135]
Performance IQ, WASI[b]	116 (±10.5) [94–135]	109 (±14.9) [75–138]
Verbal IQ, WASI	110 (±12.5) [71–137]	110 (±13.2) [84–139]
EHI	96 (±7.6) [65–100]	93 (±14.2) [25–100]
ADI-R Score		
Social[c]	-	18.1 (±5.3)
Communication[c]	-	13.6 (±4.2)
Repetitive behaviour[c]	-	4.8 (±2.2)
ADOS Score		
Social[d]	-	6.1 (±2.9)
Communication[d]	-	3.3 (±1.7)
Repetitive behaviour[d]	-	1.2 (±1.2)
AQ	-	23.6 (±10.7)
EQ	-	32.7 (±15.5)
SQ	-	64.3 (±22.3)

Numbers are means ± standard deviations. Ranges are between square brackets. AQ = Autism-Spectrum Quotient; EQ = Empathy Quotient; SQ = Systemizing Quotient; WASI = Wechsler Abbreviated Scale of Intelligence.

[a]There were no significant differences between the ASD and control groups in age, full-scale IQ, or verbal IQ at $P < 0.05$ (two-tailed).

[b]There was a significant difference in performance IQ ($P = 0.005$).

[c]Information was available for all 61 individuals with ASD. The following cut-off scores were used: ADI-R Social, > 10; Communication, > 8; and Repetitive behaviour, > 3.

[d]Information was available for 59 individuals with ASD. A cut-off of 7 was used for Communication plus Social interaction.

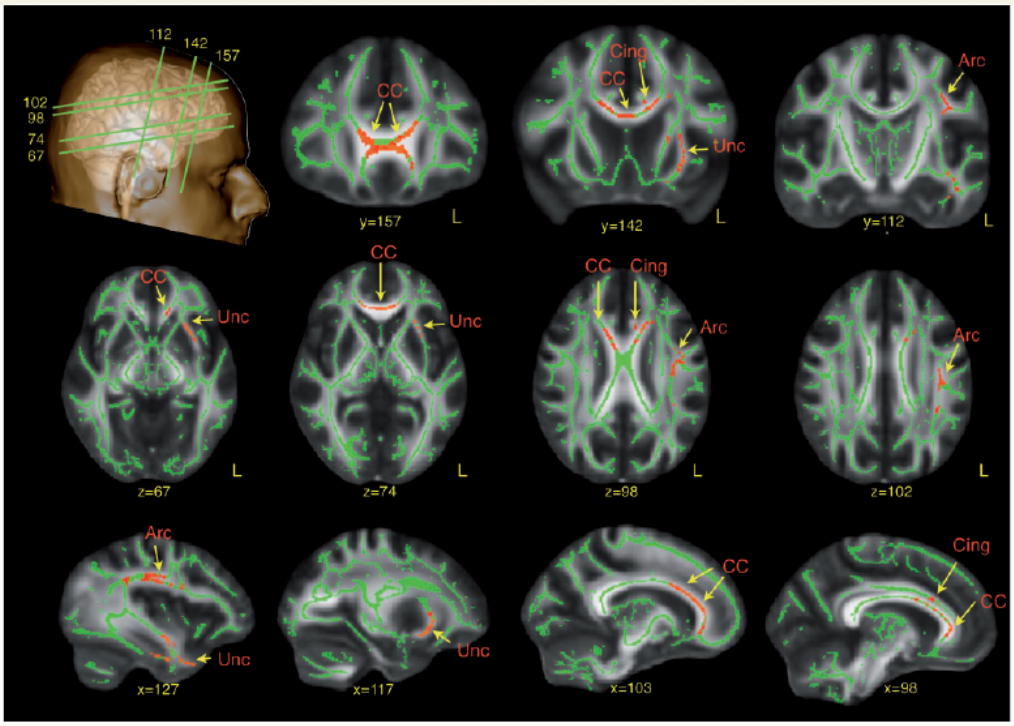

Figure 1 TBSS analysis of differences in fractional anisotropy between ASD subjects and neurotypical controls. Red regions indicate reduced fractional anisotropy values in ASD. Arc = arcuate fasciculus; CC = corpus callosum; Cing = cingulum; Unc = uncinate fasciculus.

ratings. In addition, Autism-Spectrum Quotient (AQ), Empathy Quotient (EQ), and Systemizing Quotient (SQ) were collected for all patients. The ASD sample included 24 males with an ICD10-R diagnosis of childhood autism and 37 with Asperger syndrome (see Table 1 for details).

Exclusion criteria included a history of psychotic disorders, head injury, genetic disorder associated with ASD, any medical condition affecting brain function (e.g. epilepsy), current use of antipsychotic medication, mood stabilizers, or benzodiazepines or a history of substance misuse (including alcohol).

All participants gave informed written consent in accordance with ethics approval by the National Research Ethics Committee, Suffolk, England.

MRI data acquisition

At both sites participants were scanned with MRI scanners operating at 3 T (GE Medical Systems HDx). We used the same scanning acquisition protocol at both sites to ensure data compatibility. High-resolution structural T_1-weighted volumetric images were acquired with full-head coverage, 196 contiguous slices (1.1 mm thickness, with 1.09 × 1.09 mm in-plane resolution), a 256 × 256 × 196 matrix and a repetition time/echo time of 7/2.8 ms (flip angle 20°, field of view 28 cm). An 8-channel head-coil was used for radiofrequency transmission and reception allowing a parallel imaging (ASSET) speed up factor of 2. Consistent image quality was ensured by a semi-automated quality control procedure. DT-MRI data were acquired using a spin-echo echo-planar imaging double refocused sequence providing whole head coverage with isotropic image resolution (2.4 × 2.4 × 2.4 mm; 32 diffusion-weighted volumes with different non-collinear diffusion directions with b-factor 1300 s/mm^2, and six non-diffusion-weighted volumes; 60 slices without slice gap; echo time = 104.5 ms; repetition time = 20 R-R intervals; 128 × 128 acquisition matrix; field of view 307 × 307 mm). The acquisition was gated to the cardiac cycle using a digital pulse oximeter placed on participants' forefinger.

Diffusion tensor MRI processing

Diffusion data were processed using ExploreDTI (Leemans *et al.*, 2009). Data were first preprocessed correcting for eddy current distortions and head motion. For each subject the mean rotational and translational relative movement was extracted and statistical analysis was performed to detect group differences in head movement. No statistically significant differences were found between ASD and controls. For each subject the b-matrix was then reoriented to provide a more accurate estimate of diffusion tensor orientations (Leemans and Jones, 2009). Diffusion tensor was estimated using a non-linear least square approach (Jones and Basser, 2004). Fractional anisotropy, mean diffusivity and radial

Table 2 Tract-specific measurements of the three segments of the arcuate fasciculus

Segments	Measurements	Controls	ASD	P-value
Long left	Streamlines	292 ± 108	246 ± 108	0.023
	FA	0.504 ± 0.020	0.496 ± 0.023	0.042
	MD	$0.74 \pm 0.02 \times 10^{-3}$	$0.75 \pm 0.02 \times 10^{-3}$	0.002*
	RD	$0.51 \pm 0.02 \times 10^{-3}$	$0.52 \pm 0.02 \times 10^{-3}$	0.003*
Long right	Streamlines	153 ± 116	120 ± 88	0.084
	FA	0.480 ± 0.024	0.470 ± 0.025	0.21
	MD	$0.49 \pm 0.02 \times 10^{-3}$	$0.48 \pm 0.06 \times 10^{-3}$	0.163
	RD	$0.52 \pm 0.02 \times 10^{-3}$	$0.52 \pm 0.02 \times 10^{-3}$	0.09
Anterior left	Streamlines	132 ± 78	101 ± 63	0.018
	FA	0.459 ± 0.026	0.448 ± 0.030	0.039
	MD	$0.75 \pm 0.02 \times 10^{-3}$	$0.77 \pm 0.03 \times 10^{-3}$	0.003*
	RD	$0.55 \pm 0.02 \times 10^{-3}$	$0.57 \pm 0.03 \times 10^{-3}$	0.003*
Anterior right	Streamlines	210 ± 125	192 ± 119	0.431
	FA	0.470 ± 0.027	0.464 ± 0.024	0.188
	MD	$0.76 \pm 0.02 \times 10^{-3}$	$0.77 \pm 0.02 \times 10^{-3}$	0.083
	RD	$0.55 \pm 0.02 \times 10^{-3}$	$0.55 \pm 0.02 \times 10^{-3}$	0.078
Posterior left	Streamlines	156 ± 67	170 ± 94	0.353
	FA	0.454 ± 0.026	0.453 ± 0.023	0.885
	MD	$0.75 \pm 0.02 \times 10^{-3}$	$0.76 \pm 0.02 \times 10^{-3}$	0.007
	RD	$0.54 \pm 0.02 \times 10^{-3}$	$0.55 \pm 0.03 \times 10^{-3}$	0.057
Posterior right	Streamlines	132 ± 75	131 ± 83	0.947
	FA	0.452 ± 0.028	0.451 ± 0.026	0.878
	MD	$0.76 \pm 0.02 \times 10^{-3}$	$0.77 \pm 0.03 \times 10^{-3}$	0.011
	RD	$0.55 \pm 0.02 \times 10^{-3}$	$0.56 \pm 0.03 \times 10^{-3}$	0.055

Numbers are means ± SD. *Indicates values that survive Bonferroni correction for multiple comparisons. FA = fractional anisotropy; MD = mean diffusivity; RD = radial diffusivity.

diffusivity maps were generated. Whole brain tractography was performed by selecting all seed voxels with fractional anisotropy > 0.2. Streamlines were propagated using an Euler integration (Basser *et al.*, 2000), and a tractography algorithm step size of 1 mm. Where fractional anisotropy < 0.2 or when the angle between two consecutive tractography steps was > 35°, tractography stopped. Finally, diffusion tensor maps and whole brain tractography were exported to Trackvis (Wang *et al.*, 2007) for virtual manual dissection of the tracts.

Tract-based spatial statistics analysis

Each participant's fractional anisotropy map was transformed into standard stereotactic space (using FMRIB58 template) and a mean fractional anisotropy map for the whole sample used to create the average core 'skeleton'. By using only the core of the sample's white matter the peripheral tract regions are not involved in further analysis, thus removing partial volume effects (Smith *et al.*, 2006). Skeleton images of each participant's fractional anisotropy map were then produced and projected onto the mean skeleton to identify voxels where fractional anisotropy value differs significantly between these skeletons using voxel-wise statistics. The design matrix used centre, performance IQ, and age as covariates. Five thousand permutations were applied (confidence limits for $P = 0.05$ is ± 0.0062). The TFCE value images are reported fully corrected for multiple comparisons across space using threshold free cluster enhancement with a specified significance level of $P < 0.05$.

Tractography dissections

Following the TBSS analysis, white matter regions that were found to be atypical in ASD were localized using a probabilistic digital atlas of the major white matter tracts (Catani and Thiebaut de Schotten, 2012). Tracts that were identified to be atypical in ASD by the TBSS analysis were dissected using one or two region of interest approach (Catani and Thiebaut de Schotten, 2008). The tractographer was blind to group membership of each subject and brain side.

We performed virtual dissections of the left and right arcuate fasciculus and its segments connecting frontal, parietal and temporal regions according to previous publications (Catani *et al.*, 2005) (Fig. 2). We also performed virtual dissections of the three major limbic pathways including the cingulum, uncinate fasciculus and fornix (Catani and Thiebaut de Schotten, 2008). In addition we dissected the inferior longitudinal fasciculus and the inferior fronto-occipital fasciculus to extend the analysis to pathways that contain parts of the fibres connecting limbic structures to visual and auditory associative areas (Fig. 3). The corpus callosum was dissected using a single region of interest defined on the two most medial slices of the fractional anisotropy maps. Individual portions of the corpus callosum were analysed separately according to Witelson's (1989) criteria.

Statistical analysis

Statistical comparisons of the data were performed using SPSS software (SPSS Inc, Chicago, Ill). Demographic and behavioural differences between ASD and control groups were

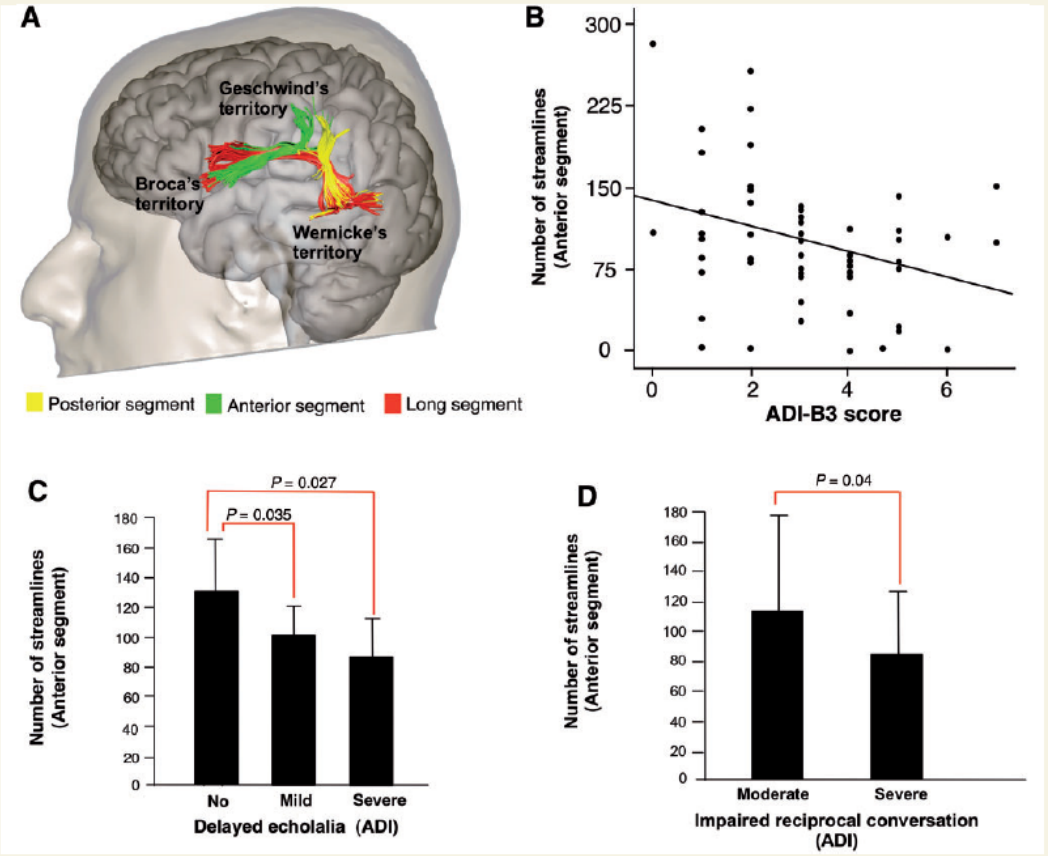

Figure 2 The anatomy of the arcuate fasciculus in relation to childhood ASD symptoms. (**A**) Tractography dissections of the three segments of the arcuate fasciculus. (**B**) Negative correlation between the number of streamlines of the left anterior segment and the B3 score (stereotyped, repetitive and idiosyncratic speech) of the ADI-R ($r = -0.340$; $P = 0.005$) in the ASD group. (**C**) In the ASD group, participants with a significant history of stereotyped utterance and delayed echolalia in childhood had a significantly lower number of streamlines in the anterior segment of the arcuate fasciculus. (**D**) Similarly, ASD subjects with severely impaired reciprocal conversation in childhood had a significantly lower number of streamlines in the anterior segment of the arcuate fasciculus compared to ASD subjects with moderate symptoms.

analysed using independent-samples *t*-tests. Repeated measures ANOVA analyses were performed separately for each measurement (i.e. number of streamlines, volume, fractional anisotropy, mean diffusivity, and perpendicular diffusivity) to examine group differences (i.e. the fixed factor) for the perisylvian network (long, posterior and anterior segments of the arcuate fasciculus) and the limbic association pathways (cingulum and uncinate fasciculus). Corpus callosum's group differences were estimated separately for each measurement (i.e. number of streamlines, volume, fractional anisotropy, mean diffusivity, and perpendicular diffusivity) using univariate ANOVA analyses. Age, centre and performance IQ were entered as covariates in all analyses. *Post hoc* comparisons for specific tracts were considered as statistically significant if they survived Bonferroni correction for multiple comparisons ($P < 0.0045$, five tracts for each hemisphere; $P < 0.008$ for the corpus callosum). Both streamline count and tract volume were calculated for each tract. Considering that both measures yielded to similar results only streamline count is reported. To study possible associations between tract abnormalities and symptom severity within the ASD group we related differences in tracts to symptom severity as measured by the relevant ADI-R and ADOS scores using Pearson correlation.

Results

Tract-based spatial statistics

Compared to controls, the ASD group had significantly (corrected for multiple comparisons) lower fractional

Table 3 Tract-specific measurements of the limbic tracts

Limbic tracts	Measurements	Controls	ASD	P-value
Uncinate left	Streamlines	180 ± 80	147 ± 68	0.019
	FA	0.462 ± 0.022	0.452 ± 0.027	0.023
	MD	$0.82 \pm 0.02 \times 10^{-3}$	$0.84 \pm 0.02 \times 10^{-3}$	0.003*
	RD	$0.59 \pm 0.03 \times 10^{-3}$	$0.61 \pm 0.03 \times 10^{-3}$	0.001*
Uncinate right	Streamlines	206 ± 81	183 ± 78	0.149
	FA	0.468 ± 0.022	0.459 ± 0.029	0.044
	MD	$0.82 \pm 0.02 \times 10^{-3}$	$0.83 \pm 0.40 \times 10^{-3}$	0.014
	RD	$0.58 \pm 0.02 \times 10^{-3}$	$0.60 \pm 0.04 \times 10^{-3}$	0.025
Cingulum left	Streamlines	666 ± 139	607 ± 149	0.036
	FA	0.479 ± 0.025	0.466 ± 0.023	0.003*
	MD	$0.78 \pm 0.02 \times 10^{-3}$	$0.79 \pm 0.02 \times 10^{-3}$	0.199
	RD	$0.55 \pm 0.02 \times 10^{-3}$	$0.56 \pm 0.02 \times 10^{-3}$	0.007
Cingulum right	Streamlines	596 ± 126	562 ± 137	0.158
	FA	0.464 ± 0.024	0.457 ± 0.025	0.083
	MD	$0.78 \pm 0.02 \times 10^{-3}$	$0.79 \pm 0.02 \times 10^{-3}$	0.147
	RD	$0.56 \pm 0.02 \times 10^{-3}$	$0.58 \pm 0.03 \times 10^{-3}$	0.064
IFOF left	Streamlines	182 ± 80	167 ± 88	0.481
	FA	0.499 ± 0.025	0.493 ± 0.025	0.272
	MD	$0.78 \pm 0.02 \times 10^{-3}$	$0.80 \pm 0.03 \times 10^{-3}$	0.008
	RD	$0.54 \pm 0.03 \times 10^{-3}$	$0.55 \pm 0.03 \times 10^{-3}$	0.025
IFOF right	Streamlines	166 ± 81	177 ± 93	0.35
	FA	0.488 ± 0.020	0.491 ± 0.025	0.5
	MD	$0.79 \pm 0.02 \times 10^{-3}$	$0.80 \pm 0.03 \times 10^{-3}$	0.023
	RD	$0.55 \pm 0.02 \times 10^{-3}$	$0.56 \pm 0.03 \times 10^{-3}$	0.277
ILF left	Streamlines	235 ± 74	222 ± 118	0.469
	FA	0.529 ± 0.027	0.524 ± 0.023	0.138
	MD	$0.79 \pm 0.03 \times 10^{-3}$	$0.81 \pm 0.03 \times 10^{-3}$	0.035
	RD	$0.53 \pm 0.02 \times 10^{-3}$	$0.54 \pm 0.03 \times 10^{-3}$	0.024
ILF right	Streamlines	265 ± 103	228 ± 93	0.021
	FA	0.516 ± 0.070	0.524 ± 0.021	0.894
	MD	$0.80 \pm 0.02 \times 10^{-3}$	$0.81 \pm 0.02 \times 10^{-3}$	0.02
	RD	$0.53 \pm 0.02 \times 10^{-3}$	$0.54 \pm 0.03 \times 10^{-3}$	0.086

Numbers are means ± SD. *Indicates values that survive Bonferroni correction for multiple comparisons. FA = fractional anisotropy; MD = mean diffusivity; RD = radial diffusivity; IFOF = inferior fronto-occipital fasciculus; ILF = inferior longitudinal fasciculus.

anisotropy in the left arcuate fasciculus ($P = 0.026$), external capsule ($P = 0.046$), anterior ($P = 0.044$) and posterior ($P = 0.032$) cingulum, and anterior corpus callosum ($P = 0.015$). There were no increases in fractional anisotropy in the ASD group compared to controls (Fig. 1).

Diffusion tractography analysis

Arcuate fasciculus

Between-groups differences were statistically significant for the mean diffusivity [$F(1\,120) = 5.618$; $P = 0.020$] and radial diffusivity [$F(1\,120)$, 4.629; $P = 0.034$]. A statistically significant Group × Hemisphere interaction for the number of streamlines [$F(2\,116) = 6.817$; $P = 0.010$] and Group × Tract interaction for the number of streamlines [$F(2, 113) = 4.045$; $P = 0.02$] was also found.

Post hoc independent sample *t*-test, Bonferroni corrected for multiple comparisons, showed that the ASD group had higher mean and radial diffusivity in the left long and left anterior segments (Table 2). Differences in the number of streamlines of the left long and anterior segments and mean diffusivity of the posterior right segment did not survive correction for multiple comparisons.

We subsequently explored whether anatomical differences in the left long and anterior segments of the arcuate fasciculus were associated with language and communication impairment. Pearson's correlations were calculated between tract-specific measurements and measures for abnormalities in language and communication, that is, ADI-R (B1-B4 subscores) and ADOS (A subscore) subscores in the 'communication' domain. A statistically significant negative correlation was found between the number of streamlines of the left anterior segment and the ADI-R B3 score for stereotyped, repetitive and idiosyncratic speech (Pearson's correlation = −0.340; $P = 0.005$) (Fig. 2B). The correlation was mainly driven by the severity of stereotyped utterances and delayed echolalia (Fig. 2C) and impaired reciprocal conversation (Fig. 2D). There were no significant correlations with the ADOS communication scores.

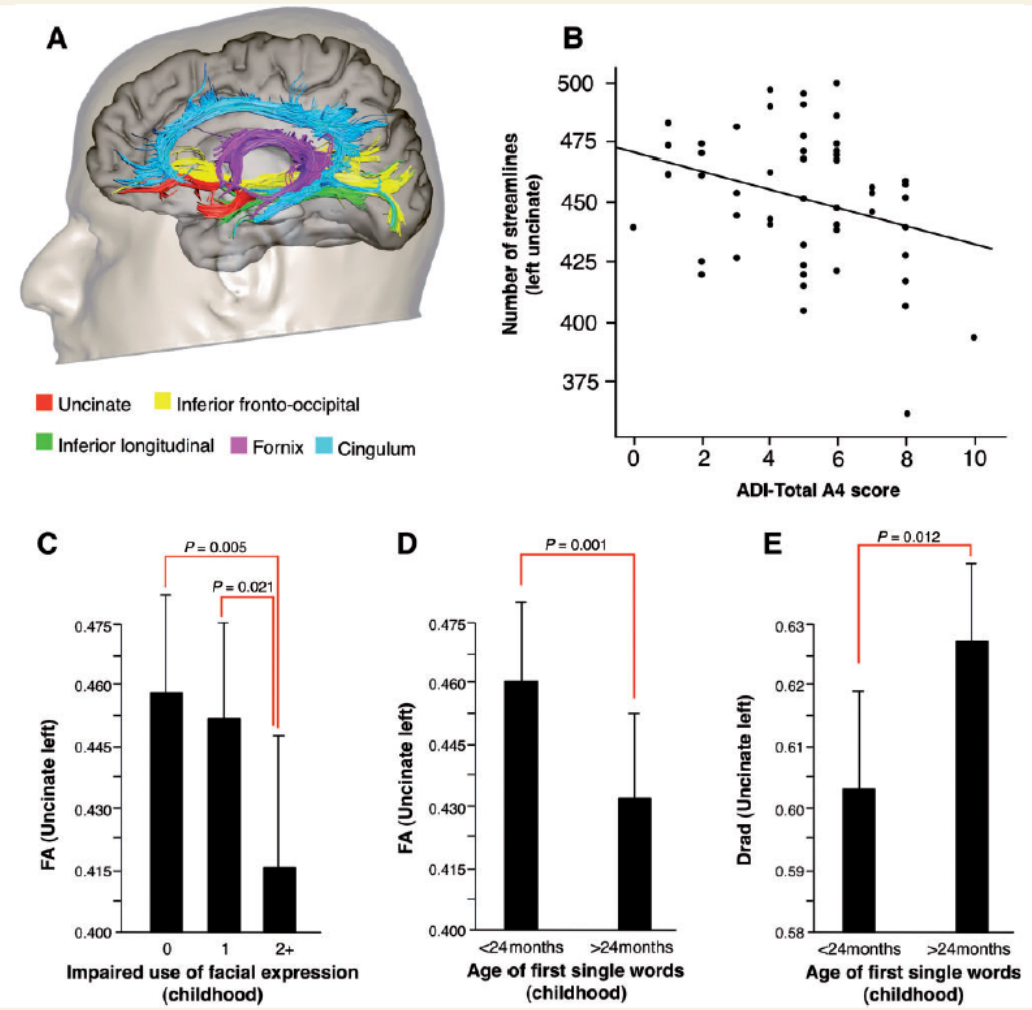

Figure 3 The anatomy of the limbic tracts in relation to childhood ASD symptoms. (**A**) Tractography reconstructions of the limbic pathways. (**B**) Negative correlation between the number of streamlines of the left uncinate fasciculus and the total A4 score for impaired socioemotional reciprocity in the ADI-R (Pearson's correlation = −0.295; $P = 0.01$) in the ASD group. ASD participants with a (**C**) significant history of impaired use of facial expression in childhood and (**D** and **E**) late use of first single words had a significantly lower fractional anisotropy (FA) and higher radial diffusivity in the left uncinate fasciculus.

Limbic tracts

A statistically significant Group × Hemisphere interaction for fractional anisotropy [$F(2\,118) = 6.197$; $P = 0.014$] was found. No other interactions were found with number of streamlines, mean diffusivity or radial diffusivity.

Post hoc independent sample *t*-test, Bonferroni corrected for multiple comparisons, showed that the ASD group had significantly higher mean diffusivity and radial diffusivity in the left uncinate and lower fractional anisotropy in the left cingulum (Table 3). Differences in the number of streamlines and fractional anisotropy of the left uncinate and radial diffusivity in the left cingulum did not survive correction for multiple comparisons.

We also explored whether anatomical differences in the left uncinate fasciculus and cingulum were associated with impaired social interaction. Pearson's correlation was calculated between tract-specific measurements and measures for abnormality in social interaction, that is, ADI-R (A1–

Table 4 Tract-specific measurements of the callosal tracts

Callosal segments	Measurements	Controls	ASD	P-value
Genu	Streamlines	914 ± 304	853 ± 192	0.197
	FA	0.572 ± 0.022	0.566 ± 0.020	0.178
	MD	$0.82 \pm 0.04 \times 10^{-3}$	$0.84 \pm 0.03 \times 10^{-3}$	0.006*
	RD	$0.51 \pm 0.03 \times 10^{-3}$	$0.53 \pm 0.03 \times 10^{-3}$	0.011
Anterior body	Streamlines	412 ± 156	427 ± 143	0.534
	FA	0.539 ± 0.022	0.532 ± 0.018	0.062
	MD	$0.82 \pm 0.03 \times 10^{-3}$	$0.83 \pm 0.03 \times 10^{-3}$	0.003*
	RD	$0.53 \pm 0.03 \times 10^{-3}$	$0.55 \pm 0.05 \times 10^{-3}$	0.004*
Centre body	Streamlines	460 ± 149	427 ± 111	0.191
	FA	0.558 ± 0.022	0.550 ± 0.020	0.04
	MD	$0.81 \pm 0.03 \times 10^{-3}$	$0.82 \pm 0.03 \times 10^{-3}$	0.04
	RD	$0.51 \pm 0.03 \times 10^{-3}$	$0.52 \pm 0.03 \times 10^{-3}$	0.022
Posterior body	Streamlines	464 ± 120	463 ± 118	0.98
	FA	0.572 ± 0.022	0.574 ± 0.018	0.537
	MD	$0.79 \pm 0.03 \times 10^{-3}$	$0.79 \pm 0.02 \times 10^{-3}$	0.741
	RD	$0.49 \pm 0.03 \times 10^{-3}$	$0.49 \pm 0.02 \times 10^{-3}$	0.994
Isthmus	Streamlines	474 ± 143	453 ± 131	0.363
	FA	0.559 ± 0.024	0.557 ± 0.020	0.723
	MD	$0.80 \pm 0.03 \times 10^{-3}$	$0.79 \pm 0.02 \times 10^{-3}$	0.532
	RD	$0.50 \pm 0.03 \times 10^{-3}$	$0.50 \pm 0.02 \times 10^{-3}$	0.722
Splenium	Streamlines	1514 ± 295	1498 ± 315	0.774
	FA	0.611 ± 0.017	0.608 ± 0.018	0.424
	MD	$0.79 \pm 0.02 \times 10^{-3}$	$0.79 \pm 0.02 \times 10^{-3}$	0.584
	RD	$0.46 \pm 0.02 \times 10^{-3}$	$0.47 \pm 0.02 \times 10^{-3}$	0.44

Numbers are means ± SD. *Indicates values that survive Bonferroni correction for multiple comparisons. FA = fractional anisotropy; MD = mean diffusivity; RD = radial diffusivity.

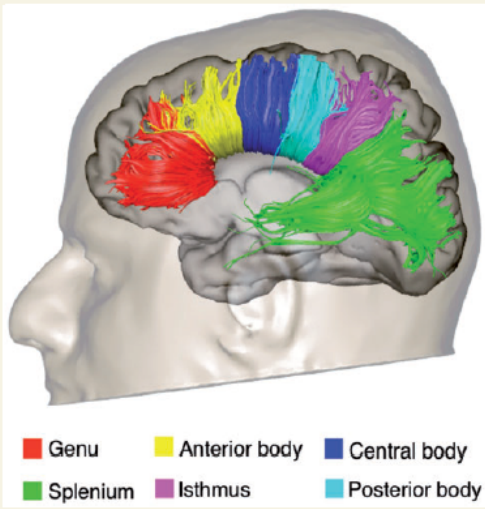

Figure 4 Tractography reconstruction of the segments of the corpus callosum according to Witelson's division (1989).

A4 subscores) and ADOS (B subscore). A statistically significant correlation was found between the number of streamlines of the left uncinate and the ADI-R total score for qualitative abnormalities in reciprocal social interactions ($r = -0.269$; $P = 0.01$), and A4 score for impaired socio-emotional reciprocity ($r = -0.295$; $P = 0.01$) (Fig. 3B). A similar correlation was found between fractional anisotropy of the left uncinate and the A4 score ($r = -0.301$; $P < 0.01$). The correlation with A4 score was mainly driven by the severity of 'inappropriate use of facial expression' (Fig. 3C). Statistically significant differences in the fractional anisotropy and radial diffusivity of the left uncinate fasciculus were also found between ASD participants who demonstrated delayed use of meaningful single words (<24 months of age) and ASD participants who developed use of single words within normal developmental ranges (Fig. 3D and E). There were no correlations between ADOS subscores and uncinate measurements, or between scores for impaired socio-emotional reciprocity on the ADI-R and ADOS and other limbic tracts.

Corpus callosum

There were no statistically significant differences between participants with ASD and controls in the number of streamlines, fractional anisotropy, mean diffusivity and radial diffusivity of the total corpus callosum.

The analysis of the segments of the corpus callosum revealed a statistically significant increase in mean diffusivity and radial diffusivity in the genu and anterior body in the ASD group as compared to controls. Differences in fractional anisotropy and radial diffusivity of the central body

did not survive correction for multiple comparisons. No statistically significant differences were found in the posterior body, isthmus and splenium. There were no significant correlations between diffusion indices of the corpus callosum and symptom severity as measured by the ADI-R and ADOS.

Discussion

In this multicentre study we investigated the anatomy of white matter networks in adults with ASD. We were able to confirm in a large population that white matter differences in ASD persist into adult life. White matter differences in ASD were localized to major association and commissural tracts of the frontal lobe. These tracts connect frontal lobe to more posterior areas of the parietal, limbic and temporal lobe. Further, white matter differences within particular networks were found to be associated with specific childhood ASD behavioural characteristics. We found, for example, differences in the left arcuate fasciculus, which plays a key role in language and social function (Catani and Bambini, 2014). Specifically, the number of streamlines of the left anterior segment of the arcuate fasciculus was negatively associated with stereotyped utterances and delayed echolalia in childhood (i.e. based on the ADI-R). Similarly, we found that ASD was associated with diffusion abnormalities of the left uncinate fasciculus, which plays a significant role in face encoding and emotional processing associated with face perception (Papagno *et al.*, 2011). Further, this correlated with 'inappropriate use of facial expression' in childhood.

Overall, our findings confirm a number of previous studies that have examined white matter tracts in ASD with varying approaches to diffusion imaging data (see Ameis and Catani, 2015 for a recent review). A recent meta-analysis of diffusion tensor imaging (voxel-based) studies that provided a collective sample of 330 people with ASD and 313 controls revealed decreases in fractional anisotropy in white matter voxels containing fibres of the left arcuate fasciculus, uncinate fasciculus and corpus callosum, and increases in mean diffusivity in the same regions (Aoki *et al.*, 2013). The meta-analysis also reported differences in the inferior longitudinal and inferior fronto-occipital fasciculus, but these did not reach statistical significance. In addition to voxel-based studies, tractography studies have also examined white matter tracts linking socio-emotional and communication regions in ASD. While the uncinate and arcuate fasciculi have been most frequently implicated as abnormal in ASD, a smaller number of studies support the presence of abnormalities in additional tracts, including the cingulum bundle, the inferior longitudinal and inferior fronto-occipital fasciculus (Ameis and Catani, 2015). Such abnormalities are generally reflected by decreased fractional anisotropy and increased diffusivity, although differences in the opposite direction have also been reported in children and adolescents, but less frequently (Cheng *et al.*, 2010; Shukla *et al.*, 2010). Some studies have also reported increased number of streamlines for the same tracts (Pugliese *et al.*, 2009; Kumar *et al.*, 2010; Thomas *et al.*, 2011). While small sample size, differences in the severity of the disorder and in the imaging approaches among studies can explain some of the contrasting findings (Lazar *et al*, 2014; Ameis and Catani, 2015), different diffusion abnormalities in the same tract in studies sampling ASD participants of different ages, likely point to an evolving picture of white matter pathology with development (Pugliese *et al.*, 2009; Kleinhans *et al.*, 2012).

An unexpected finding was the absence of significant correlations between tract-specific measurements and severity of clinical symptoms in adulthood as measured by the ADOS. One possible explanation for this negative finding is that ADOS scores, although commonly used to support a diagnosis of ASD, may not be suitable for quantifying the exact severity of current symptoms, especially in adults. It is also possible that participants with ASD compensated for their childhood deficits through observation of other people and alternative modes of communication. This has been widely documented for the language deficits by previous behavioural studies (Eisenmajer *et al.*, 1996; Gilchrist *et al.*, 2001; Howlin *et al.*, 2003). This may lead to changes at the functional, or cortical level, but not within the white matter—leading to a mismatch between white matter abnormalities and current symptoms severity. Indeed, in a recent study we showed that in ASD, current and historical language symptoms were associated with different neuroanatomical correlates (Lai *et al.*, 2014). In general there is limited evidence in the literature of a direct correlation between white matter abnormalities and clinical symptoms. The most common finding reported is a direct correlation between uncinate fasciculus abnormalities and impaired social cognition. For example, Chen *et al.* (2011) reported a negative correlation between white matter indices and social deficits in ASD, where increased Social Responsiveness Scale scores correlated with reduced fractional anisotropy in right uncinate fasciculus. Similarly Kumar et al. (2010) used tractography to show that macrostructural alterations within the uncinate fasciculus in ASD were correlated with the severity of symptoms, including socio-emotional deficits, on the Gilliam Autism Rating Scale. One interesting study that used DTI after a communication intervention in 22 low functioning young males with ASD found a positive correlation of uncinate fasciculus fractional anisotropy with both therapy duration and symptom improvement measured using the Child Autism Rating Scale (Pardini *et al.*, 2012). While all of these findings suggest that ASD is characterized by differences in white matter tracts, the exact biological mechanism modulating these differences cannot be elucidated by diffusion techniques but may be understood by other methodologies, including post-mortem studies.

Post-mortem studies have reported that ASD is associated with white matter inflammation and reduced neural size and increased packing density within frontal and temporal

limbic (grey matter) structures (Bailey *et al.*, 1998; Bauman and Kemper, 2005; Vargas *et al.*, 2005). Further, compared to controls, ASD is associated with increased number of neuronal processing units, known as cortical mini-columns (Mountcastle, 1997), within frontal and temporal cortices (Casanova *et al.*, 2002*a*, *b*). Mini-columns are highly interconnected, and a greater number of mini-columns could result in increased formation of short-range (intracortical) connections and disrupted maturation of long-range connections linking distant regions (Casanova *et al.*, 2002*a*, *b*). These findings may be of particular relevance to our study as they suggest ASD pathology induces white matter changes in the long white matter connections possibly related to axons with larger diameter, reduced myelination, or increased oedema due to inflammation (Vargas *et al.*, 2005). This interpretation could explain the findings of reduced fractional anisotropy and increased radial diffusivity in the long-range connections of the frontal lobe in the current study. This hypothesis is also supported by a recent post-mortem study in ASD, which reported reduced myelin thickness in the frontal white matter (Zikopoulos and Barbas, 2010).

It remains unclear, however, whether these changes follow an initial failure of connections to establish correct organization, or a later weakening of successfully formed white matter connections (Geschwind and Levitt, 2007) as the majority of ASD individuals studied in post-mortem analyses are older children and adults (Courchesne *et al.*, 2007). Therefore, to determine how, and when, these putative changes commence future studies would benefit from including a younger cohort. A recent *in vivo* longitudinal study has highlighted the need for this (Wolff *et al.*, 2012). In this study high-risk infants who later developed ASD were found to have reduced fractional anisotropy in limbic and association tracts including those reported in our current study, by the age they showed obvious signs of autism. This study also suggested that white matter differences are evident as early as 6 months of age in infants at risk of ASD, although abnormalities were in the opposite direction (i.e. increased fractional anisotropy in the at risk group). The initial increased fractional anisotropy could have been related to increased myelination, and/or smaller axonal diameter, in infants at risk of ASD. These findings suggest that ASD progresses through different stages during early neurodevelopment (i.e. overgrowth followed by blunted development). Realistically, it is difficult to validate these findings using post-mortem studies due to limited availability of donated brains from infants. However, the application of complimentary *in vivo* neuroimaging methods could assist in the interpretation of diffusion tensor imaging results.

Our findings also indicate an asymmetry of abnormalities with greater differences in the white matter of the left hemisphere in the ASD compared to controls. Previous diffusion studies have demonstrated that maturation of left white matter pathways in the temporal and frontal lobe is correlated with development of specific cognitive functions (Nagy *et al.*, 2004). Loss of normal interhemispheric asymmetry, both at the cortical and subcortical level, is one of the most replicated findings in ASD (Herbert *et al.*, 2005; Radua *et al.*, 2011; Ameis and Catani, 2015). This indicates that in general the underlying pathological process is rather asymmetrical in ASD and specific to those networks that show the greatest degree of lateralization in the neurotypically developing brain.

Finally, the differences in tract-specific measurements between neurotypical adults and ASD were particularly significant for the mean diffusivity and radial diffusivity in our tractography analysis. This finding suggests that, compared to fractional anisotropy and tract volume, mean diffusivity and radial diffusivity have greater intrinsic sensitivity to *in vivo* abnormalities associated with ASD pathology but also that the biophysical meaning of these indices is different. Since fractional anisotropy is a measure of anisotropy, it is by definition a 'relative' index that quantifies the difference of diffusivities of the three eigenvalues. This makes this index sensitive to changes in the overall structural organization of the tissue or the fibre architecture but it does not give information on how much faster or slower is diffusion in different directions. Conversely, mean diffusivity and radial diffusivity are absolute measures that directly provide a quantitative measure of water mobility within the tissue, either as average to the voxel (mean diffusivity) or radially to the direction of maximum diffusivity (radial diffusivity). Therefore mean diffusivity and radial diffusivity could be more specific and better related to abnormalities, such as changes in axonal membrane, extra-axonal volume density or in the myelin sheet because they may capture something not visible in a ratio or a difference in diffusivities. In support of our findings, a recent study also reported differences between typically developing adolescents and individuals with ASD only for diffusivity measures (Lisiecka *et al.*, 2015).

While the present study has several advantages compared to previous ones, its limitations include a cross-sectional design and exclusion of children, females and participants with intellectual disability, which limit our capability for generalization or confirming causal and temporal developmental effects. These criteria were implemented in order to optimize sample homogeneity. There is, for example, sex difference in arcuate tract development in the typically developing population (Catani *et al.*, 2007). Therefore our results may not generalize to females with ASD, suggesting the need for future studies to include comparable samples of females. Similarly, the exclusion of individuals with below average IQ may mean that our results are not generalizable to the proportion of those with both ASD and intellectual disability. It could be argued that the significant difference in the performance IQ between the two groups may have confounded our findings. However, this difference was dealt with by co-varying for this across all of our analyses. A multicentre design was used for MRI data acquisition, which may carry additional limitations. However, we used the same scanner model and acquisition

parameters across scanning sites. In addition intersite effects were accounted for in the statistical model (Suckling *et al.*, 2010, 2012). Therefore, the detected between-group differences cannot be fully explained by these limitations. Finally, some of the negative findings (e.g. lack of correlation between anatomy of the corpus callosum and ASD symptoms) could be explained by the use of the tensor method, which is limited in resolving fibre crossing. Future studies are necessary to improve the complete visualization of callosal tracts using advanced diffusion models (Dell'Acqua *et al.*, 2013).

In conclusion, our results suggest that male adults with ASD have regional differences in brain anatomy, which persist in adult life and correlate with specific aspects of autistic symptoms in childhood . We also found that ASD was associated with specific structural abnormalities of white matter fibres, compatible with the concept of autism being associated with atypical developmental connectivity of the frontal lobes. Future studies are needed to confirm our findings and to extend them across a wider range of autistic spectrum conditions.

Acknowledgements

We are grateful to those who agreed to be scanned and who gave their time so generously to this study. Members of the NatBrainLab (www.natbrainlab.com) provided helpful comments to the manuscript.

Funding

This study was funded by the MRC UK as the AIMS (Autism Imaging Multicentre Study) to PI's Murphy, Bullmore, Baron-Cohen and Bailey, and with support from the European Autism Interventions – A Multicentre Study for Developing New Medications (EU-AIMS, http://www.eu-aims.eu/); the research of EU-AIMS receives support from the Innovative Medicines Initiative Joint Undertaking under grant agreement n° 115300, resources of which are composed of financial contribution from the European Union's Seventh Framework Programme (FP7/2007-2013), from the EFPIA companies in kind contribution and from Autism Speaks) and the Mortimer D Sackler Foundation. Marco Catani had full access to all of the data in the study and takes responsibility for the integrity of the data and the accuracy of the data analysis. Marco Catani is the recipient of a Welcome Trust Investigator Award (103759/Z/14/Z). The research of Alexander Leemans is supported by VIDI Grant 639.072.411 from the Netherlands Organisation for Scientific Research (NWO). This study represents independent research partly funded by the National Institute for Health Research (NIHR) Biomedical Research Centre at South London and Maudsley NHS Foundation Trust and King's College London. The views expressed are those of the authors and not necessarily those of the NHS, the NIHR or the Department of Health.

References

Abell F, Krams M, Ashburner J, Passingham R, Friston K, Frackowiak R, et al. The neuroanatomy of autism: a voxel-based whole brain analysis of structural scans. Neuroreport 1999; 10: 1647–51.

Aoki Y, Abe O, Nippashi Y, Yamasue H. Comparison of white matter integrity between autism spectrum disorder subjects and typically developing individuals: a meta-analysis of diffusion tensor imaging tractography studies. Mol Autism 2013; 4: 25.

Ashwin C, Baron-Cohen S, Wheelwright S, O'Riordan M, Bullmore ET. Differential activation of the amygdala and the 'social brain' during fearful face-processing in Asperger Syndrome. Neuropsychologia 2007; 45: 2–14.

Ameis SH, Catani M. Altered white matter connectivity as a neural substrate for social impairment in Autism Spectrum Disorder. Cortex 2015; 62: 158–81.

Bailey A, Luthert P, Dean A, Harding B, Janota I, Montgomery M, et al. A clinicopathological study of autism. Brain 1998; 121(Pt 5): 889–905.

Baron-Cohen S, Ring HA, Wheelwright S, Bullmore ET, Brammer MJ, Simmons A, et al. Social intelligence in the normal and autistic brain: an fMRI study. Eur J Neurosci 1999; 11: 1891–8.

Barnea-Goraly N, Kwon H, Menon V, Eliez S, Lotspeich L, Reiss AL. White matter structure in autism: preliminary evidence from diffusion tensor imaging. Biol Psych 2004; 55: 323–26.

Barnea-Goraly N, Lotspeich LJ, Reiss AL. Similar white matter aberrations in children with autism and their unaffected siblings: a diffusion tensor imaging study using tract-based spatial statistics. Arch Gen Psych 2010; 67: 1052–60.

Basser PJ, Pajevic S, Pierpaoli C, Duda J, Aldroubi A. *In vivo* fiber tractography using DT-MRI data. Magn Reson Med 2000; 44: 625–32.

Bauman ML, Kemper TL. Neuroanatomic observations of the brain in autism: a review and future directions. Int J Dev Neurosci 2005; 23: 183–7.

Belmonte MK, Allen G, Beckel-Mitchener A, Boulanger LM, Carper RA, Webb SJ. Autism and abnormal development of brain connectivity. J Neurosci 2004; 24: 9228–31.

Bénézit A, Hertz-Pannier L, Dehaene-Lambertz G, Monzalvo K, Germanaud D, Duclap D, Guevara P, Mangin J-F, Poupon C, Moutard M-L, Dubois J. Organising white matter in a brain without corpus callosum fibres. Cortex 2015; 63: 155–71.

Billeci L, Calderoni S, Tosetti M, Catani M, Muratori F. White matter connectivity in children with autism spectrum disorders: a tract-based spatial statistics study. BMC Neurol 2012; 12: 148.

Bloemen OJ, Deeley Q, Sundram F, Daly EM, Barker GJ, Jones DK, et al. White matter integrity in Asperger syndrome: a preliminary diffusion tensor magnetic resonance imaging study in adults. Autism Res 2010; 3: 203–13.

Bonilha L, Cendes F, Rorden C, Eckert M, Dalgalarrondo P, Li LM, et al. Gray and white matter imbalance–typical structural abnormality underlying classic autism? Brain Dev 2008; 30: 396–401.

Brieber S, Neufang S, Bruning N, Kamp-Becker I, Remschmidt H, Herpertz-Dahlmann B, et al. Structural brain abnormalities in adolescents with autism spectrum disorder and patients with attention deficit/hyperactivity disorder. J Child Psychol Psychiatry 2007; 48: 1251–8.

Casanova MF, Buxhoeveden DP, Switala AE, Roy E. Asperger's syndrome and cortical neuropathology. J Child Neurol 2002a; 17: 142–5.

Casanova MF, Buxhoeveden DP, Switala AE, Roy E. Minicolumnar pathology in autism. Neurology 2002b; 58: 428–32.

Catani M, Allin MP, Husain M, Pugliese L, Mesulam MM, Murray RM, et al. Symmetries in human brain language pathways correlate with verbal recall. Proc Natl Acad Sci USA 2007; 104: 17163–8.
Catani M, Craig MC, Forkel SJ, Kanaan R, Picchioni M, Toulopoulou T, et al. Altered integrity of perisylvian language pathways in schizophrenia: relationship to auditory hallucinations. Biol Psychiatry 2011; 70: 1143–50.
Catani M, Jones DK, ffytche DH. Perisylvian language networks of the human brain. Ann Neurol 2005; 57: 8–16.
Catani M, Thiebaut de Schotten M. A diffusion tensor imaging tractography atlas for virtual *in vivo* dissections. Cortex 2008; 44: 1105–32.
Catani M, Thiebaut de Schotten M. Atlas of human brain connections. Oxford; New York, NY: Oxford University Press; 2012.
Catani M, Bambini V. A model for Social Communication And Language Evolution and Development (SCALED). Curr Opin Neurobiol 2014; 28: 165–71.
Catani M. Diffusion tensor magnetic resonance imaging tractography in cognitive disorders. Curr Opin Neurol 2006; 19: 599–606.
Cauda F, Costa T, Palermo S, D'Agata F, Diano M, Bianco F, et al. Concordance of white matter and gray matter abnormalities in autism spectrum disorders: a voxel-based meta-analysis study. Hum Brain Mapp 2014; 35: 2073–98.
Cauda F, Geda E, Sacco K, D'Agata F, Duca S, Geminiani G, et al. Grey matter abnormality in autism spectrum disorder: an activation likelihood estimation meta-analysis study. J Neurol Neurosurg Psychiatry 2011; 82: 1304–13.
Chen R, Jiao Y, Herskovits EH. Structural MRI in autism spectrum disorder. Pediatr Res 2011; 69(5 Pt 2): 63R–8R.
Cheng Y, Chou KH, Chen IY, Fan YT, Decety J, Lin CP. Atypical development of white matter microstructure in adolescents with autism spectrum disorders. NeuroImage 2010; 50: 873–82.
Cheung C, Chua SE, Cheung V, Khong PL, Tai KS, Wong TK, et al. White matter fractional anisotrophy differences and correlates of diagnostic symptoms in autism. J Child Psychol Psychiatry 2009; 50: 1102–12.
Courchesne E, Pierce K. Brain overgrowth in autism during a critical time in development: implications for frontal pyramidal neuron and interneuron development and connectivity. Int J Dev Neurosci 2005; 23: 153–70.
Courchesne E, Pierce K, Schumann CM, Redcay E, Buckwalter JA, Kennedy DP, et al. Mapping early brain development in autism. Neuron 2007; 56: 399–413.
Craig MC, Catani M, Deeley Q, Latham R, Daly E, Kanaan R, et al. Altered connections on the road to psychopathy. Mol Psychiatry 2009; 14: 946–53.
Craig MC, Zaman SH, Daly EM, Cutter WJ, Robertson DMW, Hallahan B, et al. Women with autistic-spectrum disorder: magnetic resonance imaging study of brain anatomy. Br J Psychiatry 2007; 191: 224–8.
Dell'Acqua F, Simmons A, Williams SCR, Catani M. Can spherical deconvolution provide more information than fiber orientations? Hindrance modulated orientational anisotropy, a true-tract specific index to characterize white matter diffusion. Hum Brain Mapp 2013; 34: 2464–83.
Eisenmajer R, Prior M, Leekam S, Wing L, Gould J, Welham M, et al. Comparison of clinical symptoms in autism and Asperger's disorder. J of the American Academy of Child and Adolescent Psychiatry 1996; 35: 1523–31.
Fields RD. White matter in learning, cognition and psychiatric disorders. Trends Neurosci 2008; 31: 361–70.
Fletcher PT, Whitaker RT, Tao R, DuBray MB, Froehlich A, Ravichandran C, et al. Microstructural connectivity of the arcuate fasciculus in adolescents with high-functioning autism. NeuroImage 2010; 51: 1117–25.
Forkel SJ, Thiebaut de Schotten M, Kawadler JM, Dell'Acqua F, Danek A, Catani M. The anatomy of fronto-occipital connections from early blunt dissections to contemporary tractography. Cortex 2014; 56: 73–84.
Frazier TW, Hardan AY. A meta-analysis of the corpus callosum in autism. Biol Psychiatry 2009; 66: 935–41.
Freitag CM, Luders E, Hulst HE, Narr KL, Thompson PM, Toga AW, et al. Total brain volume and corpus callosum size in medication-naive adolescents and young adults with autism spectrum disorder. Biol Psychiatry 2009; 66: 316–9.
Frith C. Is autism a disconnection disorder? Lancet Neurol 2004; 3: 577.
Geschwind DH, Levitt P. Autism spectrum disorders: developmental disconnection syndromes. Curr Opin Neurobiol 2007; 17: 103–11.
Gilchrist A, Green J, Cox A, Burton D, Rutter M, Le Couteur A. Development and current functioning in adolescents with Asperger syndrome: a comparative study. J Child Psychol Psychiatry 2001; 42: 227–40.
Groen WB, Buitelaar JK, van der Gaag RJ, Zwiers MP. Pervasive microstructural abnormalities in autism: a DTI study. J Psychiatry Neurosci 2011; 36: 32–40.
Hardan AY, Minshew NJ, Keshavan MS. Corpus callosum size in autism. Neurology 2000; 55: 1033–6.
Herbert MR, Ziegler DA, Deutsch CK, O'Brien LM, Kennedy DN, Filipek PA, et al. Brain asymmetries in autism and developmental language disorder: a nested whole-brain analysis. Brain 2005; 128(Pt 1): 213–26.
Howlin P. Outcome in high-functioning adults with autism with and without early language delays: implications for the differentiation between autism and Asperger syndrome. J of Autism and Developmental Disorders 2003; 33: 3–13.
Jones DK, Basser PJ. "Squashing peanuts and smashing pumpkins": how noise distorts diffusion-weighted MR data. Magn Reson Med 2004; 52: 979–93.
Jou RJ, Mateljevic N, Kaiser MD, Sugrue DR, Volkmar FR, Pelphrey KA. Structural neural phenotype of autism: preliminary evidence from a diffusion tensor imaging study using tract-based spatial statistics. AJNR Am J Neuroradiol 2011; 32: 1607–13.
Just MA, Cherkassky VL, Keller TA, Minshew NJ. Cortical activation and synchronization during sentence comprehension in high-functioning autism: evidence of underconnectivity. Brain 2004; 127(Pt 8): 1811–21.
Just MA, Keller TA, Malave VL, Kana RK, Varma S. Autism as a neural systems disorder: a theory of frontal-posterior underconnectivity. Neurosci Biobehav Rev 2012; 36: 1292–313.
Kanaan RA, Borgwardt S, McGuire PK, Craig MC, Murphy DG, Picchioni M, Shergill SS, Jones DK, Catani M. Microstructural organization of cerebellar tracts in schizophrenia. Biol Psychiatry 2009; 66: 1067–9.
Ke X, Hong S, Tang T, Zou B, Li H, Hang Y, et al. Voxel-based morphometry study on brain structure in children with high-functioning autism. Neuroreport 2008; 19: 921–5.
Ke X, Tang T, Hong S, Hang Y, Zou B, Li H, et al. White matter impairments in autism, evidence from voxel- based morphometry and diffusion tensor imaging. Brain Res 2009; 1265: 171–7.
Keller TA, Kana RK, Just MA. A developmental study of the structural integrity of white matter in autism. Neuroreport 2007; 18: 23–7.
Kleinhans NM, Pauley G, Richards T, Neuhaus E, Martin N, Corrigan NM, et al. Age-related abnormalities in white matter microstructure in autism spectrum disorders. Brain Res 2012; 1479: 1–16.
Kumar A, Sundaram SK, Sivaswamy L, Behen ME, Makki MI, Ager J, et al. Alterations in frontal lobe tracts and corpus callosum in young children with autism spectrum disorder. Cerebral Cortex 2010; 20: 2103–13.
Lai MC, Lombardo MV, Baron-Cohen S. Autism. Lancet 2014; 383: 896–910.

Lai MC, Lombardo MV, Ecker C, Chakrabarti B, Suckling J, Bullmore ET, et al. Neuroanatomy of individual differences in language in adult males with autism. Cereb Cortex 2015; 25: 3613–28.
Lange N, Dubray MB, Lee JE, Froimowitz MP, Froehlich A, Adluru N, et al. Atypical diffusion tensor hemispheric asymmetry in autism. Autism Res 2010; 3: 350–8.
Langen M, Durston S, Staal WG, Palmen SJ, van Engeland H. Caudate nucleus is enlarged in high-functioning medication-naive subjects with autism. Biol Psychiatry 2007; 62: 262–6.
Lazar M, Miles LM, Babb JS, Donaldson JB. Axonal deficits in young adults with High Functioning Autism and their impact on processing speed. Neuroimage Clin 2014; 4: 417–25.
Lee JE, Chung MK, Lazar M, DuBray MB, Kim J, Bigler ED, et al. A study of diffusion tensor imaging by tissue-specific, smoothing-compensated voxel-based analysis. NeuroImage 2009: 44: 870–83.
Leemans A, Jeurissen B, Sijbers J, Jones DK. ExploreDTI: a graphical toolbox for processing, analyzing, and visualizing diffusion MR data. Proc Int Soc Magn Reson Med 2009; 17: 3537.
Leemans A, Jones DK. The B-matrix must be rotated when correcting for subject motion in DTI data. Magn Reson Med 2009; 61: 1336–49.
Lisiecka DM, Holt R, Tait R, Ford M, Lai MC, Chura LR, et al. Developmental white matter microstructure in autism phenotype and corresponding endophenotype during adolescence. Transl Psychiatry 2015; e529.
Lord C, Risi S, Lambrecht L, Cook EH, Jr.Leventhal BL, DiLavore PC, et al. The autism diagnostic observation schedule-generic: a standard measure of social and communication deficits associated with the spectrum of autism. J Autism Dev Disord 2000; 30: 205–23.
Lord C, Rutter M, Le Couteur A. Autism diagnostic interview-revised: a revised version of a diagnostic interview for caregivers of individuals with possible pervasive developmental disorders. J Autism Dev Disord 1994; 24: 659–85.
McAlonan GM, Cheung V, Cheung C, Suckling J, Lam GY, Tai KS, et al. Mapping the brain in autism. A voxel-based MRI study of volumetric differences and intercorrelations in autism. Brain 2005; 128: 268–76.
McAlonan GM, Suckling J, Wong N, Cheung V, Lienenkaemper N, Cheung C, et al. Distinct patterns of grey matter abnormality in high-functioning autism and Asperger's syndrome. J Child Psychol Psychiatry 2008; 49: 1287–95.
Mountcastle VB. The columnar organization of the neocortex. Brain 1997; 120(Pt 4): 701–22.
Mueller S, Keeser D, Samson AC, Kirsch V, Blautzik J, Grothe M, et al. Convergent findings of altered functional and structural brain connectivity in individuals with high functioning autism: a multimodal MRI study. PLoS One 2013; 8: e67329.
Nagy Z, Westerberg H, Klingberg T. Maturation of white matter is associated with the development of cognitive functions during childhood. J Cogn Neurosci 2004; 16: 1227–33.
Nickl-Jockschat T, Habel U, Michel TM, Manning J, Laird AR, Fox PT, et al. Brain structure anomalies in autism spectrum disorder–a meta-analysis of VBM studies using anatomic likelihood estimation. Hum Brain Mapp 2012; 33: 1470–89.
Nordahl CW, Scholz R, Yang X, Buonocore MH, Simon T, Rogers S, et al. Increased rate of amygdala growth in children aged 2 to 4 years with autism spectrum disorders: a longitudinal study. Arch Gen Psychiatry 2012; 69: 53–61.
Noriuchi M, Kikuchi Y, Yoshiura T, Kira R, Shigeto H, Hara T, et al. Altered white matter fractional anisotropy and social impairment in children with autism spectrum disorder. Brain Res 2010; 1362: 141–9.
Papagno C, Miracapillo C, Casarotti A, Romero Lauro LJ, Castellano A, Falini A, et al. What is the role of the uncinate fasciculus? Surgical removal and proper name retrieval. Brain 2011; 134(Pt 2): 405–14.
Pardini M, Elia M, Garaci FG, Guida S, Coniglione F, Krueger F, et al. Long-term cognitive and behavioral therapies, combined with augmentative communication, are related to uncinate fasciculus integrity in autism. J Autism Dev Disord 2012; 42: 585–92.
Philip RC, Dauvermann MR, Whalley HC, Baynham K, Lawrie SM, Stanfield AC. A systematic review and meta-analysis of the fMRI investigation of autism spectrum disorders. Neurosci Biobehav Rev 2012; 36: 901–42.
Pierce K, Muller RA, Ambrose J, Allen G, Courchesne E. Face processing occurs outside the fusiform 'face area' in autism: evidence from functional MRI. Brain 2001; 124(Pt 10): 2059–73.
Pugliese L, Catani M, Ameis S, Dell'Acqua F, Thiebaut de Schotten M, Murphy C, et al. The anatomy of extended limbic pathways in Asperger syndrome: a preliminary diffusion tensor imaging tractography study. NeuroImage 2009; 47: 427–34.
Radua, J, Via E, Catani M, Mataix-Cols D. Voxel-based meta-analysis of regional white-matter volume differences in autism spectrum disorder versus healthy controls. Psychol Med 2011; 41: 1539–50.
Sahyoun CP, Belliveau JW, Mody M. White matter integrity and pictorial reasoning in high-functioning children with autism. Brain Cognit 2010; 73: 180–8.
Sethi A, Gregory S, Dell'Acqua F, Periche Thomas E, Simmons A, Murphy DGM, et al. Emotional detachment in psychopathy: involvement of dorsal default-mode connections. Cortex 2015; 62: 11–9.
Shukla DK, Keehn B, Lincoln AJ, Muller RA. White matter compromise of callosal and subcortical fiber tracts in children with autism spectrum disorder: a diffusion tensor imaging study. J Am Acad Child Adolesc Psychiatry 2010; 49: 1269–78.
Smith SM, Jenkinson M, Johansen-Berg H, Rueckert D, Nichols TE, Mackay CE, et al. Tract-based spatial statistics: voxelwise analysis of multi-subject diffusion data. NeuroImage 2006; 31: 1487–505.
Stigler KA, McDonald BC, Anand A, Saykin AJ, McDougle CJ. Structural and functional magnetic resonance imaging of autism spectrum disorders. Brain Res 2011; 1380: 146–61.
Suckling J, Barnes A, Job D, Brenan D, Lymer K, Dazzan P, et al. Power calcu-lations for multicenter imaging studies controlled by the false discovery rate. Hum Brain Mapp 2010; 31: 1183–95.
Suckling J, Barnes A, Job D, Brennan D, Lymer K, Dazzan P, et al. The Neuro/PsyGRID calibration experiment: identifying sources of variance and bias in multicenter MRI studies. Hum Brain Mapp 2012; 33: 373–86.
Thomas C, Humphreys K, Jung KJ, Minshew N, Behrmann M, et al. The anatomy of the callosal and visual- association pathways in high-functioning autism: a DTI tractography study. Cortex 2011; 47: 863–73.
Toal F, Daly EM, Page L, Deeley Q, Hallahan B, Bloemen O, et al. Clinical and anatomical heterogeneity in autistic spectrum disorder: a structural MRI study. Psychol Med 2010; 40: 1171–81.
Travers BG, Adluru N, Ennis C, Tromp do PM, Destiche D, Doran S, et al. Diffusion tensor imaging in autism spectrum disorder: a review. Autism Res 2012; 5: 289–313.
Vanderauwera J, Vandermosten M, Dell'Acqua F, Wouters J, Ghesquière P. Disentangling the relation between left temporoparietal white matter and reading: a spherical deconvolution tractography study. Hum Brain Mapp 2015; 36: 3273–87.
Vargas DL, Nascimbene C, Krishnan C, Zimmerman AW, Pardo CA. Neuroglial activation and neuroinflammation in the brain of patients with autism. Ann Neurol 2005; 57: 67–81.
Via E, Radua J, Cardoner N, Happe F, Mataix-Cols D. Meta-analysis of gray matter abnormalities in autism spectrum disorder: should Asperger disorder be subsumed under a broader umbrella of autistic spectrum disorder? Arch Gen Psychiatry 2011; 68: 409–18.
Waiter GD, Williams JH, Murray AD, Gilchrist A, Perrett DI, Whiten A. A voxel-based investigation of brain structure in male adolescents with autistic spectrum disorder. NeuroImage 2004; 22: 619–25.
Walker L, Gozzi M, Lenroot R, Thurm A, Behseta B, Swedo S, et al. Diffusion tensor imaging in young children with autism: biological effects and potential confounds. Biol Psychiatry 2012; 72: 1043–51.

Wang R, Benner T, Sorensen A, Wedeen V. Diffusion toolkit: a software package for diffusion imaging data processing and tractography. Proc Int Soc Magn Reson Med 2007; 15: 3720.
Wechsler D. Wechsler abbreviated scale of intelligence (WASI). San Antonio, TX: Harcourt Assessment; 1999.
Witelson SF. Hand and sex differences in the isthmus and genu of the corpus callosum. A postmortem morphological study. Brain 1989; 112: 799–835.
WHO. The ICD-10 classification of mental and behavioral disorders - Diagnostic criteria for research. Geneva: WHO; 1983.
Wolff JJ, Gu H, Gerig G, Elison JT, Styner M, Gouttard S, et al. Differences in white matter fiber tract development present from 6 to 24 months in infants with autism. Am J Psychiatry 2012; 169: 589–600.
Zikopoulos B, Barbas H. Changes in prefrontal axons may disrupt the network in autism. J Neurosci 2010; 30: 14595–609.

Appendix 1

The MRC AIMS Consortium is a UK collaboration of autism research centres in the UK including the Institute of Psychiatry, London, the Autism Research Centre, University of Cambridge, and the Autism Research Group, University of Oxford. It is funded by the MRC UK and headed by the Section of Brain Maturation, Institute of Psychiatry. The Consortium members are in alphabetical order:

Anthony J. Bailey, Simon Baron-Cohen, Patrick F. Bolton, Edward T. Bullmore, Sarah Carrington, Bhismadev Chakrabarti, Eileen M. Daly, Sean C. Deoni, Christine Ecker, Francesca Happé, Julian Henty, Peter Jezzard, Patrick Johnston, Derek K. Jones, Meng-Chuan Lai, Michael V. Lombardo, Anya Madden, Diane Mullins, Clodagh M. Murphy, Declan G. M. Murphy, Greg Pasco, Amber N. V. Ruigrok, Susan A. Sadek, Debbie Spain, Rose Stewart, John Suckling, Sally J. Wheelwright and Steven C. Williams.

Appendix B: Awards attributed to this thesis

2015	International Scholarship Award by the American Academy of Neurology (AAN)
2016	PhD Paper Award by King's College London
2016	Neurodegenerative Disoders Award by Rotary Milano Porta Nuova

American Academy of Neurology

is pleased to honor

Lucio D'Anna, MD

as the recipient of the

2015 International Scholarship Award

Sponsored by the American Academy of Neurology

President

AMERICAN ACADEMY OF NEUROLOGY

Executive Director/CEO

KING'S College LONDON

PhD paper award

presented to

Dr Lucio D'Anna

June 2016

Professor Patrick Leman
Dean of Education,
Institute of Psychiatry, Psychology & Neuroscience

Appendix C: Presentations attributed to this thesis

Oral Presentations:

International School of Clinical Neuroanatomy, May 2015, Ragusa Ibla. *Neuronal correlates of cognitive and psychiatric symptoms in ALS.*

XLIV Congress of Italian Society of Neurology. November 2013, Milan, Italy. *Abnormalities of the uncinate fasciculus underlie behavioural symptoms in Primary Progressive Aphasia.*

International School of Clinical Neuroanatomy-The limbic system. Bibione. May 2013. *Abnormalities of the uncinate fasciculus underly behavioural symptoms in Primary Progressive Aphasia*.

Poster presentations:

D'Anna L, Tsermenteli S, Ecker C, Dell'Acqua F, Leigh PN, Murphy D, Goldstein LH, Catani M. *Neuronal correlates of cognitive and behavioural symptoms in Amyotrophic Lateral Sclerosis.* Human Brain Mapping meeting. June 2015, Honolulu-Hawaii, USA.

D'Anna L, Mesulam Marsel M, Thiebaut de Schotten M, Dell'Acqua F, Murphy D, Wieneke C, Rogalsky E, Catani M. *Abnormalities of the uncinate fasciculus underlie behavioural symptoms in Primary Progressive Aphasia*. 67th annual meeting of the American Academy of Neurology. April 2015, Washington DC, USA.

D'Anna L, Mesulam Marsel M, Thiebaut de Schotten M, Dell'Acqua F, Murphy D, Wieneke C, Rogalsky E, Catani M. *Abnormalities of the uncinate fasciculus underlie behavioural*

symptoms in Primary Progressive Aphasia. Human Brain Mapping meeting. June 2014, Hamburg, Germany

Abnormalities of the uncinate fasciculus correlate with behavioral symptoms in primary progressive aphasia

Lucio D'Anna[1,2], Marsel M Mesulam[3,4], Michel Thiebaut de Schotten[1,5], Flavio Dell'Acqua[1], Christina Wieneke[3], Adam Martersteck[3,4], Derin Cobia[3,4], Emily Rogalski[3], Marco Catani[1]

[1]Natbrainlab, Department of Forensic and Neurodevelopmental Sciences, Institute of Psychiatry, Psychology and Neuroscience (IoPPN) , King's College London, London, UK; [2]Neurology Clinic, Department of Experimental and Clinical Medical Sciences, University of Udine Medical School, and Department of Neurosciences, "S. Maria della Misericordia" University Hospital, Udine, Italy; [3]Cognitive Neurology and Alzheimer's Disease Center, Northwestern University (NU) Feinberg School of Medicine, Chicago, IL, USA; [4]NU Feinberg School of Medicine, Department of Neurology, Chicago, IL, USA; [5]Brain and Spine Institute, CNRS UMR 7225 INSERM-UPMC UMRS 1127 La Salpêtrière, Paris, France

Background and Objective

Primary Progressive Aphasia (PPA) is characterized by a gradual breakdown of language functioning for at least two years with relatively sparing of other cognitive domains (Mesulam, 1982, Mesulam, 2001). In advanced stages patients with PPA have high risk of developing behavioural problems (Kertesz *et al.*, 1999), although the neuroanatomical basis of these symptoms remains unknown. In this study we measured cortical thickness of the orbitofrontal cortex (OFC) and the anterior temporal lobe (ATL), which are frequently affected in dementias associated with behavioural symptoms (Guo *et al.*, 2013). We also used diffusion tractography to define the microstructural organization of the major association tracts connecting to the OFC and/or ATL. Our aim is to detect anatomical abnormalities underlying behavioural symptoms in relatively early PPA.

Materials and Methods

Thirty-three patients with PPA and twenty-six healthy controls were recruited. All patients received a descriptive diagnosis of logopenic (PPA-L; 8), non-fluent/agrammatic (PPA-G; 8), semantic (PPA-S; 7), mixed (2) or unclassified/severe (8) PPA according to established guidelines (Gorno-Tempini *et al.*, 2011). Behavioural symptoms were assessed using the Frontal Behavioural Inventory (FBI) (Kertesz *et al.*, 1997). T1-weighted MPRAGE sequences (repetition time 2300 ms; echo time 2.86 ms; flip angle, 9; field of view, 256 mm; 60 slices; slice thickness 1.0mm) were acquired for cortical thickness analysis with FreeSurfer (version 4.5.0) (http://surfer.nmr.mgh.harvard.edu/). Cortical thickness estimates were calculated by measuring the distance between representations of the white–grey and pial-CSF boundaries across each point of the cortical surface (Fischl and Dale, 2000). For the tractography analysis a total of 72 contiguous near-axial slices were acquired on a 3T Siemens Trio MRI system, using an acquisition sequence fully optimized for diffusion imaging, providing isotropic (2 x 2 x 2 mm) resolution and whole head coverage. Sixty diffusion-weighted images (b-value of 1000s/mm2) were acquired together with eight images with no diffusion gradient applied. DTI processing was performed using Explore DTI (http://www.exploredti.com). Virtual tractography-based dissection was used to obtain indirect indices of white matter damage of tracts connecting to temporo-frontal regions: the uncinate fasciculus (UF) between ATL and OFC, the inferior fronto-occipital fasciculus (IFOF) between the occipital and OFC and the inferior longitudinal fasciculus (ILF) between occipital and ATL (Catani and Thiebaut de Schotten, 2008).

References

Catani M, et al. A diffusion tensor imaging tractography atlas for virtual in vivo dissections. Cortex; a journal devoted to the study of the nervous system and behavior. 2008;44(8):1105-32.Fischl B et al. Measuring the thickness of the human cerebral cortex from magnetic resonance images. Proceedings of the National Academy of Sciences of the United States of America. 2000;97(20):11050-5. Gorno-Tempini et al. et al. Classification of primary progressive aphasia and its variants. Neurology. 2011;76(11):1006-14. Guo CC et al. Anterior temporal lobe degeneration produces widespread network-driven dysfunction. Brain : a journal of neurology. 2013;136(Pt 10):2979-91. Kertesz A et al. Frontal behavioral inventory: diagnostic criteria for frontal lobe dementia. The Canadian journal of neurological sciences Le journal canadien des sciences neurologiques. 1997;24(1):29-36. Kertesz A et al. Clinical and pathological overlap between frontotemporal dementia, primary progressive aphasia and corticobasal degeneration: the Pick complex. Dementia and geriatric cognitive disorders. 1999;10 Suppl 1:46-9. Mesulam MM. Slowly progressive aphasia without generalized dementia. Annals of neurology. 1982;11(6):592-8. Mesulam MM. Primary progressive aphasia. Annals of neurology. 2001;49(4):425-32. Von Der Heide RJ et al. Dissecting the uncinate fasciculus: disorders, controversies and a hypothesis. Brain : a journal of neurology. 2013;136(Pt 6):1692-707.

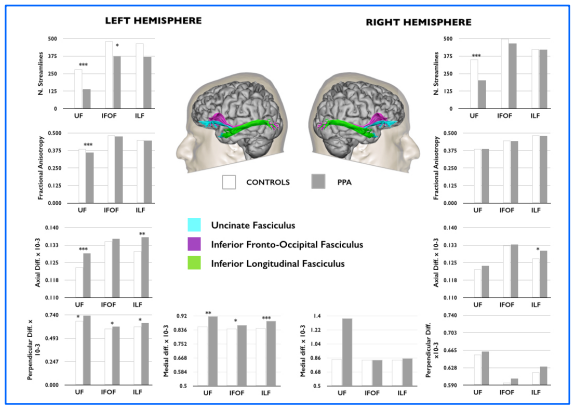

Figure 1. Differences in tract-specific measurements of the uncinate fasciculus (UF), inferior fronto-occipital fasciculus (IFOF) and inferior longitudinal fasciculus (ILF) between control subjects and patients with primary progressive aphasia (PPA). Measurements of the number of streamlines, fractional anisotropy, axial diffusivity and perpendicular diffusivity are reported for the tracts of interest (*Significant at $p < 0.05$; **Significant at $p < 0.01$; ***Significant at $p < 0.001$).

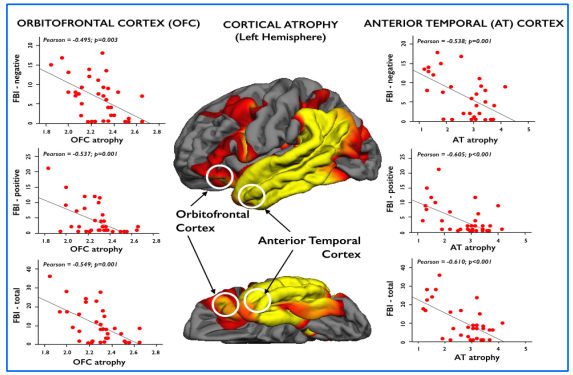

Figure 2. Correlations between left orbito-frontal cortex and anterior temporal lobe and Frontal Battery Inventory (FBI) negative, positive and total scores.

Results

White matter connections analysis (Figure 1). Compared to healthy controls, PPA patients showed statistical significantly reduced number of streamlines ($p<0.001$) fractional anisotropy ($p<0.001$) and increased axial ($p<0.001$) and perpendicular diffusivity ($p=0.020$) in the left UC. The number of streamlines was significantly reduced also in the right UC of PPA patients when compared with healthy controls ($p<0.001$). All the DTI measurements of the left UC correlated with total FBI scores and with both positive and negative FBI scores. In the right UC significant correlations were found between axial diffusivity and negative and total FBI scores and between perpendicular diffusivity and all FBI scores. In the left IFOF, the patients with PPA showed significantly lower number of streamlines ($p=0.036$) and higher perpendicular diffusivity ($p = 0.028$) when compared with healthy controls. No statistically significant differences were found for this tract in the right hemisphere. In the ILF, PPA patients showed a statistically significant increase of axial diffusivity in both sides (left: $p=0.002$; right: $p = 0.030$) and perpendicular diffusivity in the left side ($p=0.020$). We found no statistically significant correlations between any of the tractography measurements of the IFOF and ILF and the scores of the FBI.

Cortical Thickness analysis (Figure 2). A whole brain analysis showed significant cortical atrophy of the left temporal-parietal and frontal regions in the PPA compared with controls. A region of interest approach confirmed that compared with healthy controls, PPA patients showed significant atrophy in the left ($p<0.001$) and right ($p=0.014$) OFC and in the left ($p=0.001$) and right ($p=0.004$) ATL. Cortical thickness of the regions of interest in the left OFC and ATL were inversely correlated with negative scores ($p=0.003$ and $p=0.001$, respectively), positive scores ($p=0.001$ and $p<0.001$, respectively), and total scores in the FBI ($p=0.001$ and $p<0.001$, respectively). Correlations between the right ATL and the scores on the FBI were less significant. In addition significant correlations were found between DTI measurements of the left UC and cortical thickness measurements of both AT and OFC cortex. Similar correlations were found for the right UC. Not correlations were found between cortical thickness measurements and DTI measurements of the IFOF and ILF.

Discussion

Our study reports for the first time that in PPA damage to a ventral fronto-temporal network is correlated with the emergence of significant behavioral symptoms. The uncinate fasciculus is the major association pathway between the anterior part of the temporal lobe, including the amygdala, and the ventral frontal (orbitofrontal) region (Catani and Thiebaut de Schotten, 2008). These cortical areas, and the amygdala with which they are interconnected, collectively play pivotal roles in multimodal integration as well as the motivational guidance and cognitive filtering of behavior (Von Der Heide *et al.*, 2013). Our findings suggest that disruption of this network may underlie some of the behavioral abnormalities that emerge in PPA. The lack of a correlation between FBI scores and damage to the inferior fronto-occipital and inferior longitudinal fasciculi supports the relative specificity of this relationship. These results could have important implications for early detection of impending behavioral changes in PPA and in other neurodegenerative disorders.

Lucio D'Anna: lucio.d'anna@kcl.ac.uk Marco Catani: marco.l.catani@kcl.ac.uk

Appendix D: List of abbreviations

AD	Alzheimer Disease
AD	Axial Diffusivity
ADI-R	Autism Diagnostic Interview-Revised
ADC	Apparent diffusion coefficient
ALS	Amyotrophic Lateral Sclerosis
ALSFRS-R	Amyotrophic Sclerosis Functional Rating Scale Revised
AT	Anterior temporal lobe
ASD	Autism Spectrum Disorders
BA	Brodmann's area
bvFTD	behavioural variant of the frontotemporal dementia
CVLT	California Verbal Learning Test
dlPFC	dorsolateral prefrontal cortex
DTI	Diffusion tensor imaging
DWI	Diffusion-weighted imaging
FA	Fractional anisotropy
FBI	Frontal Behaviour Inventory
FAT	Frontal aslant tract
FIL	Frontal inferior longitudinal
FOP	Frontal orbito-polar
FSL	Frontal superior longitudinal
FrsBe	Frontal Systems Behavioral Scale
FTLD	Frontotemporal Lobar Degeneration
GCS	Glasgow Coma Scale

GM	Gray matter
HADS	Hospital Anxiety and Depression Scale
IFOF	Inferior Fronto-Occipital Fasciculus
KDT	Kissing and Dancing test
LMN	Lower motor neuron
mPFC	Medial prefrontal cortex
MD	Mean Diffusivity
MND	Motor Neuron Disease
MRI	Magnetic resonance imaging
OFC	Orbito-frontal cortex
PMC	Premotor cortex
PPA	Primary Progressive Aphasia
PPA-G	Agrammatic variant PPA
PPA-L	Logopenic variant PPA
PPA-S	Semantic variant PPA
PPT	Pyramid and Palm Trees test
pre-SMA	Pre-supplementary motor area
RD	Radial Diffusivity
SLF	Superior longitudinal fasciculus
SMA	Supplementary motor area
TROG-2	Test for the Reception of Grammar-second edition
UMN	Ipper motor neuron
vmPFC	ventromedial prefrontal cortex
WM	White matter
WASI	Wechsler Abbreviated Scale of Intelligence

WCST	Wisconsin Card Sorting Test